# Acceleration-induced self-interactions within a relativistic electron bunch : an analytical study

# Acceleration-induced self-interactions within a relativistic electron bunch: an analytical study

by Gianluca Geloni

# Acceleration-induced self-interactions within a relativistic electron bunch: an analytical study

PROEFSCHRIFT

ter verkrijging van de graad van doctor aan de Technische Universiteit Eindhoven, op gezag van de Rector Magnificus, prof.dr. R.A. van Santen, voor een commissie aangewezen door het College voor Promoties in het openbaar te verdedigen op vrijdag 5 september 2003 om 16.00 uur

door

Gianluca Aldo Geloni

geboren te Genova, Italia

Dit proefschrift is goedgekeurd door de promotoren:


prof.dr. M.J. van der Wiel
en
prof.dr.ir. T.J. Schep

Copromotor:
dr. J.I.M. Botman

*Larga é la foglia, stretta é la via*
*dite la vostra ch'io ho detto la mia*

Anonimo italiano

*ai miei genitori*

# Contents

# Chapter 1

# Introduction

## 1.1  INTRODUCTION AND HISTORICAL CONTEXT

The production of intense, high-brightness electron beams constitutes one of the most challenging and interesting activities for particle accelerator physicists. The growing interest of the physics community in this kind of beams is justified by important applications such as self-amplified spontaneous emission (SASE) free-electron-lasers (FELs) operating in the x-ray region (see, amongst others, [1]).

FELs are laser devices which work by exchange of energy between an electron beam and the (laser) radiation field. In order to obtain an effective exchange, the electron beam must satisfy stringent requirements: as a rule, the higher the frequency at which the laser is designed to operate, the more demanding are the constraints imposed on the electron beam. To be specific, the proposed XFEL (X-ray FEL) at DESY (Deutsches Elektronen-SYnchrotron), requires an electron bunch characterized by an energy of about 30 GeV, a charge of 1 nC, a bunch rms length of the order of 80 fs, a normalized transverse emittance of 1.6 mm mrad and a momentum spread of 0.01% in order to operate at wavelengths below 0.1 nm (see [1]).

One of the challenges faced by physicists involved in the production of these bunches is constituted by the presence of self-field induced collective effects, which may spoil the brightness of the electron beam. When an electron bunch undergoes a motion under the influence of external forces, its particles become sources of self-fields which are different from the static case (when the usual space-charge forces occur) and which obey a more general solution of Maxwell equations, derived using a retarded Green function technique: the resulting fields are known as Liénard-Wiechert expressions (see, for example, [2] or Section 2.2).

Although this subject has attained a considerable practical interest only in recent years and is completely neglected in particle accelerator textbooks, its study is a long-dated one: the first published paper we could find is due to Leonard Schiff in 1946 [3], followed by the classical article by John Nodvick and David Saxon [4] in 1954, which extends unpublished results obtained by Julian Schwinger in 1945.

These papers address the Coherent Synchrotron Radiation (CSR) emitted by an electron bunch moving in a circle[1], which is strictly related to the self-interaction

---

[1]According to the usual custom, the term 'CSR' will be used in this dissertation to designate coherent radiation from generic transversely-accelerated trajectories too, and not only from a circular

problem. In fact, collective interactions in the direction of the particle motion induce a net energy loss inside the bunch which can be detected, in the form of coherent radiation, in the 'wave zone' [2], i.e. sufficiently far away from the source so that the electromagnetic field assumes the typical characteristics of radiation [3] .

To understand the significance of these effects it is sufficient to write down and discuss the expression for the energy spectrum radiated by a system of $N$ particles undergoing an accelerated motion:

$$\left(\frac{dW}{d\omega}\right) = \left(\frac{dW}{d\omega}\right)_{sp} [N + N(N - 1) \mid \bar{F}(\omega) \mid^2] , \qquad (1.1)$$

where the subscript $sp$ identifies quantities referring to a single particle[4], while $\bar{F}(\omega)$ indicates the Fourier transform of the bunch density function.

Eq. (1.1) constitutes the basis of CSR theory. In Section 2.1 we include a thorough mathematical derivation of Eq. (1.1) adapted from [5]. The first term in $N$ between square brackets represents the ordinary incoherent synchrotron radiation, characterized by a radiated energy proportional to the number of radiating particles. The second term represents the coherent synchrotron radiation contribution. The actual coherent radiation power spectrum depends on the particle distribution in the bunch. For photon wavelengths equal to and longer than the bunch length, we expect all the particles to radiate coherently and the intensity to be, roughly, proportional to the square of the number of particles, $N^2$, rather than linearly proportional to $N$ as in the usual incoherent case. On the other hand, for a reasonably smooth behavior of the form factor $\bar{F}(\omega)$, the coherent radiation power falls off rapidly for wavelengths shorter than the rms bunch length.

Any radiation emitted corresponds to a net bunch energy loss. The quadratic effect can greatly enhance the radiation within the coherent region of the spectrum. Since the bunch population can be from $10^8$ to $10^{11}$ electrons, the magnitude of the effect can be severe.

These observations constituted the driving reason, for both the FEL and the particle accelerator community, to undertake deep investigations of self-interactions within electron beams. Self-interactions can be decomposed into longitudinal and transverse components, with respect to the direction of the velocity of a given test (or observer) particle. Studies on longitudinal self-fields (i.e. in the same direction of a specified test particle motion) aim both at determining deterioration effects on the bunch energy spread and longitudinal emittance as well as at investigating ways to use CSR as a radiation source. The need for information about the bunch evolution in the transverse direction (orthogonal to the particle motion) and estimations of transverse emittance growth triggers detailed analysis of the self-interaction in the direction orthogonal to the particles velocity. The latter is not sufficient, however, for fully characterizing the particle evolution in the transverse direction. In fact, the energy spread induced by

---

motion.

[2] Also known as radiation zone, or far field zone.

[3] We will return to this point in Section 2.2 and in Chapter 6.

[4] Here we specialized our discussion, from the beginning, to the case of Synchrotron Radiation. However, Eq. (1.1) is valid regardless the kind of radiating system we are dealing with. For example, had we imagined to have a foil instead of a magnetic system, Eq. (1.1) would have been a valid expression to describe Transition Radiation from a multi-particle system.

longitudinal self-fields has its own impact on the transverse dynamics through a magnetic system, and only a combination of both the effects in the longitudinal and the transverse direction can lead to a correct characterization of the particle behavior. As we will see in the following Sections, the full evolution problem is a formidable one; although, as we will explain in Section 1.6, in this thesis we chose to focus our attention on a more restricted part of this issue, we should make clear that the long-term goals of this kind of studies are, of course, a complete and satisfactory characterization of the bunch evolution in view of applications involving high charge, very short, ultrarelativistic bunches together with the utilization of this kind of phenomena for radiation production.

CSR and its effects on ultrashort bunches have been, of course, experimentally confirmed. The reader may refer, for example, to recent works [6] as regards beam degradation studies and [7, 8], as concerns the use of CSR as a radiation source. It is worth to mention, about beam degradation, that important effects driven by self-consistent fields take place during the passage of electron beams through magnetic chicanes, which are used for bunch compression in XFEL applications. In fact, although several techniques are currently being investigated for producing ultrashort beams (see, for example, [9]), the most reliable one, at present, consists of the following: first, accelerate a long electron bunch up to ultrarelativistic energies. Second, induce a correlated energy spread in the beam by using an RF cavity properly synchronized with the beam, so that the tail of the bunch is more energetic than the head. Third, send the beam through a magnetic chicane. The latter is a dispersive system composed of several magnets and it is designed in such a way that the more energetic particles in the tail move through a shorter path than the less energetic particles in the head, thus allowing the tail of the bunch to catch up with the head, leading to an effective bunch compression. The latest simulations for the XFEL project at DESY show significant degradation of the bunch quality due to self-interaction effects, with an expected growth of the projected transverse emittance from 0.8 mm mrad after the injector to the value of 2.6 mm mrad after compression [1].

## 1.2   THE SELF-CONSISTENT PROBLEM

The solution to the self-interaction problem is found when one is able to describe the evolution of the electron bunch particles under the action of external fields, usually induced by a magnetic system, and under the action of the fields produced by the particles themselves as they evolve in the external field. From a mathematical viewpoint this means that the equation of motion must be solved, for every particle, together with Maxwell equations. There are two main reasons why the search for the solution of this system of equations constitutes a formidable problem.

The first lies in the fact that Maxwell equations are coupled with the equation of motion. The particles in the bunch start moving under the action of the external field (for example, the magnetic field of a bending magnet) but, since they are accelerated, they also become sources of a secondary electromagnetic field (the self-interaction field) which enters, in its turn, as a driving term in the equation of motion. The problem of finding a solution for this system of coupled equations is called a "self-consistent problem".

The second reason is constituted by the fact that the electromagnetic signal propagates at finite speed, i.e. the speed of light. This means that, as an accelerated electron produces an electromagnetic signal, its effect on a second particle (the test, or observer electron) is retarded. From a practical viewpoint then, in order to include the self-field produced by the $i$-th source particle in the bunch as a driving term for the motion of a given test particle, one has to solve the following equation, known as retardation condition:

$$\left| \boldsymbol{r}(t) - {}^{i}\boldsymbol{r}({}^{i}t') \right| = c \left( t - {}^{i}t' \right) \; , \tag{1.2}$$

where $\boldsymbol{r}(t)$ is the position of the test particle at the observation time $t$, while ${}^{i}\boldsymbol{r}({}^{i}t')$ is the position of the $i$-th particle at the time at which the electromagnetic signal was emitted: as a matter of fact, to solve the self-consistent problem, one has to take into account not only the *present*, but also the *past* history of the bunch.

In Section 2.2 we provide a full mathematical presentation of the self-consistent problem making use of the covariant formalism, adapting to our purposes some of the treatment in [10]. This helps to get an eyebrow description of the issue and we feel it may be useful to report it. In our view, the choice of covariant formalism underlines the beauty and, at the same time, the entanglements of the problem with extreme elegance and compactness and it is well-suited for a general overview; moreover we will make partial use of this formalism in Chapter 5.

At this point we have given an introductory overview of the situation so that one can understand the difficulties involved in solving the self-consistent problem *in toto*: any attempt at knowing the fields must provide, first, a way to characterize the evolution of the sources but, in its turn, the evolution of the sources is only known when the fields are known, while the finite propagation velocity of the electromagnetic signal complicates the situation further. A possible solution to the problem is by means of simulation techniques, which will be briefly addressed in Section 1.5.

## 1.3   SELF-INTERACTIONS AND CSR

In the previous Section we described the self-consistent problem in a very generic fashion. There we stressed the coupling between Maxwell equations and the equations of motion, thus focusing on the self-interaction problem, more than on CSR itself. Nevertheless, as it has been said in Section 1.1, CSR and self-interactions are deeply related subjects. This relation can be made clear by means of the energy conservation theorem. In fact, the energy associated with the CSR emitted by an electron bunch must be accounted for: it obviously originates from an energy loss by the bunch which, in its turn, is caused by self-interactions. Since the rate of energy exchange between the electromagnetic field and an electron can be written as $(e\boldsymbol{E}\cdot\boldsymbol{v})$, $\boldsymbol{v}$ being the particle velocity and $\boldsymbol{E}$ the electromagnetic (self-)field acting at the position of the particle, it is obvious that the self-interaction component responsible for CSR, at least in the lowest perturbation order of the equations of motion, is the longitudinal one.

It is important to realize how close CSR and longitudinal self-interactions are. It is possible to prove, for example, (see [11, 12]) that in the case of an electron bunch moving periodically in a circular trajectory, the rate of energy loss in the bunch equals the rate of radiation energy passing through a far surface closed around the electrons.

The situation is not so straightforward in the case of a more generic trajectory. However, CSR and longitudinal self-interactions are still deeply related by the conservation laws of electromagnetism. In this thesis we will be dealing both with longitudinal self-interactions (see Chapter 3) and CSR (see Chapter 6). We feel that it is important to develop some acquaintance with the relation between the two subjects: therefore we study a particular but significant example in Section 2.3. There we begin from the conservation laws for electromagnetic fields interacting with charged particles in vacuum and we specialize them to treat the situation of a bunch entering a circular trajectory from an infinitely long straight path, pointing out the strict link which exists between CSR and longitudinal self-interactions. Our conclusion eventually confirms the logical viewpoint that the energy losses from the bunch are partly responsible for radiation detected in the wave zone, and partly for the electromagnetic field stored in the space surrounding the bunch (assuming that the bunch goes on moving indefinitely in the circle, of course).

## 1.4 SHIELDING

In the previous Section we have described the link between self-interactions in the longitudinal direction inside the bunch and CSR assuming that the bunch was moving in free space. In this sense, conditions on the electromagnetic fields were implicitly given, which specified the (absence of) surroundings of the electron bunch.

Although in this thesis we deal only with particles in free space, we spend here a few words to introduce the general problem of coping with self-interactions in the presence of surroundings other than free space. The surroundings which one has to consider are mainly constituted by the vacuum pipe around the electron beam. The problem is of course very complicated to deal with in a general situation, but a simplified analysis of simple cases is anyway possible.

In general, the presence of a conductor like, for example, a vacuum pipe, suppresses all the electromagnetic modes which do not fit the waveguide. This shielding effect is present also as regards CSR fields, even though (see [13]) the cut-off frequency turns out to be different from the usual wave-guide cutoff, depending non-linearly on the pipe dimension and on the radius of curvature of the orbit. An alternative way of thinking about this effect is to account for the formation of induced (positive) charges on the conductor surface which will produce, in their turn, an electromagnetic field. This field interacts with the primary field produced by the electrons weakening the self-interaction and the CSR effect. This effect is referred to as shielding; it obviously depends on the geometry under consideration and it becomes more and more important as the surroundings get nearer to the electrons.

There are several methods of describing this phenomenon in a quantitative way. One [13, 14] is based on the fact that, as is easily deduced from Eq. (1.1), the CSR power spectrum is proportional to the squared modulus of the Fourier transform of the current. This can be written in a more suggestive form as

$$P_{\text{CSR}}(\omega) = Z_{\text{eff}}(\omega)I^2(\omega) \, , \tag{1.3}$$

which constitutes a description of the radiating system *including* the surroundings by means of an effective impedance $Z_{\text{eff}}$: Eq. (1.3) solves, in principle, the problem of a

quantitative description of the shielding phenomenon, but a generally valid expression cannot be given, since it strongly depends on the geometry of the problem.

Another technique consists of using the image charge method [2]. Supposing the material surrounding the beam is a perfect conductor, the full system constituted by the electrons and the conductors can be proven [12] to be equivalent to another one constituted by the same electron beam and charges displaced (and moving) *ad hoc* so that the total field configuration remains the same. This method has the advantage, from a theoretical viewpoint at least, that it gives the possibility to use the same mathematical machinery used in the free space case. In the situation of an electron beam in circular motion through parallel plates separated by a distance $h$, it is found [12] that the image charges which solve the problem are constituted by an infinite array of image bunches identical to the original one, but with charges of alternating signs, displaced perpendicularly to the plates and at the same longitudinal position of the original bunch, separated by vertical displacements equal to $h$. In this case, it can be found [15] that shielding effects become important when the factor $\eta = (2\pi^3/3)^{1/2}(R/h)^{3/2}(\sigma_z/R)$ is greater than unity, where $R$ is the circle radius and $\sigma_z$ the rms bunch length.

It is easily seen that, in many cases, shielding effects constitute an important limit to coherent emission from microwave to far infrared in the situation of a bunch in a ring. For example, one can see strong shielding effects taking place [12, 15] in the case of $\sigma_z = 1$ mm, $R = 1$ m and $h = 2$ cm. These numbers correspond to a parameter $\eta \simeq 1.6$.

However, we should stress here that shielding is not always an effective mean to suppress CSR effects. For example, in the very important case of bunch compression chicanes, as the bunch gets shorter, the condition on the vacuum chamber height, $h$, becomes unpractical; for example (see [16]), the last dipole at the second LCLS (the Linac Coherent Light Source at Stanford, see [17]) chicane would require a chamber height of $h < 0.4$ mm for an effective CSR shielding.

Moreover, the estimate given above holds only in the case of circular motion, while the CSR interaction can lead to stronger power losses in case of transients between magnetic elements. A generalization of these estimates which takes into account trajectories different from the circular one can be found in [12].

We will not be dealing with shielding in this thesis since, although it is an important effect, we feel it does not add much to the physics of the problem. Therefore we refer the interested reader to specialized references given above.

## 1.5   Simulation approach

In Section 1.2 we introduced the self-consistent problem, while in Section 1.3 and 1.4 we described some of the issues related to it. In this Section we will proceed with our introduction to the self-consistent issue giving the reader an overview about its possible solutions. If one's goal is to solve the full self-consistent problem, one has to make choices about how to deal with the difficulties involved in its solution. One possibility is to perform self-consistent simulations with the help of numerical techniques. Several approaches may be followed, in principle, in order to fulfill this task.

A straightforward option (see [18]) would be to consider a model of the bunch

based on a limited number of point-like particles, each representing many electrons (in practice this consists of solving directly Eq. (2.20) and Eq. (2.21) coupled with Eq. (2.22) for a value of $N$ much smaller than the real one). The obvious advantage of this approach lies in the fact that the exact solution for the fields generated by a single particle is well-known. There are major drawbacks, though: first, the fields are singular at the particle positions and second, the temporal field-structure from a single particle scales with $R/(c\gamma^3)$, which is very short in the ultrarelativistic limit. As a result, many particles are needed in order to obtain meaningful results from this method: for example, a bunch characterized by rms length $\sigma$ should be modelled out of $N = \sigma\gamma^3/R$ particles and the number of operations needed in order to calculate all the interactions at a certain time will be of order $N^2$, often resulting in exceedingly long simulation times.

Another possible technique consists in considering distributed sources characterized by a smooth four-current $J^\mu$. The drawback here is constituted by the fact that this current must be specified over all space-time and it would require a 3D integration over space-like hypersurfaces to get the field at every observation event.

The approach which has produced, so far, the best results, consists of introducing a limited number of simplified distributed sources, called macroparticles or sub-bunches, each of which representing a large number of electrons. A macroparticle may have, for example, a Gaussian distribution, thus being a source of non-singular fields, and it may be superimposed to other macroparticles, since electrons, in general, do not cluster together in isolated structures.
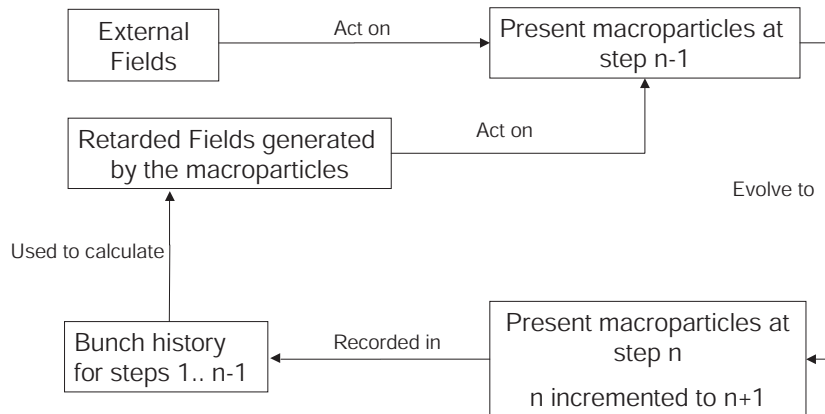


**Figure 1.1:** *Concept scheme of a self-consistent computation for the solution of the bunch evolution problem.*

The problem of tracking the bunch evolution under the action of self-forces and starting from given initial conditions can be summarized, from a general viewpoint,

as in Fig. 1.1. First a rule must be given to pass from a continuous time variable to a collection of discrete time-steps. As shown in Fig. 1.1, at each time-step the fields generated by the macroparticles at previous steps are calculated at the present position of the bunch and used, together with the external ones, as the particles evolve till the next time-step. At this point, the macroparticle states are recorded and the next time-step is considered. At the limit for zero time-steps we would recover the exact solution: it is obvious that the rule which defines the duration of the time intervals must guarantee them to be short enough to allow the calculation of the bunch evolution within a given precision and long enough to result in reasonable processing time. As the precision increases, the time-step durations decrease, complicating the situation from a numerical viewpoint, since all the macroparticle histories must be recorded and used, at every step, to calculate the retarded fields.

Several simulation codes have been built worldwide, which are based on the latter approach [19, 20, 21]. As a remarkable example we will specialize the discussion above by describing, in the following, one of these codes, TraFiC$^4$ [20]. This code has been developed at DESY and it is currently being used worldwide in order to simulate self-interaction effects in bunch dynamics, namely for XFEL purposes [1, 17]. The reason to describe this code instead of others is in the fact that, during the development of this work, we profited from a fruitful collaboration with DESY (see Chapter 4, 5 and 6), and part of the results in this thesis (Chapter 4) are devoted to an analysis of results obtained at DESY using TraFiC$^4$.

TraFiC$^4$ stands for **Tra**cking particles in the **Fi**elds of **C**ontinuous **C**harges in **C**artesian **C**oordinates. First, the code divides the beamline in different slices. As the name TraFiC$^4$ itself suggests, a cartesian coordinate system is used in order to store the information about the discretized bunch evolution.

While on the one hand the fields are generated by macroparticle source distributions, the field itself is calculated at certain sampling positions representing point-like particles. This means that the code makes use of two kinds of beam models: a generating bunch made up of macroparticles is used as field source while a cloud of (non-interacting) point-particles is used to test the field by the generating bunch, and it is therefore called sampling bunch.

The code allows two operation modes. One can choose a perturbative or a self-consistent tracking mode. If the perturbative tracking mode is selected, the (generating) bunch is first tracked along the entire beamline under the influence of the external fields alone, and the bunch history is stored. Second, a cloud of point-particles (the sampling bunch) is also tracked through the beamline but the fields from the generating bunch are summed up to the external driving forces. In other words, self-interactions are treated as a first-order perturbation to the zeroth-order motion induced by the external fields. Note that this approach basically results in considering the self-fields as external fields (in the first order approximation) which are felt by the sampling bunch but generated by an external system (the generating bunch).

If the bunch evolution is strongly coupled with the self-fields, the perturbative approach will not give realistic results. In this case the self-consistent tracking mode can be selected. When this is done, two identical bunches are created with the same initial conditions and tracked, in turn, through a step of the beamline. At each step, each bunch which is moved forward interacts with the external fields and the fields from the other bunch. Again, through this scheme the self-fields are basically considered as

external fields during a given time-step, but now the coupling with the dynamical equations is taken care of at every time-step. The relative deviation between the trajectories of the bunches gives, then, an estimate of the displacement from the self-consistent solution, which can be made smaller by using shorter time-steps and a more refined bunch population.

To end this section, it should be mentioned, for the sake of completeness, that alternative methods have been proposed [22, 23] which have been borrowed from statistical mechanics, since the latter deals with systems composed of a large number of constituents in a natural way. From our general viewpoint, we can consider an electron bunch as a fully ionized plasma composed by individuals of a single kind (the electrons). This suggests that one can seek the solution of the evolution problem trying to track directly the particle density distribution in phase space. Of course, since the system is characterized by $6N$ dimensions with $N \sim 10^8 - 10^{10}$, one will have to use all the mathematical machinery available from statistical mechanics in order to analyze the situation in a reduced 6-dimensional space, where the system evolution is governed by equations of the Vlasov-type. This kind of approach turns out to be very useful when dealing with self-interaction phenomena characterized by a time-scale which can be short with respect to the intrinsic scale associated with the macroparticle dimensions [22], like CSR-driven bunch instabilities.

CSR-driven instability is a phenomenon discovered only recently [22], which can take place also in the case self-interactions in the region from microwaves to far infrared are effectively shielded, and it can be qualitatively described in a few words. If the electron beam density presents, initially, a certain fluctuation from the ensemble expectation value and this fluctuation is characterized by a length much shorter than the bunch length, then the short structures within the bunch will start to radiate coherently and the radiation will not be shielded by the presence of the vacuum pipe, because its characteristic wavelength will be too short. This radiation can result in an amplification of the initial fluctuation which can finally end up in a phase-space fragmentation [22]. It has been pointed out that CSR instabilities constitute the first case in which an instability has first been predicted theoretically and only afterwards observed experimentally. For further information about this subject one may refer to [22, 23].

However, since this kind of phenomena will not be analyzed here we will not further investigate the Vlasov equation approach, neither from a simulation viewpoint nor from an analytical viewpoint.

## 1.6   Analytical studies: this thesis goals

TraFiC[4] and other codes are able to provide results for a number of evolution problems, an example of the application of TraFiC[4] being, as already mentioned, the modelling of the expected bunch evolution in XFEL related setups (see [1, 17]).

Nevertheless, the solution of the problem, due to its self-consistent character, merges purely electrodynamical issues with purely dynamical ones. This often results in a loss of understanding of the physics involved and in a consequent difficulty in explaining the achieved numerical results. Therefore the understanding of the electrodynamical issue, i.e. the characterization of the electrodynamical interaction, is of great importance

from the viewpoint of pure knowledge, *per se.* Nonetheless, such an understanding is
very valuable from a practical viewpoint too. In fact, benchmarks and cross-checks
of simulation results can be provided by theoretical study of the electrodynamical
problem. These cross-checks constitute critical milestones in building confidence in
simulations, which are being employed in the design of the before-mentioned large-
scale facilities around the world.

It sometimes happens, also, that this kind of theoretical analysis can be directly
applied in order to get good practical solutions for the problem, at least in a narrow
region of the parameters which specify the system setup. The results can, then, be
used for quick estimations of the magnitude of the effects under investigation and for
the development of new applications.

In this thesis we chose to investigate self-interaction problems from an electrody-
namical and fully analytical viewpoint, while ignoring the dynamical viewpoint. The
solution of the electrodynamical problem is then, in principle, ready to be used as an
input for the equations of motion to the first perturbation order in the fields. Note
that this line of action is, from a conceptual viewpoint, the same as that followed in
self-consistent simulations at each time-step, in that the code simply finds the elec-
tromagnetic fields from a given (calculated before) distribution of charges and then
includes the calculated fields into the equation of motion, tracking the system till the
next time-step.

In the present Chapter we gave a general overview of the problem, so that the
reader can easily fit the specialized discussions in the following Chapters into the more
general context.

The next Chapter 2 includes the treatment of a few selected topics which are either
at the basis of self-interaction theory or which we found useful to investigate in the
early stage of this study, as we were getting acquainted with the problem. We included
them in this thesis because we find them interesting and useful in view of the main
Chapters.

In Chapter 3 we treat the self-interaction in the longitudinal direction (parallel,
at any time, to the velocity vector by definition), which is responsible for the energy
exchange between the system and the electromagnetic field and for all CSR-related
phenomena.

The study of self-forces in the transverse direction is also important, as explained
in Section 1.1. At the time being, existing theoretical analysis of transverse self-forces
deals with the case of a circular orbit only, without considering transient collective
phenomena. We devote Chapter 4 to the study of this kind of interaction, always from
an analytical standpoint.

Very general methodological issues are often touched when dealing with practical
problems. We found that the study in Chapter 4 is actually related to the nature of
energy and momentum for an ultrarelativistic unstable system, which is a long-dated
issue. We dedicate Chapter 5 to the study of this relation.

Finally, as we have described in Section 1.3, self-interaction is deeply linked with
the CSR issue. In Chapter 6 we study subjects related to the application of CSR as
a radiation source or in a diagnostic method for monitoring the longitudinal structure
of very short, high-peak-current, ultrarelativistic bunches.

# Bibliography

[1] TESLA Technical Design Report, DESY 2001-011, edited by F. Richard et al. and http://tesla.desy.de/

[2] J.D. Jackson, *Classical Electrodynamics*, John Wiley and Sons Inc., 1998

[3] L.I. Schiff, Rev. Sci. Instr. 17, 6 (1946)

[4] J. S. Nodvick and D. S. Saxon, Phys. Rev. 96, 180 (1954)

[5] E. A. Saldin, E. A. Schneidmiller and M. V. Yurkov, DESY 02-127 (2002), ISSN 0418-9833

[6] H. H. Braun et al., Phys. Rev. Special Topics 3 (2000)

[7] G.L. Carr et al. Nature, November 2002, 153

[8] M. Abo-Bakr, J. Feikes, K. Holldack et al. Phys. Rev. Lett. 88, 254801 (2002)

[9] Fred Kiewiet, Ph.D. Thesis, Technische Universiteit Eindhoven, Nederland, 2003

[10] F. Rohrlich, *Classical Charged Particles*, Addison-Wesley publishing company inc., 1990

[11] E. L. Saldin, E. A. Schneidmiller and M. V. Yurkov, Nucl. Instr. Methods A 398, 373 (1997)

[12] R. Li, C. L. Bohn and J. J. Bisognano, in *Proceedings of the SPIE Conference, San Diego, 1997*, vol. 3154, p. 223

[13] R. L. Warnock, SLAC-PUB-5523, 1991

[14] S.A. Kheifets and B. Zotter, CERN SL-95-92 (AP), 1995

[15] C.L. Bohn, FERMILAB-Conf-02/138-T, July 2002

[16] M. Borland in *Proceedings of the LINAC2002 Conference MO202*, Gyeongju, Korea, 2002

[17] LCLS Design Study Report, SLAC reports SLAC -R521, Stanford, 1998

[18] A. Kabel, M. Dohlus, T. Limberg, Nucl. Instr. Methods A 455, 185 (2000)

[19] R. Li, in *Proceedings of the 2nd ICFA Advanced Accelerator Workshop on The Physics of High Brightness Beams, Los Angeles, 1999.*

[20] K. Rothemund, M. Dohlus and U. van Rienen, in *Proceedings of the 21st International Free Electron Laser Conference and 6th FEL Applications Workshop, Hamburg, 1999*, edited by J. Feldhaus and H. Weise

[21] M. Borland, Phys. Rev. Special Topics 4, 070701 (2001)

[22] S. Heifets and G. Stupakov, Report SLAC-PUB-8761 (2001)

[23] M. Venturini, R. Warnock, Phys. Rev. Lett, 89, 22 (2002)

# Chapter 2

# Some basic issues

In the following we treat a few selected topics which are either at the basis of self-interaction theory or which we found useful to investigate in the early stage of this study. In Section 2.1 we discuss some basic CSR physics, while in Section 2.2 we present the self-consistent problem from a covariant viewpoint. Finally in Section 2.3 we study the entrance of an electron bunch in a circular trajectory from the viewpoint of the relation between self-interactions and CSR.

## 2.1  OVERVIEW OF BASIC CSR PHYSICS

One of the fundamental results in CSR theory (see [1, 2]) and historically the first, is expressed by Eq. (1.1). We would find it incomplete to pass directly from Chapter 1 to the main Chapters of this thesis without giving here a derivation of that fundamental result. In this Section we give such a derivation adapted from [3].

Throughout this Section we will assume that the CSR-pulse energy is only a fraction of the beam energy, so that the influence of CSR can be neglected, at the lowest perturbative order, in the longitudinal equation of motion; this assumption is obviously verified in the ultrarelativistic approximation. Moreover everywhere, the cross section of the particle beam is assumed small compared to the distance to the observer detecting the CSR pulse, so that the path length differences from any point of the beam cross section to the observer are small compared to the shortest wavelength involved. The latter assumption, often valid in practice, allows one to neglect the transverse structure of the bunch, when treating CSR effects.

From a microscopic viewpoint, the electron beam current at the entrance of any magnetic system, which will act as a radiator, is made up of moving electrons with random arrival times characterized by a stochastic succession $t_k$. A stochastic distribution can be defined then, which describes the electron current at the entrance of the magnetic system:

$$I(t) = e \sum_{k=1}^{N} \delta(t - t_k) \, , \qquad (2.1)$$

where $\delta(\cdot)$ is the delta distribution, $e$ is the (negative) electron charge and $N$ is the number of electrons in the bunch. A particular choice of one bunch history out of the ensemble of all possible histories corresponds to the choice of a particular $I(t)$ which,

at this point, is just a (non-stochastic) distribution describing the behavior of a given single bunch.

The beam profile is described by the profile function $F(t)$, which is defined by the average of the beam current over a large ensemble of bunches, that is:

$$\langle I(t) \rangle = eNF(t) \ . \tag{2.2}$$

For example, the profile function for an electron beam with Gaussian current distribution is given by:

$$F(t) = \frac{1}{\sqrt{2\pi}\sigma_{\mathrm{T}}} \ \mathrm{e}^{-t^2/(2\sigma_{\mathrm{T}}^2)} \ , \tag{2.3}$$

$\sigma_{\mathrm{T}}$ being the rms electron-pulse duration. Note that, according to the definition of $F(t)$, the probability of arrival of an electron during the time interval $(t, \ t+\delta t)$, $\delta t$ being a short time interval such that $F'(t)\delta t \ll F(t)$, is simply given by $F(t)\delta t$.

Since the electron beam current, $I(t)$, and its Fourier transform, $\bar{I}(\omega)$, are connected by

$$\bar{I}(\omega) = \frac{1}{\sqrt{2\pi}} \int\limits_{-\infty}^{\infty} I(t) \ \mathrm{e}^{-i\omega t} dt = \frac{e}{\sqrt{2\pi}} \ \sum_{k=1}^{N} e^{-i\omega t_k} \ , \tag{2.4}$$

$$I(t) = \frac{1}{\sqrt{2\pi}} \int\limits_{-\infty}^{\infty} \bar{I}(\omega) \ \mathrm{e}^{i\omega t} d\omega = e \sum_{k=1}^{N} \delta(t - t_k) \ , \tag{2.5}$$

the average value of $\mid \bar{I}(\omega) \mid^2$ can be written as:

$$\langle \mid \bar{I}(\omega) \mid^2 \rangle = \langle \bar{I}(\omega)\bar{I}^*(\omega) \rangle = \frac{e^2 N}{2\pi} + \frac{e^2}{2\pi} \sum_{k \neq n} \langle \mathrm{e}^{-i\omega t_k} \rangle \langle \mathrm{e}^{i\omega t_n} \rangle. \tag{2.6}$$

The expression $\langle \mathrm{e}^{-i\omega t_k} \rangle$ is, essentially, the Fourier transform of the bunch profile function $F(t)$, since:

$$\langle \mathrm{e}^{-i\omega t_k} \rangle = \int\limits_{-\infty}^{\infty} F(t_k)\mathrm{e}^{-i\omega t_k} dt_k = \sqrt{2\pi}\bar{F}(\omega) \ . \tag{2.7}$$

Thus we can write:

$$\langle \mid \bar{I}(\omega) \mid^2 \rangle = \frac{e^2 N}{2\pi} + e^2 N(N-1) \mid \bar{F}(\omega) \mid^2 \ , \tag{2.8}$$

where the Fourier transform of the Gaussian profile function Eq. (2.3) has the form:

$$\bar{F}(\omega) = \frac{1}{\sqrt{2\pi}}\mathrm{e}^{-\omega^2 \sigma_{\mathrm{T}}^2/2} \ . \tag{2.9}$$

Up to now a characterization of the current at the entrance of the magnetic system has been given both in time and frequency domain, which completely defines the input signal of the electromagnetic device under consideration.

The next step is the derivation of the energy spectrum, which is the output signal of the device. For any given realization of the stochastic succession $t_k$, the total field experienced by the observer is given by the sum of $N$ *identical* single-particle pulses such that the $k$-th pulse is delayed by a time $t_k$ with respect to a previously set zero-time. Without loss of generality, one can decompose the field along orthogonal polarization components $\xi$ and take care to sum up the energy spectra from different polarizations at the end of the derivation.

Once the single particle field, $E_\xi^{sp}(t)$, is known, the total field, $E_\xi^{tot}(t)$, is given by:

$$E_\xi^{tot}(t) = \frac{1}{e} \int\limits_{-\infty}^{\infty} E_\xi^{sp}(t - \tau) \, I(\tau) d\tau \; . \tag{2.10}$$

Let the Fourier transform of $E_\xi^{sp}(t)$ and $E_\xi^{tot}(t)$ be indicated according to the usual notation as $\bar{E}_\xi^{sp}(\omega)$ and $\bar{E}_\xi^{tot}(\omega)$. Because of Eq. (2.10) we have

$$\bar{E}_\xi^{tot}(\omega) = \frac{\sqrt{2\pi}}{e} \bar{E}_\xi^{sp}(\omega) \bar{I}(\omega) \; . \tag{2.11}$$

It is easy to show (see for example [4, 5]), that the energy spectrum of the radiated pulse for the polarization direction $\xi$ is given by

$$\frac{dW_\xi}{d\omega} = \frac{2r_0^2}{\mu_0 c} \int d\Omega \mid \bar{E}_\xi^{tot}(\omega) \mid^2 \; , \tag{2.12}$$

$r_0$ being the distance to the observer, $c$ the speed of light in vacuum and $\mu_0$ the vacuum magnetic permeability. By using Eq. (2.11) it follows from Eq. (2.12) that the ensemble average of the energy spectrum at frequency $\omega$ is related to the average of the square modulus of the radiation field according to

$$\left\langle \frac{dW_\xi}{d\omega} \right\rangle = \left\langle \frac{2r_0^2}{\mu_0 c} \int d\Omega \mid \bar{E}_\xi^{tot}(\omega) \mid^2 \right\rangle = \frac{4\pi r_0^2}{\mu_0 c e^2} \int d\Omega \bar{E}_\xi^{sp\,2}(\omega) \langle \mid \bar{I}(\omega) \mid^2 \rangle \; . \tag{2.13}$$

The total energy spectrum $\left\langle \frac{dW}{d\omega} \right\rangle$ is given, then, by direct substitution of Eq. (2.8) in Eq. (2.13) and summation over $\xi$, which reads:

$$\left\langle \frac{dW}{d\omega} \right\rangle = \left\langle \frac{dW^{sp}}{d\omega} \right\rangle [N + 2\pi N(N-1) \mid \bar{F}(\omega) \mid^2] \; , \tag{2.14}$$

where the superscript *sp* identifies, as usual, quantities referring to a single particle. Note that Eq. (2.14) is slightly different with respect to Eq. (1.1): in fact, in Eq. (2.14) we underlined explicitly the presence of ensemble averages with the brackets $\langle ... \rangle$. Moreover the particular definition of the Fourier transform as in Eq. (2.4), which we prefer because it is completely symmetric with respect to the anti-transform, leads to the factor $2\pi$ in the second term.

## 2.2   A COVARIANT FORMULATION OF THE SELF-CONSISTENT PROBLEM

We described the self-consistent problem in Section 1.2. In that Section we did not formulate it in its natural language, that is mathematics, since our aim, there, was just to introduce it in the simplest possible way. However we feel that a more rigorous formulation of the problem is important in order to get a more thorough view of the challenges which it poses. Therefore, in this Section, we adapt some of the material in [6] to the purpose of describing the self-consistent issue in a precise way. We find that the use of the covariant formalism is very well suited for this purpose, both because of its elegance and its compactness. Moreover, this formalism will be useful in Chapter 5, where the geometrical nature of the energy-momentum pair will be discussed in the case of an unstable system.

One can write the following system of coupled equations, which describes the evolution of a system of $N$ electrons, Eq. (2.15) and Eq. (2.16) being Maxwell equations, while Eq. (2.17) being the equation of motion:

$$\partial_\nu F^{\mu\nu} = \frac{J^\mu}{\epsilon_0} \ , \tag{2.15}$$

$$\partial_\nu (*F)_{\mu\nu} = 0 \ , \tag{2.16}$$

$$\frac{e}{c} F^{\mu\nu} \, {}^i U_\nu = m \frac{\mathrm{d}({}^i U^\mu)}{\mathrm{d}\tau} \qquad i = 1... \ N. \tag{2.17}$$

Here $F_{\mu\nu}$ are the components[1] of the electromagnetic tensor in the usual coordinate basis induced by the pseudo-cartesian coordinates $\{ct, x, y, z\}$:

$$F_{\mu\nu} = \begin{pmatrix} 0 & -E_x & -E_y & -E_z \\ E_x & 0 & cB_z & -cB_y \\ E_y & -cB_z & 0 & cB_x \\ E_z & cB_y & -cB_x & 0 \end{pmatrix}, \tag{2.18}$$

and the process of raising and lowering indexes is controlled by the metric tensor of components $g_{\mu\nu}$:

$$g_{\mu\nu} = \begin{pmatrix} -1 & 0 & 0 & 0 \\ 0 & 1 & 0 & 0 \\ 0 & 0 & 1 & 0 \\ 0 & 0 & 0 & 1 \end{pmatrix}. \tag{2.19}$$

Moreover, $J^\nu$ is the total four-current density of components ($\rho$, $\boldsymbol{J}/c$), $\rho$ and $\boldsymbol{J}$ being the usual charge density and the current density respectively, while ${}^i U^\mu$ is the four-velocity of the $i$-th particle, whose components are ${}^i\gamma(1, {}^i\boldsymbol{v})$, ${}^i\gamma$ and ${}^i\boldsymbol{v}$ being the relativistic $\gamma$-factor and the velocity of the $i$-th particle respectively (note that ${}^i U^\mu$ is linked to the four-momentum by ${}^i P^\mu = m \, {}^i U^\mu$). Finally, $\tau$ indicates the proper time

---

[1] In this dissertation, Greek tensor indices are understood to run from 0 to 3, while Latin tensor indices from 1 to 3. The left superscript $i$ does not indicate a tensor index, and runs from 1 to $N$.

and $m$ the electron rest mass, while $\epsilon_0$ is the vacuum dielectric constant and $(*F)_{\mu\nu}$ designates the Hodge dual of $F_{\mu\nu}$. [2]

Eq. (2.15), Eq. (2.16) and Eq. (2.17) can be rewritten in a more specialized way separating the self-interaction fields from the external fields. The Maxwell equations for the external fields can be considered solved, i.e. the external fields are known, since the elements of the beam line are supposed to be specified. Therefore we have, with obvious notational meaning:

$$\partial_\nu F_{\text{self}}^{\mu\nu} = \frac{J_{\text{self}}^\mu}{\epsilon_0} \tag{2.20}$$

$$\partial_\nu (*F_{\text{self}})^{\mu\nu} = 0 \tag{2.21}$$

$$\frac{e}{c}(F_{\text{ext}}^{\mu\nu} + F_{\text{self}}^{\mu\nu}) \; {}^iU_\nu = m\frac{\mathrm{d}({}^iU^\mu)}{\mathrm{d}\tau} \qquad i = 1... \; N. \tag{2.22}$$

Note that if $F_{\text{self}}^{\mu\nu}$ is neglected we recover the simpler problem of charged particles evolving within a given external electromagnetic field, which can be pursued with conventional beam dynamics techniques. In the more generic case in which $F_{\text{self}}^{\mu\nu}$ can not be neglected, one has to solve Maxwell equations for the self-fields coupled with the equations for the particles motion through the self-current density, since

$$J_{\text{self}}^\mu(p) = e\sum_{i=1}^{N} \int_{-\infty}^{\infty} {}^iU^\mu(\tau) \; \delta(p - \; {}^i\lambda(\tau))d\tau, \tag{2.23}$$

where ${}^i\lambda(\tau)$ describes the world-line of the $i$-th particle and $\delta(\cdot)$ is, here, the 4-dimensional $\delta$-distribution.

In addition, of course, one has to know the initial state of every particle, which is characterized by the collection of four-vectors[3] pairs $\{({}^i\bar\lambda^\mu, \; {}^i\bar U^\mu) \mid i = 1... \; N\}$ on a given space-like surface $\sigma$; to be specific, $\sigma$ may be the one characterized by $t = 0$ in a fixed coordinate system $\{ct, x, y, z\}$. At last, specification of the surroundings of the system must be given. For example, only normal electric fields and tangential magnetic fields are expected at a boundary of a perfect conductor, and similar constraints have to be expected at the position of the metallic pipe in which the electrons move. The latter conditions translate into a set of constraints for $F^{\mu\nu}$ over a given space-like hypersurface. One cannot be more specific, since the kind of boundary depends heavily on the system setup.[4].

The system of coupled equations Eq. (2.20), Eq. (2.21) and Eq. (2.22), together with the knowledge of $F_{\text{ext}}^{\mu\nu}$, $\{({}^i\bar\lambda^\mu \; {}^i\bar U^\mu) \mid i = 1... \; N\}$ and suitable conditions on $F^{\mu\nu}$ on $\sigma$ constitute the most generic formulation of the self-consistent problem.

The situation is complicated by the fact that electromagnetic signals travel at finite speed. This means that the field at any event $p$ depends on the charges located on

---

[2]The Hodge dual on an n-dimensional manifold maps p-forms (completely antisymmetric covariant tensors in p dimensions) into (n-p)-forms by $(*A)_{\mu_1...\mu_{n-p}} = (1/p!) \; \epsilon^{\nu_1...\nu_p}{}_{\mu_1...\mu_{n-p}} A_{\nu_1...\nu_p}$, where $\epsilon_{\alpha_1...\alpha_p}$ is the Ricci tensor.

[3]Note that, strictly speaking, ${}^i\bar\lambda^\mu$ indicate the coordinates of a point in Minkowski space. However, the affine structure of the Minkowski space (the affine group is simply the Poincaré group) gives us the freedom of considering ${}^i\bar\lambda^\mu$ as the components of a four-vector.

[4]The problem of conducting surrounding has been briefly addressed in Section 1.4.

the past light-cone of $p$ only. Viceversa, a given charge at position $q$ in space-time influences the fields at $p$ if and only if $p$ is on the future light-cone of $q$. This fact defines the causal structure of Minkowski space, and the requirement

$$(p - q)^2 = 0 \quad \text{with} \quad p^0 > q^0 \tag{2.24}$$

is referred to as *retardation condition*.

In order to fully realize the difficulties involved in dealing with the self-consistent problem, one has to be familiar with the solution of Maxwell equations Eq. (2.15) and Eq. (2.16), which can be calculated once the field sources $J^\mu$ are given. For this reason it is worth to present briefly, here, a derivation of such a solution, while more details can be found in textbooks like [6, 7], stressing the fact that, in our case, this is by no means an explicit solution for the fields, since it is coupled with the equations for the particle motion: more precisely we can say it is an integro-differential presentation of the self-consistent problem.

In order to simplify the mathematical problem it is temporarily convenient (and customary) to pass from the equations for the fields to the equations for the electromagnetic potential. The electromagnetic potential can be introduced simply noting that Eq. (2.16) can be considered as a statement about the closure of the two-form $F$ defined, in components, by $F_{\mu\nu}$, that is

$$dF = 0, \tag{2.25}$$

where $d$ indicates the Cartan differential[5]. It can be shown (see for example [8, 9]) that the closure of $F$ is, in this case, a condition necessary and sufficient for $F$ to be exact too so that one can write

$$F = dA, \tag{2.26}$$

$A$ being the one form of components $A_\mu$ we were looking for.

It can be readily seen that the theory is manifestly invariant upon gauge transformations

$$A \longrightarrow A + d\lambda, \tag{2.27}$$

$\lambda$ being any zero-form (i.e. any scalar); this follows immediately from the fact that $d(d\lambda) = 0$. One choice is characterized by the Lorentz condition

$$\partial_\mu A^\mu = 0, \tag{2.28}$$

which sets $\lambda$, and therefore the gauge, in such a way that

$$\partial_\mu \partial^\mu \lambda = 0. \tag{2.29}$$

This choice is the well-known Lorentz gauge. Eq. (2.26) together with Eq. (2.15) can be easily transformed, in the Lorentz gauge, in the following set of equations:

---

[5]The Cartan differential acts on $p$-forms (completely antisymmetric covariant tensors in $p$ dimensions) $T_{\mu_1 \ldots \mu_p}$ giving back a $(p+1)$-form $(dT)_{\mu_1 \ldots \mu_{p+1}} = (p+1) \, \partial_{[\mu_1} T_{\mu_2 \ldots \mu_{p+1}]}$, where the square brackets indicate an alternating sum over indices permutations normalized to $(1/p!)$, i.e. $T_{[\mu_1 \ldots \mu_p]} = (1/p!)(T_{\mu_1 \ldots \mu_p} + \text{alternating sum over permutation of indices } \mu_1 \ldots \mu_p)$.

$$F^{\mu\nu} = \partial^\mu A^\nu - \partial^\nu A^\mu \tag{2.30}$$

and

$$\partial_\alpha \partial^\alpha A^\mu = -\frac{J^\mu}{\epsilon_0}, \tag{2.31}$$

which are equivalent to Maxwell equation Eq. (2.15) and Eq. (2.16).

Solutions of Eq. (2.31) can be found by means of the Green function method. First, solutions of the covariant equation

$$\partial_\alpha \partial^\alpha D(x - x') = -\delta(x - x') \tag{2.32}$$

are sought, where the retardation condition is enforced by requiring that

$$D(x - x') = 0 \text{ when } x'^0 > x^0. \tag{2.33}$$

Under this requirement, when Eq. (2.32) is solved, a solution for $A^\mu$, which is called *retarded solution* is also found and reads:

$$A^\mu(x) = \frac{1}{\epsilon_0} \int D(x - x') J^\mu(x') d^4 x'. \tag{2.34}$$

It is possible to show [6, 7] that the Green function we are looking for can be written in covariant form as

$$D(x) = \frac{1}{2\pi} \theta(x) \delta(x^2), \tag{2.35}$$

where $\theta(p) = 0$ if $p^0 < 0$ and $\theta(p) = 1$ when $p^0 > 0$. Substitution in Eq. (2.34) gives the final result:

$$A^\mu(x) = \frac{1}{2\pi\epsilon_0} \int J^\mu(x') \theta(x - x') \delta[(x - x')^2] d^4 x', \tag{2.36}$$

which is related to the fields $F^{\mu\nu}$ by means of Eq. (2.30). Since our specific investigation deals with a system of $N$ particles whose current density is given by Eq. (2.23), one can simplify Eq. (2.36) to the following expression:

$$A^\mu(x) = \frac{e}{4\pi\epsilon_0} \sum_{i=1}^{N} \left[ \frac{{}^i U^\mu}{{}^i U_\alpha (x - {}^i \lambda)^\alpha} \right]_{\tau = {}^i \tau_0}, \tag{2.37}$$

where

$$[x - {}^i \lambda({}^i \tau_0)]^2 = 0 \text{ with } x^0 > {}^i \lambda^0(\tau_0) \qquad i = 1... \, N \, . \tag{2.38}$$

Direct use of Eq. (2.30) gives back the expression for the retarded fields in covariant form (see [6, 7]):

$$F^{\mu\nu} = \frac{e}{4\pi\epsilon_0 c} \sum_{i=1}^{N} \left[ \frac{1}{{}^i U_\alpha (x - {}^i \lambda)^\alpha} \frac{d}{d\tau} \left( \frac{{}^i U^\mu (x - {}^i \lambda)^\nu - {}^i U^\nu (x - {}^i \lambda)^\mu}{{}^i U_\alpha (x - {}^i \lambda)^\alpha} \right) \right]_{\tau = {}^i \tau_0} \tag{2.39}$$

The latter equation can also be written in a different way. After definition of the space-like unit four-vector ${}^iN^\mu$ orthogonal to ${}^iU^\mu$ for all choices of $i = 1... N$,

$$({}^iN)^\mu({}^iN)_\mu = 1 , \qquad ({}^iN)^\mu({}^iU)_\nu = 0 , \tag{2.40}$$

one can express Eq. (2.39) as a sum of two terms:

$$F^{\mu\nu} = F_V^{\mu\nu} + F_A^{\mu\nu} , \tag{2.41}$$

where

$$F_V^{\mu\nu} = \frac{e}{4\pi\epsilon_0} \sum_{i=1}^{N} \left[ \frac{({}^iU)^\mu({}^iN)^\nu - ({}^iN)^\mu({}^iU)^\nu}{[{}^iU_\alpha(x - {}^i\lambda)^\alpha]^2} \right]_{\tau = {}^i\tau_0} \tag{2.42}$$

and

$$F_A^{\mu\nu} = \frac{e}{4\pi\epsilon_0 c} \sum_{i=1}^{N} \left\{ \frac{1}{{}^iU_\alpha(x - {}^i\lambda)^\alpha} \left[ \left( {}^iA^\mu \, {}^iU^\nu - {}^iU^\mu \, {}^iA^\nu \right) / c \right. \right.$$
$$\left. \left. - {}^iN^\mu \left( {}^iU^\nu \, {}^iA^\alpha \, {}^iN_\alpha / c + {}^iA^\nu \right) + {}^iN^\nu \left( {}^iU^\mu \, {}^iA^\alpha \, {}^iN_\alpha / c + {}^iA^\mu \right) \right] \right\}_{\tau = {}^i\tau_0} , \tag{2.43}$$

${}^iA^\mu = \mathrm{d} \, {}^iU^\mu / (\mathrm{d}\tau)$ being the four-acceleration relative to the $i$-th particle.

The importance of the presentation given by Eq. (2.41), Eq. (2.42) and Eq. (2.43) lies in the recognition that $F^{\mu\nu}$ can be decomposed into a velocity-dependent part, $F_V^{\mu\nu}$, and an acceleration-dependent part, $F_A^{\mu\nu}$. These two behave in a very different way as the observation point gets far away from the source (in the usual three dimensional sense). In order to fully appreciate this fact, it is useful to write down the non-covariant expressions for the electric and magnetic field (see again [6, 7]), following directly from Eq. (2.41):

$$\boldsymbol{E}(\boldsymbol{r_0}, t) = \boldsymbol{E_V}(\boldsymbol{r_0}, t) + \boldsymbol{E_A}(\boldsymbol{r_0}, t), \tag{2.44}$$

with

$$\boldsymbol{E_V}(\boldsymbol{r_0}, t) = \frac{e}{4\pi\varepsilon_0} \sum_{i=1}^{N} \left\{ \frac{1}{{}^i\gamma^2} \frac{{}^i\boldsymbol{n} - {}^i\boldsymbol{\beta}}{{}^iR^2 \left(1 - {}^i\boldsymbol{n} \cdot {}^i\boldsymbol{\beta}\right)^3} \right\}, \tag{2.45}$$

$$\boldsymbol{E_A}(\boldsymbol{r_0}, t) \frac{e}{4\pi\varepsilon_0} \sum_{i=1}^{N} \left\{ \frac{1}{c} \frac{{}^i\boldsymbol{n} \times \left[ \left( {}^i\boldsymbol{n} - {}^i\boldsymbol{\beta} \right) \times {}^i\dot{\boldsymbol{\beta}} \right]}{{}^iR \left(1 - {}^i\boldsymbol{n} \cdot {}^i\boldsymbol{\beta}\right)^3} \right\} \tag{2.46}$$

and

$$\boldsymbol{B}(\boldsymbol{r_0}, t) = \boldsymbol{B_V}(\boldsymbol{r_0}, t) + \boldsymbol{B_A}(\boldsymbol{r_0}, t), \tag{2.47}$$

with

$$\boldsymbol{B_V}(\boldsymbol{r_0}, t) = \frac{1}{c} \sum_{i=1}^{N} {}^i\boldsymbol{n} \times {}^i\boldsymbol{E_V} , \tag{2.48}$$

$$\boldsymbol{B_A}(\boldsymbol{r_0}, t) = \frac{1}{c} \sum_{i=1}^{N} {}^{i}\boldsymbol{n} \times {}^{i}\boldsymbol{E_A} \ . \tag{2.49}$$

Here ${}^{i}\boldsymbol{\beta}$ and ${}^{i}\dot{\boldsymbol{\beta}}$ are, respectively, the dimensionless velocity and its time derivative at the retarded time ${}^{i}t'$, all relative to the $i$-th particle, ${}^{i}R$ is the distance between the retarded position of the $i$-th source particle and the observation point and ${}^{i}\boldsymbol{n}$ is a unit vector along the line connecting those two points, while the retardation condition linking $i$-th source particle with an observation point at position $\boldsymbol{r_0}(t)$ reads:

$$\left| \boldsymbol{r_0}(t) - {}^{i}\boldsymbol{r}({}^{i}t') \right| = c \left( t - {}^{i}t' \right) \ . \tag{2.50}$$

Eqs. (2.44) to (2.49) have been first derived by Liénard in 1898 and Wiechert in 1900 and, in the form for $N = 1$, they go under the name of Liénard-Wiechert fields. In particular $\mathbf{E_V}$ and $\mathbf{B_V}$ are known as velocity fields, while $\mathbf{E_A}$ and $\mathbf{B_A}$ are referred to as acceleration fields.

The main feature of the velocity and acceleration fields is that they depend, respectively, on $R^{-2}$ and $R^{-1}$. As is well-known ([6, 7]), the dependence on $R^{-1}$ allows a net energy flow through a far surface, which is referred to as *radiation*, while the dependence $R^{-2}$ forbids it. This explains why the velocity and the acceleration fields are also commonly named Coulomb and radiation fields.

At this point the reader has a general overview of the situation and can fully understand the difficulties involved in solving the self-consistent problem *in toto*: any attempt of knowing the fields must first provide a way to characterize the evolution of the sources but in its turn, the evolution of the sources is only known when the fields are known, while the finite propagation velocity of the electromagnetic signal complicates the situation further.

## 2.3 Self-interactions and CSR, a specific example

Studying CSR is a singular learning experience in that many results are not intuitive at all if not, some times, counter intuitive. The best way to cope with this is to build up understanding step by step, starting from simple situations first and to discuss more complicated situations later. We have already mentioned in Chapter 1 that, in the case of a circular motion, there is a direct correspondence between the rate of energy lost by the bunch and the rate of energy passing through a far surface closed on the sources. In this Section we provide a thorough analysis of the relation between CSR and self-interaction in the longitudinal direction. After the introduction of general concepts we specialize our discussion to a particular case, different from the circular situation, which we found interesting and useful to build confidence with the subject.

Let us start discussing the link between the variation of the electromagnetic contents of space and the charge motions; this is presented, from a general viewpoint, in the conservation laws for electromagnetic fields interacting with charged particles in vacuum [6, 7]:

$$\partial_\mu \Theta^{\mu\nu} = -F^{\nu\beta} J_\beta, \tag{2.51}$$

where $\Theta$ is the symmetric electromagnetic stress tensor:

$$\Theta^{\mu\nu} = \epsilon_0 \left( -g^{\alpha\nu} F^{\mu\beta} F_{\alpha\beta} + \frac{1}{4} g^{\mu\nu} F^{\alpha\beta} F_{\alpha\beta} \right). \tag{2.52}$$

After substitution of Eq. (2.19) and Eq. (2.30) into Eq. (2.52), the time component of Eq. (2.51) reads:

$$\frac{\partial u}{\partial t} + \boldsymbol{\nabla} \cdot \boldsymbol{S} = -\boldsymbol{J} \cdot \boldsymbol{E}, \tag{2.53}$$

where $u = \Theta^{00} = (\epsilon_0/2)(E^2 + c^2 B^2)$ is the electromagnetic energy density and $\boldsymbol{S} = (1/\mu_0)(\boldsymbol{E} \times \boldsymbol{B})$ is the Poynting vector (note that $\Theta^{0i} = \Theta^{i0} = S^i/c$). This well-known result is referred to as the Poynting theorem.

Let us now consider a closed three-dimensional surface $\Sigma$ including a volume $V$, for example a sphere of radius $R$, in the laboratory frame where the electrons are set in motion, in the limit for a large distance of $\Sigma$ from the bunch (in space). If we integrate Eq. (2.53) over V (note that V is nothing but a space-like hypersurface) we have:

$$\left[ \oint_{\Sigma} S_n d\sigma \right](t) = - \left[ \int \boldsymbol{J} \cdot \boldsymbol{E}\ dV \right](t) - \left[ \int \frac{\partial u}{\partial t}\ dV \right](t)\ , \tag{2.54}$$

where $S_n$ is the scalar product between the Poynting vector and a unit vector orthogonal to $\Sigma$ pointing outwards, while $t$ refers to the time measured in the judgment of an observer at rest with respect to $\Sigma$, i.e. with respect to the laboratory frame.

Here, as in Section 1.1, we will assume that the CSR-pulse energy is only a fraction of the beam energy and that the path length differences from any point of the beam cross section to the observer are small compared to the shortest wavelength involved. The first term on the right hand side of Eq. (2.54) can be written as:

$$\left[ \int \boldsymbol{J} \cdot \boldsymbol{E}\ dV \right](t) = \left[ e \int_{-\infty}^{+\infty} (\boldsymbol{v} \cdot \boldsymbol{E})(s)\ F(s)\ ds \right](t), \tag{2.55}$$

where averages over a large ensemble of bunches will be systematically understood from now on. $\boldsymbol{E}(s)$ is the total electric field at a certain position $s$ along the bunch and it should include the external field, which we will set to zero assuming a motion through a magnetic system. The electric field due to interactions with the other particles is, therefore, the only non-zero term.

Moreover, when the detectors collect information on a surface $\Sigma$ and the sources are located far away, the velocity contribution can be neglected. In this case Eq. (2.54) can be written as:

$$\left[ \oint_{\Sigma} S_n d\sigma \right]_A (t) = - \left[ e \int_{-\infty}^{+\infty} (\boldsymbol{v} \cdot \boldsymbol{E})(s)\ F(s)\ ds \right](t) - \left[ \int \frac{\partial u}{\partial t}\ dV \right](t) \tag{2.56}$$

Eq. (2.56) connects the bunch energy losses to the radiation detected far away on a surface (i.e. $\Sigma$) closed around the sources.

In stationary (or periodic) situations[6] it is trivial to connect instantaneous energy loss of a bunch and flux of the Poynting vector through a distant surface; in fact the

---

[6]Here the words *stationary* and *periodic* obviously refer to the temporal dependence of $u$.

second term on the right hand side of Eq. (2.56) gives a zero contribution, and the instantaneous energy loss of a bunch must equal the radiation energy detected on a far surface, as has been verified in [10, 11]. This is, for example, the situation which one encounters in the case of uniform circular motion.

The previous consideration ceases to hold in case of a non-stationary motion, where the time derivative of the energy density in the volume surrounded by the distant surface is neither zero nor periodic. In this case its integral, i.e. the second term on the right hand side of Eq. (2.56), does not vanish anymore. Nevertheless, the conservation laws of vacuum electrodynamics still hold and in particular, Eq. (2.56) holds.
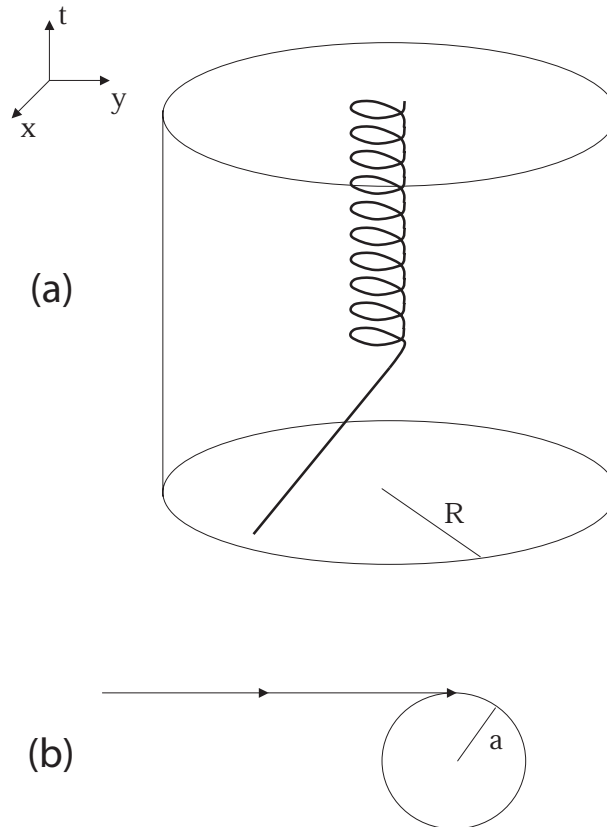


**Figure 2.1:** *(a) Space-time diagram of a single particle entering a circular trajectory from an half-infinite straight path and of a large sphere containing the circle. (b) The actual trajectory.*

In order to get a feeling for what happens in the generic case of non-stationary motion, one can consider a simple example of a bunch entering a circular motion after an half-infinite straight path. To fix the ideas it might be useful to look at Fig. 2.1: there a single particle trajectory and the corresponding single particle evolution in space-time are plotted. Also, a sphere with a large radius $R$, which represents our surface $\Sigma$, is plotted while evolving in space-time together with the particle. There is clearly a "transient" event which separates the stationary situation of the particle moving in a straight line from the periodic situation of particle moving in a circle.

Radiation is collected on the sphere of radius $R$, which is supposed to be centered at the transient point between the straight line and the circle.

Let us consider now an entire bunch following the same evolution as the single particle. Although the notion of transient event is well defined in space-time for every particle, the idea of transient for the bunch and the detectors on the far sphere are different.

A transient for the bunch can be reasonably defined as the situation which is occurring when at least one particle interacts with retarded sources both in the straight line and in the circle. On the other hand, for the detectors, the transient is defined as the situation which occurs between the two extreme configurations in which, first, no radiation at all is detected (all retarded sources are in the straight path) and, second, a constant, non-zero radiation power is detected (all retarded sources are in the circle).

Since detectors and particles undergo different evolutions in space-time, the word "transient" has different meanings, and, thus, defines different time intervals, for the bunch and for the detectors on the far surface.

Suppose that the first particle of the bunch crosses the transient point between straight and bend at time $T_{N1}$, with respect to a clock in the laboratory frame (i.e. the rest frame of the detectors).
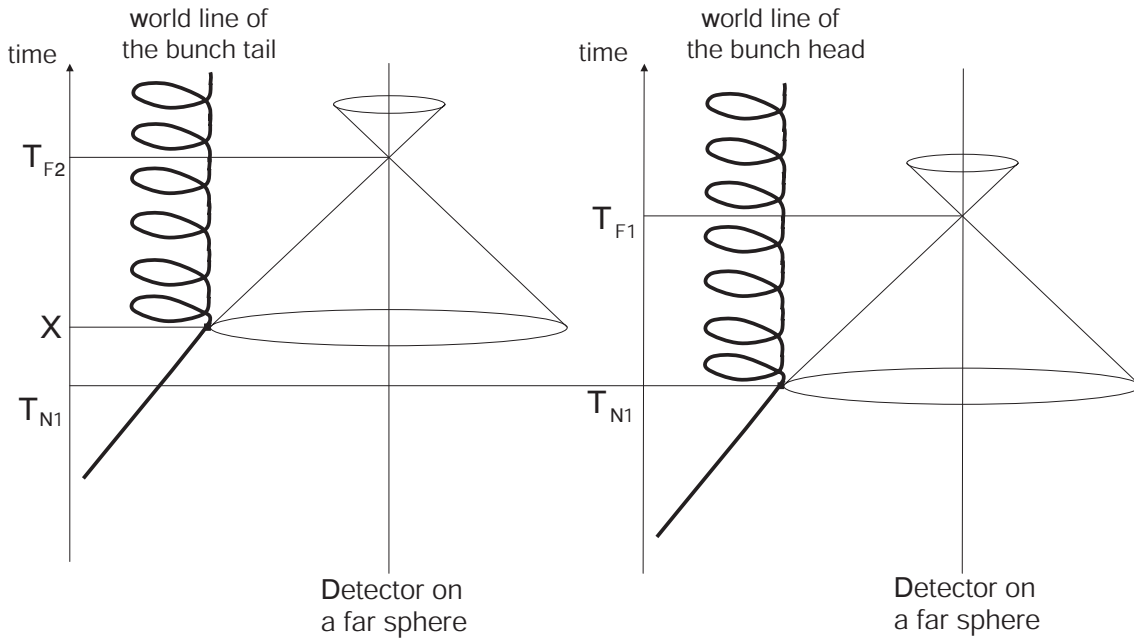


**Figure 2.2:** *Space-time diagram indicating the critical times of the transient from straight line for the bunch and for a detector far away. The event X indicates the entrance of the bunch tail in the circle.*

On the one hand, it is easy to see from Fig. 2.2 that the transient for the far sphere starts at time $T_{F1} = R/c + T_{N1}$ and finishes at time $T_{F2} = R/c + T_{N1} + \sigma/(\beta c)$, where $\sigma$ is the bunch length. Therefore, the duration of the transient in the far field is $\sigma/(\beta c)$.

On the other hand, the transient situation for the bunch begins at time $T_{N1}$ and ends at a time $T_{N2} = T_{N1} + \sigma/(\beta c) + a\phi^*/(\beta c)$; here $\phi^*$ is the angle specifying how far the first particle runs along the circle before it is reached by an electromagnetic signal

emitted by the last electron at the time of its entrance in the circle, $a$ being the radius of the circle itself. Altogether, the duration of the transient, as regards the bunch, is $\sigma/(\beta c) + a\phi^*/(\beta c)$.

In order to visualize the situation we may assume that the bunch as has a length such that $T_{N1} < T_{N2} < T_{F1} < T_{F2}$ as depicted in Fig. 2.2.

Since time intervals referred to the bunch are different from the ones referred to the detectors on the sphere, one must exercise a lot of care in telling what kind of transient one is referring to.

Of course the situation is not ambiguous at all considering the full picture in space-time, and it is easy to understand also in three-dimensional language when one compares the energy lost by the bunch during its transient and the energy detected by detectors during their transient. These quantities are different and the energy difference is simply stored in the electromagnetic field inside the sphere of radius R. This is, basically, the difference between the electromagnetic energy in the sphere when all the particles in the bunch are in the straight line and when they are in the circle.

A simple analogous situation is given by a bucket with some water in it situated under a closed tap, which is connected to a reserve of water; during the transient the tap is opened and some water flows from the reserve to the bucket, until the bucket is full and the water spills out of the bucket at a constant rate.

It is possible to express Eq. (2.56) in a different way which we find suggestive. Let us start integrating its right and left hand sides between times $T_{N1}$ and $T_{F2}$ to get:

$$\int_{T_{N1}}^{T_{F2}} dt \left[ \oint_{\Sigma} S_n d\sigma \right]_A = - \int_{T_{N1}}^{T_{N2}} dt \int_{-\infty}^{\infty} e(\boldsymbol{v} \cdot \boldsymbol{E})(s) \; F(s) \; ds$$
$$- \int_{T_{N2}}^{T_{F2}} dt \int_{-\infty}^{\infty} e(\boldsymbol{v} \cdot \boldsymbol{E})(s) \; F(s) \; ds - \int_{T_{N1}}^{T_{F2}} dt \left[ \int \frac{\partial u}{\partial t} \; dV \right]. \qquad (2.57)$$

Since $\int_{T_{N1}}^{T_{F1}} dt \left[ \oint_{\Sigma} S_n d\sigma \right]$ includes only velocity field terms, Eq. (2.57) can be written as:

$$\int_{T_{F1}}^{T_{F2}} dt \left[ \oint_{\Sigma} S_n d\sigma \right]_A + \int_{T_{N1}}^{T_{N2}} dt \int_{-\infty}^{\infty} e(\boldsymbol{v} \cdot \boldsymbol{E})(s) \; F(s) \; ds$$
$$= - \int_{T_{N2}}^{T_{F2}} dt \int_{-\infty}^{\infty} e(\boldsymbol{v} \cdot \boldsymbol{E})(s) \; F(s) \; ds - \int_{T_{N1}}^{T_{F2}} dt \left[ \int \frac{\partial u}{\partial t} \; dV \right]_A. \qquad (2.58)$$

It is easy to estimate $\int_{T_{N2}}^{T_{F2}} dt \int_{-\infty}^{\infty} e(\boldsymbol{v} \cdot \boldsymbol{E})(s) \; F(s) \; ds$. In fact, since from time $T_{N2}$ on all the particles are interacting with retarded sources in the circle one has:

$$\int_{T_{N2}}^{T_{F2}} dt \int_{-\infty}^{\infty} e(\boldsymbol{v} \cdot \boldsymbol{E})(s) \; F(s) \; ds = -(T_{F2} - T_{N2}) \int_{-\infty}^{\infty} N^2 P_{sp}(\omega) \mid \bar{F}(\omega)|^2 \; d\omega \;, \quad (2.59)$$

where $P_{sp}(\omega)$ is the single-particle power spectrum and the right hand side of Eq. (2.59) can be easily deduced from Eq. (1.1).

On the other hand one can easily estimate $\int_{T_{N1}}^{T_{F2}} dt \left[ \int \frac{\partial u}{\partial t} \; dV \right]_A$. In fact:

(a) It is the integral of a perfect differential, therefore only the edge terms must be studied in order to estimate the expression.

(b) At time $T_{F2}$ the sphere of radius $R$ reaches a state in which electromagnetic energy is flowing in at the same rate at which it is flowing out (in other words, the bucket of our analogy has been filled). Therefore the first edge term reads:

$$R/c \cdot \int_{-\infty}^{\infty} N^2 P_{sp}(\omega) \mid \bar{F}(\omega) \mid^2 \ d\omega + E_0 \ , \tag{2.60}$$

where $E_0$ is the (singular) electromagnetic energy associated to the bunch velocity field.

(c) At time $T_{N1}$ only the (singular) velocity field contribution is present. Since, during all the transient phenomena, we are understanding the sources to be very far from the sphere, we can assume this contribution is simply equal to $E_0$.

As a consequence, after obvious renormalization, Eq. (2.58) can be rewritten as

$$\int_{T_{F1}}^{T_{F2}} dt \left[ \oint_{\Sigma} S_n d\sigma \right]_A + \int_{T_{N1}}^{T_{N2}} dt \int_{-\infty}^{\infty} e(\boldsymbol{v} \cdot \boldsymbol{E})(s) \ F(s) \ ds$$
$$= -\phi^* a/(\beta c) \int_{-\infty}^{\infty} N^2 P_{sp}(\omega) \mid \bar{F}(\omega) \mid^2 \ d\omega. \tag{2.61}$$

This equation links the energy detected during the transient phenomenon for the detectors with the energy lost by the electrons during the transient for the bunch. The difference (note that the two terms on the left hand side of Eq. (2.61) are opposite in sign) is the term on the right hand side, and it is given by the power radiated in the steady state circular trajectory times a recovery time. The latter is the time that the retarded sources employ to get into the circle from the moment in which the present sources are all in the circle, i.e. $\phi^* a/(\beta c)$.

# Bibliography

[1] L.I. Schiff, Rev. Sci. Instr. 17, 6 (1946)

[2] J. S. Nodvick and D. S. Saxon, Phys. Rev. 96, 180 (1954)

[3] E. A. Saldin, E. A. Schneidmiller and M. V. Yurkov, DESY 02-127 (2002), ISSN 0418-9833

[4] A. Hofmann, CERN Accelerator School 1998, CERN 98-04

[5] H. Wiedemann, *Particle Accelerator Physics*, Springer-Verlag, 1993

[6] F. Rohrlich, *Classical Charged Particles*, Addison-Wesley publishing company, inc., 1990

[7] J.D. Jackson, *Classical Electrodynamics*, John Wiley and Sons Inc., 1998

[8] S. Hassani, *Mathematical Physics*, Springer, 1998

[9] R. Abraham, J. Marsden, *Foundations of Mechanics*, W.A. Benjamin Inc., 1967

[10] E. L. Saldin, E. A. Schneidmiller and M. V. Yurkov, Nucl. Instr. Methods A 398, 373 (1997)

[11] R. Li, C. L. Bohn and J. J. Bisognano, in *Proceedings of the SPIE Conference, San Diego, 1997*, vol. 3154, p. 223

# Chapter 3

# Longitudinal effects

In this Chapter we present analytical investigations about longitudinal self-interactions within a bunch, i.e. self-interactions in the direction of motion of the observer particles. In Section 3.1, the problem of the evaluation of radiative collective effects accompanying the accelerated motion of a short ultrarelativistic ($\gamma \gg 1$) electron bunch in vacuum is considered within the framework of a small-angle approximation; a second order expansion in the transverse velocity of electrons is performed. This results in the finding of a very flexible, new analytical presentation for the energy spread of the bunch, which can be used in very generic situations. In Section 3.2 we use the findings in Section 3.1 to address longitudinal effects during the passage of a beam with Gaussian longitudinal density distribution from a straight to a circular path. These have often been studied in a regime in which they are energy independent. Nevertheless, the approximations used in such a regime may fail in several practical situations, like in the case of low-energy injectors or for small structures within the bunch distribution in CSR-related instability problems. These situations demand a deeper investigation of longitudinal transient effects: a strong $\gamma$-dependence is found, and described, in the rate of energy change induced by CSR during the transient of a Gaussian bunch between a straight and a circular path, which has been studied with the help of the results in Section 3.1. Results show that the overall CSR longitudinal effects are reduced in the $\gamma$-dependent region. One of the outcomes of previous work by Saldin et al. has been extended to this situation and a very good agreement between the two studies has been found.

Section 3.1 is based, in part, on the article:
    **Gianluca Geloni et al., Phys. Rev. E, 64, 046504, 2001**
Section 3.2 is based, in part, on the article:
    **Gianluca Geloni et al., Phys. Rev. E, 65, 066504, 2002**

# 3.1 SMALL-ANGLE APPROXIMATION IN THE DESCRIPTION OF RADIATIVE COLLECTIVE EFFECTS WITHIN AN ULTRARELATIVISTIC ELECTRON BUNCH

## 3.1.1 Introduction

As already discussed in Section 1.1, very short, high-charge bunches of electrons are being produced by particle accelerators of the next generation. Bunch compression chicanes are expected to be often used in order to provide very high peak-current beams for X-ray SASE-FELs [1]. Electron bunches of this kind could also be interesting for the development of high-brightness Cherenkov and transition radiation sources [2]. However, their production and utilization may prove difficult due to radiative collective effects, as occurs in magnetic chicanes.

As we have seen in Chapter 1, an example of such a collective effect is the enhancement of low-frequency photon emission from a short relativistic electron bunch moving along a circular trajectory (in the rest of this work, we will refer to it as the steady state Coherent Synchrotron Radiation (CSR)): the number of photons per unit frequency interval increases dramatically in the part of spectrum where the photon wavelength becomes comparable with the size of the bunch. In this frequency range, electromagnetic waves emitted by individual particles have small phase differences. As a result, they add up coherently, thus leading to a quadratic dependence of the intensity of radiation on the number of electrons in the bunch [3]. This number is typically $10^8$-$10^{10}$, which explains the high magnitude of the effect.

Similar effects are observed when an electron bunch passes bending magnets, magnetic chicanes, and other beam-optics elements. In all such cases, signal retardation is the crucial feature. In addition to the above case of steady state CSR, in any beam-optics system also transient collective phenomena take place. Their study has been a matter of active theoretical, numerical and experimental research in the past few years. The problem of a one-dimensional (1D) electron bunch entering a circular path from a straight path in vacuum has been carefully studied in [4]. The total energy loss due to collective effects, as well as the final energy spread have been examined in several limiting cases that are of relevance for practical applications. The influence of shielding in a similar situation has been addressed in [5] and [6]. The presence of conducting walls has been shown to reduce the strength of radiative collective self-interactions in the bunch. Extensive numerical simulations have been performed in [7, 8, 9]; a comparison with experimental results can be found in [10]. Measurements and computations are in reasonable agreement.

In this Section we consider the problem of radiative collective interactions within a short electron bunch following its trajectory in vacuum without shielding. The main feature of our consideration is that we consistently apply a small-angle approximation, a natural technique for ultrarelativistic particles. This approach considerably reduces the efforts necessary for the treatment of an arbitrary trajectory and results in the finding of a very flexible, new analytical presentation for the energy spread of the bunch, which can be used in very generic situations; on the other hand, it somewhat restricts the class of allowed trajectories. Eventually, this route is expected to lead to
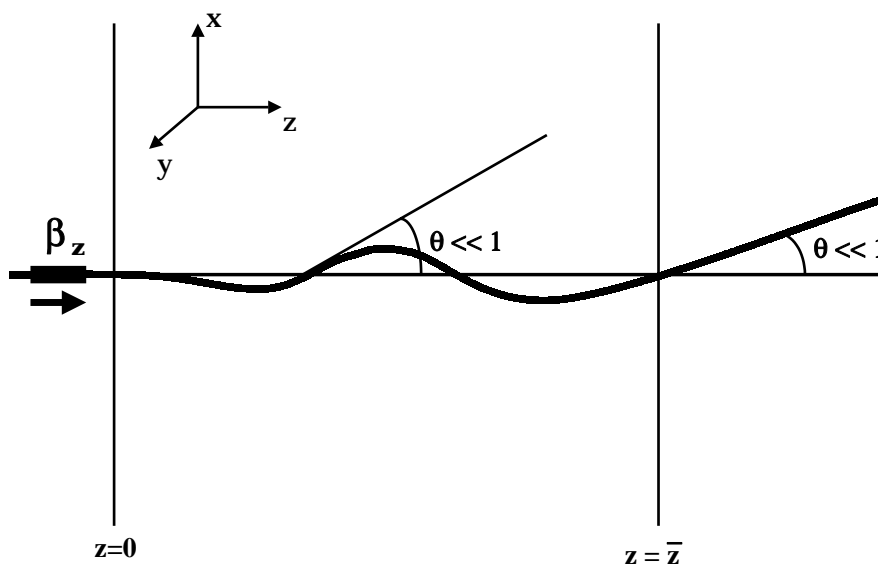
**Figure 3.1:** *Schematic of a particle trajectory in a small angle approximation.*

an efficient computational tool for the design of magnetic systems for high-peak current electron bunches.

In Section 3.1.2 the geometry of the problem is described and a small-angle approximation is introduced. Section 3.1.3 is devoted to the case of retarded interaction between two individual electrons. In Section 3.1.4 our consideration is extended to the case of a test particle interacting with the whole bunch, and the results are compared with those by other authors. Finally, Section 3.1.5 contains conclusions.

### 3.1.2 The small-angle approximation

Following other authors [4, 6, 12, 13], we will consider the bunch as a 'rigid', 1D, charged object with a given linear charge density distribution. We define a cartesian reference frame $(x, y, z)$ as shown in Fig. 3.1, where the z-axis coincides with the direction of the initial velocity.

Our consideration makes use of a small-angle approximation. That is, we assume that the bunch energy is high enough that a possible deflection of electrons from a straight line during their passage through the magnetic system is relatively small. To be specific, we will assume that, before and after the magnets ($z < 0$ or $z > \overline{z}$), the bunch moves along a rectilinear path with constant velocity, while inside the magnetic system ($0 < z < \overline{z}$) it follows a path subject to the only constraint that the angle $\theta$ formed by the velocity vector with the $z$-axis is always small, i.e. $\theta \ll 1$. Note that $\theta$ can still be small or large as compared to the other small parameter of the problem, $\gamma^{-1}$, where $\gamma \gg 1$ is the Lorentz factor: $\gamma = (\mathcal{E}/mc^2 + 1)$, $\mathcal{E}$ being the kinetic energy of the particles.

A natural assumption is $l_b(dv_{x,y}/dz) \ll v_{x,y}$ , where $l_b$ is the longitudinal extent of the bunch and $v_{x,y}(z)$ are the components of the transverse velocity of bunch electrons;
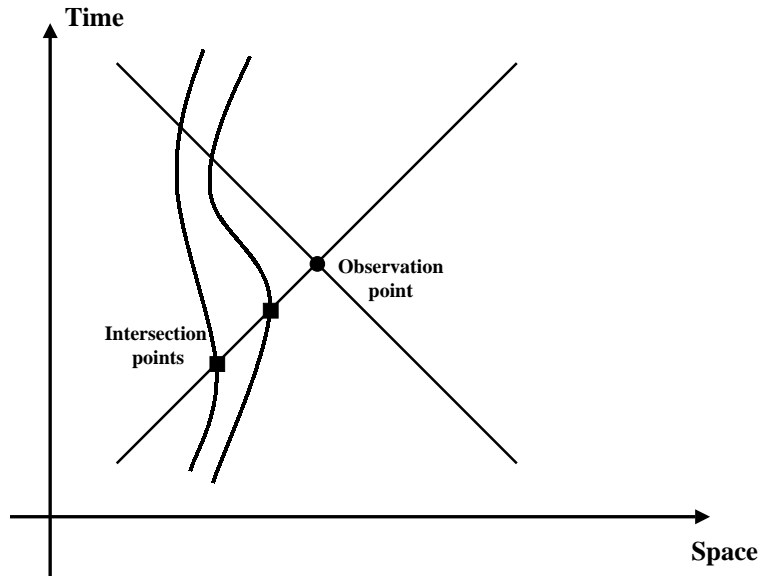
**Figure 3.2:** *Different particle world-lines intersect the light-cone of the observation event at different points in space-time.*

in other words, we will consider a situation in which differences in transverse velocities of electrons are negligible.

We will also assume zero initial energy spread in the bunch, and neglect any change of particle energy during the passage of the bunch through the magnetic system. This means that the trajectory of the bunch is pre-determined by its initial energy and by the known configuration of external fields. The back influence of radiative effects on the motion of particles is therefore assumed to be negligible; of course, this assumption has to be verified *a posteriori*: in some cases of practical interest the energy change appears to be rather significant.

The two main objects we are going to deal with in the following calculations are the local particle velocity $\mathbf{v}$ and a unit vector $\boldsymbol{n}$ connecting two points lying on the same trajectory. In the spirit of our small-angle approximation, one has to distinguish explicitly between their longitudinal and transverse components, assuming the latter to be small. Keeping first and second order terms and omitting all higher orders, one gets the following well-known expressions for $z$-components of the above vectors:

$$n_z \simeq 1 - \frac{1}{2}\boldsymbol{n}_\perp{}^2 \; , \tag{3.1}$$

$$v_z \simeq c\left(1 - \frac{1}{2\gamma^2}\right) - \frac{\boldsymbol{v}_\perp{}^2}{2c} \; . \tag{3.2}$$

Once the bunch trajectory is fixed, the problem of radiative collective effects within the bunch reduces to properly accounting for signal retardation in pairwise interactions between individual electrons. Let us consider a test particle inside the bunch. Its present velocity and its present position in the laboratory frame of reference will be denoted as $\boldsymbol{v}_0(t)$ and $\boldsymbol{r}_0(t)$, respectively. We are interested in its interaction with some

other bunch particle −the source particle− whose present position will be denoted as $\boldsymbol{r}(t)$. Causality defines the well-known retardation condition between the two particles, which we already discussed in general terms in Section 1.2:

$$|\boldsymbol{r_0}(t) - \boldsymbol{r}(t')| = c\,(t - t')\ , \tag{3.3}$$

where $\boldsymbol{r}(t')$ denotes the retarded position of the source particle ($t'$ being the so called retarded time), and $(t - t')$ is the time delay associated with signal propagation. Obviously, world-lines of different source particles are intersecting the lightcone of a certain event at different space-time points, as illustrated in Fig. 3.2.

The small-angle approximation considerably simplifies the treatment of the above retardation condition. Firstly, note that the knowledge of the transverse velocity $\boldsymbol{v}_\perp$ as a function of time fully determines the position of a particle. Indeed, using Eq. (3.2) one gets, for the transverse ($\boldsymbol{\rho} = x\,\hat{\boldsymbol{x}} + y\,\hat{\boldsymbol{y}}$) and longitudinal coordinates of a particle

$$\boldsymbol{\rho}(t) = \int_0^t \boldsymbol{v}_\perp(\tau)d\tau\ , \tag{3.4}$$

$$z(t) = z(0) + \int_0^t v_z(\tau)d\tau \simeq z(0) + \int_0^t \left[ c\left(1 - \frac{1}{2\gamma^2}\right) - \frac{\boldsymbol{v}_\perp{}^2(\tau)}{2c} \right] d\tau\ . \tag{3.5}$$

The transverse velocity, in its turn, is easily found once the configuration of external fields is defined, which makes this approach rather convenient.

Secondly, the positions of the test and of the source particle are related through

$$\boldsymbol{r_0}(t) = \boldsymbol{r}(t + \delta)\ , \tag{3.6}$$

because all particles in the bunch are assumed to follow the same trajectory. In the small-angle approximation the time difference $\delta$ is easily translated into the difference between $z$-coordinates of both particles:

$$\Delta z = z_0 - z \simeq c\delta\ . \tag{3.7}$$

It is worth mentioning that for $\delta > 0$ the position of the source particle is always *behind* that of the test particle. This is, in fact, the only case we are interested in. As has been argued in [4], interactions with particles that are *ahead* of the test particle do not contain a radiative part. Their contribution consists in trivial Coulomb repulsion, which has to be subtracted from final expressions in order to get a non-singular result (see the discussion of the Coulomb singularity in Section 3.1.3). For this reason, in the following we will always assume $\Delta z > 0$.

Thirdly, it is convenient to switch from time-retardation to a retardation condition expressed in $z$, which is possible since, in the small-angle approximation, $t$ and $z$ are uniquely mapped onto each other. The corresponding relation is easily found; namely, up to second order terms in the transverse velocity one gets:

$$t - t' \simeq \frac{(z - z')}{c}\left(1 + \frac{1}{2\gamma^2}\right) + \frac{1}{2c}\int_{z'}^z d\zeta\,\boldsymbol{\beta}_\perp{}^2(\zeta)\ , \tag{3.8}$$

where $\boldsymbol{\beta}_\perp$ is the usual notation for dimensionless velocity, $\boldsymbol{\beta}_\perp \equiv \boldsymbol{v}_\perp/c$. Upon this, the retardation condition can be re-written as

$$(z_0 - z')^2 + (\boldsymbol{\rho_0} - \boldsymbol{\rho'})^2 \simeq \left[ (z - z') \left( 1 + \frac{1}{2\gamma^2} \right) + \frac{1}{2} \int_{z'}^{z} d\zeta \boldsymbol{\beta_\perp}^2(\zeta) \right]^2 . \qquad (3.9)$$

Rearranging terms, neglecting those of order $\Delta z / (z - z') \ll 1$ and taking into account Eq. (3.4), we find

$$\left[ \int_{z'}^{z_0} d\zeta \boldsymbol{\beta_\perp}(\zeta) \right]^2 \simeq 2(z - z') \left[ \frac{(z - z')}{2\gamma^2} - \Delta z + \frac{1}{2} \int_{z'}^{z} d\zeta \boldsymbol{\beta_\perp}^2(\zeta) \right] . \qquad (3.10)$$

Finally, we represent the retardation condition in the small-angle approximation as

$$\frac{(z_0 - z')}{\gamma^2} + \int_{z'}^{z_0} d\zeta \boldsymbol{\beta_\perp}^2(\zeta) - \frac{1}{(z_0 - z')} \left( \int_{z'}^{z_0} d\zeta \boldsymbol{\beta_\perp}(\zeta) \right)^2 \simeq 2\Delta z . \qquad (3.11)$$

### 3.1.3   Liénard-Wiechert fields and Coulomb singularity

From Eq. (2.44) and Eq. (2.47) one has that the fields generated by a source particle at an observation point $\boldsymbol{r_0}(t)$ are given by the following expressions:

$$\boldsymbol{E}(\boldsymbol{r_0}, t) = \frac{e}{4\pi\varepsilon_0} \left\{ \frac{1}{\gamma^2} \frac{\boldsymbol{n} - \boldsymbol{\beta}}{R^2 \left( 1 - \boldsymbol{n} \cdot \boldsymbol{\beta} \right)^3} + \frac{1}{c} \frac{\boldsymbol{n} \times \left[ (\boldsymbol{n} - \boldsymbol{\beta}) \times \dot{\boldsymbol{\beta}} \right]}{R \left( 1 - \boldsymbol{n} \cdot \boldsymbol{\beta} \right)^3} \right\} \qquad (3.12)$$

and

$$\boldsymbol{B}(\boldsymbol{r_0}, t) = \frac{1}{c} \boldsymbol{n} \times \boldsymbol{E} , \qquad (3.13)$$

where $\boldsymbol{\beta}$ and $\dot{\boldsymbol{\beta}}$ are, respectively, the dimensionless velocity and its time derivative at the retarded time $t'$, $R$ is the distance between the retarded position of the source particle and the observation point, and $\boldsymbol{n}$ is a unit vector along the line connecting those two points.

Multiplying $e\boldsymbol{E}$ by the velocity of the test particle $\boldsymbol{v_0}$, one gets the change of the energy of the test particle due to its interacton with the source particle:

$$\left( \frac{d\mathcal{E}}{dt} \right) = e\boldsymbol{E}(\boldsymbol{r_0}, t) \cdot \boldsymbol{v_0}(t) , \qquad (3.14)$$

and hence

$$\left( \frac{d\mathcal{E}}{dt} \right) = \frac{e^2}{4\pi\varepsilon_0} \left[ \frac{c}{\gamma^2} \frac{\boldsymbol{n} \cdot \boldsymbol{\beta_0} - \boldsymbol{\beta} \cdot \boldsymbol{\beta_0}}{R^2(1 - \boldsymbol{n} \cdot \boldsymbol{\beta})^3} + \frac{(\boldsymbol{n} \cdot \dot{\boldsymbol{\beta}})(\boldsymbol{n} \cdot \boldsymbol{\beta_0} - \boldsymbol{\beta} \cdot \boldsymbol{\beta_0}) - (\boldsymbol{\beta_0} \cdot \dot{\boldsymbol{\beta}})(1 - \boldsymbol{n} \cdot \boldsymbol{\beta})}{R(1 - \boldsymbol{n} \cdot \boldsymbol{\beta})^3} \right] .$$
$$(3.15)$$

As one can see, the above expression still contains a term proportional to $R^{-2}$ as well as one proportional to $R^{-1}$, signature of the velocity (or Coulomb) field and of the acceleration (or radiation) field respectively.

As has been argued in [4], the Coulomb part is singular in the limit $R \to 0$ (that is, $\Delta z \to 0$). On the other hand, this large contribution has nothing to do with radiative effects, because it represents just trivial electrostatic repulsion of electrons. Its singular behavior is connected with the infinitely small transverse size of the bunch that we use in our model problem. Following [4], we will cure the situation by subtracting from Eq.(3.15) its purely Coulomb counterpart corresponding to rectilinear motion of the same two particles with constant velocity:

$$\left(\frac{d\widehat{\mathcal{E}}}{dt}\right) = \left(\frac{d\mathcal{E}}{dt}\right) - \frac{e^2 \beta c}{4\pi\varepsilon_0 \gamma^2 (\Delta z)^2} \ . \tag{3.16}$$

The resulting expression appears to be regular in the limit $\Delta z \to 0$. This regularized formula will be used in all following calculations.

In the small-angle approximation, one has to expand the above expressions up to second order terms in the transverse velocity. The following relations are quite helpful at this stage:

$$(1 - \boldsymbol{n} \cdot \boldsymbol{\beta}) \simeq \frac{1}{2}\left[\frac{1}{\gamma^2} + (\boldsymbol{\beta}_\perp - \boldsymbol{n}_\perp)^2\right] \ , \tag{3.17}$$

$$(\boldsymbol{n} \cdot \boldsymbol{\beta_0} - \boldsymbol{\beta} \cdot \boldsymbol{\beta_0}) \simeq \frac{1}{2}\left[\frac{1}{\gamma^2} + (\boldsymbol{\beta}_{\perp 0} - \boldsymbol{\beta}_\perp)^2 - (\boldsymbol{\beta}_{\perp 0} - \boldsymbol{n}_\perp)^2\right] \ , \tag{3.18}$$

$$(\boldsymbol{\beta_0} \cdot \dot{\boldsymbol{\beta}}) \simeq (\boldsymbol{\beta}_{\perp 0} - \boldsymbol{\beta}_\perp) \cdot \dot{\boldsymbol{\beta}}_\perp \ , \tag{3.19}$$

where $\boldsymbol{n}_\perp$ is given by

$$\boldsymbol{n}_\perp = \frac{1}{(z_0 - z')} \int_{z'}^{z_0} d\zeta \boldsymbol{\beta}_\perp(\zeta) \ . \tag{3.20}$$

Using the above formulas and putting, with the same accuracy, $R \simeq (z_0 - z')$, one gets

$$\left(\frac{d\widehat{\mathcal{E}}}{dt}\right) \simeq \frac{e^2}{4\pi\varepsilon_0}\frac{2\gamma^2}{1 + \gamma^2(\boldsymbol{n}_\perp - \boldsymbol{\beta}_\perp(z'))^2}\left\{[C] + [R]\right\} \ , \tag{3.21}$$

where $[C]$ and $[R]$ stand for the Coulomb and the Radiative part, respectively:

$$[C] \equiv \frac{2c}{(z_0 - z')^2}\left\{\frac{1 - \gamma^2\left(\boldsymbol{\beta}_\perp(z_0) - \boldsymbol{n}_\perp\right)^2 + \gamma^2\left[\boldsymbol{\beta}_\perp(z_0) - \boldsymbol{\beta}_\perp(z')\right]^2}{\left[1 + \gamma^2\left(\boldsymbol{n}_\perp - \boldsymbol{\beta}_\perp(z')\right)^2\right]^2}\right.$$
$$\left. - \frac{1 + \gamma^2\left[\boldsymbol{n}_\perp - \boldsymbol{\beta}_\perp(z')\right]^2}{\left[1 - \gamma^2\boldsymbol{n}_\perp^2 + \gamma^2\left(z_0 - z'\right)^{-1}\int_{z'}^{z_0}\boldsymbol{\beta}_\perp^2(\zeta)d\zeta\right]^2}\right\} \ , \tag{3.22}$$

$$[R] \equiv 2\gamma^2 \frac{\dot{\boldsymbol{\beta}}_\perp}{(z_0 - z')\left\{1 + \gamma^2\left[\boldsymbol{n}_\perp - \boldsymbol{\beta}_\perp(z')\right]^2\right\}^2}$$

$$\times\left\{[\boldsymbol{n}_\perp - \boldsymbol{\beta}_\perp(z')]\left[1 + \gamma^2\left(\boldsymbol{\beta}_\perp(z_0) - \boldsymbol{\beta}_\perp(z')\right)^2\right.\right.$$

$$\left.-\gamma^2\left(\boldsymbol{n}_\perp - \boldsymbol{\beta}_\perp(z_0)\right)^2\right] - [\boldsymbol{\beta}_\perp(z_0) - \boldsymbol{\beta}_\perp(z')]\left[1 + \gamma^2\left(\boldsymbol{n}_\perp - \boldsymbol{\beta}_\perp(z')\right)^2\right]\right\} .$$

$$(3.23)$$

A rather straightforward calculation shows that the obtained expression is, indeed, regular in the limit $\Delta z \to 0$ or, equivalently, $(z_0 - z') \to 0$. Namely, it is sufficient to consider the case of constant transverse acceleration $\dot{\boldsymbol{\beta}}_\perp = constant$. Without loss of generality, let us put $\dot{\beta}_x = \alpha$, $\dot{\beta}_y = 0$. By shifting the origin and denoting $z_0 - z' \equiv \tau$, one has $\beta_y(z_0) = 0$, $\beta_x(z_0) = \alpha\tau$. Upon this, the Coulomb part becomes

$$[C] = \frac{1 + \frac{3}{4}\gamma^2\alpha^2\tau^2}{\tau^2\left(1 + \frac{1}{4}\gamma^2\alpha^2\tau^2\right)^2} - \frac{1 + \frac{1}{4}\gamma^2\alpha^2\tau^2}{\tau^2\left(1 + \frac{1}{12}\gamma^2\alpha^2\tau^2\right)^2}$$

$$\simeq \frac{\gamma^2\alpha^2}{6}\frac{\left(1 - \frac{1}{3}\gamma^2\alpha^2\tau^2\right)}{\left(1 + \frac{1}{4}\gamma^2\alpha^2\tau^2\right)^2\left(1 + \frac{1}{12}\gamma^2\alpha^2\tau^2\right)^2} ,$$

$$(3.24)$$

which clearly has no pole as $\tau \to 0$. Similarly, one can check the absence of singularity in the radiative part.

### 3.1.4 Energy loss for a test particle in a one-dimensional bunch

The next step is to evaluate the energy change for a test particle interacting with the whole bunch characterized by a given electron density distribution. This latter is, in accordance with our assumptions, stationary in a co-moving frame of reference. It is also worth mentioning that, in terms of the 1D model used here, it is essentially the same (up to a numerical factor) as the longitudinal profile of the total current carried by the bunch.

As has already been said, we are interested only in the contribution coming from particles that are behind the test one; it is logical then to express the bunch density, that we will call $\lambda$, in terms of the longitudinal distance from the test particle. The corresponding variable, $\Delta z$, has been already introduced in Eq. (3.7). Then the energy change can be written as

$$\left(\frac{d\mathcal{E}}{dt}\right)_B (z_0) = \int_0^\infty \left(\frac{d\widehat{\mathcal{E}}}{dt}\right)(z_0, \Delta z)\lambda(\Delta z)d(\Delta z) , \qquad (3.25)$$

where $'B'$ stands for *Bunch* and $\lambda$ is supposed to vanish as $\Delta z \to +\infty$, so that the integral converges at the upper limit. Note that the lower limit of integration is zero.

Clearly, it is more convenient to perform integration over the retarded position $z'$ rather than over the distance between particles $\Delta z$, since this eliminates the necessity of solving Eq.(3.11) against $z'$. Upon this, Eq. (3.25) becomes

$$\left(\frac{d\mathcal{E}}{dt}\right)_B (z_0) = \int_{z_0}^{-\infty} \left(\frac{d\widehat{\mathcal{E}}}{dt}\right)(z_0, z')\lambda(\Delta z)\frac{d(\Delta z)}{dz'}dz' \ , \tag{3.26}$$

where the limits of integration correspond to the retarded position of the source particle for $\Delta z = 0$ or, respectively, $+\infty$. Note that $\lambda(\Delta z)$ is to be considered as a shorthand for $\lambda(\Delta z(z, z'))$. The expression for $\left(d\widehat{\mathcal{E}}/dt\right)(z_0, z')$ has been obtained in the previous section. As for $d(\Delta z)/dz'$, one can easily check that

$$\frac{d(\Delta z)}{dz'} = -\left(1 - \boldsymbol{n}\cdot\boldsymbol{\beta}(z')\right) \ . \tag{3.27}$$

Finally, if we want to obtain the energy loss during the entire trajectory we have to integrate over $t$ (or, equivalently, over $z_0$), which gives

$$\Delta\mathcal{E} = \int_{-\infty}^{+\infty} \left(\frac{d\mathcal{E}}{dt}\right)_B \frac{dt}{dz_0}dz_0 \ . \tag{3.28}$$

Eq. (3.28) is a closed expression for the energy loss, in the sense that all we need to know is just the transverse velocity of the bunch as function of the propagation distance. This latter is fully defined by the (pre-designed) configuration of external magnetic fields. As a results, we get for the total energy change

$$\Delta\mathcal{E} \simeq \frac{e^2}{4\pi\epsilon_0 c} \int_{-\infty}^{+\infty} dz_0 \int_{-\infty}^{z_0} dz'\{[C] + [R]\}\lambda(\Delta z) \ , \tag{3.29}$$

where $[C]$ and $[R]$ are defined by Eqs. (3.22) and (3.23), and $\Delta z$ by Eq. (3.11).

A useful, particular case of the above equation is the one of a rectangular current profile: $\lambda(\Delta z)$ is assumed to be constant, $\lambda(\Delta z) = \lambda_0$, over the whole length of the bunch $l_b$. If the test particle is situated at a distance $s_0$ from the head of the bunch, then the expression for the energy loss becomes

$$\Delta\mathcal{E}(s_0) \simeq \frac{e^2\lambda_0}{4\pi\epsilon_0 c} \int_{-\infty}^{+\infty} dz_0 \int_{z'_*(l_b-s_0)}^{z_0} dz'\{[C] + [R]\} \ , \tag{3.30}$$

where $z'_*(l_b - s_0)$ stands for the solution of Eq. (3.11) corresponding to $\Delta z = l_b - s_0$, and $s_0$ is understood positive for particles that lie behind the head of the bunch.

We have performed a comparison of the above expressions with some earlier results obtained without the use of the small-angle approximation. Following [4], general analysis of the problem of a bunch with rectangular density distribution passing through a bending magnet can be considerably simplified in several limiting cases. Namely, the authors of [4] call the magnet *short* (respectively, *long*) if it deflects electrons at an angle much smaller (much larger) than $1/\gamma$. On the other hand, an electron bunch is considered *short* or *long*, when its linear dimension is, respectively, much shorter or much longer than $A/\gamma^3$, where $A$ is the radius of curvature of the particle trajectory in the magnet. Upon this, normalized expressions for the bunch length $(\hat{l}_b = l_b\gamma^3/A)$ and for the angular dimension of the magnet $(\hat{\phi}_m = \gamma\phi_m)$ are given.

**Table 3.1:** *Energy change, in Joules, for an electron located at the head of a bunch with rectangular density distribution. A comparison is made between an evaluation with completely analytical formulas found by other authors and with our simuation. B is the magnetic field, in Tesla, $l_b$ is the bunch length in meters, $\gamma$ is the Lorentz factor, $\overline{z}$ is the length of the interaction zone, in meters and N is the number of particles considered in the bunch.*

|   | $B(T)$ | $l_b(m)$ | $\gamma$ | $\overline{z}(m)$ | $N/10^9$ | $Analysis(J)$ | $Simulation(J)$ |
|---|--------|----------|----------|-------------------|----------|---------------|-----------------|
| **1** | 0.043 | $1.0 \cdot 10^{-6}$ | 25 | $1.2 \cdot 10^{-2}$ | 6.0 | $8.7 \cdot 10^{-15}$ | $8.3 \cdot 10^{-15}$ |
| **2** | 0.085 | $1.0 \cdot 10^{-7}$ | 50 | $8.0 \cdot 10^{-3}$ | 10.0 | $1.54 \cdot 10^{-13}$ | $1.50 \cdot 10^{-13}$ |
| **3** | 0.17 | 0.45 | 50 | $9.9 \cdot 10^{-2}$ | 10.0 | $3.7 \cdot 10^{-17}$ | $3.4 \cdot 10^{-17}$ |
| **4** | 0.85 | 0.2 | 500 | 0.02 | 10.0 | $8.4 \cdot 10^{-17}$ | $9.3 \cdot 10^{-17}$ |

In one of those limiting cases, the comparison is particularly simple: if the bunch is *short* and the bending magnet is, in the normalized sense, *much longer* than the bunch then, as has been argued in [4], the transient effects at the interface between the straight path and the magnet can be neglected. This means that, in this particular case, we can assume all the retarded positions of the sources to lie within the bending magnet, and the situation becomes stationary.

For a rectangular bunch containing $N$ particles, one finds upon a calculation similar to that in Eq. (3.24)

$$\left(\frac{d\mathcal{E}}{dt}\right)_{Bunch} = -\frac{1}{4\pi\varepsilon_0}\frac{4Ne^2\gamma c}{Al_b}\frac{\gamma u_s\left(8+\gamma^2 u_s^2\right)}{\left(4+u_s^2\gamma^2\right)\left(12+\gamma^2 u_s^2\right)}\;, \tag{3.31}$$

where

$$u_s \simeq \frac{2\gamma^2(l_b-s_0)}{A}\;. \tag{3.32}$$

One can easily check that Eqs. (3.31) and (3.32) coincide with those found in [4].

In general, the expressions are rather complicated, and the corresponding comparison can only be done numerically. A computer code has been developed and benchmarked against several limiting cases given in [4]. The results are presented in table 1. Cases 1 and 2 deal with a *short* bunch and a magnet *longer* than the bunch: here the crucial factor is the energy of the beam. The difference by a factor of 2 in the Lorentz factor is responsible for the increase by a factor of 16 in the energy change. In cases 3 and 4 the magnet is *long* and the bunch is *much longer* (again in the normalized sense) than the magnet; these two cases have been computed, respectively, with low- and high-energy bunches.

In all cases we observe a good agreement between our numerical computations and the corresponding analytical estimates (a relatively large discrepancy of order 10% in cases 3 and 4 is presumably a result of the logarithmic accuracy of the analytical expressions in [4]). It is also worth mentioning that in all four cases the total energy change is small as compared to the initial particle energy; specifically, the largest
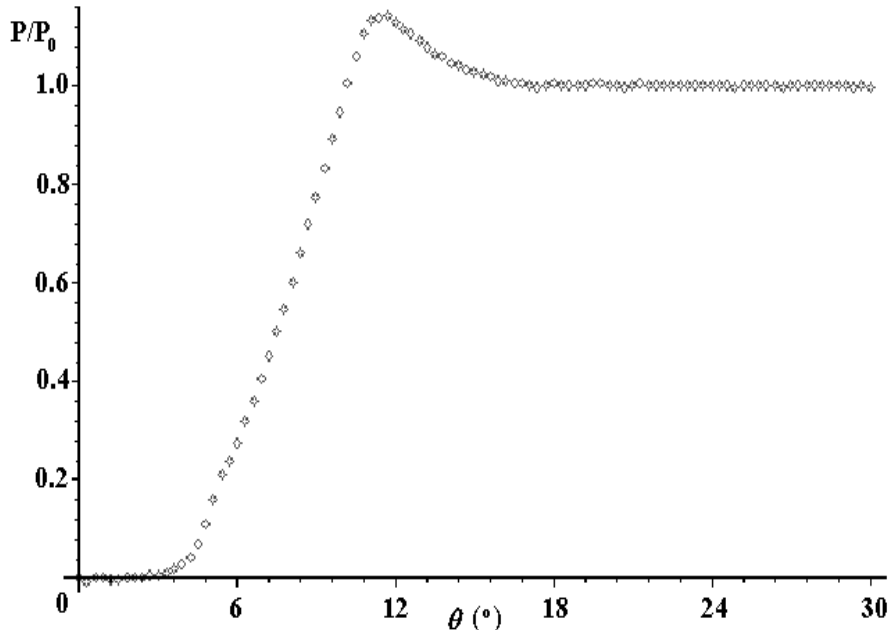
**Figure 3.3:** *Normalized transient power loss for a bunch with rectangular density distribution going into a bend.*

relative energy change of about 4% is found in case 2. This confirms consistency of the computational scheme, as has been discussed in Section 1.1.

As one more test, we have calculated the instantaneous power radiated by a particle located at the head of a bunch that enters into bending magnet. This case demonstrates pronounced transient collective effects. To be specific, we considered a 1 mm-long, 40 MeV bunch with rectangular electron density distribution entering a circular trajectory with a radius $A = 1$ m from a straight path. The dependence of the radiated power on the angle of deflection $\theta$ is shown in Fig. 3.3. After the bunch enters the bend the radiated power is seen to increase till it reaches a peak at $\theta \simeq 12^o$. Upon this it decreases to its steady state value, $P_0$, which has been used as an overall normalization factor in Fig. 3.3.

The observed dependence is in agreement with well-known results [5], [6]. Basically, the transient in the figure connects two steady state situations. The first one corresponds to the bunch before the bend: clearly, no power is radiated in this case. The second stationary regime is the steady state CSR $-$ that is, when the retarded positions of source particles interacting with the test particle are all in the bend. The transient describes a 'mixed' situation when the retarded positions of source particles are partially in the bend and partially in the straight line preceeding the bend.

## 3.1.5   Conclusions

A new analytical approach to the problem of radiative collective effects within an ultrarelativistic electron bunch has been developed. The systematical use of a small-angle approximation results in a new expression for the energy exchange between a test particle and the bunch. This expression is closed, in the sense that we only need

to know the transverse velocity of the bunch as a function of the propagation distance, which is directly determined by the external field configuration.

Analytical and numerical comparison of the obtained formulas with earlier results by other authors has been performed and a good agreement has been demonstrated. The technique is applicable to a wide class of trajectory: the condition of a small deflection angle $\theta$, still keeps open the possibility of comparison with $1/\gamma$, so that one can treat all important practical cases for $\theta \ll 1/\gamma$ (undulator) and $\theta \gg 1/\gamma$ (wigglers, compression chicanes).

## 3.2   COHERENT SYNCHROTRON RADIATION TRANSIENT-EFFECTS IN THE ENERGY-DEPENDENT REGION

### 3.2.1   Introduction

In this Section we will apply the results obtained in the previous one to address longitudinal effects during the passage of a beam with Gaussian longitudinal density distribution from a straight to a circular path.

The problem of the characterization of self-interaction effects at the transient between a straight path and a region of constant bending radius has been a matter of active theoretical research (see, for example, [4] and [6]) in the last few years, this subject being of fundamental importance for a proper understanding of CSR phenomena. Other more general works, both numerical and theoretical (see, among others, [8] to [20]) followed.

Some of these investigations (e.g. [15] to [20]) deal with ultra relativistic beams in which the value of the Lorentz factor, $\gamma$, is always above a certain threshold, as the fundamental result in [4], upon which they are based, is derived in that approximation.

Nevertheless, in several practical situations, like for example the case of low energy injectors (see, for example, [21]), we deal with ultrarelativistic beams for which the value of $\gamma$, in combination with the bunch length and the choice of the trajectory, may be low enough so that the latter approximation fails. Moreover, recent research (see [16] to [18]) has shown there is reason of concern about beam instabilities induced by CSR in storage rings as well as in bunch compressors. In fact, as it has been discussed earlier in Section 1.5, CSR has been shown to amplify small sinusoidal perturbations of the bunch distribution during the evolution of the beam: once again, one should make sure that the perturbation wavelength (in combination with the beam-energy and the geometry of the magnetic system) satisfies the approximations above before using results in [4] (or alternatively, for steady state regime, in [13]).

These observations demand a deeper investigation of CSR effects in such situations. In this Section, and with the help of the method discussed in Section 3.1, the problem of a Gaussian bunch crossing a transient between a straight path and a region of constant bending radius in the low-energy region has been studied. Results show a strong dependence of the CSR longitudinal force on the Lorentz factor.

Next, the formula in [4] for the rate of energy change of an electron has been extended in such a way that it is valid independently of the choice of $\gamma$, and it is used

to treat the same problem: a comparison between the two studies shows a very good agreement.

In Section 3.2.2 the main results obtained in Section 3.1 is applied to a low-$\gamma$ transient case. Then, in Section 3.2.3, an extension of the formula in [4] to the $\gamma$-dependent region is presented and a perfect agreement is shown between such an extension and the previous results in this article. Finally, Section 3.1.5 is dedicated to conclusions.

## 3.2.2 Small-angle approximation and its application to a transient in the low-$\gamma$ region

An expression for the rate of energy change of a test particle within a rigid, 1D bunch with generic density distribution function moving along a generic trajectory has been presented in Section 3.1. Such an expression was derived by means of a consistent use of the paraxial approximation explained in Fig. 3.1. As it has been explained in Section 3.1, such an approximation is applicable to a very wide class of trajectories.

Referring to Section 3.1, and therefore to the geometry in Fig. 3.1, $z_0$ is defined, again, as the present z-position of a test electron and $z$ as the present z-position of a source electron; moreover $\Delta z = z_0 - z$ with $\Delta z > 0$, the contributions to CSR effects from the case $\Delta z < 0$ being negligible (see Section 3.1, [4]). Then, always following Section 3.1, the rate of energy change for a test particle can be written as

$$\frac{d\mathcal{E}}{d(ct)} \simeq \frac{e^2}{4\pi\epsilon_0 c^2} \int_{-\infty}^{z_0} dz' \{[C] + [R]\}\lambda(\Delta z) , \qquad (3.33)$$

where $\lambda$ is the bunch density. Here $[C]$ and $[R]$ stand for the terms due to Coulomb and the Radiative parts of the retarded fields, already defined in Eq. (3.22) and Eq. (3.23) respectively.

As already said in Section 3.1, a computer code has been developed in order to integrate Eq. (3.33) at different positions of the test particle within the bunch and at different locations of the bunch within the magnet, obtaining, therefore, the instantaneous rate of energy change of any particle within the bunch for different values of $\gamma$. Let us make use of this code in order to deal with a particular case.

Consider, as in [4], a rigid, 1D bunch with Gaussian particle density distribution $\lambda(s)$ ($s$ being the coordinate inside the moving bunch) entering a hard-edge bending magnet after coming from an infinitely long straight section. The bunch standard deviation will be indicated with $\sigma = 50$ $\mu$m, and the total charge will be $q = 1$ nC. In the actual simulation the gaussian beam will be truncated at $\pm 10$ $s/\sigma$, where the distribution is understood to be centered at $s/\sigma = 0$, that is

$$\lambda(s) = \lambda_0 e^{-s^2/2\sigma^2}. \qquad (3.34)$$

The magnet has hard edges and a curvature radius $R = 1.5$ m.

The rate of energy change of an electron as a function of its position along the Gaussian bunch and at several positions of the bunch after the beginning of the magnet have been plotted in Fig. 3.4. These positions cover all the transient phenomenon, in which there are retarded sources both in straight section and bending magnet. Simulation results for different values of $\gamma$ are plotted at every position. These values have been chosen large enough to keep the system ultrarelativistic but at the same time

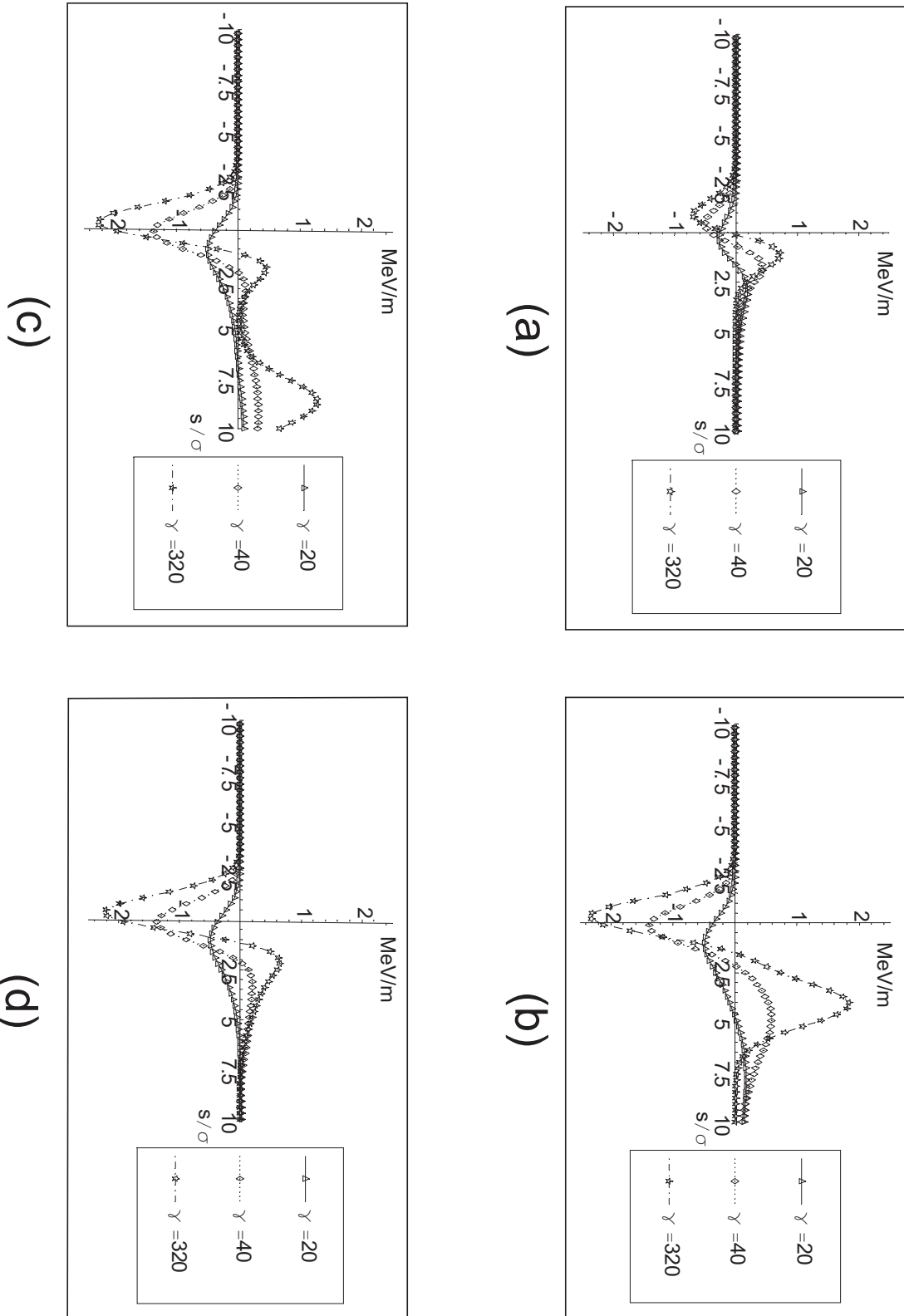**Figure 3.4:** *Rate of energy change of an electron in MeV/m as a function of its position along the Gaussian bunch $s/\sigma$ entering a hard-edge magnet, as calculated using our approach. Every picture shows results for different values of $\gamma$. Parameters are $R = 1.5$ m, $\sigma = 50$ $\mu$m, $q = 1$ nC (a) 5 cm after the entrance; (b) 14 cm after the entrance; (c) 18 cm after the entrance; (d) 25 cm after the entrance.*

small enough (in combination with the bunch length and the radius of curvature of the magnet, as will be discussed in detail in Section 3.2.3) so that the usual regime of applicability of the formula in [4], which has referred to in Section 3.2.1, is abandoned.

As one can see by inspection from Fig. 3.4, results are strongly dependent on the beam energy. When $\gamma$ grows enough (again, this statement will be specified quantitatively in Section 3.2.3), the energy-dependent region is abandoned, and curves in Fig. 3.4 converge to a $\gamma$-independent behavior. Note, in particular, that case (*d*) in Fig. 3.4 already belongs to the steady state regime: therefore it can be said that the study given up to now shows energy-dependence in both the transient and the steady state.

### 3.2.3   Generalization and comparison

In order to describe, in the same situation presented in Section 3.2.2, the rate of energy change of an electron within a Gaussian bunch entering a hard edge magnet, the following approximated formula is used in [4]:

$$\frac{d\mathcal{E}}{d(ct)} \simeq -\frac{1}{4\pi\epsilon_0} \frac{2e^2 N}{3^{1/3}(2\pi)^{1/2} R^{2/3}\sigma^{4/3}}$$

$$\times \left[ \rho^{-1/3}\left(e^{-(\xi-\rho)^2/2} - e^{-(\xi-4\rho)^2/2}\right) + \int_{\xi-\rho}^{\xi} \frac{d\xi'}{(\xi-\xi')^{1/3}} \frac{d}{d\xi'} e^{-\xi'^2/2} \right], \qquad (3.35)$$

where $\xi = s/\sigma$, $\rho = R\phi^3/24\sigma$ and $\phi$ is an angle fixing the position of the bunch inside the magnet (see Fig. 3.5).
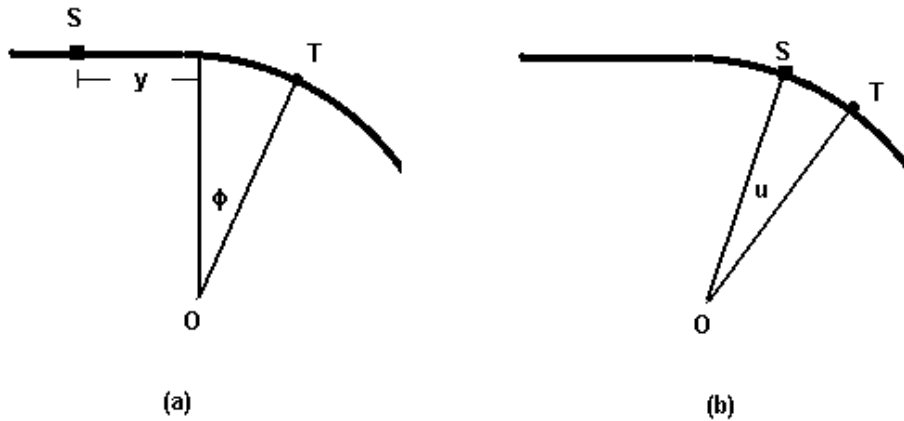


**Figure 3.5:** *Geometry for the present position of a test particle T and the retarded position of a source particle S. (a) S is in the straight line. (b) S is in the bend.*

It is worth underlining, once again, the importance of Eq. (3.35) that (in its generalized form for any bunch density distribution function) has been used as a basis for several CSR analysis and computations (see [15] to [20]).

Eq. (3.35) is completely independent of $\gamma$, as one can easily realize by inspection. A comparison between the results that one can obtain by direct integration of Eq. (3.35)

(these results are well known, and presented in [4]) and the results, obtained in this Section, for the case $\gamma = 320$ (reproduced also in Fig. 3.4) is plotted in Fig. 3.6.

It has been pointed out in Sec. 3.2.2 that curves in Fig. 3.4 saturate, for high values of the Lorentz factor, to a $\gamma$-independent behaviour: Fig. 3.6 shows that they reproduce, asymptotically, i.e. for large values of $\gamma$, the behaviour predicted by Eq. (3.35). The reason why the agreement is only asymptotic lies in the approximations used to derive Eq. (3.35).

Moreover it is important to note that, as Fig. 3.4 and Fig. 3.6 directly show, an acritical use of the energy-independent Eq. (3.35) may lead to an over-estimation of all CSR longitudinal effects in the energy-dependent regime.

In the following, the hypothesis upon which Eq. (3.35), taken from [4], was built will be briefly reviewed. By considering the transient phenomenon *in toto*, that is up to saturation to the steady state regime (when all the retarded sources are in the bend) it has been implicitly assumed that the bending magnet is long enough to allow the entire bunch to enter such a regime. Besides this assumption, Eq. (3.35) was derived, in [4], when the following condition is met:

$$\frac{R}{\gamma^3}\frac{d\lambda(s)}{ds} \ll \lambda(s). \tag{3.36}$$

This basically means that the bunch length is much larger than $R/\gamma^3$. For a Gaussian beam with characteristic length $\sigma$, Eq. (3.36) can be written as

$$\gamma \gg \left(\frac{Rs}{\sigma^2}\right)^{1/3}. \tag{3.37}$$

Taking $s \simeq \sigma$ this means $\gamma \gg 30$.

Moreover, always in [4], the Gaussian beam is treated as a superposition of bunches with rectangular density distribution satisfying the following condition

$$\hat{\phi}_b \gg 1, \tag{3.38}$$

where $\hat{\phi}_b$ is defined by the retardation condition

$$\frac{\hat{\phi}_b}{2} + \frac{\hat{\phi}_b^3}{24} = \frac{\gamma^3}{R}l_b, \tag{3.39}$$

where $l_b$ is the bunch length. When equation (3.38) is satisfied, equation (3.39) reads

$$\left(\frac{24\gamma^3 l_b}{R}\right)^{1/3} \gg 1, \tag{3.40}$$

or

$$\gamma \gg \left(\frac{R}{24l_b}\right)^{1/3}. \tag{3.41}$$

Taking $l_b \simeq \sigma$ this means $\gamma \gg 10$.

From the previous discussion it follows, as a conclusion, that Eq. (3.36) and Eq. (3.38) set a lower limit (expressed, explicitly, by Eq. (3.37) and Eq. (3.41)) to the values of $\gamma$ above which Eq. (3.35) is valid. Note that such a limit is in agreement with the fact
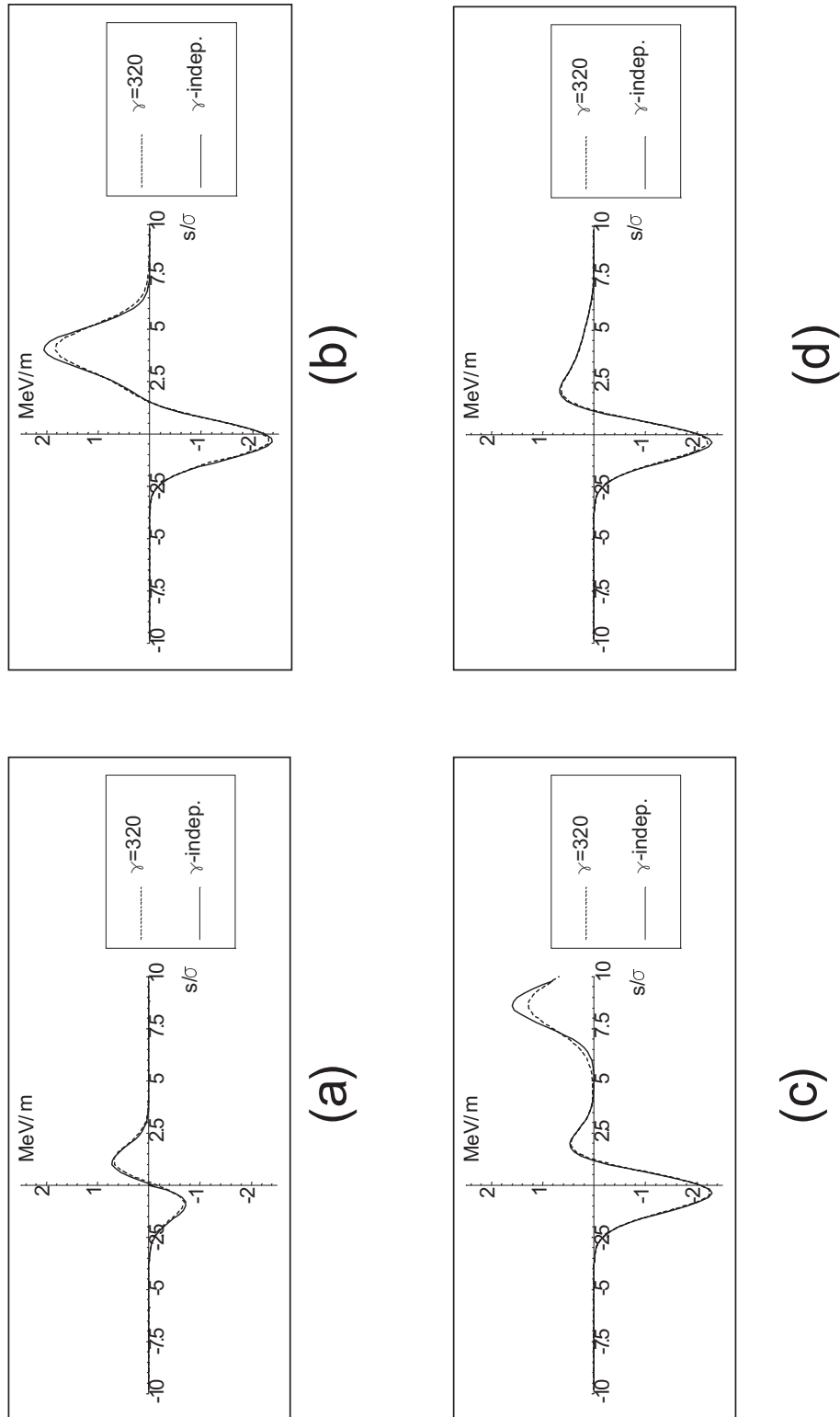
**Figure 3.6:** *Comparison between analytical results from literature [4] and our results shown in Fig. 3.4 for $\gamma = 320$. Rate of energy change of an electron in MeV/m as a function of its position along the Gaussian bunch $s/\sigma$ entering a hard edge magnet. Parameters are $R = 1.5$ m, $\sigma = 50$ $\mu$m, $q = 1$ nC. The plots are $\gamma$-independent. (a) 5 cm after the entrance. (b) 14 cm after the entrance. (c) 18 cm after the entrance. (d) 25 cm after the entrance.*

that simulation results approach the analytical expectation in [4] for high values of $\gamma$, as has been already discussed above in this Section.

As one more comment, remember that recent research (see [16] to [18]) has shown there is reason for concern about beam instabilities induced by CSR in storage rings as well as in bunch compressors. In fact, CSR has been shown to amplify small sinusoidal perturbations of the bunch distribution during the evolution of the beam in magnetic systems: in all these cases, one should make sure that the perturbation wavelength (in combination with the beam-energy and the geometry of the magnetic system) satisfies Eq. (3.36) and Eq. (3.38) before actually using an energy-independent wake to describe CSR effects.

An extension of Eq. (3.35) will be now sought that is valid regardless of whether such conditions are met, with the intent of comparing it with results in Fig. 3.4. In order to do so consider first Fig. 3.5, and the equations, also derived in [4], for the rate of energy change of a test particle $T$ at some point in the bend due to the interaction with source particles $S$ whose retarded position are in the straight line before the bend

$$\frac{d\mathcal{E}}{d(ct)} = \frac{2e^2\gamma\lambda_0}{4\pi\epsilon_0 R}\int_0^\infty d\hat{y}\left\{\frac{(\hat{\phi}+\hat{y})^2+\hat{\phi}^3(3\hat{\phi}/4+\hat{y})}{[(\hat{\phi}+\hat{y})^2+\hat{\phi}^4/4]^2} - \frac{(\hat{\phi}+\hat{y})^2+\hat{\phi}^4/4}{[(\hat{\phi}+\hat{y})^2+(\hat{\phi}^3/12)(\hat{\phi}/4+\hat{y})]^2}\right\},$$
(3.42)

or inside the arc

$$\frac{d\mathcal{E}}{d(ct)} = \frac{2e^2\gamma\lambda_0}{4\pi\epsilon_0 R}\int_0^{\hat{\phi}} d\hat{u}\left(1+\frac{\hat{u}^2}{4}\right)\left\{\frac{\hat{u}^2/4-1}{2(1+\hat{u}^2/4)^3} + \frac{1}{\hat{u}^2}\left[\frac{1+3\hat{u}^2/4}{(1+\hat{u}^2/4)^3} - \frac{1}{(1+\hat{u}^2/12)^2}\right]\right\}.$$
(3.43)

Eq. (3.42) and Eq. (3.43) are valid in the case of an infinitely long electron bunch with constant particle density distribution $\lambda_0$. Here, as in [4], $\hat{\phi} = \gamma\phi$, $\hat{y} = y\gamma/R$ and $\hat{u} = \gamma u$ being the meaning of $y$, $\phi$ and $u$ explained in Fig. 3.5. Moreover, always in [4], we find the following relations, that hold, respectively, when S is in the straight line

$$(\hat{s}-\hat{s}') = \frac{\hat{\phi}+\hat{y}}{2} + \frac{\hat{\phi}^3}{24}\frac{\hat{\phi}+4\hat{y}}{\hat{\phi}+\hat{y}}\ ,$$
(3.44)

or in the bend

$$(\hat{s}-\hat{s}') = \frac{\hat{u}}{2} + \frac{\hat{u}^3}{24},$$
(3.45)

where $(\hat{s}-\hat{s}') = (s-s')\gamma^3/R$, and $(s-s')$ is the curvilinear distance between the test particle and a source *at the same time*.

By means of Eqs. (3.42) to (3.45), the following extension of Eq. (3.35) can be written down for the total rate of energy change of an electron entering a bending magnet as a function of its position along the Gaussian bunch:

$$\frac{d\mathcal{E}}{d(ct)} = \frac{2e^2\gamma\lambda_0}{4\pi\epsilon_0 R}\left\{\int_0^\infty d\hat{y}\left[\frac{(\hat{\phi}+\hat{y})^2 + \hat{\phi}^3(3\hat{\phi}/4+\hat{y})}{[(\hat{\phi}+\hat{y})^2 + \hat{\phi}^4/4]^2} - \frac{(\hat{\phi}+\hat{y})^2 + \hat{\phi}^4/4}{[(\hat{\phi}+\hat{y})^2 + (\hat{\phi}^3/12)(\hat{\phi}/4+\hat{y})]^2}\right]\right.$$

$$\times e^{-\frac{\left\{s - (R/\gamma^3)(\hat{\phi}+\hat{y})/2 + (\hat{\phi}^3/24)(\hat{\phi}+4\hat{y})/(\hat{\phi}+\hat{y})\right\}^2}{2\sigma^2}}$$

$$+ \int_0^{\hat{\phi}} d\hat{u}\left(1 + \frac{\hat{u}^2}{4}\right)\left[\frac{\hat{u}^2/4 - 1}{2(1+\hat{u}^2/4)^3} + \frac{1}{\hat{u}^2}\left(\frac{1 + 3\hat{u}^2/4}{(1+\hat{u}^2/4)^3} - \frac{1}{(1+\hat{u}^2/12)^2}\right)\right.$$

$$\left.\left.\times e^{-\frac{\left\{s - (R/\gamma^3)(\hat{u}/2 + \hat{u}^3/24)\right\}^2}{2\sigma^2}}\right]\right\}.$$

$$(3.46)$$

Note that the first and the second integral on the right side of Eq. (3.46) deal, respectively, with retarded sources in the straight line and in the bend. The correct contribution by a source to the rate of energy change of the test particle is given by the integrands of Eq. (3.42) and Eq. (3.43) weighted with the particle density distribution (expressed by Eq. (3.34)), where the latter is evaluated at the retarded position of the source (Eq. (3.44) and Eq. (3.45), respectively).

Next, Eq. (3.46) is integrated, numerically, for the same positions of the beam in the magnet and for the same values of $\gamma$ that are reported in Fig. 3.4 and in Fig. 3.6. Results are shown in Fig. 3.7.

Note that the main features of Fig. 3.4 (or Fig. 3.7) can be explained, in the high-$\gamma$ case, just by inspecting Eq. (3.35). For example, the behaviour of the maximum in the rate of energy change, present in both simulation results (for $\gamma = 320$) and analytical results (see Fig. 3.6) can be just understood observing that one gets the maximum value at the right hand side of Eq. (3.35) when $s = R\phi^3/6$. In fact, for that value of $s$, one has $\lambda(s - R\phi^3/6) = e^{-(\xi-4\rho)^2/2} = 1$ while the other terms get close to zero. When $R = 1.5$ m and the bunch is 14 cm inside the bend the maximum is , therefore, at $s \simeq 5\sigma$; when the bunch is 18 cm inside the bend the maximum has moved at position $s \simeq 8\sigma$, in agreement with the plots. This explains the evolution of the maximum in Fig. 3.4 for the high-$\gamma$ case (or Fig. 3.6, or Fig. 3.7). By inspecting Fig. 3.4 and Fig. 3.7, for the case of lower values of $\gamma$, one can see that the peak is still there, still evolving towards the right hand side part of the plots, even if much less pronounced.

In order to get a quantitative evaluation of the agreement between the curves in Fig. 3.4 and the respective twins in Fig. 3.7, points have been sampled from every curve in Fig. 3.4 and in Fig. 3.7. Then, for every pair of corresponding sampled points (referring to corresponding curves), the differences normalized to the values given by Eq. (3.35) (shown in Fig. 3.7) have been taken. Next, the rms value of these quantities has been considered as a measure of agreement between every pair of twin curves. For every curve it has been found an agreement within 1 percent (this small difference is ascribed to computational inaccuracies).

The very good matching between Fig. 3.4 and Fig. 3.7 reflects the fact that the general small-angle approximation in Section 3.1 was successfully applied to the particular case of a transient between a straight line and a bend: in other words, as expected,
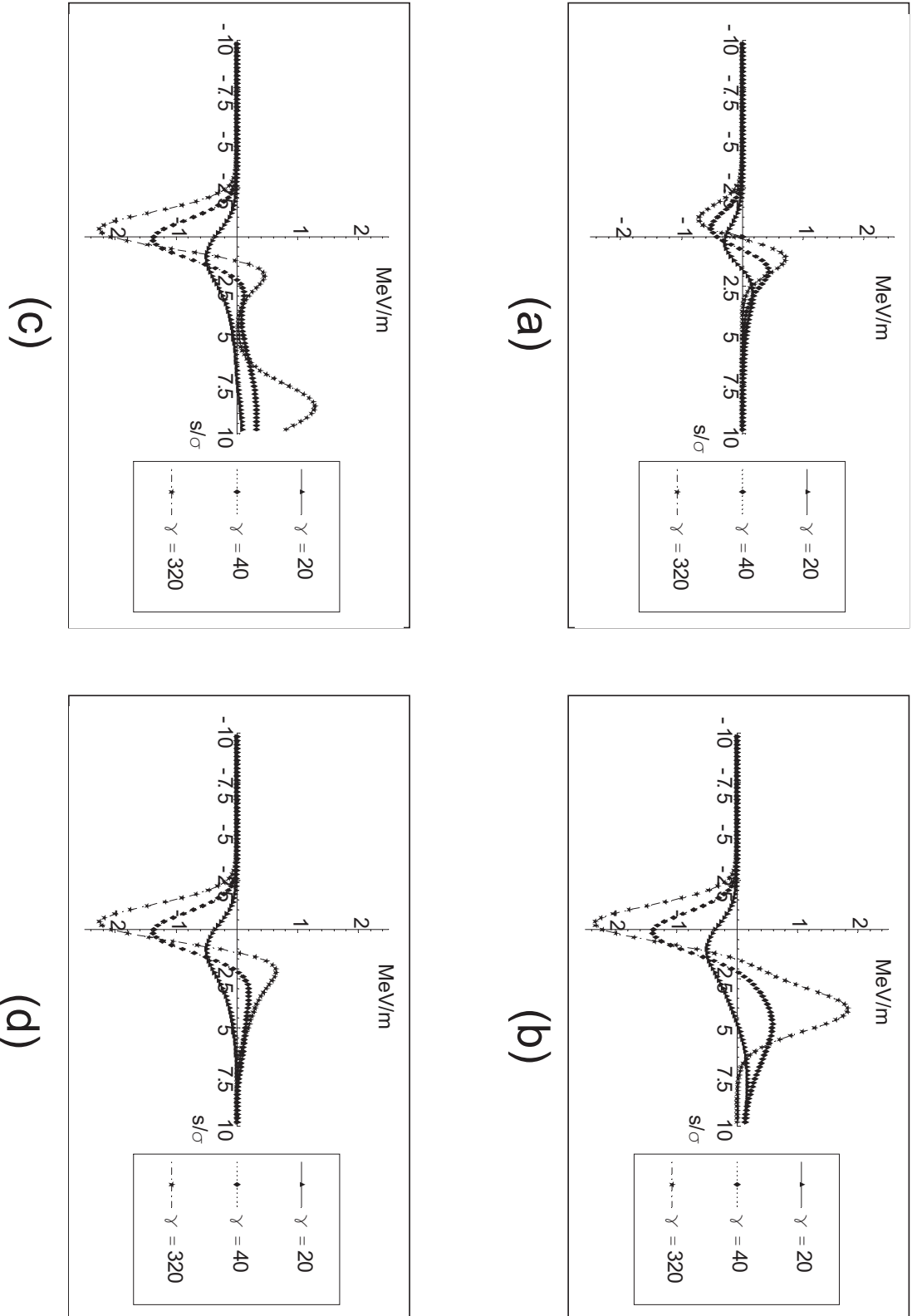
**Figure 3.7:** *Rate of energy change of an electron in MeV/m as a function of its position $s/\sigma$ along the Gaussian Bunch entering a hard edge magnet, as calculated using a generalization of Eq. (3.35). Every picture shows results for different values of $\gamma$. Parameters are $R = 1.5$ m, $\sigma = 50$ $\mu$m, $q = 1$ nC (a) 5 cm after the entrance. (b) 14 cm after the entrance. (c) 18 cm after the entrance. (d) 25 cm after the entrance.*

Eq. (3.33) reduces to Eq. (3.46) when that particular trajectory (straight line followed by a bend) is selected. Of course, as it must be, both reduce to Eq. (3.35) as soon as the conditions expressed in Eq. (3.36) and Eq. (3.38) are satisfied.

### 3.2.4    Conclusions

In the last few years, CSR longitudinal effects have been studied widely, both in the framework of analytical and numerical investigations. Many of these studies are based on Eq. (3.35), found in [4], that constitute an important result in CSR theory.

With a systematic use of a small-angle approximation we were able to derive, in Section 3.1, an expression for the energy exchange between a test particle and the bunch: this expression is closed, in the sense that all one needs to know in order to evaluate it is the transverse velocity of the bunch as a function of the propagation distance, which is directly determined by the external field configuration.

CSR longitudinal transient effects from a straight to a circular path have often been studied under approximations Eq. (3.36) and Eq. (3.38), in which they are energy-independent. With the help of the method described in Section 3.1, the case in which these approximations are no longer valid is addressed instead. In this situation, results (see Fig. 3.4) show a strong dependence of the CSR longitudinal force on the Lorentz factor (both in the steady state and in the transient case) and an asymptotic agreement, for large values of $\gamma$, with Eq. (3.35) (see Fig. 3.6). A conclusion is that, in such energy-dependent regime, the use of the energy-independent Eq. (3.35) leads to an overall over-estimation of all CSR longitudinal effects.

The study proposed in the present Section 3.2 is of practical interest for low-energy injector design as well as in the framework of CSR-related instabilities: in the first case one considers ultrarelativistic beams whose value of $\gamma$ (in combination with the bunch length and the choice of the trajectory) may be low enough not to fulfill Eq. (3.36) and Eq. (3.38). Similarly, in the second case, when short wavelength perturbations of the bunch distribution do not meet the requirements in Eq. (3.36) and Eq. (3.38), one should use $\gamma$-dependent wake fields in order to model CSR interactions. Further investigations may address these practical situations in a more quantitative way.

Results have been compared with an extension of the $\gamma$-independent formula in [4] for the rate of energy change of an electron (Eq. (3.35)), and a very good agreement between the two outcomes has been demonstrated. This reflects the fact that the general approach in [14] perfectly succeeded in dealing with the particular case of a transient. In other words Eq. (3.33), valid for any trajectory (under the constraint of the paraxial approach explained in [14]), reduces to Eq. (3.46) when the correct trajectory (straight line followed by a bend) is selected.

# Bibliography

[1] TESLA Technical Design Report, DESY 2001-011, edited by F. Richard et al. and http://tesla.desy.de/

[2] W. Knulst, J. Luiten, M. van der Wiel and J. Verhoeven, Applied Physics Letters 79, 2999 (2001)

[3] J. S. Nodvick and D. S. Saxon, Phys. Rev. 96, 180 (1954)

[4] E. L. Saldin, E. A. Schneidmiller and M. V. Yurkov, Nucl. Instr. Methods A 398, 373 (1997)

[5] R. Li, in *Proceedings of the Particle Accelerator Conference, New York, 1999*, edited by A. Luccio and W. MacKay, p. 118

[6] R. Li, C. L. Bohn and J. J. Bisognano, in *Proceedings of the SPIE Conference, San Diego, 1997*, vol. 3154, p. 223

[7] R. Li, in *Proceedings of the 2nd ICFA Advanced Accelerator Workshop on The Physics of High Brightness Beams, Los Angeles, 1999.*

[8] R. Li, Nucl. Instrum. Methods A 429, 310 (1998).

[9] K. Rothemund, M. Dohlus and U. van Rienen, in *Proceedings of the 21st International Free Electron Laser Conference and 6th FEL Applications Workshop, Hamburg, 1999*, edited by J. Feldhaus and H. Weise

[10] H. H. Braun et al., Phys. Rev. Special Topics 3 (2000)

[11] B. E. Carlsten, Phys. Rev. E 54, 838 (1996)

[12] E. L. Saldin, E. A. Schneidmiller and M. V. Yurkov, Nucl. Instr. Methods A 417, 158 (1998)

[13] Ya. S. Derbenev, J. Rossbach, E. L. Saldin and V. D. Shiltsev, TESLA-FEL Report No. 95-05, DESY, Hamburg, 1995

[14] G. Geloni, V. Goloviznin, J. Botman and M. van der Wiel, Phys. Rev. E 64, 046504

[15] S. Heifets and G. Stupakov, Report SLAC-PUB-8761 (2001)

[16] S. Heifets and G. Stupakov, Report SLAC-PUB-8758 (2001)

[17] S. Heifets and G. Stupakov, Report SLAC-PUB-8988 (2001)

[18] E. L. Saldin, E. A. Schneidmiller, M. V. Yurkov, TESLA-FEL 2002-02 (2002)

[19] M. Borland, Phys. Rev. Special Topics 4, 070701 (2001)

[20] M. Borland, Phys. Rev. Special Topics 4, 074201 (2001)

[21] F. B. Kiewiet, O. J. Luiten, G. J. H. Brussaard, J.I.M. Botman and M.J. van der Wiel in *Proceedings of Eurpean Particole Accelerator Conference, Wien, 2000*, edited by J.L. Laclare, W. Mitaroff et al.

# Chapter 4

# Transverse effects

Much of the theoretical analysis about transverse self-forces deals with the case of a bunch moving along a circular orbit only, without considering the situation of a bending magnet with a finite length. The need of understanding and cross-checking results by the code TraFiC[4] for the self-interaction in the transverse direction calls for a thorough investigation of transverse self-interactions from a purely electrodynamical viewpoint. After a general introduction in Section 4.1 we propose, in Section 4.2, an analysis of transverse self-fields which originate, at the position of a test particle, from an ultrarelativistic line of charges moving in an arc of a circle. The problem will be first addressed within a two-particle system. We then extend our consideration to a line bunch with a stepped density distribution, a situation which can be easily generalized to the case of an arbitrary density distribution. Our approach turns out to be also useful in order to get a better insight in the physics involved in the case of simple circular motion. Further on, in Section 4.3, we treat an electron bunch with a given vertical (i.e. perpendicular to the orbital plane) size by a generalization of our previous work to the case of a test particle with vertical displacement interacting with a line bunch. In fact, since a bunch with vertical extent can always be thought of as a superposition of displaced charge lines, all the relevant physical aspects of the problem are included in the study of that simple model. Our generalization results in a physically meaningful and quantitative explanation of the main features of simulations obtained with the code TraFiC[4] as well as in successful cross-checking of the code.
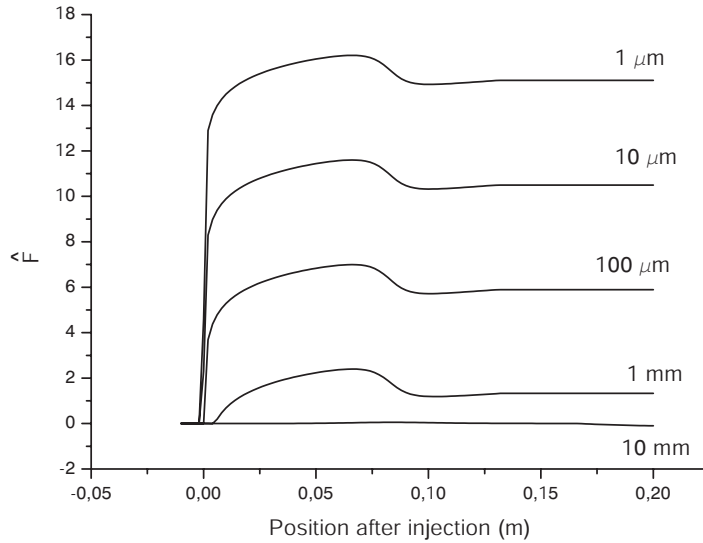
**Figure 4.1:** *Radial force normalized to $e^2\lambda/(4\pi\varepsilon_0 R)$, $\hat{F}$, felt by a particle with different vertical displacements $h$ positioned at the center of a line bunch 200 $\mu$m long as the bunch enters a circle of radius $R = 1$m. Here $\gamma = 100$. These simulations were obtained by means of the code TraFiC$^4$.*

## 4.1  INTRODUCTION

As already pointed out, in all self-interaction issues the equations for the field form, together with the dynamical equations for the particle motion, a formidable self-consistent problem. Its complete solution, that is the evolution of the bunch distribution, is obtained only when one is able to solve simultaneously the equations for the fields (electrodynamical problem) and the equations of motion (dynamical problem): this task can be performed with the help of self-consistent computer simulations. An example of such codes is given (see [1]) by the program TraFiC[4], which has been briefly discussed in Chapter 1 and of which results will be used throughout this Chapter.

TraFiC[4] has been used to predict self-field related effects in the bunch compressor chicanes to be used in front of the main linac for the XFEL at DESY and it is, at the time being, the only fully developed code for XFEL modelling both at DESY and SLAC. Results show that the projected transverse emittance of the bunch grows from 0.8 mm mrad after the injection to the significantly enhanced value of 2.6 mm mrad after the compressor [2].

Transverse dynamics is addressed by the code in two steps: first, the transverse electromagnetic forces, which are well defined and measurable physical quantities, are calculated separately and, second, the equation of motion is solved in a self-consistent way. However, numerical results alone are not sufficient in order to reach an understanding of how electromagnetic forces act. Consider for example the plot in Fig. 4.1, obtained by using the electromagnetic solver of TraFiC[4].

The figure shows the normalized radial force (i.e. the force normalized to $e^2\lambda/(4\pi\varepsilon_0 R)$

in the direction orthogonal to the test particle velocity and still lying on the bending plane) felt by a test particle entering into a hard-edge magnet. Here $\lambda$ is the bunch density while $h$ is a vertical (orthogonal to the bending plane) displacement with respect to the center of a one-dimensional bunch with rectangular density distribution function.

The plot shows interesting characteristics: a very sharp feature at the injection position, a transient and a steady state, which we can observe but for which there is no intuitive physical explanation. The electromagnetic problem is, of course, only a part of the evolution problem but its understanding is *per se* an important physical issue.

Self-forces in the transverse direction were first addressed, in the case of a circular motion, and from an electrodynamical viewpoint, in [3]. Further analysis ([4] to [7]) considers, again, the case of circular motion both from an electrodynamical and a dynamical viewpoint: transient collective phenomena have not been considered so far.

Analytical investigations of transient cases are therefore needed in order to see the meaning of the simulation results (i.e. to explain the features of the electromagnetic interaction), besides providing, from a more practical viewpoint, important cross-checks with the code. In Section 4.2 we will restrict our attention to the simpler situation of a rigid line bunch (whose particles are characterized by a vertical extent $h = 0$) evolving through an arc of a circle, under the influence of the electromagnetic fields generated by its own motion. In Section 4.3 we will eventually show that, through a generalization of this kind of study, we can understand the features of Fig. 4.1 from a physical viewpoint, deal with characteristic times and lengths and, as a very practical result, validate the simulation results by producing analytical cross-checks.

## 4.2 Transverse self-fields within an electron bunch moving in an arc of a circle

### 4.2.1 Introduction

In this Section we report, as a first step towards a quantitative explanation of phenomena like those in Fig. 4.1, a fully electrodynamical analysis of transverse self-fields originating, at the position of a test particle, from an ultrarelativistic line of charges moving in an arc of a circle, thus extending the treatment of the basic situation of circular motion to the case of a transient between a straight line and a hard-edge magnet (and, viceversa, from a bend to a straight line).

Consistently with the choice to analyze the electrodynamical aspect of the problem only, a zero energy-spread will be understood when considering the evolution of an electron bunch. The results obtained can be directly applied only in the case in which the zero energy-spread hypothesis is verified *a posteriori*.

First, a two-particle model is adopted in order to study the transverse force produced by a single particle and then, by summing up all the contributions from different electrons, the case of a line-bunch model characterized by a rectangular density distribution is analyzed: this can easily be generalized further to the situation of an arbitrary density distribution.

Besides providing results in the case of a finite hard-edge bending magnet, our

approach also turns out to be useful in order to get a better insight of the physics involved in a simple circular motion.

The study is organized as follows. The transverse interaction between two electrons moving on a circle is treated in Section 4.2.2. In Section 4.2.3 we deal with a stepped-profile electron bunch interacting with a test particle again in a circle, and discuss also the applicability region of the line model with respect to the transverse beam size, $h$. Within such applicability limits, we find results which are independent of the bunch transverse dimension. Transient behavior (from straight to circular path and viceversa) for the transverse self-forces between two particles are then studied in Section 4.2.4. Results for the transient of a stepped-profile bunch are given in Section 4.2.5, where a treatment for the case of a more generic bunch density is also proposed. A regularization technique for cancelling the singularity in the expression for the transverse force (which always arises in the limit of a near-zero distance between test particle and sources) is then applied. Finally, in Section 4.2.6, we come to a summary of the results obtained and to conclusions.

## 4.2.2   Transverse interaction between two electrons moving in a circle

Let us begin our study considering two electrons moving in a circle of radius $R$. The case of the test particle following the source (tail-head interaction) has already been treated in [3] (we will treat here too for the sake of completeness), while the case of the test particle preceding the source (head-tail interaction) has always been neglected before. The electro-magnetic force which one of the two particles (designated with "T", i.e. the test particle) feels, due to the interaction with the other one (designated with "S", i.e. the source particle), is given by

$$\boldsymbol{F}(\boldsymbol{r_T}, t) = e\boldsymbol{E}(\boldsymbol{r_T}, t) + ec\boldsymbol{\beta_T} \times \boldsymbol{B}(\boldsymbol{r_T}, t), \tag{4.1}$$

where $\boldsymbol{r_T}$ is the position of the test particle, $e$ is the electron charge with its own (negative) sign, $\boldsymbol{\beta_T}$ is the velocity of the test particle normalized to the speed of light, $c$, while $\boldsymbol{E}(\boldsymbol{r_T}, t)$ and $\boldsymbol{B}(\boldsymbol{r_T}, t)$ are, respectively, the electric and the magnetic field generated at a given time $t$ by the source particle S, at the position of the test particle T, given by the Liénard-Wiechert expressions discussed in Chapter 2 and Chapter 3 (see e.g. Eq. (3.12) and Eq. (3.13)).

The transverse direction (on the orbital plane) is, by definition, orthogonal to $\boldsymbol{\beta_T}$. The transverse component of Eq. (4.1) can be written, in a similar fashion as the longitudinal component, as the sum of contributions from the velocity ("C", Coulomb) and the acceleration ("R", Radiation) fields, namely

$$\boldsymbol{F_\perp}(\boldsymbol{r_T}, t) = \boldsymbol{F_{\perp C}}(\boldsymbol{r_T}, t) + \boldsymbol{F_{\perp R}}(\boldsymbol{r_T}, t), \tag{4.2}$$

where

$$\boldsymbol{F_{\perp C}}(\boldsymbol{r_T}, t) = \frac{e^2}{4\pi\varepsilon_0} \frac{\boldsymbol{n_\perp}\left(1 - \boldsymbol{\beta_S} \cdot \boldsymbol{\beta_T}\right) - \boldsymbol{\beta_{\perp S}}\left(1 - \boldsymbol{n} \cdot \boldsymbol{\beta_T}\right)}{\gamma_S^2 R_{ST}^2 \left(1 - \boldsymbol{n} \cdot \boldsymbol{\beta_S}\right)^3} \tag{4.3}$$
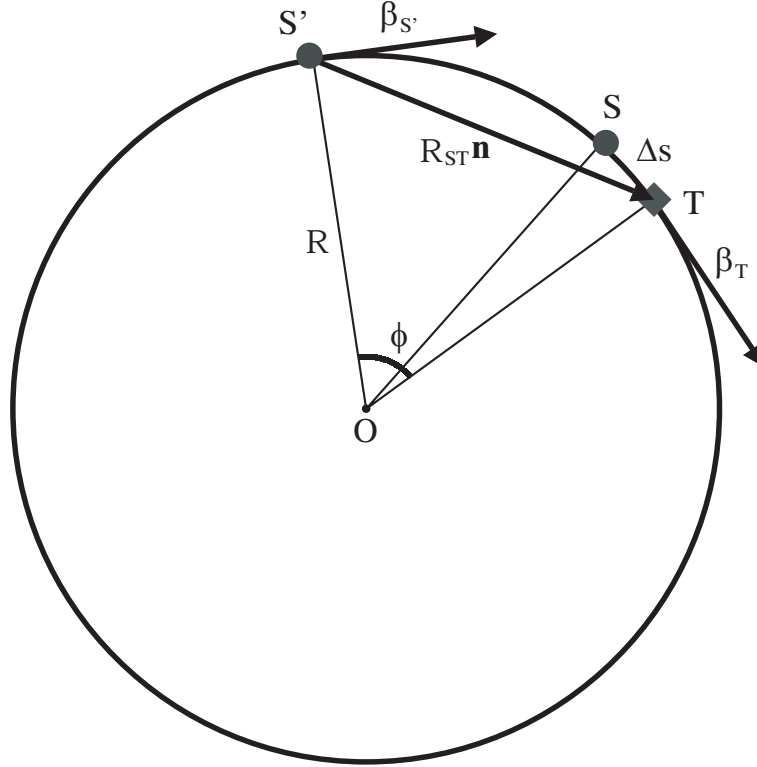
**Figure 4.2:** *Geometry for the two-particle system in the steady state situation, with the test particle ahead of the source. Here T is the present position of the test particle, S is the present position of the source, while S' indicates the retarded position of the source.*

and

$$\boldsymbol{F}_{\perp \mathbf{R}}(\boldsymbol{r_T}, t) = \frac{e^2}{4\pi\varepsilon_0 c} \left[ \frac{\boldsymbol{n_\perp}\left(\boldsymbol{n}\cdot\dot{\boldsymbol{\beta}}_{\mathbf{S}}\right)\left(1-\boldsymbol{\beta_S}\cdot\boldsymbol{\beta_T}\right) - \boldsymbol{\beta_{\perp S}}\left(\boldsymbol{n}\cdot\dot{\boldsymbol{\beta}}_{\mathbf{S}}\right)\left(1-\boldsymbol{n}\cdot\boldsymbol{\beta_T}\right)}{R_{\mathrm{ST}}\left(1-\boldsymbol{n}\cdot\boldsymbol{\beta_S}\right)^3} \right.$$
$$\left. - \frac{\dot{\boldsymbol{\beta}}_{\perp\mathbf{S}}\left(1-\boldsymbol{n}\cdot\boldsymbol{\beta_T}\right) + \boldsymbol{n_\perp}\left(\boldsymbol{\beta_T}\cdot\dot{\boldsymbol{\beta}}_{\mathbf{S}}\right)}{R_{\mathrm{ST}}\left(1-\boldsymbol{n}\cdot\boldsymbol{\beta_S}\right)^2} \right] . \quad (4.4)$$

Let us first consider the case in which the test particle is in front of the source. In this case, referring to Fig. 4.2, we can define with $\Delta s$ the curvilinear distance between the present position of the test and of the source particle; $\phi$ will indicate, instead, the angular distance between the retarded position of the source and the present position of the test electron, and it will be addressed to as the retarded angle.

In the following we will assume $\beta_{\mathrm{S}} = \beta_{\mathrm{T}} = \beta$. This hypothesis will naturally lead, further on, to the assumption of a zero energy-spread when one considers the evolution of an electron bunch, and, as already discussed in Sec. 4.2.1, it is consistent with our choice to analyze only the electrodynamical aspect of the problem. Therefore we can write Eq. (4.3) and Eq. (4.4) in the following way:

$$F_{\perp \mathrm{C}} = \frac{e^2}{4\pi\varepsilon_0} \frac{1+\beta^2-2\beta\cos(\phi/2)}{4R^2\gamma^2\sin(\phi/2)(1-\beta\cos(\phi/2))^3} \; , \quad (4.5)$$

$$F_{\perp \mathrm{R}} = \frac{e^2}{4\pi\varepsilon_0} \frac{\beta^2}{2R^2} \left[ \frac{1}{\sin(\phi/2)\,(1 - \beta\cos(\phi/2))} - \frac{(1 - \beta^2)\sin\phi/2}{(1 - \beta\cos(\phi/2))^3} \right] . \tag{4.6}$$

On the other hand, the retardation condition linking $\Delta s$ and $\phi$ (see [8]) can be readily derived:

$$\Delta s = R\phi - 2\beta R \sin\frac{\phi}{2} , \tag{4.7}$$

or its approximated form

$$\Delta s = (1 - \beta)R\phi + \frac{R\phi^3}{24} . \tag{4.8}$$

As one can see by inspecting Eq. (4.7), when we impose reasonable values for $\Delta s \ll R$ we obtain corresponding values of $\phi \ll 1$. We will therefore assume $\phi \ll 1$ throughout this Section and verify *a posteriori* the validity of this assumption when studying particular situations. Note that, by fixing $\phi \ll 1$ we keep open the possibility of comparing $\phi$ with the synchrotron radiation formation angle $1/\gamma$ (a deflection angle smaller or larger than $1/\gamma$ is characteristic of the cases, respectively, of undulator or synchrotron radiation).

We can now expand Eq. (4.5) and Eq. (4.6) to the second non-vanishing order in $\phi$ thus obtaining

$$F_{\perp \mathrm{C}} \simeq \frac{e^2\gamma^3}{4\pi\varepsilon_0 R^2} \Phi_{\mathrm{C}}(\hat{\phi}) \tag{4.9}$$

and

$$F_{\perp \mathrm{R}} \simeq \frac{e^2\gamma^3}{4\pi\varepsilon_0 R^2} \Phi_{\mathrm{R}}(\hat{\phi}) , \tag{4.10}$$

where we define $\Phi_{\mathrm{C}}$ and $\Phi_{\mathrm{R}}$ as

$$\Phi_{\mathrm{C}}(\hat{\phi}) = \frac{\hat{\phi}^2}{\hat{\phi}(1 + \hat{\phi}^2/4)^3} \tag{4.11}$$

and

$$\Phi_{\mathrm{R}}(\hat{\phi}) = \frac{2 - \hat{\phi}^2 + \hat{\phi}^4/8}{\hat{\phi}(1 + \hat{\phi}^2/4)^3} . \tag{4.12}$$

Here and above $\hat{\phi} = \gamma\phi$. This normalization choice, already treated in [8], is quite natural, $1/\gamma$ being the synchrotron radiation formation-angle at the critical wavelength. In the derivation of Eq. (4.9) and Eq. (4.10) (and in the following, too) we understood $\hat{\phi} \gg 1/\gamma$, which is justified by the ultrarelativistic approximation.

The following expression can be then trivially derived, which is valid for the total transverse force felt by the test particle

$$F_{\perp} \simeq \frac{e^2\gamma^3}{4\pi\varepsilon_0 R^2} \Phi(\hat{\phi}) , \tag{4.13}$$

where $\Phi$ is defined by
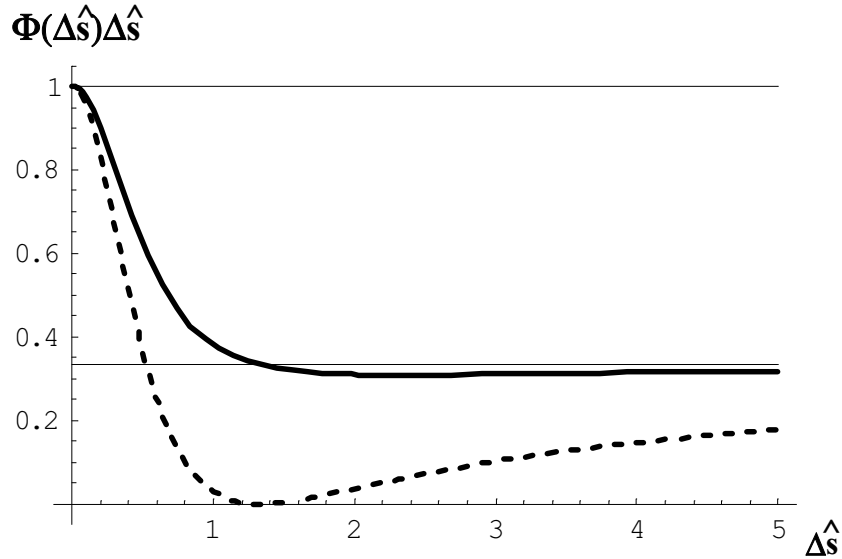
**Figure 4.3:** *Plot of $\Phi(\Delta\hat{s})\Delta\hat{s}$ (solid line) and comparison with the asymptotic values, 1 and 1/3. The dashed line shows the acceleration contribution $\Phi_{\mathrm{R}}(\Delta\hat{s})\Delta\hat{s}$ alone.*

$$\Phi(\hat{\phi}) = \frac{2 + \hat{\phi}^4/8}{\hat{\phi}(1 + \hat{\phi}^2/4)^3} \ . \tag{4.14}$$

Note that Eq. (4.14) is completely independent of the parameters of the system: it is then straightforward to study the asymptotic behaviors of $\Phi$.

It is evident that $\Phi(\Delta\hat{s}) \to 1/(3\Delta\hat{s})$ when $\hat{\phi} \gg 1$ and $\Phi(\Delta\hat{s}) \to 1/(\Delta\hat{s})$ when $\hat{\phi} \ll 1$, having introduced the normalized quantity $\Delta\hat{s} = (\gamma^3/R)\Delta s$. This normalization choice is linked to the fact that the critical synchrotron radiation wavelength, $R/\gamma^3$, is also the minimal characteristic distance of our system: two particles nearer than such a distance can be considered as a single one radiating, up to the critical frequency, with charge $2e$ (see [8]).

The asymptotic behavior above suggests to study the function $\Phi(\Delta\hat{s})\Delta\hat{s}$. We plotted such a function in Fig. 4.3 (together with the radiative contribution alone) for values of $\Delta\hat{s}$ running from 0 to 5.

It is interesting to underline the fact that, as one can see from Fig. 4.3, the transverse force is always centrifugal, for any distance between the two particles. This fact can be explained by means of a simple relativistic argument which holds, qualitatively, for all particle distances: in order to build the two-particle system, i.e. to bring them together, one needs to work against the electromagnetic field. Then, the total mass of the system accounts for this interaction energy too, and is therefore bigger than the simple sum of the particles masses. Hence, also the equilibrium orbit radius must be larger than $R$, and a centrifugal self-force is to be expected.

It is also worthwhile to note that $\Phi_{\mathrm{R}}$ has the same asymptotic behavior as $\Phi$, and that $\Phi_{\mathrm{C}}$ gives important contributions to $\Phi$ only for values between the two asymptotes (see Fig. 4.3). This may find intuitive explanation in the following reasoning. As is
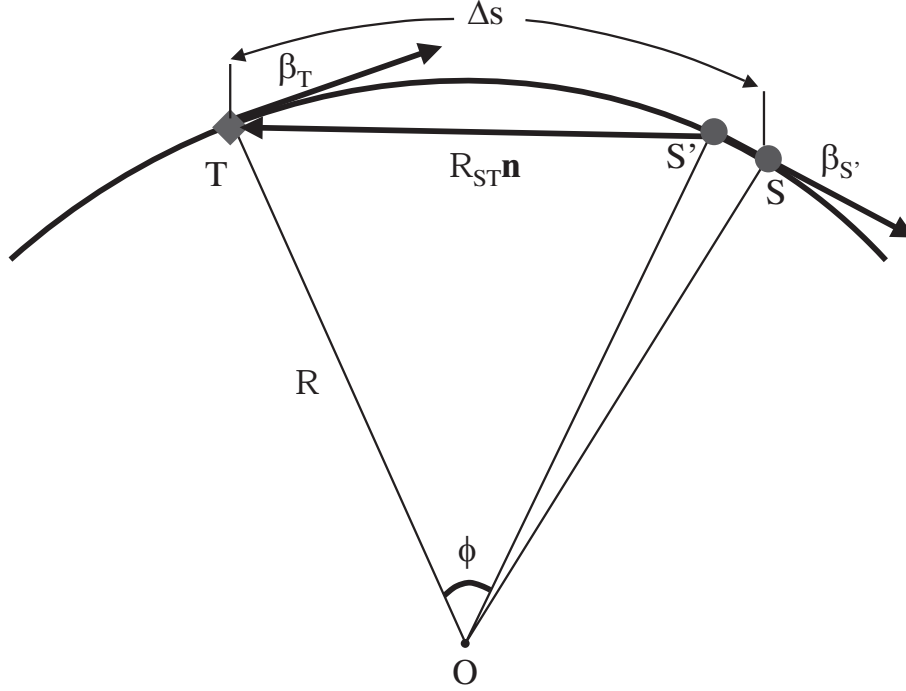
**Figure 4.4:** *Geometry for the two-particle system in the steady state situation, with the source particle ahead of the test one. Here T is the present position of the test particle, S is the present position of the source, while S' indicates the retarded position of the source.*

well known (see, for example, [9]), the velocity field of an ultrarelativistic electron is radial, with respect to the "virtual" position which the particle would assume if it moved with constant velocity starting from the retarded point, but the line forces are not isotropically distributed, and resemble more and more the plane wave configuration as $\beta \to c$. Therefore, the test particle is influenced by the velocity field of the source particle only when such a field "shines right on the test electron" (quoted from [10]), which does not happen for asymptotic values of $\hat{\phi}$.

Let us now analyze, in the framework of our line model, the case in which the source particle is in front of the test particle. The geometry is qualitatively sketched in Fig. 4.4.

The difference with respect to the situation in which the test electron is in front of the source is that the test electron "runs against" the electromagnetic signal emitted by the source, while in the other case it just "runs away" from it. Therefore the relative velocity between the signal and the test electron is equal to $(1+\beta)c$, instead of $(1-\beta)c$ in the other situation. Hence the retardation condition reads (here $\Delta s < 0$):

$$| \Delta s | = R\phi + 2\beta R \sin \frac{\phi}{2} \tag{4.15}$$

or, solved for $\phi$ in its approximated form,

$$\phi \simeq \frac{| \Delta s |}{R(1 + \beta)} \ . \tag{4.16}$$

In this situation, $\boldsymbol{\beta_{S'}}$ is almost parallel to (and equal to) $\boldsymbol{\beta_T}$ and antiparallel to $\boldsymbol{n}$: it turns out that the only important contribution to the transverse force is given by the second term on the right side of Eq. (4.4), and it is easy to check that

$$F_\perp \simeq \frac{e^2}{4\pi\varepsilon_0 R \mid \Delta s \mid} \; . \tag{4.17}$$

It may be worthwhile to underline that the force in Eq. (4.17) is, evidently, of the same magnitude as the force in Eq. (4.13).

An interpretation for the electromagnetic transverse forces from the viewpoint of relativistic dynamics in the limit $\mid \Delta s \mid \ll R/\gamma^3$ is given in Chapter 5.

### 4.2.3    Transverse interaction between an electron and a bunch moving in a circle

In this Section we discuss the transverse force felt by an electron due to the interaction with a line bunch (with rectangular density distribution) moving in a circle. The geometry is described in Fig. 4.5, and will be considered rigid, i.e. fixed during the entire evolution of the system.

Before beginning actual calculations, we provide here a discussion about the applicability region of our line model. In the case of contributions from particles behind the test particle, the region of applicability of the line model follows straightforwardly from the retardation condition: one can easily check that the inclusion of a transverse dimension of the bunch, already designated with $h$ in Section 4.2.1, adds to Eq. (4.8) a term of magnitude $h^2/(R\phi)$. Such a term is negligible with respect to the others in the retardation condition, whenever $h \ll R/\gamma^2$, which specifies the region of applicability of our model as regards the transverse bunch size.

The situation becomes more complicated when one considers contributions from electrons in front of the test particle. In fact, in the case $\Delta s < 0$ (source particle in front) and $|\Delta s| < h$, we have a situation in which the test electron overtakes the source before it is reached by the electromagnetic signal: this means that, even if the test particle is behind the source, the present position of the test particle is, anyway, in front of the retarded position of the source. Then, the line model constitutes a valid description of the situation only when $|\Delta s| \gg h$. The cases that do not verify such a condition are studied in Section 4.3.

Now, in order to actually evaluate the transverse electromagnetic force which the bunch exerts on the test particle one has to sum up the contributions from all the retarded sources. Since the two-particle interaction has been calculated in Section 4.2.2 as a function of the retarded angle $\phi$, it is convenient to switch the integration variable from $\Delta s$ to $\phi$,

$$\frac{d\Delta s}{d\phi} = R \left(1 - \beta \cos\frac{\phi}{2}\right) \; , \tag{4.18}$$

being the Jacobian of the transformation. Therefore, from Eq. (4.5), Eq. (4.6) and Eq. (4.18) one has
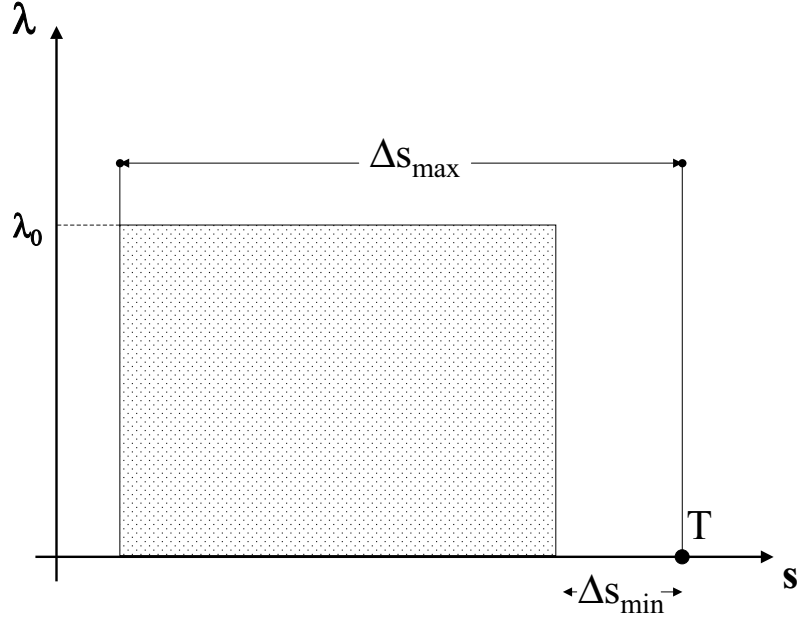
**Figure 4.5:** *Schematic of the test electron T and the stepped-profile bunch; $\Delta s_{\min}$ indicates the distance between the electron and the head of the bunch; $\Delta s_{\max}$ is the sum of the bunch length and $\Delta s_{\min}$.*

$$F_{\perp C}^{B} = \lambda_0 \int_{\phi_{\min}}^{\phi_{\max}} F_{\perp C}(\phi)\ R\left(1 - \beta\cos(\phi/2)\right) d\phi$$

$$= \frac{e^2 \lambda_0}{4\pi\varepsilon_0 R} \frac{1}{2\gamma^2} \left[ -\frac{\beta}{1 - \beta\cos(\phi/2)} - \ln(\tan(\phi/4)) \right]_{\phi_{\min}}^{\phi_{\max}} \tag{4.19}$$

and

$$F_{\perp R}^{B} = \lambda_0 \int_{\phi_{\min}}^{\phi_{\max}} F_{\perp R}(\phi)\ R\left(1 - \beta\cos(\phi/2)\right) d\phi$$

$$= \frac{e^2 \lambda_0}{4\pi\varepsilon_0 R} \left[ \beta^2 \ln(\tan(\phi/2)) + \frac{\beta(1 - \beta^2)}{1 - \beta\cos(\phi/2)} \right]_{\phi_{\min}}^{\phi_{\max}} \quad , \tag{4.20}$$

where the superscript "B" stands for "bunch", and $\lambda_0$ is the constant linear density of the bunch. If we now expand in $\phi_{\min} \ll 1$ and $\phi_{\max} \ll 1$ the trigonometric functions in Eq. (4.19) and Eq. (4.20) we have

$$F_{\perp C}^{B} \simeq \frac{e^2 \lambda_0}{4\pi\varepsilon_0 R} \left[ -\frac{1}{2\gamma^2} \ln\left(\frac{\phi_{\max}}{\phi_{\min}}\right) - \frac{1}{2\gamma^2}\left( \frac{1}{1 - \beta + \beta\phi_{\max}^2/8} - \frac{1}{1 - \beta + \beta\phi_{\min}^2/8} \right) \right] \tag{4.21}$$

and

$$F_{\perp R}^{B} \simeq \frac{e^2 \lambda_0}{4\pi\varepsilon_0 R} \left[ \ln\left(\frac{\phi_{\max}}{\phi_{\min}}\right) + \frac{1}{\gamma^2}\left( \frac{1}{1 - \beta + \beta\phi_{\max}^2/8} - \frac{1}{1 - \beta + \beta\phi_{\min}^2/8} \right) \right] . \tag{4.22}$$

The second term on the right side of Eq. (4.21) is centrifugal, as well as the first one on the right side of Eq. (4.22). The other ones are centripetal. Note that the logarithmic term in Eq. (4.21) is unimportant (in the limit of large values for $\gamma$) with respect to the one in Eq. (4.22), while the second term in Eq. (4.21) modifies for a factor $1/2$ the analogous centripetal term in Eq. (4.22). Therefore, the total transverse force on the test electron is given by:

$$F_\perp^{\mathrm{B}} \simeq \frac{e^2 \lambda_0}{4\pi\varepsilon_0 R} \left[ \ln\left(\frac{\hat{\phi}_{\max}}{\hat{\phi}_{\min}}\right) + \left(\frac{4}{4+\hat{\phi}_{\max}^2} - \frac{4}{4+\hat{\phi}_{\min}^2}\right) \right] , \qquad (4.23)$$

which is the sum of a logarithmic centrifugal term and a centripetal term. It is easy to check that Eq. (4.23) can be also obtained by direct integration of Eq. (4.13).

A natural assumption is to consider our bunch density such that there are many particles within a distance $R/\gamma^3$ which, as already underlined, is the minimal characteristic distance of the system: if the test particle is to be considered at the head of our bunch, then it is straightforward to assume $\Delta s_{\min} \ll R/\gamma^3$ which, by means of the retardation condition Eq. (4.8), gives us back the condition: $\phi_{\min} \ll 1/\gamma$, the non-linear term in $\phi_{\min}$ of Eq. (4.8) being, in this case, negligible.

Under the latter assumption we can easily investigate the two cases of a short bunch, that is $\phi_{\max} \ll 1/\gamma$ (in which the linear term in $\phi_{\max}$ of Eq. (4.8) dominates), and of a long bunch, that is $\phi_{\max} \gg 1/\gamma$ (in which the linear term in $\phi_{\max}$ of Eq. (4.8) is negligible). These two cases correspond, of course, to the asymptotic situations for the two-particle interaction discussed in Section 4.2.2.

Let us consider first the case $\phi_{\max} \ll 1/\gamma$. Eq. (4.21), Eq. (4.22) and Eq. (4.23), then, read

$$F_{\perp\mathrm{C}}^{\mathrm{B}} \simeq \frac{e^2 \lambda_0}{4\pi\varepsilon_0 R} \left[ -\frac{1}{2\gamma^2} \ln\left(\frac{\hat{\phi}_{\max}}{\hat{\phi}_{\min}}\right) + \frac{1}{4}\hat{\phi}_{\max}^2 \right] \simeq \frac{e^2 \lambda_0}{4\pi\varepsilon_0 R} \left[ -\frac{1}{2\gamma^2} \ln\left(\frac{\Delta\hat{s}_{\max}}{\Delta\hat{s}_{\min}}\right) + \Delta\hat{s}_{\max}^2 \right] ,$$
$$(4.24)$$

$$F_{\perp\mathrm{R}}^{\mathrm{B}} \simeq \frac{e^2 \lambda_0}{4\pi\varepsilon_0 R} \left[ \ln\left(\frac{\hat{\phi}_{\max}}{\hat{\phi}_{\min}}\right) - \frac{1}{2}\hat{\phi}_{\max}^2 \right] \simeq \frac{e^2 \lambda_0}{4\pi\varepsilon_0 R} \left[ \ln\left(\frac{\Delta\hat{s}_{\max}}{\Delta\hat{s}_{\min}}\right) - 2\Delta\hat{s}_{\max}^2 \right] \qquad (4.25)$$

and

$$F_\perp^{\mathrm{B}} \simeq \frac{e^2 \lambda_0}{4\pi\varepsilon_0 R} \left[ \ln\left(\frac{\hat{\phi}_{\max}}{\hat{\phi}_{\min}}\right) - \frac{1}{4}\hat{\phi}_{\max}^2 \right] \simeq \frac{e^2 \lambda_0}{4\pi\varepsilon_0 R} \left[ \ln\left(\frac{\Delta\hat{s}_{\max}}{\Delta\hat{s}_{\min}}\right) - \Delta\hat{s}_{\max}^2 \right] . \qquad (4.26)$$

From Eq. (4.26) we see that the centripetal term tends, asymptotically, to zero as $(\gamma\phi_{\max})^2$.

In the case $\phi_{\max} \gg 1/\gamma$, instead, we have

$$F_{\perp\mathrm{C}}^{\mathrm{B}} \simeq \frac{e^2 \lambda_0}{4\pi\varepsilon_0 R} \left[ -\frac{1}{2\gamma^2} \ln\left(\frac{\hat{\phi}_{\max}}{\hat{\phi}_{\min}}\right) + 1 \right] \simeq \frac{e^2 \lambda_0}{4\pi\varepsilon_0 R} \left[ -\frac{1}{2\gamma^2} \ln\left(\frac{(24\Delta\hat{s}_{\max})^{1/3}}{\Delta\hat{s}_{\min}}\right) + 1 \right] ,$$
$$(4.27)$$

$$F_{\perp\mathrm{R}}^{\mathrm{B}} \simeq \frac{e^2\lambda_0}{4\pi\varepsilon_0 R}\left[\ln\left(\frac{\hat{\phi}_{\max}}{\hat{\phi}_{\min}}\right)-2\right] \simeq \frac{e^2\lambda_0}{4\pi\varepsilon_0 R}\left[\ln\left(\frac{(24\Delta\hat{s}_{\max})^{1/3}}{\Delta\hat{s}_{\min}}\right)-2\right] \qquad (4.28)$$

and

$$F_{\perp}^{\mathrm{B}} \simeq \frac{e^2\lambda_0}{4\pi\varepsilon_0 R}\left[\ln\left(\frac{\hat{\phi}_{\max}}{\hat{\phi}_{\min}}\right)-1\right] \simeq \frac{e^2\lambda_0}{4\pi\varepsilon_0 R}\left[\ln\left(\frac{(24\Delta\hat{s}_{\max})^{1/3}}{\Delta\hat{s}_{\min}}\right)-1\right] , \qquad (4.29)$$

which means that the centripetal term saturates to a constant value in the limit of a long bunch.

Note that, in order to obtain Eq. (4.29), we had to integrate contributions from $\hat{\phi} \ll 1$ to $\hat{\phi} \gg 1$: we can give a simple explanation for the centripetal constant force term just analyzing Eq. (4.13) and its asymptotic behaviors. The product of Eq. (4.13) with the Jacobian (Eq. (4.18)) of the transformation between $\Delta\hat{s}$ and $\hat{\phi}$ is equal, in the limits for $\hat{\phi} \gg 1$ and $\hat{\phi} \ll 1$, to $1/\hat{\phi}$: then we can conclude that the logarithmic centrifugal term in Eq. (4.29) (or in Eq. (4.27) or in Eq. (4.28)) takes into account the $1/\hat{\phi}$-behavior of the transverse force for the two-particle system, while the constant centripetal term brings information about the way in which the transverse force for a two-particle system changes in the intermediate region between the limits $\hat{\phi} \ll 1$ and $\hat{\phi} \gg 1$. Note, however, that there is no physical ground to distinguish between the first (centrifugal) and the second (centripetal) term in Eq. (4.29): the total force is always centrifugal, and both terms are consequence of the integration of a unique expression for the force between a two-particle system (which, of course, is always centrifugal too).

## 4.2.4   Transverse interaction between two electrons moving in an arc of a circle

We will now discuss the case of a two-particle system during the passage from a straight path to a circular one and from a circular path to a straight one. The four possible cases are sketched in Fig. 4.6 for the case in which the test particle is in front of the source.

The case in which both particles are in the bend, depicted in Fig. 4.6b, has already been discussed in Section 4.2.2. Moreover, note that the situation in which the source particle is ahead of the test electron can be treated immediately for all three (a, c and d) transient cases in Fig. 4.6 (of course, with respect to the figure, test and source particle exchange roles) on the basis of Eq. (4.17). In fact in such a case, we can assume the retarded angle $\phi$ small enough (the test particle "runs against" the electromagnetic signal) so that the actual trajectory followed by the particles is not essential and one can use Eq. (4.17) to describe also the transient cases. Now, the important contribution from the source particle comes from the acceleration part of the Liénard-Wiechert fields. Then, within our approximations, the only non-negligible contribution is constant and identical to the one in Eq. (4.17), and it is present in the situation (again, with the roles of test and source particle inverted) depicted in Fig. 4.6a only (Fig. 4.6b is the already discussed steady-state case). We will discuss more extensively the consequences of this fact in Section 4.2.5.

Let us now focus on the cases in which the source particle is behind the test particle and, in particular, let us first deal with the case in Fig. 4.6a; such a situation occurs when the following condition is met (see [8]):

$$\Delta \hat{s} > \frac{\hat{\eta}}{2} + \frac{\hat{\eta}^3}{24}. \tag{4.30}$$

Let us designate with $y$ the distance, along the straight line before the bend, between the retarded source particle and the beginning of the magnet. The retardation condition, in its approximated form, reads (see [8]):

$$\Delta \hat{s} \simeq \frac{\hat{\eta} + \hat{y}}{2} + \frac{\hat{\eta}^3}{24} \frac{\hat{\eta} + 4\hat{y}}{\hat{\eta} + \hat{y}}, \tag{4.31}$$

where we introduced the normalized quantity $\hat{y} = y\gamma/R$, which is just $y/R$ normalized to the synchrotron radiation formation angle, $1/\gamma$.

In the situation considered, the source particle is only responsible for a velocity contribution, therefore $F_\perp = F_{\perp C}$. By direct use of Eq. (4.3), one can find the exact expression for $F_\perp$:

$$F_\perp = \frac{e^2}{4\pi\varepsilon_0\gamma^2} \frac{\beta^2 R(1 - \cos\eta) - \beta\sin\eta[(y + R\sin\eta)^2 + R^2(1 - \cos\eta)^2]^{1/2} + R - R\cos\eta + y\sin\eta}{\{[(y + R\sin\eta)^2 + R^2(1 - \cos\eta)^2]^{1/2} - \beta y - R\beta\sin\eta)^3\}}. \tag{4.32}$$

Expanding the trigonometric functions in Eq. (4.32) and using normalized quantities one finds:

$$F_\perp \simeq \frac{e^2}{4\pi\varepsilon_0} \frac{4\gamma^3}{R^2} \hat{\eta}(\hat{y} + \hat{\eta})^2 \frac{\hat{y}^2 + \hat{y}(\hat{\eta} + \hat{\eta}^3/2) + \hat{\eta}^4/4}{[(\hat{y} + \hat{\eta})^2 + \hat{\eta}^4/4]^3}. \tag{4.33}$$

It can be easily verified that, as it must be, Eq. (4.33) reduces to Eq. (4.9) in the limit $y \to 0$.

It is now possible, by means of Eq. (4.33), to plot the normalized transverse force $\hat{F} = F_\perp/[e^2/(4\pi\varepsilon_0 R\Delta s)]$ as a function of the position after injection (defined by the entrance of the test particle in the hard-edge magnet) for different values of $\Delta\hat{s} = \Delta s\gamma^3/R$. In Fig. 4.7 we compared such a plot with numerical results from the code TraFiC$^4$ (see [1]).

Note that, at the position which corresponds to the entrance of the retarded source in the magnet there is a discontinuity in the plots. This is linked to our model choice, and it is due to the abrupt (hard edge magnet) switching on of the acceleration fields.

As general remark to Fig. 4.7 (and to the following ones) it might be worthwhile to stress that the perfect agreement (with graphical accuracy) between our calculations and numerical results by TraFiC$^4$ provides, *per se*, an excellent cross-check between analysis and simulations, which enhance one's level of confidence on both these approaches.

Let us now consider the case depicted in Fig. 4.6c, in which the source particle has its retarded position inside the bend and the test particle has its present position in the straight line following the magnet. We will define with $x$ the distance, along the straight line after the magnet, between the end of the bend and the present position of the test particle. In this situation the following condition is verified (see [8]):
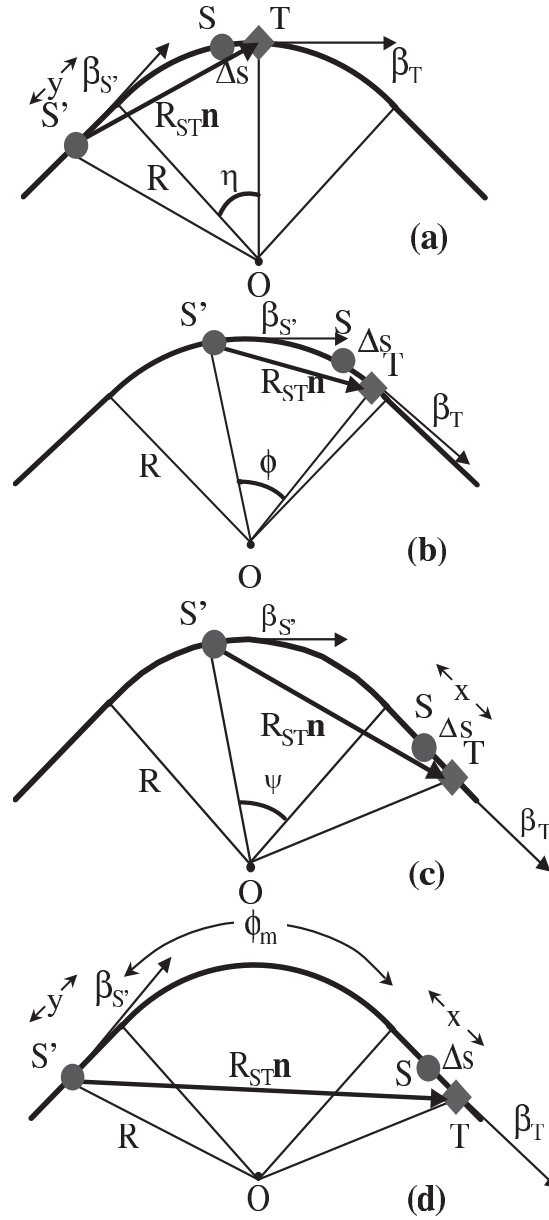
**Figure 4.6:** *Relative configuration of the retarded source point S' and the test point T for a system of two electron passing a bending magnet.*

**Figure 4.7:** *Normalized transverse force ($\hat{F} = F_\perp/[e^2/(4\pi\varepsilon_0 R\Delta s)]$) for a two-particle system entering a hard-edge bending magnet as a function of the position after injection. The solid lines show analytical results; the circles describe the outcome from TraFiC$^4$. We plotted several outcomes from different values of the normalized distance between the two particles.*

$$\Delta\hat{s} < \frac{\hat{\phi}_\mathrm{m} + \hat{x}}{2} + \frac{\hat{\phi}_\mathrm{m}^3}{24}\frac{\hat{\phi}_\mathrm{m} + 4\hat{x}}{\hat{\phi}_\mathrm{m} + \hat{x}}, \tag{4.34}$$

where $\hat{\phi}_\mathrm{m} = \gamma\phi_\mathrm{m}$, $\phi_\mathrm{m}$ being the angular extension of the magnet, and $\hat{x} = \gamma x/R$ (the reason for this normalization choice for $x$ is identical to that for $y$) .

The retardation condition reads

$$\Delta\hat{s} \simeq \frac{\hat{\psi} + \hat{x}}{2} + \frac{\hat{\psi}^3}{24}\frac{\hat{\psi} + 4\hat{x}}{\hat{\psi} + \hat{x}}. \tag{4.35}$$

In contrast with the case of Fig. 4.6a, here we have contributions from both velocity and acceleration field. Again, by direct use of Eq. (4.3) and Eq. (4.4) one can find the exact expression for the transverse electromagnetic force exerted by the source particle on the test particle

$$F_\perp = F_{\perp\mathrm{C}} + F_{\perp\mathrm{R}} , \tag{4.36}$$

where

$$F_{\perp\mathrm{C}} = \frac{e^2}{4\pi\varepsilon_0\gamma^2} \frac{R(1 - \cos\psi)(1 - \beta^2\cos\psi) - \beta\sin\psi\left[\left((x + R\sin\psi)^2 + R^2(1 - \cos\psi)^2\right)^{1/2} - \beta x - \beta R\sin\psi\right]}{\left[\left((x + R\sin\psi)^2 + R^2(1 - \cos\psi)^2\right)^{1/2} - \beta x\cos\psi - \beta R\sin\psi\right]^3}$$

$$\tag{4.37}$$

and

$$
F_{\perp\mathrm{R}} = \frac{e^2}{4\pi\varepsilon_0} \frac{\beta^2}{R} \left\{ \frac{-\cos\psi \left[ \left((x + R\sin\psi)^2 + R^2(1 - \cos\psi)^2\right)^{1/2} - \beta x - \beta R\sin\psi \right] - \beta R(1 - \cos\psi)\sin\psi}{\left[ \left((x + R\sin\psi)^2 + R^2(1 - \cos\psi)^2\right)^{1/2} - \beta x\cos\psi - \beta R\sin\psi \right]^2} \right.
$$

$$
+ \frac{(R + x\sin\psi - R\cos\psi)}{\left[ \left((x + R\sin\psi)^2 + R^2(1 - \cos\psi)^2\right)^{1/2} - \beta x\cos\psi - \beta R\sin\psi \right]^3} \left[ R(1 - \cos\psi)(1 - \beta^2\cos\psi) \right.
$$

$$
\left. \left. - \beta\sin\psi \left[ \left((x + R\sin\psi)^2 + R^2(1 - \cos\psi)^2\right)^{1/2} - \beta x - \beta R\sin\psi \right] \right] \right\} .
$$

$$(4.38)$$

Expanding the trigonometric functions in Eq. (4.37) and Eq. (4.38), and using normalized quantities one finds:
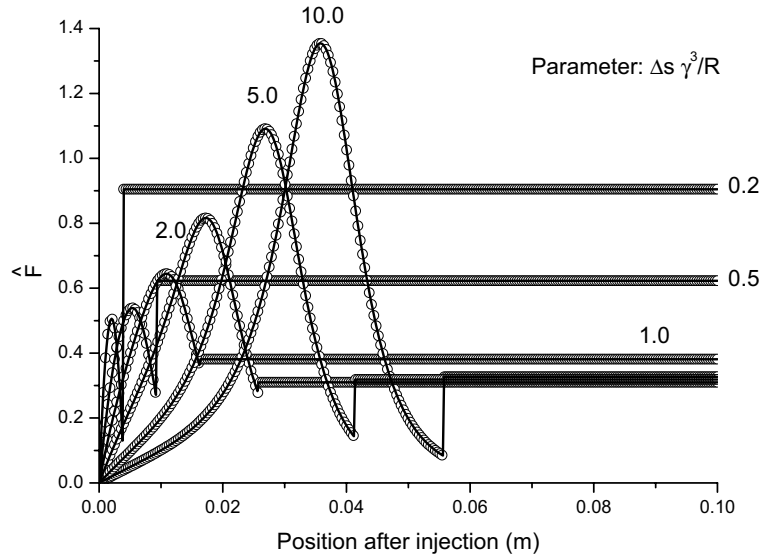


**Figure 4.8:** *Normalized transverse force* ($\hat{F} = F_\perp / [e^2/(4\pi\varepsilon_0 R\Delta s)]$) *for a two-particle system leaving a hard-edge bending magnet as a function of the position after the ejection. The solid lines show analytical results; the circles describe the outcome from* TraFiC[4]. *We plotted several outcomes from different values of the normalized distance between the two particles.*

$$
F_{\perp\mathrm{C}} = \frac{2e^2\gamma^3}{4\pi\varepsilon_0 R^2} \hat{\psi}(\hat{x} + \hat{\psi})^2 \frac{-2\hat{x}^2 + \hat{x}\left(\hat{\psi}^3 - 2\hat{\psi}\right) + \hat{\psi}^4/2}{\left[ (\hat{x} + \hat{\psi})^2 + (\hat{\psi}^2/4)(2\hat{x} + \hat{\psi})^2 \right]^3} \tag{4.39}
$$

and

$$F_{\perp\mathrm{R}} = \frac{2e^2\gamma^3}{4\pi\varepsilon_0 R^2}(\hat{x}+\hat{\psi})\left\{ \frac{\hat{x}^2 + \hat{x}\hat{\psi}(2-\hat{\psi}^2) + \hat{\psi}^2 - 3/4\hat{\psi}^4}{\left[(\hat{x}+\hat{\psi})^2 + (\hat{\psi}^2/4)(2\hat{x}+\hat{\psi})^2\right]^2} \right.$$

$$\left. + \frac{(\hat{x}+\hat{\psi})(\hat{x}+\hat{\psi}/2)\hat{\psi}^2\left[-2\hat{x}^2 + \hat{x}\hat{\psi}(-2+\hat{\psi}^2) + \hat{\psi}^4/2\right]}{\left[(\hat{x}+\hat{\psi})^2 + (\hat{\psi}^2/4)(2\hat{x}+\hat{\psi})^2\right]^3} \right\} . \tag{4.40}$$

Similarly to the latter case, it can be easily verified that Eq. (4.39) and Eq. (4.40) reduce to Eq. (4.9) and Eq. (4.10), respectively, in the limit $x \to 0$. Again, it is possible to plot the normalized transverse force $\hat{F}$ (defined above) as a function of the position after the ejection (defined by the exit of the test particle from the hard-edge magnet) for different values of $\Delta\hat{s} = \Delta s\gamma^3/R$. In Fig. 4.8 we compared such a plot with numerical results from TraFiC$^4$.

Again, at the position which corresponds to the exit of the retarded source from the magnet there is a discontinuity in the plots. This is linked to our model choice, and it is due to the fact that, for particles on axis, when the retarded source leaves the magnet there is only Coulomb repulsion directed along the longitudinal direction.
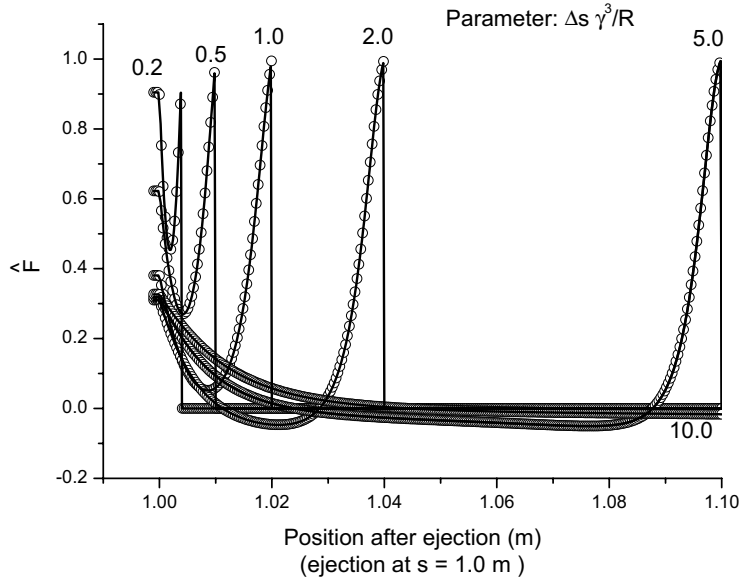


**Figure 4.9:** *Normalized transverse force ($\hat{F} = F_{\perp}/[e^2/(4\pi\varepsilon_0 R\Delta s)]$) for a two-particle system crossing a hard-edge bending magnet as a function of the position of the test particle inside the magnet in the case of a short magnet $\phi_{\mathrm{m}} \ll 1$. The solid lines show analytical results; the circles describe the outcome from TraFiC$^4$. Here the normalized distance between the two particles is $\Delta\hat{s} = 0.2$. We plotted several outcomes from different values of the normalized magnet angle $\hat{\phi}_{\mathrm{m}} = 0.1, 0.2, 0.3, 0.4, 0.5, 1.0$.*

The last case left to discuss is depicted in Fig. 4.6d; the source particle has its

retarded position in the straight line before the bend, and the test particle has its present position in the straight line following the magnet. This case occurs when

$$\Delta\hat{s} > \frac{\hat{\phi}_{\mathrm{m}} + \hat{x}}{2} + \frac{\hat{\phi}_{\mathrm{m}}^3}{24}\frac{\hat{\phi}_{\mathrm{m}} + 4\hat{x}}{\hat{\phi}_{\mathrm{m}} + \hat{x}}. \tag{4.41}$$

The retardation condition reads

$$\Delta\hat{s} \simeq \frac{\hat{\phi}_{\mathrm{m}} + \hat{x} + \hat{y}}{2} + \frac{\hat{\phi}_{\mathrm{m}}^3}{24}\frac{\hat{\phi}_{\mathrm{m}} + 4(\hat{x} + \hat{y}) + 12\hat{x}\hat{y}/\hat{\phi}_{\mathrm{m}}}{\hat{\phi}_{\mathrm{m}} + \hat{x} + \hat{y}} \ . \tag{4.42}$$

In this case we have only velocity contributions. The exact expression for the electromagnetic transverse force on the test particle is

$$F_\perp = \frac{e^2}{4\pi\varepsilon_0\gamma^2}\Big\{(R + y\sin\phi_{\mathrm{m}} - R\cos\phi_{\mathrm{m}})(1 - \beta^2\cos\phi_{\mathrm{m}}) - \beta\sin\phi_{\mathrm{m}}\Big[\big(2R^2 + x^2$$
$$+y^2 + \cos\phi_{\mathrm{m}}(2xy - 2R^2) + 2R(x + y)\sin\phi_{\mathrm{m}}\big)^{1/2} - \beta(x + y\cos\phi_{\mathrm{m}} + R\sin\phi_{\mathrm{m}})\Big]\Big\}$$
$$\times\Big\{\big[2R^2 + x^2 + y^2 + 2\cos\phi_{\mathrm{m}}(xy - R^2) + 2R(x + y)\sin\phi_{\mathrm{m}}\big]^{1/2} - \beta\cos\phi_{\mathrm{m}}$$
$$\times(x + y\cos\phi_{\mathrm{m}} + R\sin\phi_{\mathrm{m}}) - \beta\sin\phi_{\mathrm{m}}(R + y\sin\phi_{\mathrm{m}} - R\cos\phi_{\mathrm{m}})\Big\}^{-3}. \tag{4.43}$$

Expanding the trigonometric functions in Eq. (4.43) and using normalized quantities one finds the following approximated expression for $F_\perp$:

$$F_\perp \simeq \frac{e^2}{4\pi\varepsilon_0 R^2}8\gamma^3(\hat{x} + \hat{y} + \hat{\phi}_{\mathrm{m}})^2\hat{\phi}_{\mathrm{m}}\big\{-\hat{x}^2/2 + \hat{y}^2/2 + (\hat{\phi}_{\mathrm{m}}^2/2)\hat{x}\hat{y}$$
$$+\hat{x}(\hat{\phi}_{\mathrm{m}}^3/4 - \hat{\phi}_{\mathrm{m}}/2) + \hat{y}(\hat{\phi}_{\mathrm{m}}^3/4 + \hat{\phi}_{\mathrm{m}}/2) + \hat{\phi}_{\mathrm{m}}^4/8\big\}\big\{(\hat{x} + \hat{y} + \hat{\phi}_{\mathrm{m}})$$
$$\times\Big[\hat{x}(1 + \hat{\phi}_{\mathrm{m}}^2) + \hat{y} + \hat{\phi}_{\mathrm{m}} + \hat{\phi}_{\mathrm{m}}^3/3\Big] - (\hat{\phi}_{\mathrm{m}}^2/12)[12\hat{x}\hat{y} + 4(\hat{x} + \hat{y})\hat{\phi}_{\mathrm{m}} + \hat{\phi}_{\mathrm{m}}^2]\big\}^{-3} \ .$$
$$\tag{4.44}$$

It is easy to verify that Eq. (4.44) reduces, respectively, to Eq. (4.9) when $x = 0$ and $y = 0$, to the transient case in Fig. 4.6a when $x = 0$ (Eq. (4.33)) and to the transient case in Fig. 4.6c when $y = 0$ (Eq. (4.39)). Following the treatment of the transient situations in Fig. 4.6a and in Fig. 4.6c it is possible to plot, for this case too, a normalized expression for the transient force, i.e. the usual $\hat{F}$, as a function of the curvilinear position of the test particle (s=0 indicates the entrance of the magnet) for different values of $\Delta\hat{s} = \Delta s\gamma^3/R$ and for different magnet lengths. In Fig. 4.9, Fig. 4.10 and Fig. 4.11 we compared our analytical results with numerical results from TraFiC[4], for the cases $\Delta\hat{s} = 0.2$, $\Delta\hat{s} = 1.0$ and $\Delta\hat{s} = 5.0$ respectively.

## 4.2.5 Transverse interaction between an electron and a bunch entering a bend from a straight path

In the previous Section 4.2.4 we dealt with all the possible configurations for a two-particle system moving in an arc of a circle. Now, one can consider a bunch moving on the same trajectory and calculate the transverse force on a test particle as the sum of contributions from all the source particles within the bunch.
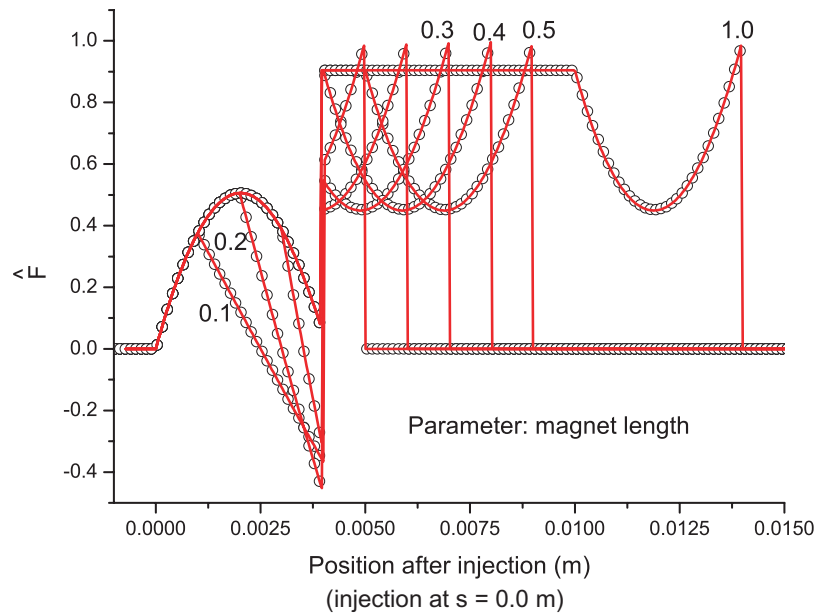
**Figure 4.10:** *Normalized transverse force ($\hat{F} = F_\perp/[e^2/(4\pi\varepsilon_0 R\Delta s)]$) for a two-particle system crossing a hard-edge bending magnet as a function of the position of the test particle inside the magnet in the case of a short magnet $\phi_m \ll 1$. The solid lines show analytical results; the circles describe the outcome from TraFiC$^4$. Here the normalized distance between the two particles is $\Delta\hat{s} = 1.0$. We plotted several outcomes from different values of the normalized magnet angle $\hat{\phi}_m = 0.1, 0.2, 0.5, 1.0, 1.5, 2.0$.*

As an example, we will study here the case of a bunch entering a long bending magnet. Such a case is important, as mentioned before, for code benchmark purposes and for direct application in restricted regions of parameters (negligible transverse bunch size and bunch energy spread).

**Head-Tail interaction.** First we will analyze the case of a bunch with rectangular density function, and we will assume the test particle to be behind the bunch. Such an analysis will be performed using our line model and it is therefore valid only for transverse dimension of the bunch much smaller than the distance between the test particle and the bunch $\Delta s_{min}$. After the discussions, in Section 4.2.2 and 4.2.4, about a two-particle system with the test particle behind the source electron, one is led to conclude that, within an electron bunch, interactions between sources in front of the test particle and the test particle itself are important and, in general, they must be responsible, at the entrance and at the exit of the bending magnet, for sharp changes in the transverse forces acting on the test electron. The quantitative change depends, of course, on the position of the test particle inside the bunch: the extreme cases are for the test particle at the head of the bunch, where there are just interactions with electrons behind the test particle (no head-tail interactions), and for the test particle at the tail of the bunch, where all the sources are in front of it (only head-tail
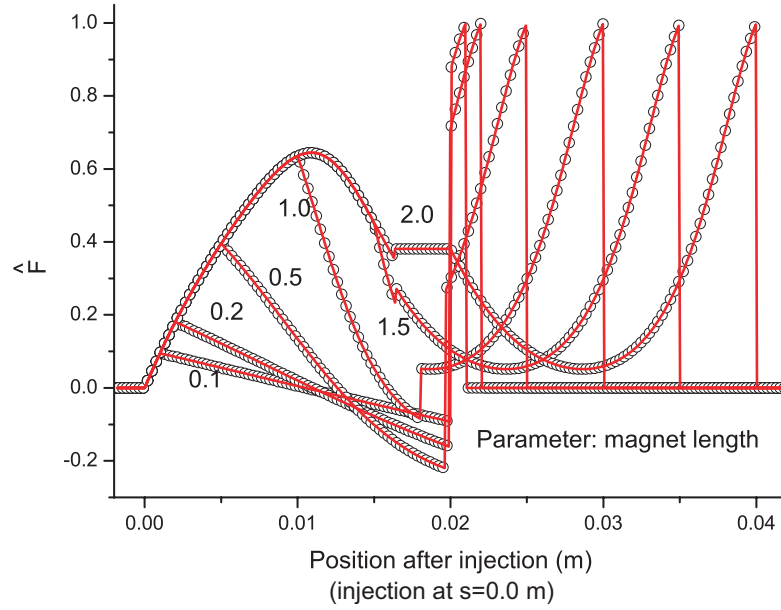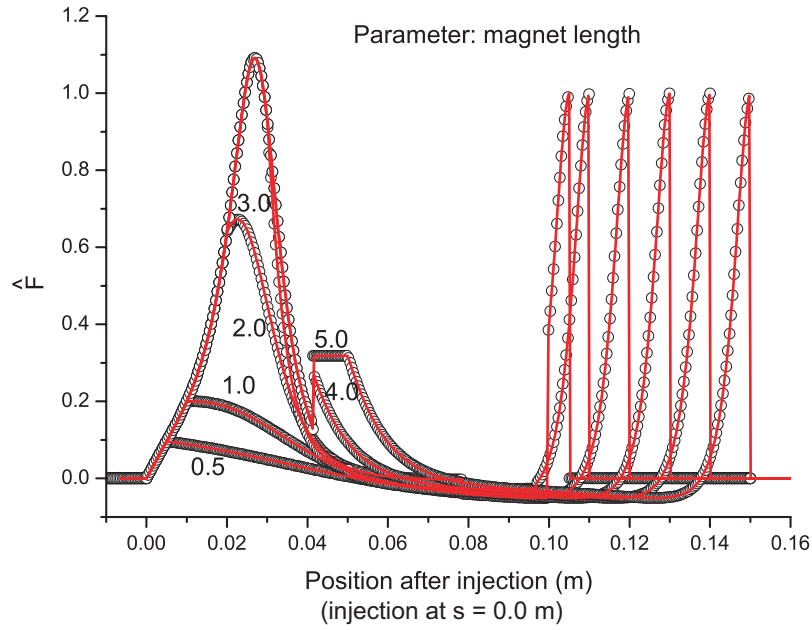
**Figure 4.11:** *Normalized transverse force ($\hat{F} = F_\perp/[e^2/(4\pi\varepsilon_0 R\Delta s)]$) for a two-particle system crossing a hard-edge bending magnet as a function of the position of the test particle inside the magnet in the case of a short magnet $\phi_m \ll 1$. The solid lines show analytical results; the circles describe the outcome from TraFiC$^4$. Here the normalized distance between the two particles is $\Delta\hat{s} = 5.0$. We plotted several outcomes from different values of the normalized magnet angle $\hat{\phi}_m = 0.5,\ 1.0,\ 2.0,\ 3.0,\ 4.0,\ 5.0$.*

interactions). It may be worthwhile to underline that the sharp jumps in the transverse force are expected to take place in a space interval comparable, at most, with half of the bunch length in the case of the test electron at the tail of the bunch. In order to show this, one can easily calculate the transverse force acting on a test particle behind a bunch with rectangular density distribution entering a hard-edge magnet. If, as usual, we indicate with $\Delta s_{\max}$ the distance from the test particle to the head of the bunch and with $\Delta s_{\min}$ the distance from the test particle to the tail of the bunch (both understood as positive quantities), then one can easily derive such an expression from Eq. (4.16) and Eq. (4.17):

$$
F_{\perp\ \mathrm{HT}}^{\mathrm{B}}(y) \simeq
\begin{cases}
0 & y > \Delta s_{\max}/(1+\beta) \\[2ex]
\frac{e^2\lambda_0}{4\pi\varepsilon_0 R}\ \ln\left[\frac{\Delta s_{\max}}{y(1+\beta)}\right] & \Delta s_{\min}/(1+\beta) < y < \Delta s_{\max}/(1+\beta) \\[2ex]
\frac{e^2\lambda_0}{4\pi\varepsilon_0 R}\ \ln\left[\frac{\Delta s_{\max}}{\Delta s_{\min}}\right] & y < \Delta s_{\min}/(1+\beta)
\end{cases}
,
$$

$$(4.45)$$

where "HT" stands for "head-tail" and $y$ is the (positive) distance of the test particle from the magnet entrance.



**Figure 4.12:** *Normalized transverse force $F_\perp/f_1$ acting on a test particle behind a bunch with rectangular density distribution. As the bunch enters a hard-edge bending magnet we plot the normalized force as a function of the position of the test particle inside the magnet (solid line) and we compare with results by TraFiC⁴ (circles). The parameter choices are: bunch length $= 100~\mu m$, $\gamma = 100$, $R = 1$ m; the value of $\Delta s_{\min}$ is $1~\mu m$.*

The following step is to actually plot the transverse force in Eq. (4.45). It is convenient to choose, as normalization factor for the transverse force, the value $f_1 = e^2\lambda_0/(4\pi\varepsilon_0 R)\ln[\Delta s_{\max}/\Delta s_{\min}]$. Our results, compared once again with simulations by `TraFiC`⁴, are shown in Fig. 4.12 for a bunch length $\Delta s_{\max} - \Delta s_{\min} = 100~\mu m$, $\gamma = 100$, $R = 1$ m and for $\Delta s_{\min} = 1~\mu m$. This means that, according to the validity limits of our model, this result can be applied only when $h \ll 1~\mu m$. Nevertheless, this simple example shows that the code `TraFiC`⁴ is actually able to account for head-tail interactions. Note that, as expected, the transient has a spatial extent of about one half of the bunch length ($\Delta s_{\max}/(1+\beta)$).

**Tail-Head interaction.** We will now analyze the case of a bunch with rectangular density function with the test particle in front of the bunch, as depicted in Fig. 4.5. In the injection case we have contributions from retarded sources both in the bend and in the straight line before the bend. The contribution from the retarded sources in the magnet is given, basically, by Eq. (4.23), and reads

$$F_{\perp m}^{B} \simeq \frac{e^2\lambda_0}{4\pi\varepsilon_0 R}\left[\ln\left(\frac{\hat{\phi}_{\max}}{\hat{\phi}_{\min}}\right) + \frac{4}{4+\hat{\phi}_{\max}^2} - \frac{4}{4+\hat{\phi}_{\min}^2}\right]~,\qquad(4.46)$$

where "m" reminds that the contributions treated by Eq. (4.46) are all from the "magnet". All that is left to do now, is the investigation of the values which $\hat{\phi}_{\min}$ and $\hat{\phi}_{\max}$ assume. Let us first define with $\hat{\phi}^*$ the solution of the retardation equation $\Delta\hat{s}_{\min} = \hat{\phi}^*/2 + \hat{\phi}^{*3}/24$. Then let us remember that $\hat{\eta}$ indicates the normalized angular position of the test particle inside the bending magnet. If $\hat{\phi}^* < \hat{\eta}$, the retarded position of the first source particle is in the bending magnet, and $\hat{\phi}_{\min} = \hat{\phi}^*$. On the other hand, when $\hat{\phi}^* > \hat{\eta}$ there are no contributions to the transverse force from the bend. Next, we define with $\hat{\phi}^{**}$ the solution of $\Delta\hat{s}_{\max} = \hat{\phi}^{**}/2 + \hat{\phi}^{**3}/24$. Supposing $\hat{\phi}^* < \hat{\eta}$, if $\hat{\phi}^{**} < \hat{\eta}$ too, then all the particles contribute from the bend, and $\hat{\phi}_{\max} = \hat{\phi}^{**}$. On the other hand, when $\hat{\phi}^{**} > \hat{\eta}$, we have a mixed situation, in which part of the particles contribute from the bend and others from the straight line before the magnet. In this case $\hat{\phi}_{\max} = \hat{\eta}$.

The contribution from the retarded sources in the straight path before the bend is given by

$$F_{\perp s}^{B} = \lambda_0 \int_{\Delta\hat{s}_1}^{\Delta\hat{s}_2} \frac{R}{\gamma^3} F_{\perp}(\hat{y}(\Delta\hat{s}, \hat{\eta}), \hat{\eta}) d\Delta\hat{s} \ , \qquad (4.47)$$

where "s" stands for "straight path", and where the expression for $F_{\perp}$ in the integrand is given by Eq. (4.33). It is convenient, as done before, to switch the integration variable from $\Delta\hat{s}$ to $\hat{y}$. The Jacobian of the transformation is given by

$$\frac{d\Delta\hat{s}}{d\hat{y}} \simeq \frac{(\hat{\eta} + \hat{y})^2 + \hat{\eta}^4/4}{2(\hat{\eta} + \hat{y})^2} \ . \qquad (4.48)$$

After substitution of Eq. (4.48) and Eq. (4.33) in Eq. (4.47), one can easily carry out the integration, thus getting

$$F_{\perp s}^{B} \simeq \frac{2e^2\lambda_0}{4\pi\varepsilon_0 R} \left[ \frac{\hat{\eta}\,(4\hat{y}_{\min} + 2\hat{\eta} + \hat{\eta}^3)}{4\hat{y}_{\min}^2 + 8\hat{y}_{\min}\hat{\eta} + 4\hat{\eta}^2 + \hat{\eta}^4} - \frac{\hat{\eta}\,(4\hat{y}_{\max} + 2\hat{\eta} + \hat{\eta}^3)}{4\hat{y}_{\max}^2 + 8\hat{y}_{\max}\hat{\eta} + 4\hat{\eta}^2 + \hat{\eta}^4} \right] \ . \qquad (4.49)$$

As done before for $\hat{\phi}_{\min}$ and $\hat{\phi}_{\max}$, we can now investigate the values of $\hat{y}_{\min}$ and $\hat{y}_{\max}$. Let us start with $\hat{y}_{\min}$. First, we define with $\hat{y}^*$ the solution of the retardation condition $\Delta\hat{s}_{\min} = (\hat{\eta} + \hat{y}^*)/2 + (\hat{\eta}^3/24)(4\hat{y}^* + \hat{\eta})/(\hat{y}^* + \hat{\eta})$. If $\hat{y}^* > 0$, the retarded position of the first source particle is in the straight line before bending magnet, and $\hat{y}_{\min} = \hat{y}^*$. On the other hand, when $\hat{y}^* < 0$, the retarded position of the first source particle is in the bend, and $\hat{y}_{\min} = 0$.

Next, we define with $\hat{y}^{**}$ the solution of $\Delta\hat{s}_{\max} = (\hat{\eta} + \hat{y}^{**})/2 + (\hat{\eta}^3/24) \times (4\hat{y}^{**} + \hat{\eta})/(\hat{y}^{**} + \hat{\eta})$. Consider the case $\hat{y}^{**} < 0$: all the particles contribute from the bend, that is we entered the steady-state situation. In this case $\hat{y}_{\max} = \hat{y}_{\min} = 0$. On the other hand, when $\hat{y}^{**} > 0$, we have again a mixed situation, in which part of the particles contribute from the bend and others from the straight line before the magnet. In this case $\hat{y}_{\max} = \hat{y}^{**}$.

The following step is to actually plot the transverse force on an electron from a bunch with rectangular distribution entering a long bend. It is convenient to choose, as normalization factor for the transverse force, the value $f = e^2\lambda_0/(4\pi\varepsilon_0 R)\ln(\Delta\hat{s}_{\max})$. Our results, compared, once again, with simulations by TraFiC[4], are shown in Fig. 4.13 for a bunch length of 100 $\mu$m, $\gamma = 100$, $R = 1$ m and for different values of $\Delta\hat{s}_{\min}$.

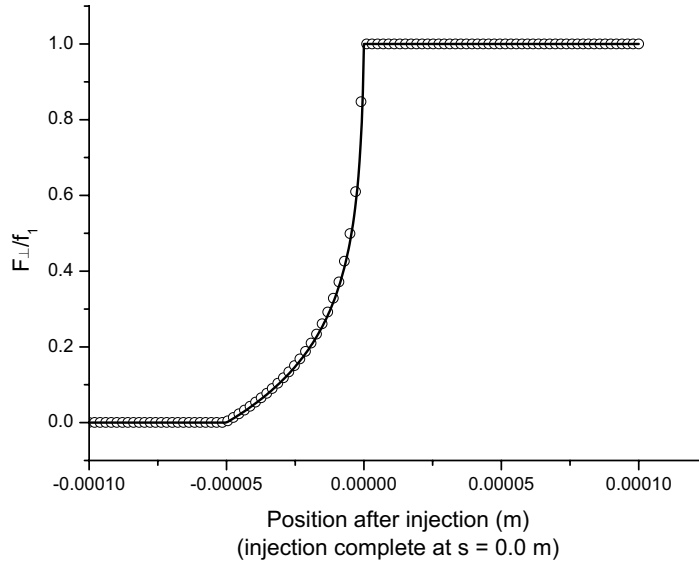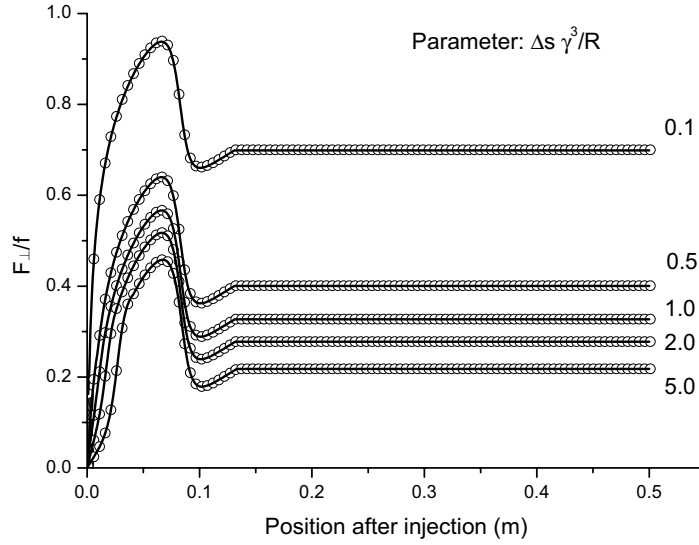**Figure 4.13:** *Normalized transverse force $(F_\perp/f)$ acting on a test particle from a bunch with rectangular density distribution entering a hard-edge bending magnet as a function of the position of the test particle inside the magnet. The solid lines show analytical results; the circles describe the outcome from TraFiC⁴. We chose $\Delta s_{\mathrm{max}} = 100~\mu m$, $\gamma = 100$, $R = 1$ m; graphs are plotted for several values of the parameter $\Delta \hat{s}_{\mathrm{min}}$.*

It is interesting to calculate the asymptotic expression for $F_{\perp\mathrm{s}}^{\mathrm{B}}$ in the limit for a long bunch ($\Delta \hat{s}_{\mathrm{max}} \gg 1$) and for a short distance between the test particle and the head of the bunch ($\Delta \hat{s}_{\mathrm{min}} \ll 1$). First let us indicate with $\hat{\phi}_{\mathrm{b}}$ the solution of the retardation condition for the circular motion, so that within our approximations $\hat{\phi}_{\mathrm{b}} \simeq (24\Delta \hat{s}_{\mathrm{max}})^{1/3}$. By means Eq. (4.31) it is easy to prove that, when $\hat{\eta}$ decreases, $\hat{y}_{\mathrm{max}}$ takes bigger and bigger values, with an upper limit $\hat{y}_{\mathrm{max}} = 2\Delta \hat{s}_{\mathrm{max}}$. On the other hand, when $\hat{\eta}$ increases, $\hat{y}_{\mathrm{max}}$ takes always decreasing values, with a lower limit $\hat{y}_{\mathrm{max}} = 0$. Assuming $\hat{y}_{\mathrm{min}} \ll 1$, one may check that, in the long bunch limit, Eq. (4.49) reads

$$F_{\perp\mathrm{s}}^{\mathrm{B}} \simeq \begin{cases} e^2\lambda_0/(2\pi\varepsilon_0 R) & \hat{\eta}/\hat{\phi}_{\mathrm{b}} < 2^{-2/3} \\ 0 & \hat{\eta}/\hat{\phi}_{\mathrm{b}} > 2^{-2/3} \end{cases}, \tag{4.50}$$

which is a boxcar function. Note that in the passage from Eq. (4.49) to Eq. (4.50) we used the fact that $\hat{\eta} \gg 1$. In order to visualize the limiting process we plotted, in Fig. 4.14, $F_{\perp\mathrm{s}}^{\mathrm{B}}$, as it is given in Eq. (4.49) and normalized to $f = e^2\lambda_0/(4\pi\varepsilon_0 R)\ln(\Delta \hat{s}_{\mathrm{max}})$ (i.e. $v = F_{\perp\mathrm{s}}^{\mathrm{B}}/f$, in the plot), as a function of the position after injection, normalized to $\hat{\phi}_{\mathrm{b}}$ (i.e. $u = R\hat{\eta}/(\gamma\hat{\phi}_{\mathrm{b}})$, in the plot). The plots in Fig. 4.14a, b, c and d refer to different bunch lengths (respectively $10^2\mu m$, $10^3\mu m$, $10^4\mu m$ and $10^5\mu m$). For every choice of the bunch length we show different outcomes for several choices of $\Delta \hat{s}_{\mathrm{min}}$. As one can see from Fig. 4.14, in the limit for $\Delta \hat{s}_{\mathrm{min}} \ll 1$ and $\Delta \hat{s}_{\mathrm{max}} \gg 1$, one approaches the boxcar function described by Eq. (4.50). Note that, here, the radius of the bend is

$R = 1$ m and $\gamma = 100$, therefore we have $2^{-2/3}R/\gamma \simeq 6.3 \cdot 10^{-3}$ m, while the maximum value for $v$, due to the normalization choice, is given, from Eq. (4.50), by $2/\ln(\Delta\hat{s}_{\max})$. In the case of Fig. 4.14d, for example, we have $2/\ln(\Delta\hat{s}_{\max}) \simeq 0.174$ (in agreement, of course, with the maximum value found in the plot).
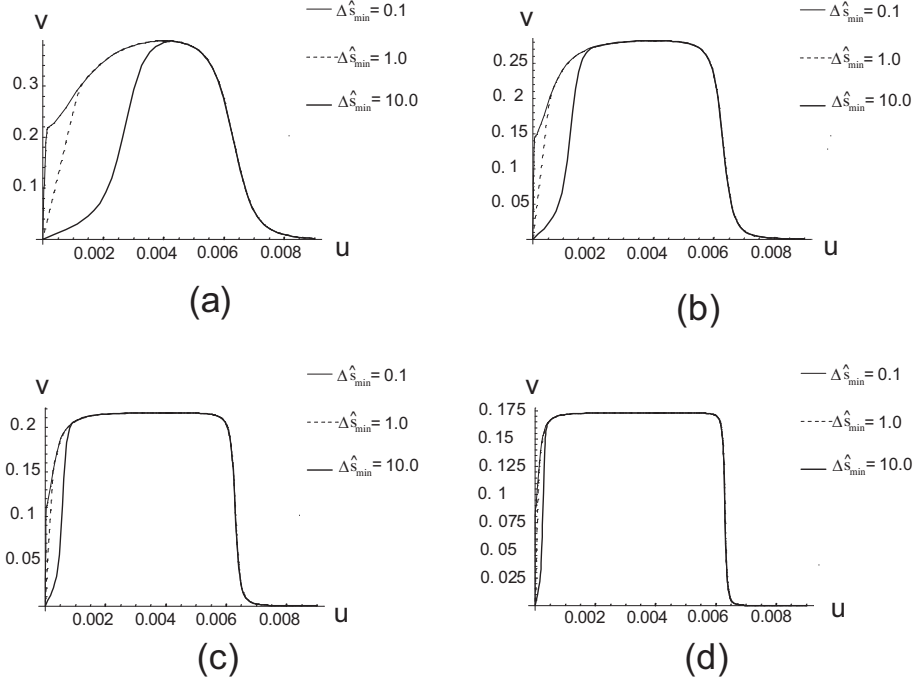


**Figure 4.14:** *Plot of $v = F_{\perp s}^{B}/f$ as a function of $u = R\hat{\eta}/(\gamma\hat{\phi}_b)$; here $R = 1$ m and $\gamma = 100$. Case (a) the bunch length is $10^2$ $\mu m$, (b) $10^3$ $\mu m$, (c) $10^4$ $\mu m$ and (d) $10^5$ $\mu m$. Each case is parameterized with respect to different values of $\Delta\hat{s}_{\min} = \gamma^3 \Delta s_{\min}/R$ (see the legends in the plots).*

On the other hand, again in the same limits, one can find the asymptotic expression for the contribution from particles with retarded position in the bend: this is given, indeed, by Eq. (4.46), with the limit expressions for $\hat{\phi}_{\min}$ in the case of a small distance $\Delta\hat{s}_{\min}$, and for $\hat{\phi}_{\max}$ in the long bunch limit. For $\hat{\phi}_{\min}$ we have, from the retardation condition in Eq. (4.8) $\hat{\phi}_{\min} = 2\Delta\hat{s}_{\min}$. For $\hat{\phi}_{\max}$, if $\Delta\hat{s}_{\max} < \hat{\eta}^3/24$ we have, again from the retardation condition, $\hat{\phi}_{\max} = \hat{\phi}_b = (24\Delta\hat{s}_{\max})^{1/3}$. Otherwise, when $\Delta\hat{s}_{\max} > \hat{\eta}^3/24$ we obtain $\hat{\phi}_{\max} = \hat{\eta}$.

By means of these results one can build an expression for the transverse force in the case of a bunch with general density distribution $\lambda$, by considering it as a composition of rectangular bunches with length $(s - s')$ and linear density $ds'd\lambda(s')/ds'$, under the constraint that the important bunches for such a composition are long enough to neglect all linear terms in the expression for the retardation condition (i.e. $\lambda(s)\gamma^3/R \gg d\lambda(s')/ds'$, see [8]). In this case, the contribution from particles in the straight line reads

$$F_{\perp s}^{\text{tot}} \simeq \int_{-\infty}^{s - R\eta^3/6} F_{\perp s}^{B}(\eta, s - s')\frac{d\lambda(s')}{ds'}ds' = \frac{e^2}{2\pi\varepsilon_0 R}\lambda(s - R\eta^3/6) \, . \qquad (4.51)$$

Note that the expression above does not depend on $\Delta s_{\min}$. On the other hand the contribution from particles in the bend is

$$F_{\perp m}^{\text{tot}} \simeq \int_{-\infty}^{s-s_{\min}} F_{\perp m}^{\text{B}}(\eta, s - s') \frac{d\lambda(s')}{ds'} ds'$$

$$= \frac{e^2}{2\pi\varepsilon_0 R} \int_{-\infty}^{s-s_{\min}} \frac{1}{2} \left[ -1 + \frac{1}{3} \ln\left( \frac{24\gamma^3}{R} \Delta s_{\max} \right) - \ln\left( \frac{2\gamma^3}{R} \Delta s_{\min} \right) \right] \frac{d\lambda(s')}{ds'} ds' \ , \ (4.52)$$

which, instead, depends on $\Delta s_{\min}$. It is very interesting to show that this dependence on $\Delta s_{\min}$ cancels with the dependence on $\Delta s_{\min}$ of the steady-state force: in fact this constitutes a general result independent from the choice of the position of the test particle. In order to show this, let us first note that Eq. (4.52) can be written as

$$F_{\perp m}^{\text{tot}} \simeq \frac{e^2}{4\pi\varepsilon_0 R} \left\{ \int_{s-\eta^3 R/24}^{s-s_{\min}} \left[ -1 + \ln(\hat{\phi}_{\text{b}}(s')) - \ln(\hat{\phi}_{\min}) \right] \frac{d\lambda(s')}{ds'} ds' \right.$$

$$\left. + \int_{-\infty}^{s-\eta^3 R/24} \left[ -1 + \ln(\hat{\eta}) - \ln(\hat{\phi}_{\min}) \right] \frac{d\lambda(s')}{ds'} ds' \right\} , \qquad (4.53)$$

while the steady state contribution is given by

$$F_{\perp \text{steady}}^{\text{tot}} \simeq \frac{e^2}{4\pi\varepsilon_0 R} \int_{-\infty}^{s-s_{\min}} \left[ -1 + \ln(\hat{\phi}_{\text{b}}(s')) - \ln(\hat{\phi}_{\min}) \right] \frac{d\lambda(s')}{ds'} ds' \ . \qquad (4.54)$$

Subtracting side by side Eq. (4.54) from Eq. (4.53), and adding the contribution from the straight path, one finally gets the following "regularized" expression for the transient transverse force:

$$\widetilde{F}_{\perp}^{\text{tot}} \simeq \frac{e^2}{2\pi\varepsilon_0 R} \left[ \lambda(s - R\eta^3/6) - \frac{1}{6} \int_{-\infty}^{s-R\eta^3/24} \ln\left( \frac{24(s-s')}{R\eta^3} \right) \frac{d\lambda(s')}{ds'} ds' \right] , \qquad (4.55)$$

which is completely independent from $\Delta s_{\min}$ and, therefore, free from singularity in the limit $\Delta s_{\min} \to 0$. It might be worthwhile to remark that usual regularization techniques take place, in the study of longitudinal (CSR) self-interactions (see Chapter 3 and [8]) at the stage of the two-particle system and *before* integration of the contributions from all the retarded sources within the bunch. The situation is reversed here, where regularization takes place *after* integration.

## 4.2.6 Summary and conclusions

In Section 4.2 we presented a fully electrodynamical study of transverse self-forces within an electron bunch moving in an arc of a circle. Our analysis is based on a line-bunch model. In the case of test particles in front of the source, our model is valid whenever $h \ll R/\gamma^2$, where $h$ indicates the transverse beam size. On the other hand, when the source electron is in front of the test electron, then the situation is more

complicated and the model can be applied only for $|\Delta s| \gg h$. The cases that do not fulfill these conditions are treated in the next Section.

In Section 4.2.2 we first studied the situation of a two-particle system moving on a circular path, finding an approximated expression for the transverse self-forces which is the product of a factor dependent on the parameters that specify the system setup and a universal function (i.e. a function independent of such parameters): for every distance between the particles we found a centrifugal force, which has a qualitative explanation by means of simple arguments from relativistic dynamics. We concluded that both the tail-head and head-tail interactions are important: in the first case the velocity interaction plays a role besides the acceleration one, while in the second only acceleration contributions are present.

Further on, in Section 4.2.3, after discussing the applicability region of our model, we integrated the results for a two-particle system, thus finding an expression for the transverse interaction between a line bunch and a particle in front of it. Such an expression is structured as the sum of a centrifugal logarithmic part and a centripetal term, of which we studied the asymptotic behaviors in the limit of short and long bunch, both with a small distance between the test particle and the bunch head.

In particular, in the limit of a short bunch, we found that the centripetal force tends to zero as $(\gamma\phi_{\max})^2$, while in the limit of a long bunch we found results already well known in literature. We were able to explain the constant centripetal term in the latter case as an overall effect of the transient between the asymptotic behavior (identical in $\phi$, different in $\Delta s$) of the transverse force in the two-particle system, respectively for small or long distance between the two electrons. We concluded that the centripetal term is therefore only of mathematical nature, and there is no physical ground to distinguish it from the centrifugal term: from a physical viewpoint there is, in fact, just an overall centrifugal force.

In Section 4.2.4, again within the region of applicability of our model, we extended our considerations to a two-particle system moving in an arc of a circle, thus finding, for the first time, both exact and approximated analytical expressions for the transverse force in all the possible transient configurations (see Fig. 4.6), including the case in which the source particle is in front of the test particle. Furthermore we plotted the expression for the transverse force in several practical cases, which are important for a quick evaluation of the magnitude of the effect and for cross-checks between computer codes. In particular we report a very good agreement with `TraFiC`[4], which demonstrates that such a code can deal, from a numerical viewpoint, with the transverse transient problem.

In Section 4.2.5, we analyzed the situation of the transverse interaction between a line bunch and a test particle moving in an arc of a circle. We treated, in particular, the case of the injection from a straight section into a hard-edge bending magnet. Firstly we calculated both exact and approximated expressions for the transverse force; secondly, following what we did in Section 4.2.4, we provided a few graphical examples; thirdly we analyzed our expressions in the limit for a long bunch and a short minimal distance between the test particle and the head of the bunch.

We showed that the contribution from the particles whose retarded positions are in the straight line before the bend is well described, as a function of the normalized angular position of the test particle inside the bend, by a boxcar function. By simple composition of rectangular bunches we provided an expression for the calculation of

the transverse interaction in the case of a long bunch with an arbitrary density distribution. We showed that, in the chosen limits, the contribution from the particles in the bend is independent from $\Delta s_{\min}$ and that, in contrast to this, the contribution from the particles in the straight line is dependent on $\Delta s_{\min}$. Finally we proved that such a dependence can be removed by subtraction of the steady-state transverse self-interaction, thus providing a "regularized" expression for $F_\perp$.

The case of injection provides a useful example for a quick evaluation of the transverse self-field magnitude as well as for computer codes benchmark. By means of the same approach one can analyze also the case of ejection, which is left to future work.

Before our study in Section 4.2 there was no explanation for the simulation results shown in Fig. 4.1. The work in Section 4.2 provides a qualitative explanation of these results: such qualitative character of the explanation is due to the fact that the model therein is one-dimensional, and does not allow any quantitative investigation when (as in Fig. 4.1) a vertical displacement is introduced. Still it was possible to demonstrate that the sharp feature near the injection point is due to interactions of the test particle with particles in front of it.

## 4.3    Transverse self-fields within an electron bunch with vertical extent moving in an arc of a circle

### 4.3.1   Introduction

In Section 4.2 we proposed a fully electrodynamical analysis of a bunch moving in an arc of a circle where, for the reasons explained in Section 4.1, we were not interested in the full evolution problem, but only in the electrodynamical one. We addressed the issue of understanding the electromagnetic interactions only in the framework of a 1D model.

In this Section we aim at an extension of the model proposed in Section 4.2 which allows a fully electrodynamical analysis of a bunch endowed with a vertical dimension. Since a bunch with vertical extent can be always thought of as a superposition of displaced charge lines, all the relevant physical aspects of the problem are included in the study of a simpler model, constituted by a one-dimensional line bunch and a test particle with vertical displacement, which is the situation studied in Fig. 4.1. In this Section, our explanation of the features in Fig. 4.1 will be refined to a quantitative level.

The work is organized as follows. We first treat, in Section 4.3.2, the transverse interaction between two particles moving in an arc of a circle, supposing that one of the two particles has a vertical displacement $h$ with respect to the source. By integration of our results we consider, in Section 4.3.3, a stepped-profile electron bunch interacting with a test particle with vertical displacement entering an arc of a circle and we discuss all the characteristic lengths involved. Finally, in Section 4.3.4, we come to a summary of the results obtained and to conclusions.

## 4.3.2 Transverse interaction between two electrons

We will first address the case of two electrons moving in an arc of a circle of radius $R$ in such a way that one of the two is displaced, with respect to the reference trajectory, by a quantity $h$ in the vertical (perpendicular to the bending plane) direction. We will see that, as concerns the interaction in the radial direction (in the bending plane) it does not matter which particle is endowed with this displacement.

The electromagnetic force which one of the two particles (designated with "T", i.e. the test particle) feels, due to the interaction with the other one (designated with "S", i.e. the source particle), is given by Eq. (4.1).

In contrast to the case studied in Section 4.2, the transverse (by definition, orthogonal to $\boldsymbol{\beta_T}$) projection of $\boldsymbol{F}(\boldsymbol{r_T}, t)$ has now components both in the bending plane and perpendicular to it. We will introduce, therefore, two unit vectors $\hat{\mathbf{e}}_\mathbf{h}$, in the direction perpendicular to the bending plane, and $\hat{\mathbf{e}}_\mathbf{p}$, in the radial direction, i.e. orthogonal to $\boldsymbol{\beta_T}$ and lying in the bending plane. Of course, the transverse component of $\boldsymbol{F}(\boldsymbol{r_T}, t)$ can still be written, following Section 4.2, as the sum of contributions from the velocity ("C", Coulomb) and the acceleration ("R", Radiation) fields, namely

$$\boldsymbol{F_\perp}(\boldsymbol{r_T}, t) = \boldsymbol{F_{\perp C}}(\boldsymbol{r_T}, t) + \boldsymbol{F_{\perp R}}(\boldsymbol{r_T}, t), \tag{4.56}$$

where

$$\boldsymbol{F_{\perp C}}(\boldsymbol{r_T}, t) = \frac{e^2}{4\pi\varepsilon_0} \frac{\boldsymbol{n_\perp}\left(1 - \boldsymbol{\beta_S} \cdot \boldsymbol{\beta_T}\right) - \boldsymbol{\beta_{\perp S}}\left(1 - \boldsymbol{n} \cdot \boldsymbol{\beta_T}\right)}{\gamma_S^2 R_{ST}^2 \left(1 - \boldsymbol{n} \cdot \boldsymbol{\beta_S}\right)^3} \tag{4.57}$$

and

$$\boldsymbol{F_{\perp R}}(\boldsymbol{r_T}, t) = \frac{e^2}{4\pi\varepsilon_0 c} \left[ \frac{\boldsymbol{n_\perp}\left(\boldsymbol{n} \cdot \dot{\boldsymbol{\beta}}_\mathbf{S}\right)\left(1 - \boldsymbol{\beta_S} \cdot \boldsymbol{\beta_T}\right) - \boldsymbol{\beta_{\perp S}}\left(\boldsymbol{n} \cdot \dot{\boldsymbol{\beta}}_\mathbf{S}\right)\left(1 - \boldsymbol{n} \cdot \boldsymbol{\beta_T}\right)}{R_{ST}\left(1 - \boldsymbol{n} \cdot \boldsymbol{\beta_S}\right)^3} \right.$$
$$\left. - \frac{\dot{\boldsymbol{\beta}}_{\perp\mathbf{S}}\left(1 - \boldsymbol{n} \cdot \boldsymbol{\beta_T}\right) + \boldsymbol{n_\perp}\left(\boldsymbol{\beta_T} \cdot \dot{\boldsymbol{\beta}}_\mathbf{S}\right)}{R_{ST}\left(1 - \boldsymbol{n} \cdot \boldsymbol{\beta_S}\right)^2} \right]. \tag{4.58}$$

**Tail-Head interaction: case of two particles in circular motion.** We will first consider the situation in which the test particle is in front of the source. In this case, one can refer to Fig. 4.6 for all the possible configurations of the present position of the test electron and the retarded position of the source with respect to the arc. The vertical displacement $h$ of one of the two particles is to be imagined in the direction perpendicular to the figure plane. Let us start with the steady state case in Fig. 4.6b. We can define with $\Delta s$ the curvilinear distance between the present positions of the test and of the source particle; $\phi$ will indicate the angular distance between the retarded position of the source and the present position of the test electron, and it will be designated as the retarded angle. Finally, $h$ will be the vertical displacement.

We will assume $\beta_S = \beta_T = \beta$. Therefore we can write Eq. (4.57) and Eq. (4.58) in the following way:

$$\boldsymbol{F_{\perp C}} = \frac{e^2}{4\pi\varepsilon_0 \gamma^2} \frac{\hat{\mathbf{e}}_\mathbf{h}\left[h(1 - \beta^2 \cos\phi)\right] + \hat{\mathbf{e}}_\mathbf{p}\left[2R\sin^2(\phi/2)(1 + \beta^2) - \beta\sin\phi(h^2 + 4R^2\sin^2(\phi/2))^{1/2}\right]}{\left[(h^2 + 4R^2\sin^2(\phi/2))^{1/2} - 2\beta R\sin(\phi/2)\cos(\phi/2)\right]^3},$$

$$(4.59)$$

$$
\boldsymbol{F}_{\perp \mathbf{R}} = \frac{e^2 \beta^2}{4\pi\varepsilon_0} \left\{ -\frac{\hat{\mathbf{e}}_\mathbf{h} \left[ h\beta \sin\phi \right] + \hat{\mathbf{e}}_\mathbf{p} \left[ \beta R \sin\phi - \cos\phi (h^2 + 4R^2 \sin^2(\phi/2))^{1/2} \right]}{R \left[ (h^2 + 4R^2 \sin^2(\phi/2))^{1/2} - 2\beta R \sin(\phi/2)\cos(\phi/2) \right]^2} + 2\sin^2(\phi/2) \right.
$$

$$
\left. \times \frac{\hat{\mathbf{e}}_\mathbf{h} \left[ h(1 - \beta^2 \cos\phi) \right] + 2\hat{\mathbf{e}}_\mathbf{p} \sin(\phi/2) \left[ R\sin(\phi/2)(1 + \beta^2) - \beta\cos(\phi/2)(h^2 + 4R^2 \sin^2(\phi/2))^{1/2} \right]}{\left[ (h^2 + 4R^2 \sin^2(\phi/2))^{1/2} - 2\beta R \sin(\phi/2)\cos(\phi/2) \right]^3} \right\} .
$$

$$(4.60)$$

The retardation condition linking $\Delta s$, $h$ and $\phi$ reads

$$
\Delta s = R\phi - \beta \left[ h^2 + 4R^2 \sin^2 \frac{\phi}{2} \right]^{1/2} . \qquad (4.61)
$$

As one can readily see by inspecting Eq. (4.61), when we impose reasonable values for $\Delta s \ll R$ and $h \ll R$ we obtain corresponding values of $\phi \ll 1$. We will therefore assume $\phi \ll 1$ throughout this Section, and verify *a posteriori* the validity of this assumption when studying particular situations. Note that, as already pointed out in Section 4.2, by fixing $\phi \ll 1$ we keep open the possibility of comparing $\phi$ with the synchrotron radiation formation angle $1/\gamma$ (note that a deflection angle smaller or larger than $1/\gamma$ is characteristic of the cases, respectively, of undulator or synchrotron radiation). We can therefore expand Eq. (4.59) and Eq. (4.60) to the second non-vanishing order in $\phi$ thus obtaining

$$
\boldsymbol{F}_{\perp \mathbf{C}} \simeq \frac{e^2 \gamma^3}{4\pi\varepsilon_0 R^2} \boldsymbol{\Phi}_{\mathbf{C}}(\hat{\phi}) \qquad (4.62)
$$

and

$$
\boldsymbol{F}_{\perp \mathbf{R}} \simeq \frac{e^2 \gamma^3}{4\pi\varepsilon_0 R^2} \boldsymbol{\Phi}_{\mathbf{R}}(\hat{\phi}) , \qquad (4.63)
$$

where we define $\boldsymbol{\Phi}_{\mathbf{C}}$ and $\boldsymbol{\Phi}_{\mathbf{R}}$ as

$$
\boldsymbol{\Phi}_{\mathbf{C}}(\hat{\phi}) = \frac{4\hat{\mathbf{e}}_\mathbf{h} \left[ \hat{h} + 2\hat{h}/\hat{\phi}^2 \right] + \hat{\mathbf{e}}_\mathbf{p} \left[ \hat{\phi}^2 - 4\hat{h}^2/\hat{\phi}^2 \right]}{\hat{\phi} \left[ 1 + \hat{\phi}^2/4 + \hat{h}^2/\hat{\phi}^2 \right]^3} \qquad (4.64)
$$

and

$$
\boldsymbol{\Phi}_{\mathbf{R}}(\hat{\phi}) = \frac{\hat{\mathbf{e}}_\mathbf{h}\hat{\phi}^2\hat{h} \left[ 1 - 4\hat{h}^2/\hat{\phi}^4 \right] + \hat{\mathbf{e}}_\mathbf{p} \left[ 2 - \hat{\phi}^2 + \hat{\phi}^4/8 - 3\hat{h}^2 + 4\hat{h}^2/\hat{\phi}^2 \right]}{\hat{\phi} \left[ 1 + \hat{\phi}^2/4 + \hat{h}^2/\hat{\phi}^2 \right]^3} . \qquad (4.65)
$$

Here and above $\hat{\phi} = \gamma\phi$. This normalization choice, already treated in [8], is quite natural, $1/\gamma$ being the synchrotron radiation formation angle at the critical wavelength. In the derivation of Eq. (4.62) and Eq. (4.63) (and in the following, too) we understood $\hat{\phi} \gg 1/\gamma$, which is justified by the ultrarelativistic approximation. Moreover we defined

$\hat{h} = h\gamma^2/R$; in order to understand this definition we first write down the retardation condition Eq. (4.61) in an approximate form. Since we are already working in the limit $\Delta s/R \ll 1$ and $\phi \ll 1$, in order to have $\Delta s > 0$ it must be $h < R\phi$. We will automatically recover from our results that the assumption $h \ll R\phi$ is sufficiently good for our purposes. Therefore Eq. (4.61) can be approximated with:

$$\Delta s = (1 - \beta)R\phi + \frac{R\phi^3}{24} - \frac{h^2}{2R\phi} \; . \tag{4.66}$$

The latter can be written down in dimensionless form too as

$$\Delta\hat{s} = \frac{\hat{\phi}}{2} + \frac{\hat{\phi}^3}{24} - \frac{\hat{h}^2}{2\hat{\phi}} \; , \tag{4.67}$$

which explains the choice of the definition for $\hat{h}$.

The reader may easily check that Eq. (4.64), Eq. (4.65) and Eq. (4.67) (as well as Eq. (4.59) and Eq. (4.60)) are generalizations of the expressions given in Section 4.2 by taking their limit for $\hat{h} \longrightarrow 0$.

The following expression, which is valid for the total transverse force felt by the test particle can be then trivially derived

$$\boldsymbol{F}_\perp \simeq \frac{e^2\gamma^3}{4\pi\varepsilon_0 R^2}\boldsymbol{\Phi}(\hat{\phi}) \; , \tag{4.68}$$

where $\Phi$ is defined by

$$\boldsymbol{\Phi}(\hat{\phi}) = \boldsymbol{\Phi_R}(\hat{\phi}) + \boldsymbol{\Phi_C}(\hat{\phi}), \tag{4.69}$$

**Tail-Head interaction: case (a).** Let us now consider the other cases depicted in Fig. 4.6a, c and d. While the case in Fig. 4.6b deals with the steady state situation in which the present position of the test and the retarded position of the source electron are both in the bend, Fig. 4.6a, c and d deal with transient situations in which we can find the retarded source and the present test particle in the straight line before and after the bend too.

Consider the situation in Fig. 4.6a. In this case, under the assumption $h \ll (y + R\eta)$, the retardation condition reads

$$\Delta\hat{s} \simeq \frac{\hat{y} + \hat{\eta}}{2} - \frac{1}{2}\frac{\hat{h}^2 - (\hat{\eta}^3/3)(\hat{y} + \hat{\eta}/4)}{\hat{y} + \hat{\eta}} \; , \tag{4.70}$$

where we introduced the normalized quantity $\hat{y} = y\gamma/R$, which is just $y/R$ normalized to the synchrotron radiation formation angle, $1/\gamma$.

In this case the source particle is only responsible for a velocity field contribution, therefore $\boldsymbol{F}_\perp = \boldsymbol{F}_{\perp C}$. By direct use of Eq. (4.57), one can find the exact expression for $\boldsymbol{F}_\perp$:

$$\boldsymbol{F}_\perp = \frac{e^2}{4\pi\varepsilon_0\gamma^2}\frac{\hat{\mathbf{e}}_{\mathbf{h}}\left\{h[1 - \beta^2\cos\eta]\right\} + \hat{\mathbf{e}}_{\mathbf{p}}\left\{-R_{ST}\beta\sin\eta + [R(1 + \beta^2)(1 - \cos\eta) + y\sin\eta]\right\}}{\left\{R_{ST} - \beta(y + R\sin\eta)\right\}^3} \; ,$$
$$\tag{4.71}$$

$R_{ST}$ being given by

$$R_{ST} = \left[(y + R\sin\eta)^2 + R^2(1 - \cos\eta)^2 + h^2\right]^{1/2} . \tag{4.72}$$
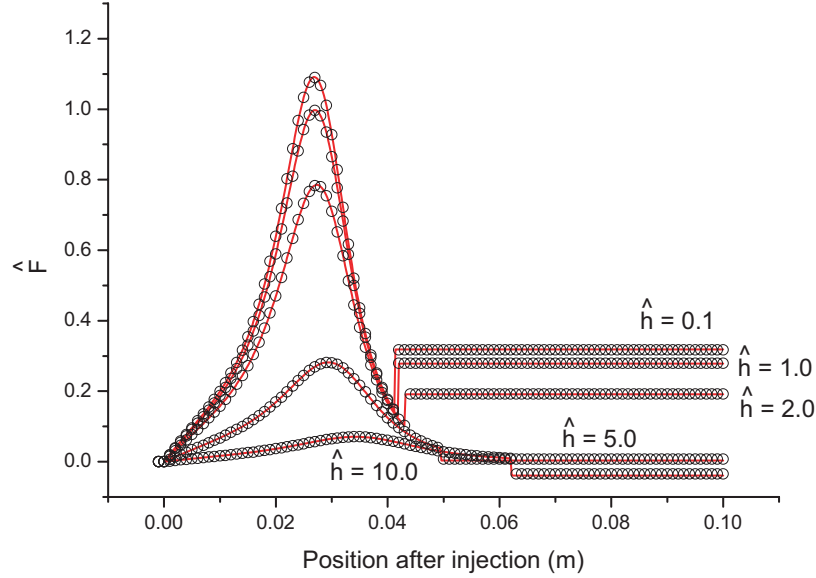


**Figure 4.15:** *Normalized radial force $\hat{F}$ for a two-particle system entering a hard-edge bending magnet as a function of the position after injection. Results for different values of $\hat{h}$ are shown. The solid lines show analytical results; the circles describe the outcome from TraFiC$^4$. Here $\Delta\hat{s} = 5.0$.*

Expanding the trigonometric functions in Eq. (4.71) and using normalized quantities one finds:

$$\boldsymbol{F}_\perp \simeq \frac{e^2}{4\pi\varepsilon_0} \frac{4\gamma^3}{R^2} (\hat{y}+\hat{\eta})^2 \frac{\left\{\hat{\mathbf{e}}_\mathbf{h}\left[\hat{h}(\hat{y}+\hat{\eta})(2+\hat{\eta}^2)\right] + \hat{\mathbf{e}}_\mathbf{p}\left[\hat{y}^2\hat{\eta} + \hat{y}(\hat{\eta}^2 + \hat{\eta}^4/2) + \hat{\eta}^5/4 - \hat{h}^2\hat{\eta}\right]\right\}}{\left[(\hat{y}+\hat{\eta})^2 + \hat{\eta}^4/4 + \hat{h}^2\right]^3} . \tag{4.73}$$

It can be easily verified that, as it must be, Eq. (4.73) reduces to Eq. (4.62) in the limit $\hat{y} \to 0$. Also, the reader may check that in the limit $\hat{h} \to 0$, Eq. (4.73) reduces to already derived expressions in Section 4.2.

Let us now define the normalized radial force $\hat{F} = F_p/[e^2/(4\pi\varepsilon_0 R\Delta s)]$. It is possible, by means of Eq. (4.73), to plot $\hat{F}$ as a function of the position after the injection (defined by the entrance of the test particle in the hard-edge magnet) for a fixed value of $\Delta\hat{s} = \Delta s\gamma^3/R = 5.0$ and different values of $h$. In Fig. 4.15 we compare such a plot with numerical results from the code TraFiC$^4$ (see [1]).

Note that, as already pointed out in Section 4.2, at the position which corresponds to the entrance of the retarded source in the magnet there is a discontinuity in the

plots. This is linked to our model choice, and it is due to the abrupt (hard-edge magnet) switching on of the acceleration fields.

As general remark to Fig. 4.15 and, in fact, to Fig. 4.16, Fig. 4.18 and Fig. 4.23, the perfect agreement between our calculations and numerical results by $\texttt{TraFiC}^4$ provides, *per se*, an excellent cross-check between our analytical results (with their assumptions and applicability region) and simulations.

**Tail-Head interaction: case (c).** We will now move to the case depicted in Fig. 4.6c, in which the source particle has its retarded position inside the bend and the test particle has its present position in the straight line following the magnet. We will define with $x$ the distance, along the straight line after the magnet, between the end of the bend and the present position of the test particle. Here $\hat{\phi}_{\mathrm{m}} = \gamma \phi_{\mathrm{m}}$, $\phi_{\mathrm{m}}$ being the angular extension of the magnet, and $\hat{x} = \gamma x / R$, the reason for this normalization choice for $x$ being identical to that for $y$.

The retardation condition reads

$$\Delta \hat{s} \simeq \frac{\hat{\psi} + \hat{x}}{2} + \frac{\hat{\psi}^3}{24} \frac{\hat{\psi} + 4\hat{x}}{\hat{\psi} + \hat{x}} - \frac{\hat{h}^2}{2(\hat{\psi} + \hat{x})}. \tag{4.74}$$

In contrast with the case of Fig. 4.6a, here we have contributions from both velocity and acceleration field. Again, by direct use of Eq. (4.57) and Eq. (4.58) one can find the exact expression for the transverse electromagnetic force exerted by the source particle on the test particle

$$\boldsymbol{F}_{\perp} = \boldsymbol{F}_{\perp \mathrm{C}} + \boldsymbol{F}_{\perp \mathrm{R}} , \tag{4.75}$$

where

$$\boldsymbol{F}_{\perp\mathrm{C}} = \frac{e^2}{4\pi\varepsilon_0\gamma^2} \frac{\hat{\mathbf{e}}_{\mathbf{h}}\left[(1-\beta^2\cos\psi)h\right] + \hat{\mathbf{e}}_{\mathbf{p}}\left[R(1-\cos\psi)(1-\beta^2\cos\psi) - \beta\sin\psi\,(R_{ST} - \beta x - \beta R\sin\psi)\right]}{\left[R_{ST} - \beta x\cos\psi - \beta R\sin\psi\right]^3}$$

$$(4.76)$$

and

$$\boldsymbol{F}_{\perp\mathrm{R}} = \frac{e^2\beta^2}{4\pi\varepsilon_0 R}\left\{\left[\frac{\hat{\mathbf{e}}_{\mathbf{h}}\left[h(1-\beta^2\cos\psi)(R + x\sin\psi - R\cos\psi)\right]}{\left[R_{ST} - \beta x\cos\psi - \beta R\sin\psi\right]^3}\right.\right.$$

$$+ \frac{\hat{\mathbf{e}}_{\mathbf{p}}\left[(R + x\sin\psi - R\cos\psi)(R(1-\cos\psi)(1-\beta^2\cos\psi) - \beta\sin\psi(R_{ST} - \beta x - \beta R\sin\psi))\right]}{\left[R_{ST} - \beta x\cos\psi - \beta R\sin\psi\right]^3}\right]$$

$$\left. - \frac{\hat{\mathbf{e}}_{\mathbf{h}}\left[h\sin\psi\right] + \hat{\mathbf{e}}_{\mathbf{p}}\left[R(1-\cos\psi)\beta\sin\psi + \cos\psi(R_{ST} - \beta x - \beta R\sin\psi)\right]}{\left[R_{ST} - \beta x\cos\psi - \beta R\sin\psi\right]^2}\right\},$$

$$(4.77)$$

$R_{ST}$ being now

$$R_{ST} = \left((x + R\sin\psi)^2 + R^2(1-\cos\psi)^2 + h^2\right)^{1/2} .$$

$$(4.78)$$

Expanding the trigonometric functions in Eq. (4.76) and Eq. (4.77), and using normalized quantities one finds:
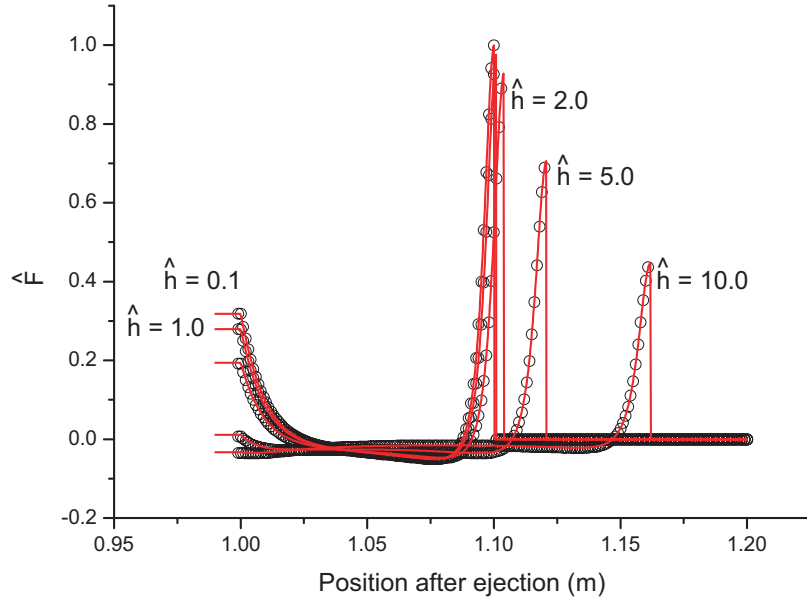


**Figure 4.16:** *Normalized radial force $\hat{F}$ for a two-particle system leaving a hard-edge bending magnet as a function of the position after the ejection. Results for different values of $\hat{h}$ are shown. The solid lines show analytical results; the circles describe the outcome from TrafiC[4]. Here $\Delta\hat{s} = 5.0$.*

$$\boldsymbol{F}_{\perp\mathrm{C}} = \frac{2e^2\gamma^3}{4\pi\varepsilon_0 R^2}\,\frac{2\hat{\mathbf{e}}_{\mathbf{h}}\left[\hat{h}(2+\hat{\psi}^2)(\hat{x}+\hat{\psi})^3\right] + \hat{\mathbf{e}}_{\mathbf{p}}\hat{\psi}(\hat{x}+\hat{\psi})^2\left[-2\hat{x}^2 + \hat{x}\left(\hat{\psi}^3 - 2\hat{\psi}\right) + \hat{\psi}^4/2 - 2\hat{h}^2\right]}{\left[(\hat{x}+\hat{\psi})^2 + (\hat{\psi}^2/4)(2\hat{x}+\hat{\psi})^2 + \hat{h}^2\right]^3}\,,$$

$$(4.79)$$

and

$$\boldsymbol{F}_{\perp\mathrm{R}} = \frac{2e^2\gamma^3}{4\pi\varepsilon_0 R^2}(\hat{x}+\hat{\psi})\Bigg\{\frac{-2\hat{\mathbf{e}}_{\mathbf{h}}\left[\hat{h}\hat{\psi}(\hat{x}+\hat{\psi})\right] + \hat{\mathbf{e}}_{\mathbf{p}}\left[\hat{x}^2 + \hat{x}\hat{\psi}(2-\hat{\psi}^2) + \hat{\psi}^2 - (3/4)\hat{\psi}^4 + \hat{h}^2\right]}{\left[(\hat{x}+\hat{\psi})^2 + (\hat{\psi}^2/4)(2\hat{x}+\hat{\psi})^2 + \hat{h}^2\right]^2} +$$

$$+ \frac{2\hat{\mathbf{e}}_{\mathbf{h}}(\hat{x}+\hat{\psi})^2(2+\hat{\psi}^2)(\hat{x}+\hat{\psi}/2)\hat{\psi}\hat{h} + \hat{\mathbf{e}}_{\mathbf{p}}(\hat{x}+\hat{\psi})(\hat{x}+\hat{\psi}/2)\hat{\psi}^2\left[-2\hat{h}^2 - 2\hat{x}^2 + \hat{x}\hat{\psi}(-2+\hat{\psi}^2) + \hat{\psi}^4/2\right]}{\left[(\hat{x}+\hat{\psi})^2 + (\hat{\psi}^2/4)(2\hat{x}+\hat{\psi})^2 + \hat{h}^2\right]^3}\Bigg\}.$$

$$(4.80)$$

Similarly to the latter case, it can be easily verified that Eq. (4.79) and Eq. (4.80) reduce to Eq. (4.62) and Eq. (4.63), respectively, in the limit $x \to 0$. Moreover, in the limit $h \to 0$, they reduce to already known expressions given in Section 4.2. Again, one can plot the normalized radial force $\hat{F}$ as a function of the position after the ejection, defined by the exit of the test particle from the hard-edge magnet, for different values of $\hat{h}$ and a fixed value of $\Delta\hat{s} = \Delta s\gamma^3/R = 5.0$. In Fig. 4.16 we compare such a plot with numerical results from `TraFiC`[4].

At the position which corresponds to the exit of the retarded source from the magnet there is a discontinuity in the plots. This, again, is linked to our model choice, and it is due to the fact that, in the orbital plane, after the retarded source has left the magnet there is only Coulomb repulsion along the longitudinal direction.

It is suggestive to notice the resemblance of the peaks shown in Fig. 4.16 with half of the time pulse of the radial electric field from usual synchrotron radiation process (see Fig. 4.17 and Chapter 5). This is not a coincidence. The test particle is, indeed, far away from the source with respect to the formation length $R/\gamma^3$ and the magnetic field contribution to the Lorentz force can be expected to have the same behavior of the electric field contribution, since $\boldsymbol{B} = (\boldsymbol{n} \times \boldsymbol{E})/c$. The only difference is that the observer is now "running away" from the electromagnetic signal which will result in a spreading of the pulse of about a factor $(1-\beta)^{-1}$. Since $R = 1$ m and $\gamma = 100$ we expect the pulse to be long about $(R/\gamma^3)(1-\beta)^{-1} \sim 10^{-2}$ m.

**Tail-Head interaction: case (d).** The last tail-head case left to discuss is depicted in Fig. 4.6d; the source particle has its retarded position in the straight line before the bend, and the test particle has its present position in the straight line following the magnet. The retardation condition reads

$$\Delta\hat{s} \simeq \frac{\hat{\phi}_{\mathrm{m}} + \hat{x} + \hat{y}}{2} + \frac{\hat{\phi}_{\mathrm{m}}^3/24\left[\hat{\phi}_{\mathrm{m}} + 4(\hat{x}+\hat{y}) + 12\hat{x}\hat{y}/\hat{\phi}_{\mathrm{m}}\right] - \hat{h}^2/2}{\hat{\phi}_{\mathrm{m}} + \hat{x} + \hat{y}} \qquad . \qquad (4.81)$$
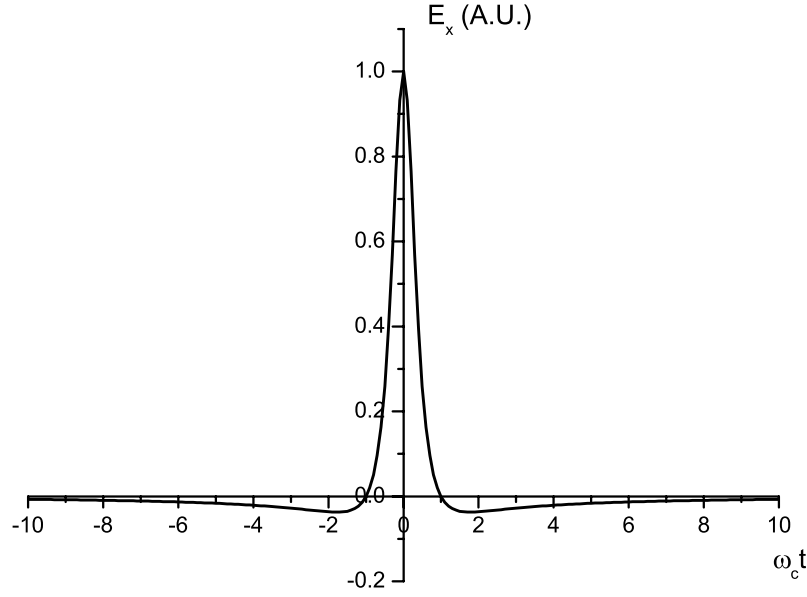
**Figure 4.17:** *Time variation of a synchrotron radiation pulse generated by a highly relativistic electron moving in a circle as seen by an observer in the orbital plane*

In this case we have only velocity contributions. The exact expression for the electromagnetic transverse force on the test particle is

$$\boldsymbol{F}_\perp = \frac{e^2}{4\pi\varepsilon_0\gamma^2} \frac{\hat{\mathbf{e}}_\mathbf{h}\left[\sin\theta(1-\beta^2\cos\phi_\mathrm{m})\right] + \hat{\mathbf{e}}_\mathbf{p}\left[\sin\delta\cos\theta(1-\beta^2\cos\phi_\mathrm{m}) - \beta\sin\phi_\mathrm{m}(1-\cos\delta\cos\theta)\right]}{R_{ST}^2\left[1 - \beta\sin\phi_\mathrm{m}\sin\delta\cos\theta - \beta\cos\phi_\mathrm{m}\cos\delta\cos\theta\right]^3},$$

(4.82)

where

$$\sin\theta = \frac{h}{R_{ST}} \,,$$

(4.83)

$$\cos\theta = \frac{(R_{ST}^2 - h^2)^{1/2}}{R_{ST}} \,,$$

(4.84)

$$\sin\delta = \frac{R + y\sin\phi_\mathrm{m} - R\cos\phi_\mathrm{m}}{R_{ST}\cos\theta}$$

(4.85)

and

$$\cos\delta = \frac{x + y\cos\phi_\mathrm{m} + R\sin\phi_\mathrm{m}}{R_{ST}\cos\theta} \,,$$

(4.86)

where $R_{ST}$ can be retrieved by the latter two equations and some trivial trigonometry.

Once again, expanding the trigonometric functions in Eqs. (4.82) to (4.85) and using normalized quantities one finds the following approximated expression for $\boldsymbol{F}_\perp$:
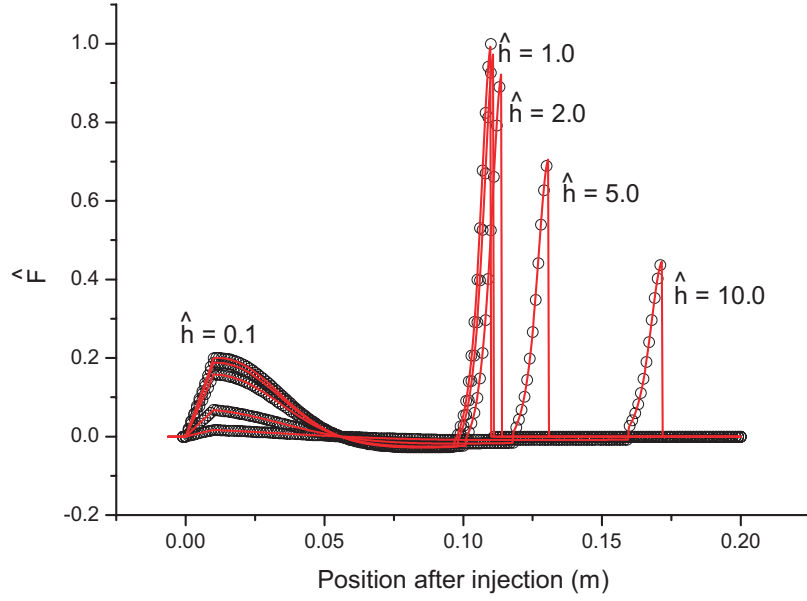
**Figure 4.18:** *Normalized radial force $\hat{F}$ for a two-particle system crossing a hard-edge bending magnet as a function of the position of the test particle inside the magnet in the case of a short magnet $\phi_{\mathrm{m}} \ll 1$. Results are shown for different values of $\hat{h}$. The solid lines show analytical results; the circles describe the outcome from TraFiC$^4$. Here the normalized distance between the two particles is $\Delta\hat{s} = 5$, while $\hat{\phi}_{\mathrm{m}} = 1$.*

$$\boldsymbol{F}_{\perp} \simeq \frac{e^2}{4\pi\varepsilon_0 R^2} 4\gamma^3 (\hat{x} + \hat{y} + \hat{\phi}_{\mathrm{m}})^2 \hat{\phi}_{\mathrm{m}}$$

$$\times \frac{\hat{\mathbf{e}}_{\mathbf{h}}\left[(2/\hat{\phi}_{\mathrm{m}} + \hat{\phi}_{\mathrm{m}})(\hat{x} + \hat{y} + \hat{\phi}_{\mathrm{m}})\hat{h}\right] + \hat{\mathbf{e}}_{\mathbf{p}}\left[-\hat{x}^2 + \hat{y}^2 + (\hat{\phi}_{\mathrm{m}}^2)\hat{x}\hat{y} + \hat{x}(\hat{\phi}_{\mathrm{m}}^3/2 - \hat{\phi}_{\mathrm{m}}) + \hat{y}(\hat{\phi}_{\mathrm{m}}^3/2 + \hat{\phi}_{\mathrm{m}}) + \hat{\phi}_{\mathrm{m}}^4/4 - \hat{h}^2\right]}{\left\{(\hat{x} + \hat{y} + \hat{\phi}_{\mathrm{m}})\left[\hat{x}(1 + \hat{\phi}_{\mathrm{m}}^2) + \hat{y} + \hat{\phi}_{\mathrm{m}} + \hat{\phi}_{\mathrm{m}}^3/3\right] - (\hat{\phi}_{\mathrm{m}}^2/12)[12\hat{x}\hat{y} + 4(\hat{x} + \hat{y})\hat{\phi}_{\mathrm{m}} + \hat{\phi}_{\mathrm{m}}^2] + \hat{h}^2\right\}^3} .$$

$$(4.87)$$

It is easy to verify that Eq. (4.87) reduces, respectively, to the steady state (Eq. (4.62)) when $x = 0$ and $y = 0$, to the transient case in Fig. 4.6a when $x = 0$ (Eq. (4.73)) and to the transient case in Fig. 4.6c when $y = 0$ (Eq. (4.76)). Moreover the reader may verify that, in the limit $h \longrightarrow 0$, Eq. (4.87) reduces to already known results in Section 4.2. Following the treatment of the transient situations in Fig. 4.6a and in Fig. 4.6c we plot, for this case too, a normalized expression for the transient force, i.e. the usual $\hat{F}$, as a function of the curvilinear position of the test particle ($s = 0$ indicates the entrance of the magnet) for different values of $\hat{h}$ and a fixed value of $\Delta\hat{s} = \Delta s\gamma^3/R$ and of $\hat{\phi}_{\mathrm{m}}$. In Fig. 4.18, we compare our analytical results with numerical results from TraFiC$^4$, for a fixed value of $\Delta\hat{s} = 5.0$ and $\hat{\phi}_{\mathrm{m}} = 1$ and for different values of the vertical displacement $\hat{h}$.

**Head-Tail interaction.**   Finally we can deal with the situation in which the source particle is ahead of the test electron, i.e. $\Delta s < 0$; we will talk, in this case, of head-tail

interaction. On the one hand it is evident that, when $\Delta s < 0$, the source particle is
ahead of the test electron at any time; on the other hand it is not true that the retarded
position of the source particle is, in general, ahead of the present position of the test
particle. As already suggested in Section 4.2, if $\Delta s < 0$ and, approximatively, $|\Delta s| < h$
the test particle overtakes the retarded position of the source before the electromagnetic
signal reaches it. In this case, although we may still talk about head-tail interaction,
since $\Delta s < 0$, its real character is very much similar to the case $\Delta s > 0$, in which the
electromagnetic signal has to catch up with the test particle. In order to understand
the physics involved in this situation it is sufficient to study the cases $\Delta s < 0$ and
$|\Delta s| > h$. The case $\Delta s < 0$ with $|\Delta s| < h$ will be treated from a qualitative viewpoint
only: its quantitative analysis, which may be interesting to perform for the sake of
completeness, presents stronger mathematical difficulties and is left for future study.
Anyway a qualitative treatment of this situation is enough to reach a full understanding
of the interaction physics, which is our goal here.

Consider therefore the case $\Delta s < 0$ with $|\Delta s| > h$. It is important to note that,
once the steady state case is studied, the situation in which the source particle is ahead
of the test electron can be treated immediately for all three (a, c and d) transient cases
in Fig. 4.6 (of course, with respect to the figure, test and source particle exchange
roles) on the basis of the steady state case alone. In fact in that situation, as it has
already been said in Section 4.2, we can assume the retarded angle $\phi$ small enough
(the test particle "runs against" the electromagnetic signal) that the actual trajectory
followed by the particles is not essential and one can use the steady state expression to
describe also the transient cases. It can be shown that the only important contribution
from the source particle comes from the acceleration part of the Liénard-Wiechert
fields. Within our approximations, the only non-negligible contribution is present in
the situation (again, with the roles of test and source particle inverted) depicted in
Fig. 4.6a and Fig. 4.6b, the latter being just the steady state case.

Let us deal with the steady state case of the head-tail interaction when $|\Delta s| > h$.
As already discussed in Section 4.2, the difference with respect to the situation in which
the test electron is in front of the source is that the test electron "runs against" the
electromagnetic signal emitted by the source, while in the other case it just "runs away"
from it. Therefore the relative velocity between the signal and the test electron is equal
to $(1+\beta)c$, instead of $(1-\beta)c$ as in the other situation. Hence the retardation condition
reads

$$| \Delta s | \simeq R\phi + \beta \left[ R^2\phi^2 + h^2 \right]^{1/2} \tag{4.88}$$

or, solved for $\hat{\phi}$,

$$\hat{\phi} \simeq | \Delta \hat{s} | - \left[ \Delta \hat{s}^2 \left( 1 - \frac{1}{\gamma^2} \right) + \hat{h}^2 \right]^{1/2} . \tag{4.89}$$

Note that, in the asymptotic for $| \Delta \hat{s} | \gg \gamma \hat{h}$ we recover the result in Section 4.2 for
the one-dimensional case.

In the general case, $\boldsymbol{\beta_S}$ is almost parallel to (and equal to) $\boldsymbol{\beta_T}$ and antiparallel
to the projection of $\boldsymbol{n}$ on the bending plane: it turns out that the only important
contribution to the radial force on the orbital plane is given by the second term on the
right side of Eq. (4.58), and it is easy to check that

$$F_\perp \simeq \frac{e^2}{4\pi\varepsilon_0 R \mid \Delta s \mid} \ . \tag{4.90}$$

It may be worthwhile to underline that the force in Eq. (4.90) is, structurally, identical to the result in Section 4.2 although, of course, $\Delta s$ is now a function of $h$.

### 4.3.3   Transverse interaction between an electron and a bunch entering a bend from a straight path

In Section 4.3.2 we dealt with all the possible configurations for a two-particle system moving in an arc of a circle. Now we are ready to provide a quantitative explanation of Fig. 4.1.

After the discussion, in Section 4.3.2, about head-tail interactions within a system with the test particle behind the source electron, one is led to the qualitative conclusion that, within an electron bunch, interactions between sources in front of the test particle and the test particle itself are important and, in general, they must be responsible, at the entrance and at the exit of the bending magnet, for sharp changes in the transverse forces acting on the test electron. The quantitative change depends, of course, on the position of the test particle inside the bunch: the extreme cases are for the test particle at the head of the bunch, where there are just interactions with electrons behind the test particle (no head-tail interactions), and for the test particle before the tail of the bunch, at a distance $\Delta s_{\min} > h$, where all the sources are in front of it (only head-tail interactions in the regime $|\Delta s| > h$).

**Head-Tail interaction.**   Consider now the situation in which a one-dimensional line bunch interacts with a particle positioned at the center of the line but vertically displaced by a quantity $h$. As already said we will discuss, analytically, the head-tail interaction for $|\Delta s| > h$ only. Since the trajectory followed by the bunch is not important we can simply integrate Eq. (4.90) and find the contribution

$$F_{\text{p HT}}^{\text{B}}(y) \simeq \begin{cases} 0 & y > R\Phi(h, \Delta s_{\max}) \\ e^2\lambda_0/(4\pi\varepsilon_0 R) \ \ln\left[\Delta s_{\max}/(y + \beta(y^2 + h^2)^{1/2})\right] & R\Phi(h, \beta h) < y < R\Phi(h, \Delta s_{\max}) \\ e^2\lambda_0/(4\pi\varepsilon_0 R) \ \ln[\Delta s_{\max}/h] & y < R\Phi(h, \beta h) \end{cases} , \tag{4.91}$$

where "HT" stands for "head-tail", $y$ is the distance between the test particle and the beginning of the magnet and $\Phi(h, \mid \Delta s \mid)$ is the solution, in $\phi$, of Eq. (4.88) at vertical displacement $h$ and longitudinal distance $\mid \Delta s \mid$, $\Delta s_{\max}$ being the (positive) longitudinal distance between the test particle and the source at the bunch head.

When a bunch longer than the vertical displacement $h$ enters the magnet, the particles in front of the bunch will interact with the test electron following Eq. (4.91), which models the radial interaction on the basis of Eq. (4.90). Nevertheless, Eq. (4.90) cannot describe the situation when the sources at a distance shorter than $\beta h$ begin to interact with the test electron. As a result the head-tail interaction has two characteristic formation lengths. The first one indicates the distance that the test electron travels from the moment it is reached by the electromagnetic signal from the first particle entering the bend, till the moment it is reached by the electromagnetic signal emitted as the
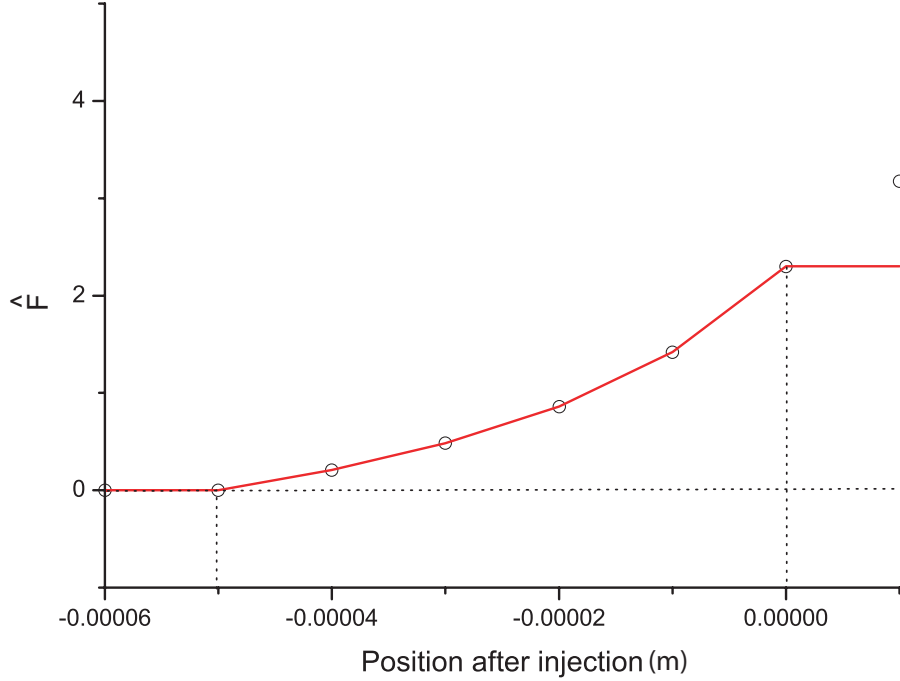
**Figure 4.19:** *Normalized radial force $\hat{F}$ from the head of the bunch ($\Delta s < 0$) to the tail as the bunch progresses inside the bend ($z = 0$ corresponds to the injection of the test particle in the magnet). Here $R = 1$ m, $\gamma = 100$, $h = 10$ $\mu$m and the bunch length is 200 $\mu$m. The test particle is located in the middle of the bunch.*

particle at $\Delta s = -\beta h$ enters the bend. This is given by $L_1 = \beta R(\phi_2 - \phi_1) = \beta R \phi_2$, $\phi_2$ and $\phi_1$ being the (non normalized) solutions of the retardation condition when $\Delta s = -\Delta s_{\max}$ and $\Delta s = -\beta h$, respectively (the reader will recognize that $\phi_1 = 0$). In the limit for $h << \Delta s_{\max}$, Eq. (4.89), substituted in the expression for $L_1$, gives the rule of thumb $L_1 \simeq \Delta s_{\max}/2$. The second characteristic length is given by the distance that the test electron travels from the moment it is reached by the electromagnetic signal from the particle at $\Delta s = -\beta h$ till the moment it is reached by the electromagnetic signal emitted by the particle with $\Delta s = 0$ as it enters the bend. This can be estimated roughly to be equal to $\gamma h$, at least when $h$ is not too large. In fact, in order to know the present angular position of the test particle when $\Delta s = 0$ one should solve the retardation condition in $\phi$

$$R\phi = \beta \left[ h^2 + 4R^2 \sin^2(\phi/2) \right]^{1/2} . \tag{4.92}$$

In the limit in which $\sin(\phi/2) \simeq \phi/2$ we have $\phi \simeq \gamma h/R$ and $L_2 \simeq \gamma h$.

This reasoning can explain pretty well the features in Fig. 4.19, where the normalized radial force has been redefined as $F_p/(e^2 \lambda_0/(4\pi\epsilon_0 R))$ since, here and in the following, we are dealing with a bunch and not with a two-particle system. The radial force grows exactly as described in Eq. (4.91) starting from a curvilinear abscissa of about $s = -l_b/4 = 50$ $\mu$m until $s = 0$ (which is roughly the first formation length). Note that the source located at $\Delta s = -\beta h$ corresponds to a retarded angle $\phi = 0$, which means that the electromagnetic signal emitted from this source at the magnet entrance will reach the test particle when this is also entering the magnet, at $s = 0$.
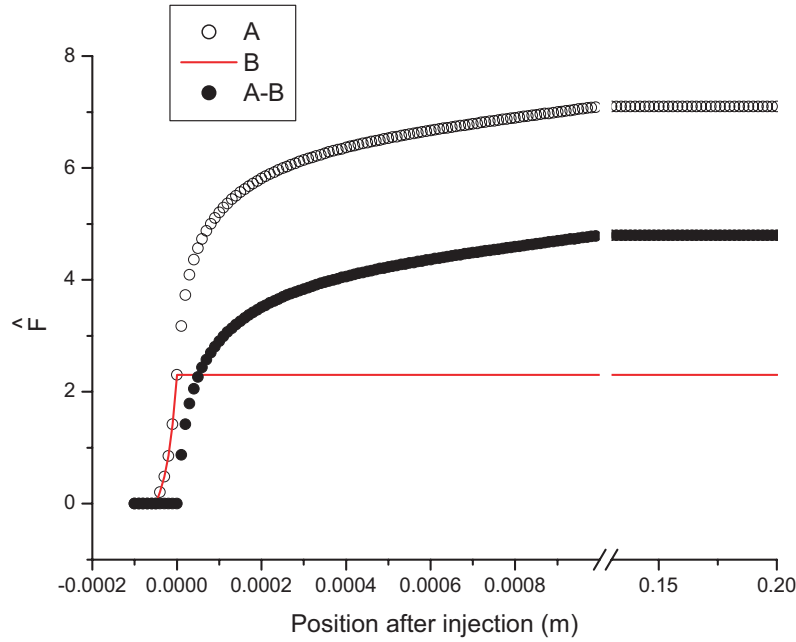
**Figure 4.20:** *The same as Fig. 4.19 for a different range. Normalized radial force from the head of the bunch ($\Delta s < 0$) to the tail as the bunch progresses inside the bend ($z = 0$ corresponds to the injection of the test particle in the magnet). Here $R = 1$ m, $\gamma = 100$, $h = 10$ $\mu$m and the bunch length is 200 $\mu$m. The test particle is located in the middle of the bunch. Curve A corresponds to the simulation by TraFiC$^4$, curve B is the contribution, given by Eq. (4.91), of the particles with $|\Delta s| > h$; A-B is the difference between the two curves, ascribed to the contribution from the particles with $|\Delta s| < h$.*

After $s = 0$, the test particle begins to interact with the sources located at $|\Delta s| < h$ while the ones at $|\Delta s| > h$ reach a steady state, in the sense that they keep on interacting in the same way with the test electron.

This is illustrated by Fig. 4.20, where the normalized radial force $\hat{F}$ is plotted in a different range. The difference between the simulation results and the analytical estimation in Eq. (4.91) gives, quantitatively, the radial interaction due to the sources at $|\Delta s| < h$. For $h = 10$ $\mu$m and $\gamma = 100$, as in our case, one expects a second formation length equal to $10^{-3}$ m which is exactly what one gets: the actual data show, in fact, that a maximum is reached when $s = 0.001$ m at $\hat{F} \simeq 7.098$. Fig. 4.20 also shows the steady state regime, when all the particles in front of the test particle interact with the latter from inside the bend. The solid line in Fig. 4.20 shows, once again, the interaction with the sources located at $|\Delta s| > h$. Finally, in Fig. 4.21 we present the results from TraFiC$^4$ for several values of $h$. Of course, when $h \gtrsim \Delta s_{\max}$, i.e. $h \gtrsim 100$ $\mu$m there are no sources characterized by $|\Delta s| > h$ at all.

One may expect that the system enters the steady state at $z \simeq \gamma h$, which is correct for $h = 1$ $\mu$m, $h = 10$ $\mu$m and, by figure inspection, for $h = 100$ $\mu$m. Nevertheless, in
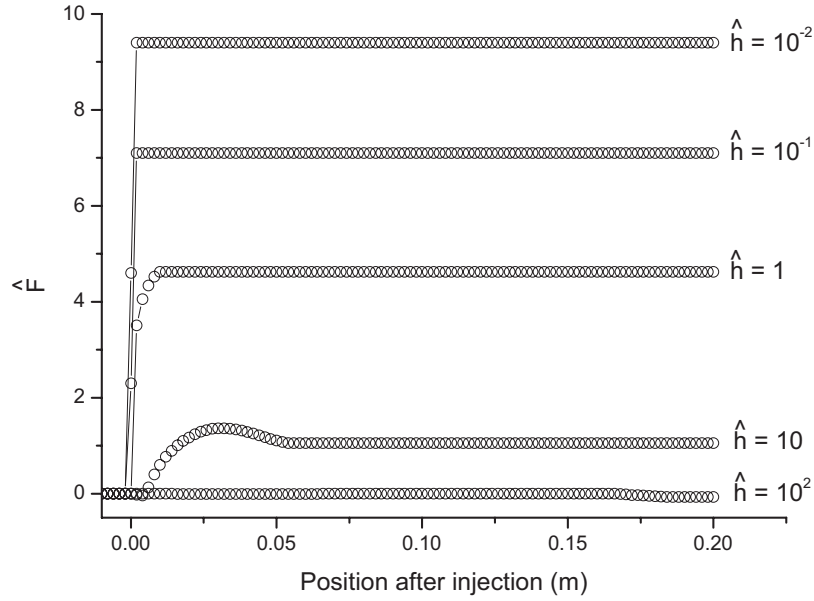
**Figure 4.21:** *Normalized radial force from the head of the bunch ($\Delta s < 0$) to the tail as the bunch progresses inside the bend ($z = 0$ corresponds to the injection of the test particle in the magnet). Here $R = 1$ m and $\gamma = 100$. Here we plot the results from TraFiC$^4$ for several values of $\hat{h}$. The bunch length is 200 $\mu$m. The test particle is located in the middle of the bunch.*

the case $h = 1$ mm and $h = 10$ mm the system enters the steady state at, respectively, $s \simeq 0.054$ m and $s \simeq 0.186$ m, which are clearly smaller than $\gamma h$. The reason for this apparent discrepancy is due to the approximation $\sin(\phi/2) \simeq \phi/2$ which has been used to derive the rule of thumb $L_2 \simeq \gamma h$ starting from Eq. (4.92). A comparison between the rule of thumb proposed before (dashed line) and the real solution of the retardation condition (solid line) is given in Fig. 4.22: one can easily see that, when $h = 1$ mm, $\phi \simeq 0.054$. In the same way, at $h = 10$ mm, $\phi \simeq 0.186$ (remember that $R = 1$ m).

**Tail-Head interaction.** We will now analyze the tail-head part of the interaction when $\Delta s > 0$. In the case where the bunch enters the bend we have contributions from retarded sources both in the bend and in the straight line before the bend. The contribution from the retarded sources in the magnet can be obtained by simple integration of Eq. (4.68), and reads

$$F_{\perp m}^{B} \simeq \frac{e^2 \lambda_0}{4\pi\varepsilon_0 R} \left[ \ln\left( \frac{\hat{\phi}_{max}}{\hat{\phi}_{min}} \right) + \frac{4(2\hat{h}^2 + \hat{\phi}_{max}^2)}{4\hat{h}^2 + 4\hat{\phi}_{max}^2 + \hat{\phi}_{max}^4} - \frac{4(2\hat{h}^2 + \hat{\phi}_{min}^2)}{4\hat{h}^2 + 4\hat{\phi}_{min}^2 + \hat{\phi}_{min}^4} \right] , \quad (4.93)$$

where "m" is a reminder that the contributions treated by Eq. (4.93) are all from the "magnet". All that is left to do now, is to investigate the values which $\hat{\phi}_{min}$ and $\hat{\phi}_{max}$ assume.
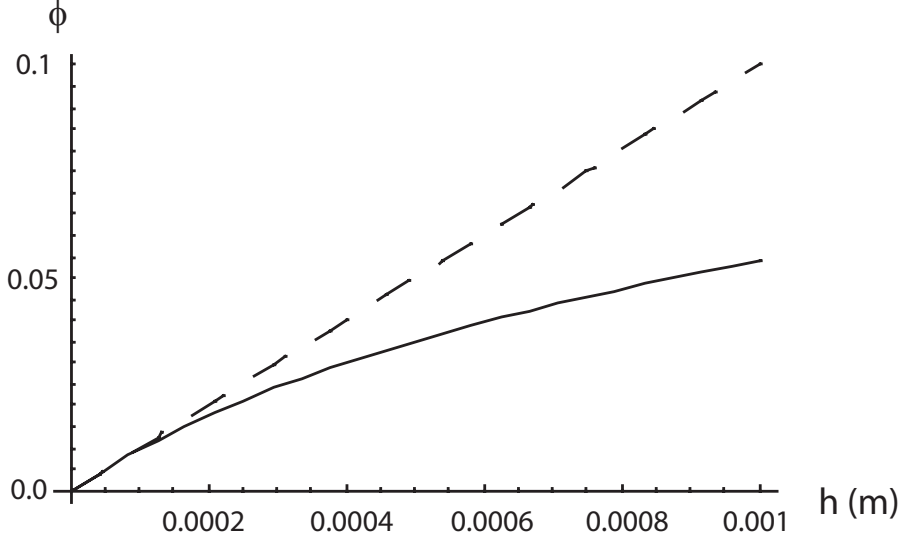
**Figure 4.22:** *Solution of the retardation condition (solid line) at $\Delta s = 0$ as a function of $h$ and comparison with $\phi = \gamma h$ (dashed line)*

Let us first remember that $\hat{\eta}$ indicates the normalized angular position of the test particle inside the bending magnet. Now define with $\hat{\phi}^*$ the solution of the retardation equation $\Delta \hat{s}_{\min} = \hat{\phi}^*/2 + \hat{\phi}^{*3}/24 - \hat{h}^2/(2\hat{\phi}^*)$. If $\hat{\phi}^* < \hat{\eta}$, the retarded position of the first source particle is in the bending magnet, and $\hat{\phi}_{\min} = \hat{\phi}^*$. On the other hand, when $\hat{\phi}^* > \hat{\eta}$ there are no contributions to the radial force from the bend.

Next, we define with $\hat{\phi}^{**}$ the solution of $\Delta \hat{s}_{\max} = \hat{\phi}^{**}/2 + \hat{\phi}^{**3}/24 - \hat{h}^2/(2\hat{\phi}^{**})$ (in our case $\Delta \hat{s}_{\max}$ will be equal to one half of the normalized bunch length). Supposing $\hat{\phi}^* < \hat{\eta}$, if $\hat{\phi}^{**} < \hat{\eta}$ too, then all the particles contribute from the bend, and $\hat{\phi}_{\max} = \hat{\phi}^{**}$. On the other hand, when $\hat{\phi}^{**} > \hat{\eta}$, we have a mixed situation, in which part of the particles contribute from the bend and others from the straight line before the magnet: in this case $\hat{\phi}_{\max} = \hat{\eta}$.

The contribution from the retarded sources in the straight path before the bend is given by

$$F_{\perp s}^{B} = \lambda_0 \int_{\Delta \hat{s}_1}^{\Delta \hat{s}_2} \frac{R}{\gamma^3} F_{\perp}(\hat{y}(\Delta \hat{s}, \hat{\eta}, \hat{h}), \hat{\eta}) d\Delta \hat{s} \; , \tag{4.94}$$

where "s" stands for "straight path", and where the expression for $F_{\perp}$ in the integrand is given by Eq. (4.73). It is convenient, as done before, to switch the integration variable from $\Delta \hat{s}$ to $\hat{y}$. The Jacobian of the transformation is given by

$$\frac{d\Delta \hat{s}}{d\hat{y}} \simeq \frac{(\hat{\eta} + \hat{y})^2 + \hat{\eta}^4/4 + \hat{h}^2}{2(\hat{\eta} + \hat{y})^2} \; . \tag{4.95}$$

After substitution of Eq. (4.95) and Eq. (4.73) in Eq. (4.94), one can easily carry out the integration, thus getting
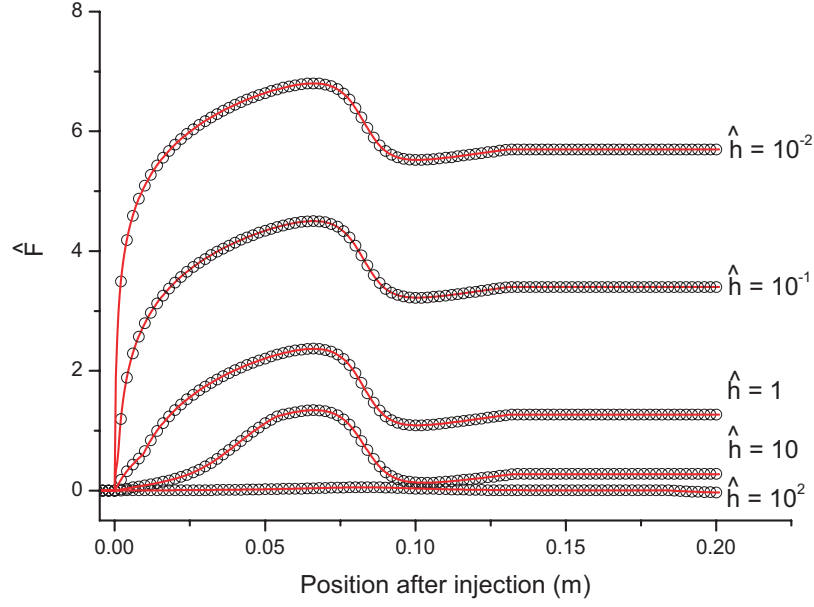
**Figure 4.23:** *Normalized radial force acting on a test particle from a bunch with
rectangular density distribution entering a hard-edge bending magnet as a function
of the position of the test particle inside the magnet. The solid lines show analytical
results; the circles describe the outcome from TraFiC⁴. We chose $\Delta s_{\max} = 100$ $\mu m$,
$\gamma = 100$, $R = 1$ m; the graphs are plotted for several values of the parameter $\hat{h}$.*

$$F_{\perp s}^{\mathrm{B}} \simeq \frac{2e^2\lambda_0}{4\pi\varepsilon_0 R}\left[\frac{\hat{\eta}\left(4\hat{y}_{\min}+2\hat{\eta}+\hat{\eta}^3\right)}{4(\hat{y}_{\min}^2+\hat{h}^2)+8\hat{y}_{\min}\hat{\eta}+4\hat{\eta}^2+\hat{\eta}^4}-\frac{\hat{\eta}\left(4\hat{y}_{\max}+2\hat{\eta}+\hat{\eta}^3\right)}{(4\hat{y}_{\max}^2+\hat{h}^2)+8\hat{y}_{\max}\hat{\eta}+4\hat{\eta}^2+\hat{\eta}^4}\right].$$
(4.96)

As done before for $\hat{\phi}_{\min}$ and $\hat{\phi}_{\max}$, we can now investigate the values of $\hat{y}_{\min}$ and $\hat{y}_{\max}$.

Let us start with $\hat{y}_{\min}$. First, we define with $\hat{y}^*$ the solution of the retardation
condition $\Delta\hat{s}_{\min} = (\hat{\eta}+\hat{y}^*)/2+(\hat{\eta}^3/24)(4\hat{y}^*+\hat{\eta})/(\hat{y}^*+\hat{\eta})-\hat{h}^2/(2\hat{y}^*+2\hat{\eta})$. If $\hat{y}^* > 0$, the
retarded position of the first source particle is in the straight line before the bending
magnet, and $\hat{y}_{\min} = \hat{y}^*$. On the other hand, when $\hat{y}^* < 0$, the retarded position of the
first source particle is in the bend, and $\hat{y}_{\min} = 0$.

Next, we define with $\hat{y}^{**}$ the solution of $\Delta\hat{s}_{\max} = (\hat{\eta}+\hat{y}^{**})/2+(\hat{\eta}^3/24)$
$\times(4\hat{y}^{**}+\hat{\eta})/(\hat{y}^{**}+\hat{\eta})-\hat{h}^2/(2\hat{y}^{**}+2\hat{\eta})$ (again, in our case $\Delta\hat{s}_{\max}$ is just half the bunch
length normalized to $R/\gamma^3$). Consider the case $\hat{y}^{**} < 0$: all the particles contribute from
the bend, that is we entered the steady-state situation. In this case $\hat{y}_{\max} = \hat{y}_{\min} = 0$.
On the other hand, when $\hat{y}^{**} > 0$, we have again a mixed situation, in which part
of the particles contribute from the bend and others from the straight line before the
magnet. In this case $\hat{y}_{\max} = \hat{y}^{**}$.

The following step is to actually plot the radial force exerted on an electron by
a bunch with rectangular distribution entering a long bend. Our results, compared,

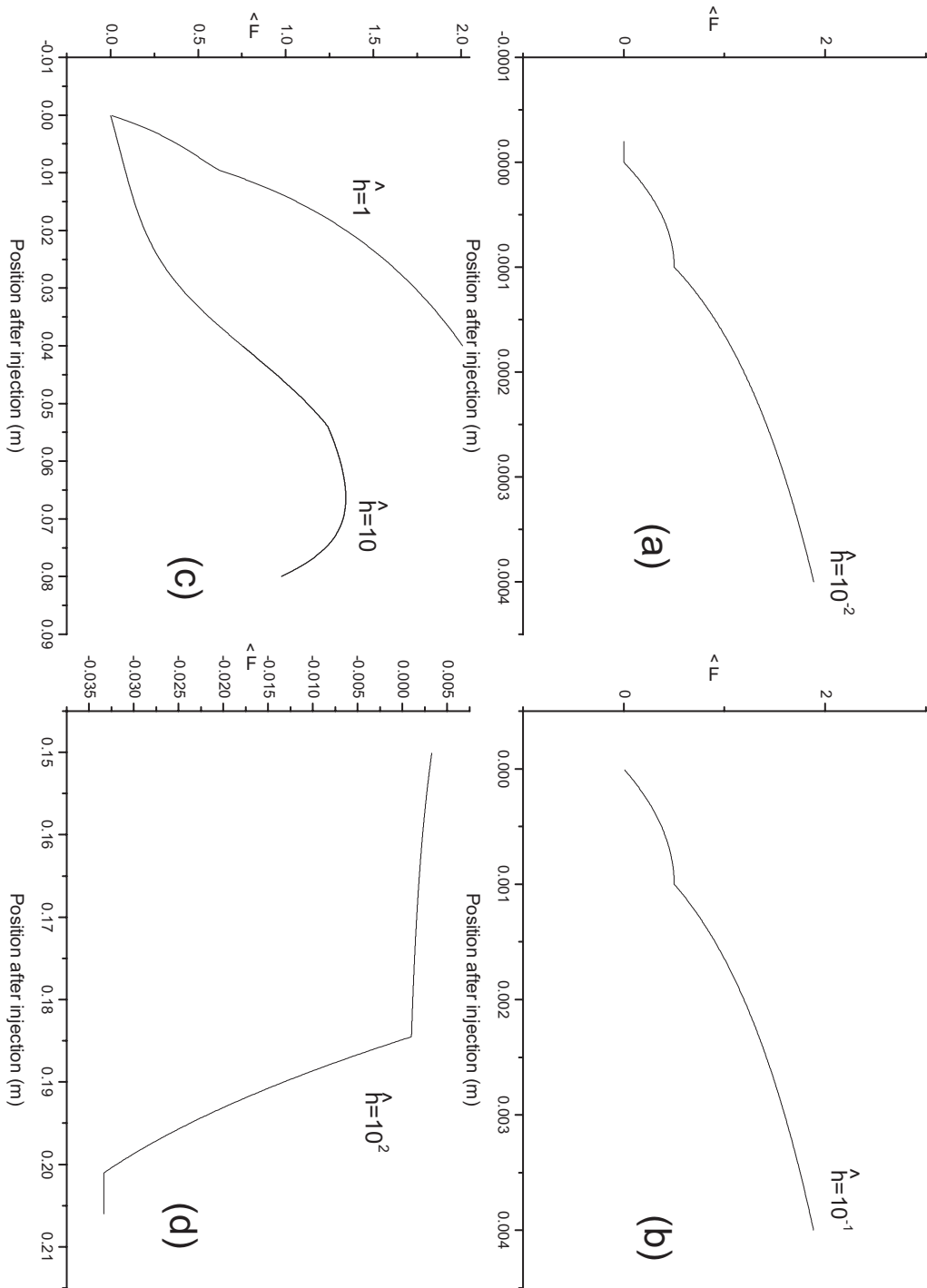**Figure 4.24:** *Normalized radial force (analytical result) acting on a test particle from a bunch with rectangular density distribution entering a hard-edge bending magnet as a function of the position of the test particle inside the magnet. We chose $\Delta s_{\max} = 100\mu m$, $\gamma = 100$, $R = 1$ m; several curves for different values of $\hat{h}$ are shown. A clear discontinuity in the first derivative is visible.*

once again, with simulations by `TraFiC`[4], are shown in Fig. 4.23 for $\Delta s_{\max} = 100 \; \mu$m, $\gamma = 100$, $R = 1$ m and for different values of $\hat{h}$. A perfect agreement is obtained with the results by `TraFiC`[4]. A first characteristic length is obviously given by the solution of the retardation condition with $\Delta s = \Delta s_{\max}$, and gives the position at which the test particle begins to feel a steady interaction from the tail sources. There is a second characteristic length more difficult to see, though: a careful inspection of Fig. 4.23 shows, in fact, a small irregularity (actually a discontinuity in the first derivative) in the curve for $\hat{h} = 1$ at the position $s \simeq 1$ cm. Such irregularities are present in all the curves in Fig. 4.23, although one has to look carefully for them by magnifying parts of the plots, as shown in Figs. 4.24a to 4.24d. It is this fact which actually suggests the presence of a second formation length.

When the value of $h$ is small the discontinuity is located, approximately, at $s \simeq \gamma h$: for example when $h = 1 \; \mu$m, in Fig. 4.24a, we have a discontinuity in the first derivative of the curve at $s \simeq 0.1$ mm. Nevertheless, this value changes as we increase h. In fact, when $h = 1$ mm, in Fig. 4.24c, the discontinuity is at $s \simeq 5.4$ cm, while when $h = 1$ cm, in Fig. 4.24d, we find a value of $s \simeq 18.6$ cm: these are the same numerical values found when discussing the entrance in the steady state of the head-tail interaction in the previous subsection. The reader will remember that these are, in fact, the solutions of Eq. (4.92). From a physical viewpoint, the solution of Eq. (4.92) is the position at which the test particle begins to feel the electromagnetic signal from the source at $\Delta s = 0$ entering the bend .

Before that point, the test particle feels interaction from particles behind it but only due to velocity fields, since the retarded positions of all the electrons behind the test one are not yet in the bend. After that particular point, the force on our test electrons has a component due to the acceleration field too. This suggests that the physical meaning of the presence of this second formation length is simply the switching on of the contribution of the acceleration field. As a last remark it is interesting to note that tail-head and head-tail interactions have a characteristic length in common, but for completely different reasons.

### 4.3.4 Summary and conclusions

In Section 4.3 we presented a fully electrodynamical study of transverse self-forces within an electron bunch moving in an arc of a circle in the case the test particle is endowed with a vertical displacement $h$. We strived for a generalization of the results obtained in Section 4.2 in order to obtain a better qualitative and quantitative explanation of the physics involved in the problem and, in particular, to explain the behavior of the self-interaction depicted in Fig. 4.1.

First we generalized the results in Section 4.2 in the case of a two-particle system. Then, by integration of these results, the case of a line bunch and a test particle with a vertical displacement was studied. This case includes all the relevant physics present in the situation of a bunch with vertical size.

Besides allowing one to generalize results obtained in Section 4.2, our study aimed at a physical understanding of the results by `TraFiC`[4]: we found that the bunch can be divided into four separate regions (over which one can integrate the two-particle interaction) corresponding to four different types of source-test interaction, namely

head-tail with $|\Delta s| < h$, head-tail with $|\Delta s| > h$, tail-head with velocity fields alone, and tail-head with contributions from both acceleration and velocity field. These regions within the bunch correspond to four different contributions to the transverse self-interaction force; these contributions are in one-to-one correspondence with four characteristic formation lengths, which can be determined quantitatively by simple analytical calculations.

For the first, the third, and the fourth region, we could use relatively simple analytical results in order to describe the situation and perform cross-checking with `TraFiC`[4]. The perfect agreement we found gives us much information: this constitutes, in fact, a reliable cross-check. Moreover, we have physical explanations of the self-interactions in terms of formation-lengths and type of source-test interaction.

Because of mathematical difficulties linked with the structure of the retardation condition we left the quantitative discussion of the second region (head-tail with $|\Delta s| < h$) for future work. Nevertheless we were able to understand the physical meaning of this region and to determine its formation length.

# Bibliography

[1] K. Rothemund, M. Dohlus and U. van Rienen, in *Proceedings of the 21st International Free Electron Laser Conference and 6th FEL Applications Workshop, Hamburg, 1999*, edited by J. Feldhaus and H. Weise

[2] TESLA Technical Design Report, DESY 2001-011, edited by F. Richard et al., and http://tesla.desy.de

[3] R. Talman, Phys. Rev. Letters, 56, 14, p. 1429 (1986)

[4] R. Li, in *Proceedings of the 2nd ICFA Advanced Accelerator Workshop on The Physics of High Brightness Beams, Los Angeles, 1999.*

[5] E. P. Lee, Partcle Accelerators, 25, 241 (1990)

[6] Y. Derbenev and V. Shiltsev, in *Fermilab-TM-1974* (1996)

[7] G. Stupakov, in *Proceedings of the ICFA Conferfence Arcidosso, 1998*

[8] E. L. Saldin, E. A. Schneidmiller and M. V. Yurkov, Nucl. Instr. Methods A 398, 373 (1997)

[9] John David Jackson, *Classical electrodynamics*, third edition, Chapter 16, John Wiley & Sons Inc., 1998

[10] R. Li, C. L. Bohn and J. J. Bisognano, in *Proceedings of the SPIE Conference, San Diego, 1997*, vol. 3154, p. 223

# Chapter 5

# On energy and momentum of an ultrarelativistic unstable system

The issue of covariance of the energy-momentum pair for the classical model of the electron was first raised a hundred years ago by Abraham and Lorentz, and solved by Poincaré with the introduction of Poincaré stresses. He pointed out that covariance and stability of a system are deeply related issues. Forty years ago Rohrlich, following an early work by Fermi, proposed a fully covariant approach to describe a stable charged particle which is in agreement with the work by Poincaré. However, the study by Rohrlich was sometimes mistaken as a proof of the fact that stability and covariance are unrelated matters. In this Chapter we revisit the problem using our study in Chapter 4. An electron bunch is, indeed, a perfect example of an unstable electromagnetic system. We make use of a paradox to show that, in the case of en electron bunch (or any other unstable system), there is no mean to define, in a physically meaningful way, a total energy-momentum four-vector: covariance of the energy-momentum pair follows from the stability of the system and viceversa, as originally pointed out by Henry Poincaré.

Chapter 5 is based, in part, on the article:

# 5.1  INTRODUCTION

Nearly one hundred years have passed since Abraham and Lorentz calculated their famous expressions for the energy and momentum of a purely electromagnetic, spherically symmetric distribution of charges [1, 2]. This distribution constitutes an attempt to build a classical model of the electron: according to Lorentz's initial idea, mass, energy and momentum of the electron could, indeed, be of completely electromagnetic nature.

Nevertheless, the energy (divided by the speed of light in vacuum, as we will understand through this Chapter) and momentum of such an electromagnetic electron do not constitute a four-vector. In fact (as Abraham [3] pointed out already in 1904 probably, at that time, without a clear understanding of what a four-vector is), in a frame moving with velocity $\boldsymbol{v}$ with respect to the system rest frame, we have

$$E_e = \gamma U'(1 + 1/3\beta^2) \tag{5.1}$$

and

$$\boldsymbol{P}_e = 4/3\gamma\boldsymbol{v}U'/c^2, \tag{5.2}$$

where the index $e$ indicates the electromagnetic nature of the energy $E_e$ and momentum $\boldsymbol{P}_e$, $\gamma$ is the usual Lorentz factor, $\beta$ is the velocity $v/c$ (normalized to the speed of light in vacuum $c$), and $U'$ indicates the electromagnetic energy in the electron rest frame [4],

$$U' = \epsilon_0/2 \int \boldsymbol{E}'^2 dV', \tag{5.3}$$

$\epsilon_0$ being the free space permittivity. $U'$ is purely an electrostatic quantity (in this Chapter the prime will always indicate quantities calculated in the rest frame; therefore $\boldsymbol{E}'$ and $dV'$ are, respectively, the electric field and the volume element in the rest frame of the system).

It is worth to mention here that the factor $4/3$ in Eq. (5.2) and the term proportional to $1/3\beta^2$ in Eq. (5.1) depend on the choice of spherical symmetry made on the charge distribution: had we chosen, for instance, an infinitely long line distribution in the direction of $\boldsymbol{v}$, we would have found

$$E_{e2} = \gamma U'(1 + \beta^2) \tag{5.4}$$

and

$$\boldsymbol{P}_{e2} = 2\gamma\boldsymbol{v}U'/c^2, \tag{5.5}$$

while, in the case of a line charge oriented perpendicularly to the direction of $\boldsymbol{v}$,

$$E_{e3} = \gamma U' \tag{5.6}$$

and

$$\boldsymbol{P}_{e3} = \gamma\boldsymbol{v}U'/c^2, \tag{5.7}$$

which only incidentally, due to the particular choice of the distribution, behaves as a four-vector.

Henry Poincaré solved the problem of the lack of covariance shown in Eq. (5.1) and Eq. (5.2) by introducing, in the electron model, energies and momenta of non-electromagnetic nature [5]. These are actually due to non-electromagnetic interactions which keep the electron together. By doing so he strongly related the covariance of energy and momentum with the stability of the system: the electromagnetic energy-momentum pair alone is not a four-vector, but the total energy-momentum pair, accounting for the non-electromagnetic interaction, is a regular four-quantity.

In 1922, Enrico Fermi developed an original, early relativistic approach to the 4/3 problem [6]; about forty years later a redefinition of the energy-momentum pair related to Fermi's work was proposed by Rohrlich [7], which leaves untouched the total energy-momentum vector, but splits it into electromagnetic and non-electromagnetic contributions in such a way that covariance is granted for both the electromagnetic and the non-electromagnetic part of the energy-momentum pair.

It is possible to show [8, 9] that the treatments by Poincaré and Rohrlich are not in contradiction.

Nevertheless, the approach by Rohrlich [7] was sometimes taken (see e.g. [10]) as the proof that stability and covariance are unrelated matters since, upon redefinition, the electromagnetic part alone is a four-vector.

We will show here that such a conclusion is incorrect. The stability of the system is related to the covariance of the total energy-momentum vector, according to the original work by Poincaré: the redefinition procedure mentioned above is indeed acceptable only in the case one is interested in the total energy-momentum vector of a stable system (i.e. a system whose constituents are and stay at rest in a particularly chosen frame), and not in the separate electromagnetic and non-electromagnetic part. Only in that case the arbitrariness included in the recombination of these two contributions does not affect the equation of motion for the system (which deals, in fact, with the total energy-momentum vector).

In Chapter 4 we addressed the problem of describing the transverse self-fields originating within an ultrarelativistic electron bunch moving in a fixed trajectory.

This, as already discussed, is a particularly relevant problem in modern particle accelerator physics, in view of the need for very high-peak current, low emittance beams to be used, for example, in self-amplified spontaneous emission (SASE)-free-electron lasers operating in the x-ray regime (see for example [11, 12]): in fact, the good quality of the beam may be spoiled by self-interactions occurring within the bunch.

Besides practical relevance (which stresses how, after one hundred years, pure academical problems become relevant to applied physics too), an electron bunch is also a very good example of an unstable system subject to purely electromagnetic interactions. For such a system, the total (interaction) energy and the total momentum in any frame, are just of electrodynamical nature. We will show that (according to our previous statement about the relation between stability and covariance) there is no way, in this case, to define the total energy-momentum pair in a covariant way. In fact, in contrast to what happens for stable systems, there is no way to describe the evolution of an unstable system without the knowledge of the (electromagnetic) field theory governing the (self-)interactions between its constituents.

## 5.2   A PARADOX AND ITS SOLUTION

Let us consider a short electron bunch moving, in a given laboratory frame, in a circular orbit. We can simplify the description of this system accounting only for two electrons which will represent the head and the tail of our bunch.

Imagine that the two particles are moving, initially with the same Lorentz factor $\gamma \gg 1$, in a circular orbit of radius $R$, and separated by a (curvilinear) distance $\Delta s \ll R/\gamma^3$.

In this situation the two electrons are near enough to be considered travelling with the same velocity vector: indeed it can be shown [13], that they radiate as a single particle of charge $2e$ ($e$ being the electron charge) up to frequencies much above the synchrotron radiation critical frequency (note that, from a quantitative viewpoint, the expression "much above" is trivially connected to "how much" $\Delta s \ll R/\gamma^3$). The requirements specified before consist, from a geometrical viewpoint, in assuming that at the beginning of the evolution the two particle world-lines are very close: actually, considering our resolution in space equal to $R/\gamma^3$, they initially coincide.

This assumption justifies the presence of an inertial frame in which both particles are, with good approximation, at rest during the initial part of their evolution. We will refer to it simply as the rest frame. A quantitative definition of the initial part of the evolution may be given when a choice is made about how close to zero are the velocities of the particles in the rest frame. Note that the existence of the rest frame is central for our study because, referring to it, one can easily analyze the energy and momentum of the system constituted by the two particles together with their electromagnetic fields.

By means of a Lorentz transformation, then, we can recover the same quantities in the laboratory frame.

Starting with the study in the rest frame we will refer, separately, to mechanical and electromagnetic quantities.

Obviously, in the rest frame, the mechanical momentum of the system, $\boldsymbol{P}'_{ne}$, is zero, and the mechanical energy, $E'_{ne}$, is just equal to $2mc^2$, where $m$ is the electron rest mass.

The study of the electromagnetic contributions to energy and momentum is also trivial. Since the electrons are at rest they produce electric field only. Therefore the Poynting vector vanishes and $\boldsymbol{P}'_e = 0$. Moreover $E_e$ is given, simply, by the work $U'$ done against the field to bring the two particles together (quasistatically) from a situation in which they are separated by an infinite distance.

By doing so, of course, we are neglecting, in both $\boldsymbol{P}'_e$ and $E'_e$, the contributions from the acceleration (self-)fields generated by the system.

This approximation is justified by the fact that we are discussing the asymptotic behavior for the two particles separated by a very small distance: then, as it will be clear from Eq. (5.16) and Eq. (5.20), we may assume that the acceleration field contribution are unimportant, when compared with the Coulomb one. In fact acceleration effects saturate in the asymptotic limit of small distance between the two particles (see [13] and Chapter 3), while Coulomb ones are singular; once again it must be clear that we are discussing the asymptotic case for small distance between the two particles. Therefore we have:

$$E'_e = U' = e^2/(4\pi\epsilon_0\gamma\Delta s) \tag{5.8}$$

and

$$\boldsymbol{P}'_e = 0. \tag{5.9}$$

Summing up the electromagnetic and mechanical contributions one gets the total energy and momentum for the system:

$$E'_{tot} = E'_{ne} + E'_e = 2mc^2 + U' \tag{5.10}$$

and

$$\boldsymbol{P}'_{tot} = \boldsymbol{P}'_{ne} + \boldsymbol{P}'_e = 0. \tag{5.11}$$

As already said, one may now use a Lorentz transformation in order to calculate these quantities in the laboratory frame. Again, since we are interested at the beginning of the evolution, it follows from our assumptions that the two particles evolve with the same four-velocity vector. Therefore a direction of motion (which we will designate with z) is well defined for the system in the laboratory frame and the Lorentz transformation from the rest frame is a simple boost in the $-z$ direction (note that a good definition of the $z$ direction is equivalent to a good definition of the rest frame). We will represent this boost with a matrix with components $\Lambda^\mu_{\ \nu}$ with $\mu, \nu = 0... 3$ (where the third component corresponds to the $z$ direction):

$$\Lambda^\mu_{\ \nu} = \begin{pmatrix} \gamma & 0 & 0 & \beta\gamma \\ 0 & 1 & 0 & 0 \\ 0 & 0 & 1 & 0 \\ \beta\gamma & 0 & 0 & \gamma \end{pmatrix}. \tag{5.12}$$

The use one makes of $\Lambda^\mu_{\ \nu}$ is a critical point in our derivation. If one (erroneously) assumes that energy and momentum constitute a four-vector, then he gets straightforwardly:

$$(E_{tot}/c, \boldsymbol{P}_{tot})^\mu = \Lambda^\mu_{\ \nu}(E'_{tot}/c, \boldsymbol{P}'_{tot})^\nu \ ; \tag{5.13}$$

therefore

$$E_{tot} = \gamma \left(2mc^2 + U'\right), \tag{5.14}$$

and

$$P_{tot} = \gamma \left(2m + U'/c^2\right) \beta c \ , \tag{5.15}$$

where $P_{tot}$ is a scalar quantity, since we understand that $\boldsymbol{P}_{tot}$ is oriented along the $z$ direction.

We can now project the equation of motion, $\boldsymbol{F}_{\text{syst}} = d\boldsymbol{P}_{tot}/dt$, onto the transverse direction (perpendicular to $z$ and lying on the orbital plane) thus getting, within our approximations:

$$F_{\perp\text{syst}} = -2eB\beta c - \frac{e^2}{4\pi\varepsilon_0 R\Delta s} \ . \tag{5.16}$$

As the reader will remember, we addressed the description of the transverse self-fields originating within an electron bunch moving in a circle in Chapter 4. There, an approach has been proposed which involves purely electrodynamical considerations, based on the retarded Green function solution of Maxwell equations.

In particular, in part of Chapter 4 we treated the case of two particles separated by a distance $\Delta s$ (non necessarily much smaller than $R/\gamma^3$), moving rigidly in a circle (see Fig. 4.2) of radius $R$. Those results are in disagreement with Eq. (5.16).

Let us briefly justify the latter statement. The total transverse force (orthogonal to its velocity and lying on the orbital plane) felt by the head electron and due to the tail electron source turned out to be given by Eq. (4.13), that is:

$$F_\perp \simeq \frac{e^2\gamma^3}{4\pi\varepsilon_0 R^2}\Phi(\hat{\phi}) \; , \qquad (5.17)$$

where $\Phi$ is defined by Eq. (4.14), which, as already observed, is completely independent on the parameters of the system.

In Chapter 4 we also plotted the function $\Phi(\Delta\hat{s})\Delta\hat{s}$ as a function of $\Delta\hat{s}$. This result has been presented in Fig. 4.3. As it is seen from the figure, the contribution from the velocity field is not important in the asymptotic limit for particles very nearby (as in our case here) or very far away. When, in particular, $\Delta s \ll R\gamma^3$ we can approximate Eq. (5.17) by

$$F_\perp \simeq \frac{e^2}{4\pi\varepsilon_0 R\Delta s} \; . \qquad (5.18)$$

On the other hand, as regards the force felt by the tail particle (see Fig. 4.4), it is easily seen (Chapter 4, or [13]) that the test electron, which now is the tail particle, "runs against" the electromagnetic signal emitted by the source (while in the previous case it just "runs away" from it).

In this situation, $\boldsymbol{\beta_S}$ is almost parallel (and equal) to $\boldsymbol{\beta_T}$ and antiparallel to $\boldsymbol{n}$ (which is the unit vector oriented as the line connecting the retarded source to the present test particle): it turns out that the only important contribution to the transverse force results from the acceleration field and is given by Eq. (4.17):

$$F_\perp \simeq \frac{e^2}{4\pi\varepsilon_0 R\Delta s} \; , \qquad (5.19)$$

where $\Delta s$ is considered as a positive distance, as everywhere in this Chapter. In the case under study, since $\Delta s \ll R/\gamma^3$, the total self-force acting on the system is given by the sum of Eq. (5.18) and Eq. (5.19):

$$F_\perp \simeq 2\frac{e^2}{4\pi\varepsilon_0 R\Delta s} \; , \qquad (5.20)$$

which is in disagreement of a factor 2 with respect to the self-force term in Eq. (5.16). In other words, had we erroneously assumed covariance, we would have encountered a paradox. Again, note that we are treating the asymptotic limit of a small distance between the two electrons: in this limit we can neglect the contribution from the acceleration field in the equation of motion Eq. (5.16). In fact this contribution saturates for small distance between the two particles (see [13] and Chapter 3), while the term

missing by comparison between Eq. (5.16) and Eq. (5.20) is singular (and, therefore, dominating) in the limit when $\Delta s$ goes to zero.

This situation should not be too much surprising for the reader familiar with the works [1, 2, 3] which led to Eq. (5.1) and Eq. (5.2): the derivation of Eq. (5.16) is, in fact, performed under the explicit assumption that energy and momentum constitute a four-vector.

As we will immediately see, in the case of unstable systems (like the one we are dealing with), the use of correct transformation laws for the electromagnetic stress tensor solves the problem but spoils the covariance of the energy-momentum pair.

The energy and momentum of an electromagnetic system in the laboratory frame is given by

$$E = \int T'^{\mu\nu} \Lambda^0{}_\mu \Lambda^0{}_\nu \frac{dV'}{\gamma} \tag{5.21}$$

and

$$P^i = \frac{1}{c} \int T'^{\mu\nu} \Lambda^i{}_\mu \Lambda^0{}_\nu \frac{dV'}{\gamma}, \tag{5.22}$$

where $T'^{\mu\nu}$ are the components (in the rest frame) of the electromagnetic stress tensor of the system, which contain all the information about the (electromagnetic) field theory governing the interactions between the particles. The process of lowering and raising indexes is governed in the usual way by the metric tensor. Here the latin index $i$ runs from 1 to 3 and, as already said, the quantities with prime refer to the rest frame. In our case we will consider the only important component, i.e. the third (along $z$).

Note that the integrals in Eq. (5.21) and Eq. (5.22) include both a single-particle term and an interaction term (compare also with [9]). Here we are interested in the interaction term alone: in fact we will treat the (trivial) mechanical contributions to the energy-momentum pair separately and, once again, we will neglect the acceleration-field contributions. Therefore, in the following, we will understand that $T'$ refers to the interaction term alone.

Then, since the mechanical energy-momentum pair of a single particle is a 4-vector, one gets:

$$(E_{ne}/c, P_{ne})^\mu = \Lambda^\mu{}_\nu (E'_{ne}/c, P'_{ne})^\nu \,, \tag{5.23}$$

hence

$$E_{ne} = 2\gamma mc^2 \tag{5.24}$$

and

$$P_{ne} = 2\beta\gamma mc, \tag{5.25}$$

while

$$E_e = \beta^2 \gamma \int T'^{33} dV' + \gamma U', \tag{5.26}$$

$$P_e = \gamma\beta U'/c + \gamma\beta/c \int T'^{33} dV'. \tag{5.27}$$

We should note, here (but this is a valid methodological remark also as regards the previous, incorrect approach), that the particles are subject to a long-range interaction (the electromagnetic interaction) and, therefore, a covariant definition of the total energy and momentum is not straightforward even when one is considering the two particles alone, without including (as we did, instead) the electromagnetic fields in the system. Therefore, strictly speaking, one may object that Eq. (5.23) does not make any sense at all.

Indeed, if the interaction occurred at a single point in space-time (short-range scattering case), the particle velocities would have been constant, in the view of any inertial observer, before and after the scattering took place. Then, if two observers related by a Lorentz boost compared their judgments about the particles velocities, they would have found that these are linked by a Lorentz transformation, the same which transforms from one observer to the other. Nevertheless, this is a particular case. We must remember that in general, according to the theory of relativity, the concept of simultaneity depends on the observer. Therefore, when (as in the situation under study) one deals with a long-range interaction, the velocities of the particles, in the judgment of the two observers above, are not related by a Lorentz transformation anymore (see [14]): the objection about the correct definition of the mechanical energy-momentum vector follows directly from this observation.

However this objection does not concern us here since, as already implicit in the definition of the $z$ direction, we discuss about that region of space-time in which the two particles world-lines are very close and are roughly characterized by the same Lorentz factor, that is, once again, at the beginning of the evolution.

Then we can use Eqs. (5.23) to (5.27) to get, by summation, the total energy and momentum of the system in the laboratory frame and in the direction of motion (see also [4] and [15]):

$$E_{tot} = \gamma \left( 2mc^2 + U' + \beta^2 \int T'^{33} \, dV' \right), \qquad (5.28)$$

and

$$P_{tot} = \gamma \left( 2m + U'/c^2 + \frac{1}{c^2} \int T'^{33} \, dV' \right) \beta c \, . \qquad (5.29)$$

Note that Eq. (5.28) and Eq. (5.29) can be used to obtain Eq. (5.1) and Eq. (5.2), as well as Eqs. (5.4) to (5.7): different distributions of charge give different expressions for the electromagnetic stress tensor and for the electromagnetic energy.

In our case of two electrons we already know the explicit expression for $U'$. In fact we remind that, as has already been said, the electromagnetic interaction energy is simply given by the work done against the field to bring the two particles together, quasistatically, from a situation in which they are separated by an infinite distance:

$$U' \simeq \frac{e^2}{4\pi\varepsilon_0 \gamma \Delta s} \, . \qquad (5.30)$$

On the other hand it is easy to calculate $T'^{33}$ (in the rest frame, since we need to integrate over $V'$). To this purpose we remind that, in the rest frame (and at short distance $\gamma \Delta s \ll R/\gamma^2$, so that the acceleration field contributions are unimportant),

the space-space components of the total (comprehensive of both single-particle and interaction part) symmetric energy-momentum tensor read (see Chapter 1 or [4]):

$$T_{tot}^{\prime ij} = -\varepsilon_0(E^{\prime i}E^{\prime j} - \delta^{ij}E^{\prime 2}/2) \; , \tag{5.31}$$

where, here, $i, j = 1... 3$. The discussion above shows that, for us, the only interesting component is $T^{\prime 33}$. With the help of [9] it can be proven that the interaction part alone is just

$$\int T^{\prime 33} \, dV' = U' \; . \tag{5.32}$$

Note that Eq. (5.32) describes also the case of a charged line distribution oriented in the direction of motion (in the case of a charged line, of course, the single-particle term is not present at all).

The equations for the energy and the momentum of the system in the laboratory frame now read:

$$E_{tot} = \gamma \left[2mc^2 + U'(1 + \beta^2)\right] \tag{5.33}$$

and

$$P_{tot} = \gamma \left(2m + 2U'/c^2\right) \beta c \; , \tag{5.34}$$

whose electromagnetic parts are the same of Eq. (5.4) and Eq. (5.5).

From the transverse component of the equation of motion for the system one gets

$$F_{\perp\text{syst}} \simeq -2eB\beta c - 2\frac{e^2}{4\pi\varepsilon_0 R\Delta s} \; . \tag{5.35}$$

Eq. (5.35) is now in perfect agreement with our result in Eq. (5.20). Both the terms on the right hand side of Eq. (5.35) are centripetal as well as the ones in Eq. (5.16) (although, of course, Eq. (5.16) and Eq. (5.35) are in disagreement as concerns the magnitude of the self-interaction term); the first is due to an external magnetic field, while the second is linked with the presence, in the system, of electromagnetic fields: an extra centripetal (external) force is needed, if one wants to keep the system moving in a circle of radius $R$, compensating for the centrifugal self-field contributions calculated in Chapter 4 (or in Eq. (5.20)).

## 5.3   Discussion

In order to reach the agreement between Eq. (5.20) and Eq. (5.35), one has to give up the covariance of the energy-momentum pair of our system, as it is seen directly from Eq. (5.33) and Eq. (5.34).

We can sum up the discussion in Section 5.2 by saying that the assumption of covariance for the transformation of the energy-momentum pair of an unstable system leads to a paradox. Such a paradox can be solved introducing the correct transformation laws for the energy-momentum tensor. In this way, it is seen that the energy-momentum pair for an unstable system (particles and electromagnetic field) is not a four-vector. We already mentioned in Section 5.1, that the non-covariant character of energy and

momentum is also present when one discusses some classical problems which involve the relativistic dynamics of a charged particles stable system. Nevertheless, in these cases, covariance can be always restored by introducing non-electromagnetic stresses which keep the system together or, equivalently, by redefinition (see [7]) of the energy-momentum pair. In particular we can refer to the 4/3 problem in the classical electron model (as done above in Section 5.1) but also to other problems like, for example, the explanation of the Trouton-Noble paradox, which has been treated extensively in literature (see [8], [16] to [19]) all over the last century.

As we already said in Section 5.1, there is one major difference with respect to our case, though: our system, in contrast with the latter ones, is unstable by nature; there is no reference frame such that its components are and stay at rest. This fact leads to a major difference in the treatment of the total energy and momentum.

In the case of a stable system, the total energy and momentum of the system (including non-electromagnetic binding forces) constitute a four-vector, a well-defined geometrical entity.

On the contrary, in the case of an unstable system, this pair of quantities has no geometrical meaning, although it is possible to give, of course, separate definitions of total energy and momentum in the judgment of any observer.

In the situation discussed in Section 5.2 this is a direct consequence of the fact that we deal with a fully electrodynamical system and there is no way to introduce, in a straightforward way, an analogue of Poincaré stresses. As a result we must conclude that stability of the system and covariance of the energy-momentum pair are bound together.

Let us discuss the latter statements in detail, starting with a review of well-known arguments for stable systems.

Stable systems are characterized by a zero (total self-) four-force density. When the four-force density can be derived from an energy-momentum tensor $T^{\mu\nu}$, the latter property is equivalent to (see [4]):

$$\partial_\mu T^{\mu\nu} = 0 \; , \tag{5.36}$$

which is the requirement for a zero-divergency energy-momentum tensor.

However, Eq. (5.36) refers to the total energy-momentum tensor, while the electromagnetic part of it is not divergenceless at all (its divergence is, simply, the Lorentz four-force density).

On the other hand, since stability is characterized by a zero total four-force density, non-electromagnetic stresses must be present (Poincaré stresses), which balance the Lorentz four-force density, thus insuring stability for the system. Poincaré stresses also insure covariance for the energy-momentum pair which is, therefore, a well-defined four-vector: to prove this, one can remember the definition of the total energy-momentum pair (see [4, 8]):

$$P^\mu = \frac{1}{c} \int_\sigma T^{\mu\nu} d\sigma_\nu \; , \tag{5.37}$$

where the integration is carried out over any hypersurface at $t = constant$ (actually $\sigma$ may be, more generally, any spacelike surface, see [8]) for any inertial observer.

It can be easily proved (see [8]) that Eq. (5.37) is independent from the choice of the integration hypesurface. Such a proof is based on Eq. (5.36).

The choice of different inertial observers is equivalent to the choice, on the space-time manifold, of different time-like unit vectors. The different families of hypersurfaces orthogonal to these vectors represent the physical space at a certain time in the judgement of different observers. From the independence of the definition in Eq. (5.37) of the choice of the integration hypersurface follows, therefore, the independence of $P^\mu$ on the reference frame used to evaluate it, and this constitutes the proof that $P^\mu$ is a well-defined four-vector.

Since $P^\mu$ is independent from the choice of the integration hypersurface, we are free to choose the one which helps better in solving problems. Historically, two choices have been used in explaining, for example, the Trouton-Noble paradox. The first (see [8]) consists in considering the surface at $t = constant$ for any observer. This leads to the usual expressions for the electromagnetic energy and momentum in a given frame (see [4]):

$$\frac{E_e}{c} = P_e^0 = \frac{1}{2c} \int \left( \epsilon_0 \boldsymbol{E}^2 + \frac{\boldsymbol{B}^2}{\mu_0} \right) dV \tag{5.38}$$

and

$$\boldsymbol{P}_e = \frac{1}{\mu_0 c^2} \int (\boldsymbol{E} \times \boldsymbol{B}) \, dV, \tag{5.39}$$

where $\mu_0$ is the free space permeability.

While Eq. (5.38) and Eq. (5.39) do not constitute a four-vector, one can straightforwardly solve the problem of the lack of covariance by introducing Poincaré stresses.

The second choice consists in selecting $t = constant$ in the rest frame of the system (see [4, 20]):

$$\frac{E_e}{c} = P_e^0 = \frac{\gamma^2}{2c} \int \left( \epsilon_0 \boldsymbol{E}^2 - \frac{\boldsymbol{B}^2}{\mu_0} \right) dV \tag{5.40}$$

and

$$\boldsymbol{P}_e = \frac{\gamma^2 \boldsymbol{\beta}}{2c} \int \left( \epsilon_0 \boldsymbol{E}^2 - \frac{\boldsymbol{B}^2}{\mu_0} \right) dV \; ; \tag{5.41}$$

the electromagnetic part of the total energy-momentum pair is, then, a four-vector (see [4]). This is, in fact, the same redefinition of the four-momentum that Rohrlich used to deal with the electron problem [7]. One can easily check (see [8]) that, in this case, the non-electromagnetic part of the total energy-momentum pair is zero.

All this illustrates the well-known fact that the introduction of Poincaré stresses or the Rohrlich redefinition of energy and momentum are, in fact, equivalent in essence. The choice of the integration hypersurface is a matter of taste for stable systems, since the only important quantity from a geometrical viewpoint is the total energy-momentum four-vector, given by the sum of the electromagnetic and the non-electromagnetic part; this sum, by definition, is independent from such a choice. In other words, different choices of the hypersurface just split the same total quantity onto two parts (electromagnetic and non-electromagnetic) in distinct ways but,

as quoted from [8]: "The split into electromagnetic and non-electromagnetic parts is quite arbitrary".

Our point is that this situation is completely different in the case of unstable systems, where only electromagnetic forces are present and Poincaré stresses are not. In the case of unstable systems there is no way one can define the total energy-momentum four-vector. This statement is justified, from a mathematical viewpoint, by the following inequality:

$$\partial_\mu T_{tot}^{\mu\nu} = \partial_\mu T_e^{\mu\nu} \neq 0 \; ; \tag{5.42}$$

in fact, from the previous discussion, we know that divergenceless is an essential ingredient for the independence of the total energy-momentum pair from the choice of the integration hypersurface.

Note that Eq. (5.42) means that there is a non-vanishing four-force density field over the space-time. In the case discussed in Section 5.2 we gave a practical example of the statements above.

Of course, also for unstable systems we may consider an observer and find out the energy and the momentum of the system with respect to that observer, but this quantities will not be covariant, nor we can recover covariance by integrating the energy-momentum tensor over a suitable hypersurface (as done with stable systems), since the electromagnetic energy-momentum pair (which coincides now with the total energy-momentum pair) would change Eq. (5.33) and Eq. (5.34), thus giving an unphysical result on the second term of Eq. (5.35), when compared with Eq. (5.20). The latter discrepancy, to our view, is similar to the one encountered in [9]. In that paper a system composed by two electron is studied too and a comparison is proposed between energy-derived mass $m_u$ (electrostatic energy divided by $c^2$), momentum-derived mass $m_p$ (momentum divided by $\gamma v$, being $v$ the system velocity) and self-force-derived mass $m_s$ (self-force divided by $\gamma^3 a$, $a$ being the system acceleration). The authors of [9] point out that $m_s = m_p \neq m_u$ and that the inequality between $m_p$ and $m_u$ can be solved by redefining, following Rohrlich (see [7]) the energy-momentum pair. Nevertheless, in this case, one is left with a discrepancy between $m_s$ and $m_u$. This fact is perceived by the authors of [9] as an unsolved paradox. Actually, the derivation of Eq. (5.16) (or equivalently, of $m_u$, treated with Rohrlich's method) is performed under the explicit assumption that energy and momentum constitute a four-vector, which is true only in the case of a stable system. As a result, by comparing Eq. (5.16) and Eq. (5.20) or, which is the same, $m_u$ (treated by Rohrlich's method or, equivalently, by introducing Poincaré stresses) with $m_s$, one is comparing quantities which refer to a stable system with quantities which refer to an unstable one, thus giving a paradoxical result.

Consider, as a last example, an unstable system formed by different subsystems initially at rest in a certain frame (as in the case discussed in Section 5.2). In general, while dealing with unstable systems, the knowledge of dynamical quantities for the subsystems cannot bring any information about the behavior of the system as a whole, unless we have knowledge of the (electromagnetic) field theory governing the interactions (which make the system unstable).

In our example of Section 5.2, even if we can measure, in a certain frame, the particle velocities when they are far away from each other (thus no more interacting) and if we know their rest masses, we cannot say anything about the energy and the

momentum of the total system without the knowledge of the stress tensor, and the reason for this is the presence of a non-zero four-force density field (which we can account for only knowing the stress tensor, i.e. the interaction theory) on that part of the four-dimensional manifold on which we want to have information.

Suppose our system was stable (think about an ideal "rope" responsible for Poincaré stresses, or think, instead of the case of two electrons, about a nuclear fission process in which electromagnetic fields are, before the fission event, balanced by the strong interaction). Put ourselves in the laboratory frame and imagine that, at a certain moment, for a certain reason (a collision with a neutron, for example) the Poincaré stresses are not present anymore. Thus the system becomes unstable, it breaks in two subsystems and the electromagnetic interaction (if you are thinking about the nucleus imagine we are talking about a charged ion) takes over. If we wait for enough time the two particles will get far away from each other and we can consider them no more interacting.

At this point, the kinetic energy of the particles is equal to the energy previously stored in the electromagnetic field when the system was stable: thus we are able to get information about the total energy-momentum vector of the stable system even if we do not know anything about the stress tensor and the theory of the interaction between the subsystems. In fact, the sum of the momenta of the two free particles and the sum of their energies will give us, respectively, the energy and the momentum of the stable system, which form a four-vector again.

The reason is, simply, that there is no four-force density field in that part of the space-time on which we want to have information: from a general viewpoint we can conclude that the presence of a four-force density, which characterizes unstable systems, spoils without remedy the covariance of the energy-momentum pair. The only way to recover such covariance would be to introduce a balancing four-force density, i.e. to make the system stable.

In other words, in agreement with Poincaré, from the stability of the system follows the covariance of the system and, viceversa, from covariance follows stability: the energy-momentum pair of an unstable system does not constitute a four-vector. This conclusion may seem, at first glance, of academical importance only. It has very practical consequences in modern electron beam physics. Energy and momentum of an electron bunch are measurable quantities and an electron bunch itself is a practical example of an unstable system. Nowadays, technology allows the production of ultra-high brightness, intense electron beams to be used, for example, in self-amplified spontaneous emission (SASE)-free-electron lasers operating in the x-ray regime. The production of such bunches is one of the most challenging activities for particle accelerators physicists. The description of these systems would be completely incorrect without accounting for self-interactions in the right way. We can conclude that any simulation code or analytical consideration relying on the covariance of the energy-momentum pair would give, *a priori*, wrong results which may be immediately confuted by experiment. Technological developments often transform, as in this case, purely methodological issues into very practical ones.

# Bibliography

[1] M. Abraham, *Theorie der Elektrizitat, vol II: Elektromagnetische Theorie der Stralung*, Teubner, Leipzig, 1905

[2] H.A. Lorentz, *The Theory of electrons*, Leipzig, Teubner, 1909

[3] M. Abraham, Phys. Z., 5, 1904

[4] J. D. Jackson, *Classical Electrodynamics*, Wiley, N.Y.

[5] H. Poincaré, *On the dynamics of the electron*, Rendiconti del Circolo Matematico di Palermo 21, 129, 1906

[6] E. Fermi, Il Nuovo Cimento, 25, 159-170, 1923

[7] F. Rohrlich, *Classical Charged Particles*, Addison-Wesley, 1990, Sec. 6-3

[8] S. A. Teukolsky, Am. J. Phys. 64 (9), 1104, 1996

[9] D. J. Griffiths and R. E. Owen, Am. J. Phys. 51 (12), 1120, 1983

[10] M. H. Mac Gregor, *The enigmatic electron*, Kluwer Academic Publishers, Dordrecht/Boston/London, edited by Alwyn van der Merwe, 1992, pp. 19-24

[11] TESLA Technical Design Report, DESY 2001-011, edited by F. Richard et al. and http://tesla.desy.de/

[12] The LCLS Design Study Group, LCLS Design Study Report, SLAC reports SLAC -R521, Stanford (1998)
and http://www-ssrl.slac.stanford.edu/lcls/CDR

[13] E. L. Saldin, E. A. Schneidmiller and M. V. Yurkov, Nucl. Instr. Methods A 398, 373 (1997)

[14] M.A. Trump at al., *Classical Relativistic Many-Body Dynamics*, Kluwer Academic Publishers, Dordrecht, 1999

[15] C. Möller, *The theory of relativity*, second edition, Chapter 7, Clarendon press, Oxford, 1972

[16] M. v. Laue, Ann. Phys. 35, 524, 1911

[17] W. Pauli, *The theory of relativity*, Pergamon, New York, 1958

[18] A. K. Singal, Am. J. Phys. 61, 428, 1993

[19] J. W. Butler, Am. J. Phys. 36, 936, 1968

[20] J. W. Boyer, Phys. Rev. D. 25, 12, 1982

# Chapter 6

# Applications of Coherent Synchrotron Radiation

In this Chapter we discuss subjects related to possibilities and limits under which CSR can be employed as a radiation source or as a diagnostic method for monitoring the longitudinal structure of very short, high-peak current, ultrarelativistic bunches. We first characterize the CSR pulse from an electron bunch moving in an arc of a circle and then we present a systematic discussion about the limits of validity of the famous Schwinger formulas, which are widely used in synchrotron radiation and CSR theory and usually considered universally valid. It turns out that the standard theory of synchrotron radiation uses several approximations whose applicability limits are too often forgotten. Any attempt to set up a CSR source or a bunch diagnostics system based on CSR detection should take into account these considerations.

Chapter 5 is based, in part, on the article:
**Gianluca Geloni et al., DESY 03-31, ISSN 0418-9833, 2003**

# 6.1  INTRODUCTION

The application of CSR as a powerful far-infrared source, especially in the Terahertz (THz) spectral range, has been considered in several facilities around the world, and first experiments have been performed or proposed [1, 2, 3]. This kind of application is particularly interesting for the community in that, compared with currently available THz sources, CSR sources are characterized by a radiative power several order of magnitude higher.

Besides its utilization as a radiation source, CSR is also a promising tool for bunch diagnostics. As discussed in the previous Chapters, the bunch length for XFEL applications is of the order of 100 femtoseconds. Since detailed understanding of longitudinal dynamics in this new domain of accelerator physics is of paramount importance for FEL performance, experiments on this subject are planned in test facilities. The femtosecond time scale is beyond the range of standard electronic display instrumentation and the development of nondestructive methods for the measurement of the longitudinal beam current distribution in such short bunches is undoubtedly a challenging problem. As a general remark, coherent radiation has the advantage to get simpler to be measured as the bunch shortens, since the minimum coherent wavelength is of the order of the bunch length. In particular, CSR has already been used as a tool to monitor bunch length variations (see [4]) but never to achieve longitudinal bunch-distribution measurements in the femtosecond time scale, as it has been proposed in [5] for the DESY case.

Whenever one plans to use CSR as a far-infrared source or as a tool for bunch diagnostics, one has to carefully characterize the CSR pulse. In this Chapter we discuss topics related to CSR pulse characterization from dipole magnets in the time domain.

In Section 6.2 we first introduce synchrotron radiation theory in the time domain, with special emphasis on the case of radiation from a finite bending magnet. In fact, while Schwinger formulas are valid in order to describe radiation from a dipole in the X-ray range, their long wavelength asymptote is not valid, in general. Analytical study of this matter was first performed in the 80's [6], but since synchrotron radiation users are normally interested in the high frequency range, Schwinger formulas are often considered as always directly applicable. This is not true in the case of CSR from a dipole magnet, because the interesting wavelength range is in the far-infrared. In Section 6.3 we provide a new expression which gives an analytical characterization of the CSR pulse from a bunch moving in an arc of a circle. We use a synthetic approach to present the material: the simpler situation of a circular motion is studied first, and then generalized to the case of an arc. Standard theory of synchrotron radiation relies upon other approximations too, and it is important to pay attention to their region of applicability. To be specific, two important limitations are discussed in Section 6.4. First, it is usually assumed that the observer is located at infinite distance from the source. Second, in real experimental conditions, the radiation is seen by the detector through some limited aperture. Both finite distance effects and diffraction effects are usually ignored. The aperture sizes and the distances are such that these effects must be accounted for in practical situations. Finally, in Section 6.5, we come to some summing up and conclusions.
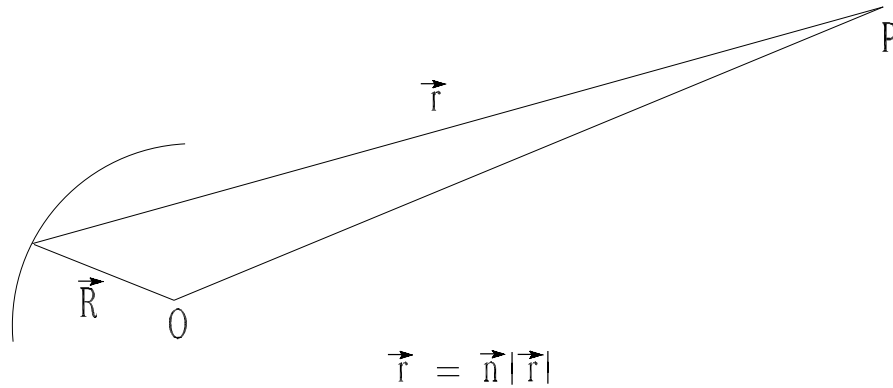
**Figure 6.1:** *Geometry for synchrotron radiation production from a bending magnet.*

## 6.2 Single-particle radiation from a dipole magnet

The typical textbook treatment of single-particle synchrotron radiation (see for example [7, 8, 9]) consists in finding the expression for the synchrotron radiation spectrum from an electron moving in a circle. However, no attention is usually paid to the region of applicability of the derived expressions. For instance, the standard extension of the theory to the case of radiation from a dipole magnet is based on the assumption that the energy spectrum formula is equivalent to the famous Schwinger formula [10]. While this formula is valid for the X-ray range, it does not provide a satisfactory description in the long wavelength asymptotic [6], which is the only region of interest as regards CSR phenomena. In view of its application to CSR theory in the next Section, it is therefore useful to review, here, how a single electron radiates as it moves in a dipole magnet.

Fig. 6.1 shows the relationship between the observer at a fixed point $P$, whose coordinates are $(\boldsymbol{r_0}, t)$, and the radiating electron at $(\boldsymbol{R}, t')$, $t'$ being the emission (or retarded) time. The fundamental laws of electrodynamics tell that the electric field of a charge $e$ moving along an arbitrary trajectory is given by the Liénard-Wiechert fields.

As already discussed, these consist of two terms. The first is inversely proportional to the square of the distance between radiation source and observer, depends only on the charge velocity and is known as velocity or Coulomb field. The second is inversely proportional to the distance from the charge, depends also on the charge acceleration and is known as acceleration or radiation field. At large distances from the moving electron, the acceleration-related term dominates, and is usually associated to the electromagnetic radiation of the charge. The region of space where the radiation field dominates is called far (or wave) zone and the radiative electric field in the far-zone is given by the formula
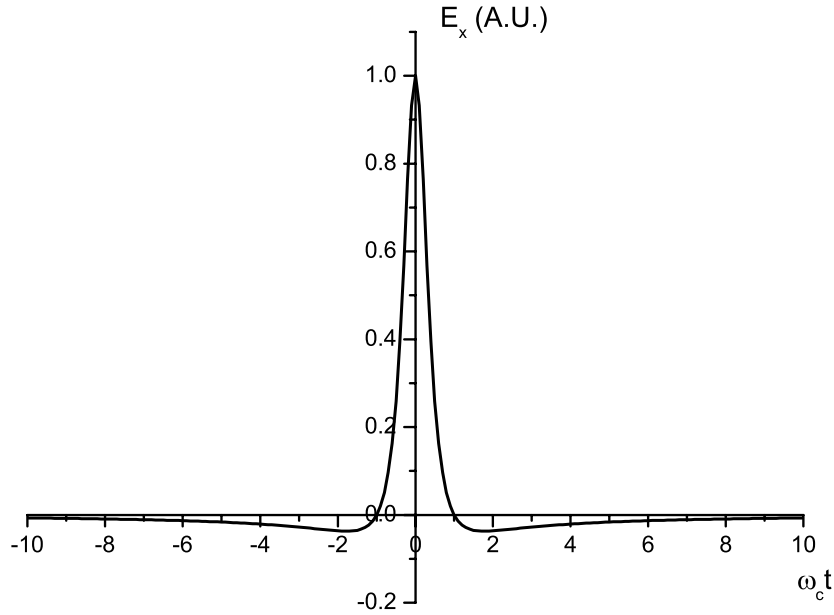
**Figure 6.2:** *Time variation of a synchrotron radiation field-pulse generated by a highly relativistic electron moving in a circle as seen by an observer in the orbital plane.*

$$\boldsymbol{E}_{\mathrm{r}}(t) = \frac{e}{4\pi\epsilon_0 c \mid \boldsymbol{r}_0 \mid} \left[ \frac{\boldsymbol{n} \times [(\boldsymbol{n} - \boldsymbol{\beta}) \times \dot{\boldsymbol{\beta}}]}{(1 - \boldsymbol{n} \cdot \boldsymbol{\beta})^3} \right]_{\mathrm{r}} . \tag{6.1}$$

The usual theory of synchrotron radiation is based, after Schwinger, on the assumption that the electron is moving on a circle and radiation is observed from the whole circular trajectory, so that in each cycle we get a sharp pulse of electric field. A far-field computation of the predicted time-dependence of the synchrotron radiation from an electron in circular motion (of radius R) is presented in Fig. 6.2.

The horizontal component of the electric field is plotted versus the normalized variable $\omega_{\mathrm{c}}t$, where $\omega_{\mathrm{c}} = 3\gamma^3 c/(2R)$ is the critical frequency of synchrotron radiation. The field in the orbital plane has a zero around $t = \omega_{\mathrm{c}}^{-1}$. Numerically, from Fig. 6.2 one obtains

$$\int_{-\infty}^{\infty} \boldsymbol{E}_{\mathrm{r}} \, \mathrm{d}\, t = 0 . \tag{6.2}$$

It is interesting to stress the fact that Eq. (6.2) is strictly related to the well-known result that a uniformly charged ring does not radiate. In fact, starting from Eq. (6.2) one can show that a system of $N$ identical equidistant charges $q$ moving with constant velocity $v$ along a circle does not radiate in the limit for $N \to \infty$ and $qN = $ constant, and that the electric and the magnetic fields of the system are the usual static values.

It is important to realize that Eq. (6.2) is valid only when the electron is moving on a closed trajectory. By inspecting Figs. 6.3 to 6.5, one can see that when the electron

**Figure 6.3:** *Time variation of a synchrotron radiation pulse generated by a highly relativistic electron moving along an arc of a circle. The normalized bending angle is $\hat{\phi}_\mathrm{m} = \gamma\phi_\mathrm{m} = 2.5$.*
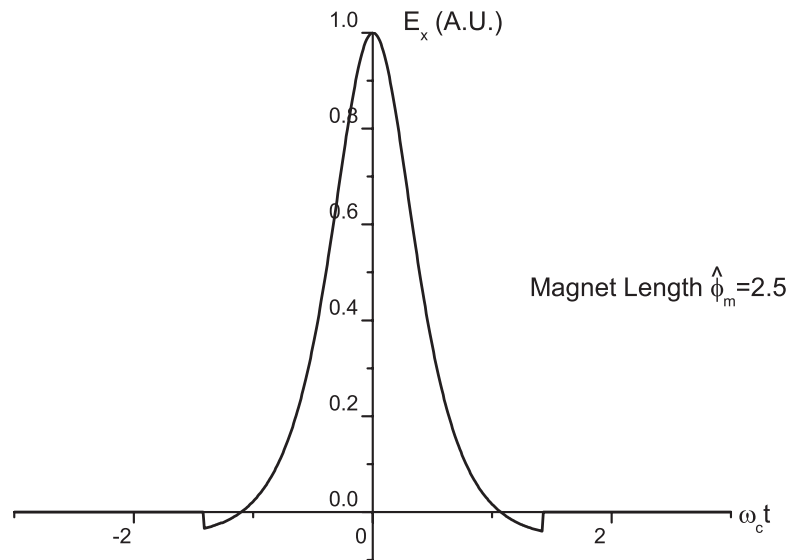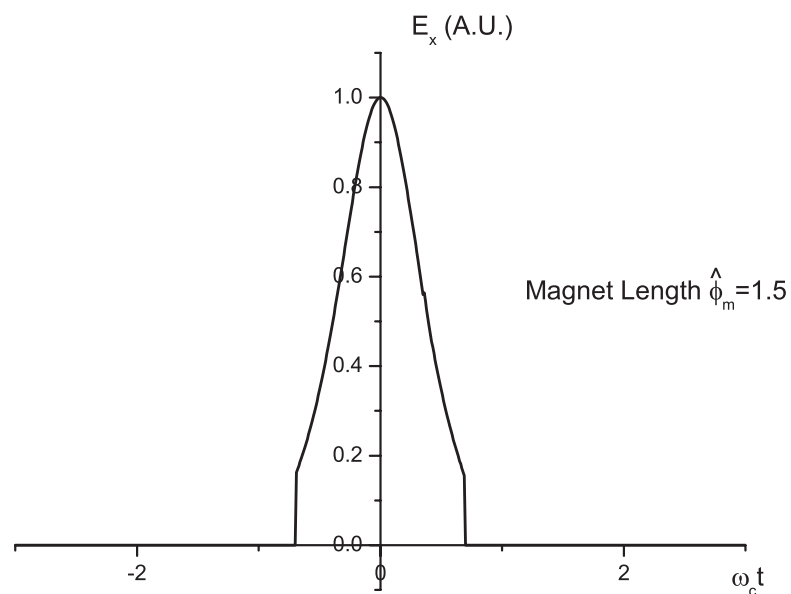


**Figure 6.4:** *Time variation of a synchrotron radiation pulse generated by a highly relativistic electron moving along an arc of a circle. The normalized bending angle is $\hat{\phi}_\mathrm{m} = \gamma\phi_\mathrm{m} = 1.5$.*
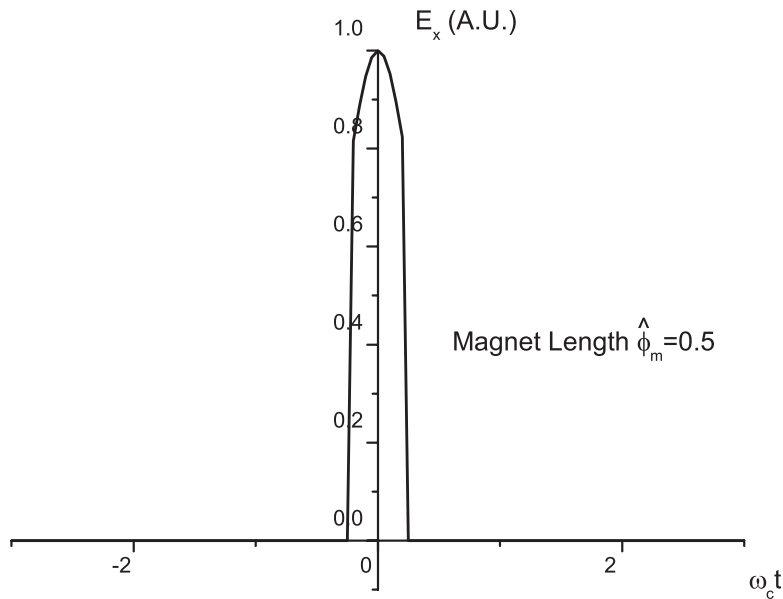
**Figure 6.5:** *Time variation of a synchrotron radiation pulse generated by a highly relativistic electron in a short bending magnet. The normalized bending angle is $\hat{\phi}_\mathrm{m} = \gamma\phi_\mathrm{m} = 0.5$.*

moves in arcs of circle with different angular extensions $\phi_\mathrm{m}$, the time-average of the electric field is non-zero.

Let us consider for a moment (in parallel with what has been done in the case of a circle) a system of $N$ uniformly distributed charges moving with constant (in magnitude) velocity $v$ in an arc of a circle preceded and followed by infinite straight paths in the limit of $N \to \infty$ and $qN = \text{constant}$, as in Fig. 6.6. The fact that the average electric field from a single particle is different from zero means that the acceleration field from our infinite circuit (arc and straight paths) must be different from zero too. Then we have to deal with an intriguing paradox, since it is a well known result that a uniform electron current does not radiate, not only in the case of circular motion, but independently from the trajectory.

It is possible to explain this contradiction in very simple terms as follows. First of all the velocity (electric) field from a line current (including our case) is proportional to $1/\mid \boldsymbol{r}_\perp \mid$, where $\mid \boldsymbol{r}_\perp \mid$ is the distance of the observer from the line charge. Second, in our case the acceleration part of the electric field is proportional to $1/\mid \boldsymbol{r} \mid$, where $\mid \boldsymbol{r} \mid$ is the distance of the observer from the magnet (since the acceleration field sources are strictly limited to the particles in the magnet only). The situation is depicted in Fig. 6.6: the ratio $\mid \boldsymbol{r}_\perp \mid / \mid \boldsymbol{r} \mid$ is finite for any position of the observer; therefore there is no region in space where the acceleration field dominates. This last observation solves our paradox since, in the case of infinite charge current in an arc of a circle, we cannot talk about far-zone at all, although a non-zero acceleration field is present.
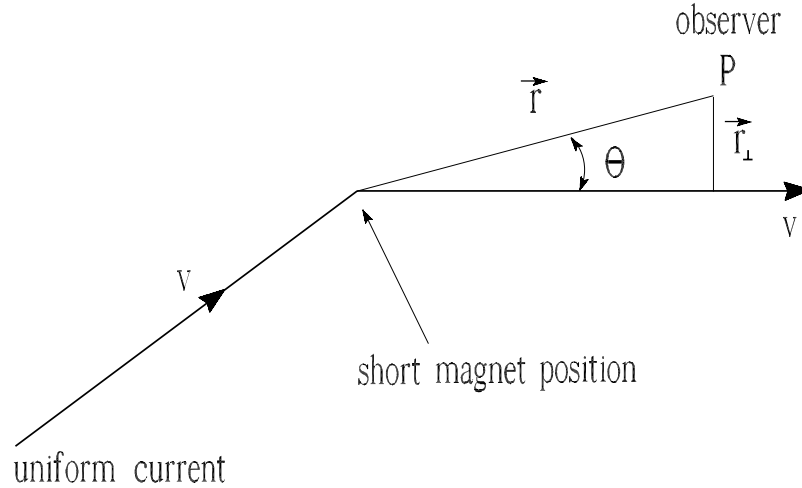
**Figure 6.6:** *Geometry for a uniform current progressing through an arc of a circle and relative position of an observer.*

## 6.3 CSR FIELD IN THE TIME DOMAIN

We can now start to discuss the shape of the coherent synchrotron radiation field pulse associated with different particle trajectories. What we have been dealing with before is simply a far field analysis of the single-particle radiation field. When a large number of electrons move together, the total field will be a linear superposition of the individual particle fields. Of course the result depends upon the longitudinal distribution of the electrons.

### 6.3.1 "Short" magnet limit case

One aspect of the problem that we can immediately deal with is the coherent synchrotron radiation production from a "short" magnet, i.e. in the asymptotic limit $\phi_m \ll 1/\gamma$. We can assert that the field appears as shown in Fig. 6.7. In fact the time-dependence of the field has, for every electron, approximatively, the shape shown in Fig. 6.5 and the total field emitted by the electron bunch is represented by a sum of these pulses, one for each radiating electron. In the limit for short magnets, the time profile of the electron bunch density is linearly encoded onto the electric field of the radiation pulse. The width of the temporal profile of the electric field corresponds directly to the electron bunch length, and the shape of the temporal profile is proportional to the longitudinal bunch distribution.

We have just argued that the bunch density is linearly encoded onto the electric field as in Fig. 6.7; nevertheless, in Fig. 6.7, we illustrate small fluctuations which occur in the field amplitude too. The reason for this is that the electron bunch is composed of a large number of electrons, thus fluctuations always exist in the electron beam density due to shot noise effects. For any synchrotron radiation beam there is some characteristic time, which determines the time scale of the random field fluctuations. This characteristic time is called coherence time $\tau_c$ of synchrotron radiation and its
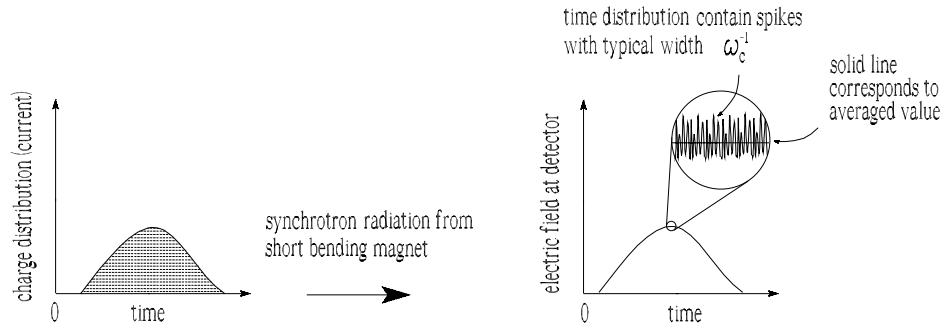
**Figure 6.7:** *Coherent synchrotron radiation production from a "short" magnet. The time profile of the electron bunch density is linearly encoded onto the electric field of the radiation pulse. The spikes correspond to spontaneous radiation, and the average value of the electric field corresponds to CSR. The width of the temporal profile of the electric field corresponds directly to the electron bunch length, and the shape of the temporal profile is proportional to the longitudinal distribution within the bunch.*

magnitude is of the order of the pulse duration from one electron. The physical significance of these fluctuations is that there is a short wavelength radiation component of the radiation in the range of the inverse pulse duration from a single electron. Simple physical considerations show that the energy spectrum of this hard radiation component is order of $P(\omega) \simeq N p(\omega)$. This explains the relation between small fluctuations of the radiation field amplitude and spontaneous (incoherent) emission of synchrotron radiation.

## 6.3.2   Circular motion case

Up to this point we only talked about coherent radiation from a "short" magnet (i.e. in the limit $\phi_{\mathrm{m}} \ll 1/\gamma$). Ultimately we want to relax the assumption $\phi_{\mathrm{m}} \ll 1/\gamma$ and consider CSR production from an arc of a circle in a more generic case. A first step in this direction consists in the analysis of the CSR time pulse from a circular motion. It is possible, indeed, to derive a new, simple analytical expression for the CSR pulse from a bunch with an arbitrary distribution of the linear density satisfying the following condition:

$$\frac{R}{c\gamma^3} \frac{\mathrm{d}\,F(t)}{\mathrm{d}\,t} \ll F(t) \ . \tag{6.3}$$

This condition simply tells that the characteristic length of the bunch is much longer than $R/\gamma^3$. Let us express the total CSR pulse as a superposition of single particle fields:

$$E_{\mathrm{CSR}}(t) = \int\limits_{-\infty}^{\infty} \boldsymbol{E}_{\mathrm{r}}(t-\tau)NF(\tau)\,\mathrm{d}\tau \; , \tag{6.4}$$

where we calibrated the observer time in such a way that, when $F(\tau) = \delta(\tau)$, the single particle radiation pulse has its maximum at $t = 0$. To calculate the integral in Eq. (6.4) one should take into account the property Eq. (6.2) of the kernel $\boldsymbol{E}_{\mathrm{r}}(t-\tau)$ which has been discussed above. Using Eq. (6.2) and condition (6.3) one can simplify Eq. (6.4) in the following way. The integral in Eq. (6.4) is written down as a sum of three integrals

$$\boldsymbol{E}_{\mathrm{CSR}}(t) = \int\limits_{-\infty}^{t-\delta_1} \boldsymbol{E}_{\mathrm{r}}(t-\tau)NF(\tau)\,\mathrm{d}\tau$$

$$+ \int\limits_{t-\delta_1}^{t+\delta_2} \boldsymbol{E}_{\mathrm{r}}(t-\tau)NF(\tau)\,\mathrm{d}\tau + \int\limits_{t+\delta_2}^{\infty} \boldsymbol{E}_{\mathrm{r}}(t-\tau)NF(\tau)\,\mathrm{d}\tau \; , \tag{6.5}$$

where $\delta_{(1,2)}$ satisfy the following conditions:

$$\delta_{(1,2)} \gg \frac{R}{c\gamma^3} \; , \quad \delta_{(1,2)}\frac{\mathrm{d}\,F(t)}{\mathrm{d}\,t} \ll F(t) \; . \tag{6.6}$$

The limitations (6.6) define a "slowly" varying function of the time and we simply take $F(\tau)$ outside the integral sign and call it $F(t)$ when calculating the second integral of Eq. (6.5):

$$\int\limits_{t-\delta_1}^{t+\delta_2} \boldsymbol{E}_{\mathrm{r}}(t-\tau)NF(\tau)\,\mathrm{d}\tau \simeq NF(t)\int\limits_{t-\delta_1}^{t+\delta_2} \boldsymbol{E}_{\mathrm{r}}(t-\tau)\,\mathrm{d}\tau \; . \tag{6.7}$$

Then we remember that the average of the electric field over time is zero when an electron is moving in a circle. As a result, we can write:

$$\int\limits_{t-\delta_1}^{t+\delta_2} \boldsymbol{E}_{\mathrm{r}}(t-\tau)\,\mathrm{d}\tau = - \left[ \int\limits_{-\infty}^{t-\delta_1} \boldsymbol{E}_{\mathrm{r}}(t-\tau)\,\mathrm{d}\tau + \int\limits_{t+\delta_2}^{\infty} \boldsymbol{E}_{\mathrm{r}}(t-\tau)\,\mathrm{d}\tau \right] \; . \tag{6.8}$$

Taking into account Eq. (6.7) and Eq. (6.8), the expression for the CSR pulse becomes

$$\boldsymbol{E}_{\mathrm{CSR}}(t) = \int\limits_{-\infty}^{t-\delta_1} \boldsymbol{E}_{\mathrm{r}}(t-\tau)NF(\tau)\,\mathrm{d}\tau - NF(t)\int\limits_{-\infty}^{t-\delta_1} \boldsymbol{E}_{\mathrm{r}}(t-\tau)\,\mathrm{d}\tau$$

$$+ \int\limits_{t+\delta_2}^{\infty} \boldsymbol{E}_{\mathrm{r}}(t-\tau)NF(\tau)\,\mathrm{d}\tau - NF(t)\int\limits_{t+\delta_2}^{\infty} \boldsymbol{E}_{\mathrm{r}}(t-\tau)\,\mathrm{d}\tau \; . \tag{6.9}$$
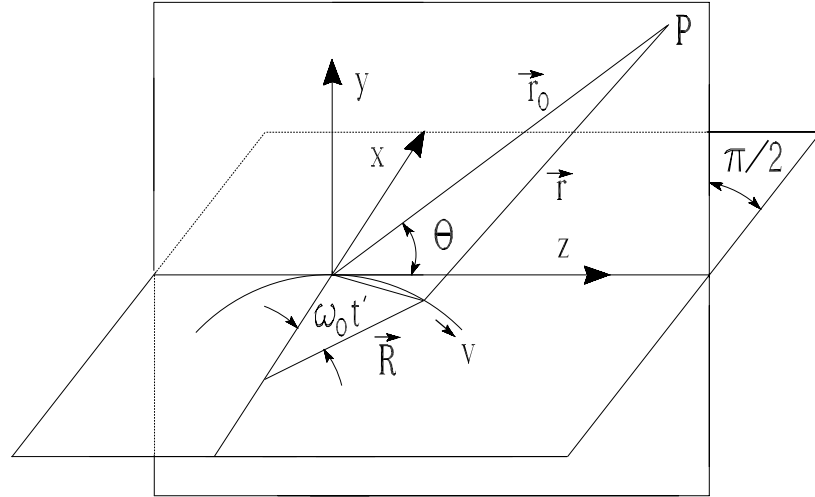
**Figure 6.8:** *Geometry for synchrotron radiation from circular motion.*

Integrating by parts, the first pair of integrals on the right hand side of Eq. (6.9) can be joined in a single one; the same can be done with the second pair:

$$
\boldsymbol{E}_{\mathrm{CSR}}(t) = - \int_{-\infty}^{t-\delta_1} \Phi\left[\boldsymbol{E}_{\mathrm{r}}\right](t-\tau)N\frac{\mathrm{d}\,F(\tau)}{\mathrm{d}\,\tau}\,\mathrm{d}\,\tau
$$

$$
- \int_{t+\delta_2}^{\infty} \Phi\left[\boldsymbol{E}_{\mathrm{r}}\right](t-\tau)N\frac{\mathrm{d}\,F(\tau)}{\mathrm{d}\,\tau}\,\mathrm{d}\,\tau \; , \tag{6.10}
$$

where $\Phi\left[\boldsymbol{E}_{\mathrm{r}}\right]$ is a primitive of $\boldsymbol{E}_{\mathrm{r}}$. What is left to do now is to evaluate a primitive of the radiation field from one electron.

To calculate the primitive of $\boldsymbol{E}_{\mathrm{r}}$ we use Eq. (6.1) and we note that the electric field is expressed in terms of quantities at the retarded time $t'$. The calculation is simplified if we use the following consideration: since (see [7]), in general, $\mathrm{d}\,t/\,\mathrm{d}\,t' = (1 - \boldsymbol{n}\cdot\boldsymbol{\beta})$ and

$$
\frac{\mathrm{d}}{\mathrm{d}\,t'}\left[\frac{\boldsymbol{n}\times[(\boldsymbol{n}\times\boldsymbol{\beta})]}{(1-\boldsymbol{n}\cdot\boldsymbol{\beta})}\right] = \left[\frac{\boldsymbol{n}\times[(\boldsymbol{n}-\boldsymbol{\beta})\times\dot{\boldsymbol{\beta}}]}{(1-\boldsymbol{n}\cdot\boldsymbol{\beta})^2}\right] \; , \tag{6.11}
$$

we also have

$$
\frac{\mathrm{d}}{\mathrm{d}\,t}\left[\frac{\boldsymbol{n}\times[(\boldsymbol{n}\times\boldsymbol{\beta})]}{(1-\boldsymbol{n}\cdot\boldsymbol{\beta})}\right] = \left[\frac{\boldsymbol{n}\times[(\boldsymbol{n}-\boldsymbol{\beta})\times\dot{\boldsymbol{\beta}}]}{(1-\boldsymbol{n}\cdot\boldsymbol{\beta})^3}\right] \; . \tag{6.12}
$$

Thus we can write $\boldsymbol{E}_{\mathrm{CSR}}(t)$ as

$$\boldsymbol{E}_{\text{CSR}}(t) = \frac{-e}{4\pi\epsilon_0 c \mid \boldsymbol{r}_0 \mid} \int\limits_{-\infty}^{t-\delta_1} \left[ \frac{\boldsymbol{n} \times [(\boldsymbol{n} \times \boldsymbol{\beta})]}{(1 - \boldsymbol{n} \cdot \boldsymbol{\beta})} \right]_{(t-\tau)} N \frac{\mathrm{d}\, F(\tau)}{\mathrm{d}\,\tau} \,\mathrm{d}\,\tau$$

$$+ \frac{-e}{4\pi\epsilon_0 c \mid \boldsymbol{r}_0 \mid} \int\limits_{t+\delta_2}^{\infty} \left[ \frac{\boldsymbol{n} \times [(\boldsymbol{n} \times \boldsymbol{\beta})]}{(1 - \boldsymbol{n} \cdot \boldsymbol{\beta})} \right]_{(t-\tau)} N \frac{\mathrm{d}\, F(\tau)}{\mathrm{d}\,\tau} \,\mathrm{d}\,\tau \; , \tag{6.13}$$

where the quantity in brackets must be evaluated at the retarded time $t' = (t - \tau) - \frac{1}{c} \mid \boldsymbol{r}(t') \mid$. Since the conditions (6.6) hold, we can substitute the function in brackets in both integrals on the right hand side of Eq. (6.13) with its asymptotic behavior at $\mid \tau \mid \gg R/(c\gamma^3)$. Because the angles are very small and the relativistic factor $\gamma$ is very large, it is useful to express Eq. (6.13) in a small angle approximation. The triple vector product is calculated from Fig. 6.8:

$$\boldsymbol{n} \times [\boldsymbol{n} \times \boldsymbol{\beta}] = \omega_0 t' \boldsymbol{e}_x + \theta \boldsymbol{e}_y \; . \tag{6.14}$$

Here $\theta$ is the vertical angle, $\omega_0 = \beta c/R$ is the revolution frequency and $\boldsymbol{e}_{x,y}$ are unit vectors directed along the $x$ and $y$ axis of the fixed Cartesian coordinate system $(x, y, z)$ shown in Fig. 6.8. The definition of $\boldsymbol{n}$ and $\boldsymbol{R}$ can be used to compute the scalar product in the denominators in Eq. (6.13) so that

$$\boldsymbol{n} \cdot \boldsymbol{\beta} = \beta \cos\theta \cos\omega_0 t' \simeq \beta(1 - \theta^2/2)(1 - (\omega_0 t')^2/2) \; . \tag{6.15}$$

We assume, here, that the vertical angle is small enough so that we can leave out the cosine factor. We can now write $\boldsymbol{E}_{\text{CSR}}(t)$ as

$$\boldsymbol{E}_{\text{CSR}}(t) = \frac{-2e}{4\pi\epsilon_0 c \mid \boldsymbol{r}_0 \mid} \left\{ \int\limits_{-\infty}^{t-\delta_1} \left[ \frac{(\omega_0 t' \boldsymbol{e}_x + \theta \boldsymbol{e}_y)}{(\omega_0 t')^2} \right]_{(t-\tau)} N \frac{\mathrm{d}\, F(\tau)}{\mathrm{d}\,\tau} \,\mathrm{d}\,\tau \right.$$

$$\left. + \int\limits_{t+\delta_2}^{\infty} \left[ \frac{(\omega_0 t' \boldsymbol{e}_x + \theta \boldsymbol{e}_y)}{(\omega_0 t')^2} \right]_{(t-\tau)} N \frac{\mathrm{d}\, F(\tau)}{\mathrm{d}\,\tau} \,\mathrm{d}\,\tau \right\} \; . \tag{6.16}$$

Part of the integrand in Eq. (6.16) is still expressed as a function of $t'$, which has to be converted into a function of $t - \tau$ using the explicit dependence

$$t - \tau = t' + \frac{1}{c} \mid \boldsymbol{r}(t') \mid = t' + \frac{\mid \boldsymbol{r}_0 \mid}{c} - \frac{R}{c} \cos\theta \sin\omega_0 t' \; . \tag{6.17}$$

Since we assume the vertical angle is very small, we may use again the replacement $\cos\theta \simeq 1$. We can therefore approximate $t - \tau$ by

$$t' + \frac{1}{c} \mid \boldsymbol{r}(t') \mid = \frac{\mid \boldsymbol{r}_0 \mid}{c} + t'(1 - \beta) + \frac{\omega_0^2 (t')^3}{6} \; . \tag{6.18}$$

We conventionally fixed $\boldsymbol{E}_{\text{r}}(0)$ as the maximum value of the field (in time) and we are interested in the asymptote for $\mid \tau \mid \gg R/(c\gamma^3)$ only, therefore we can simply write $t - \tau = \omega_0^2 (t')^3/6$ . The solution of this equation allows us to write Eq. (6.16) as

$$\boldsymbol{E}_{\text{CSR}}(t) = \frac{-2eN}{4\pi\epsilon_0 c \mid \boldsymbol{r}_0 \mid} \left\{ \int\limits_{t+\delta_2}^{\infty} \frac{\left[[6\omega_0(t-\tau)]^{1/3}\boldsymbol{e}_x + \theta\boldsymbol{e}_y\right]}{[6\omega_0(t-\tau)]^{2/3}} \frac{\mathrm{d}\,F(\tau)}{\mathrm{d}\,\tau}\,\mathrm{d}\,\tau \right.$$

$$\left. + \int\limits_{-\infty}^{t-\delta_1} \frac{\left[[6\omega_0(t-\tau)]^{1/3}\boldsymbol{e}_x + \theta\boldsymbol{e}_y\right]}{[6\omega_0(t-\tau)]^{2/3}} \frac{\mathrm{d}\,F(\tau)}{\mathrm{d}\,\tau}\,\mathrm{d}\,\tau \right\} \, . \qquad (6.19)$$

Limitations in (6.6) indicate that the contribution from the integrands in the right hand side of Eq. (6.19) are negligible in the region $(t-\delta_1, t+\delta_2)$ and therefore we can rewrite Eq. (6.19) in its final form, which is a new and elegant result:

$$\boldsymbol{E}_{\text{CSR}}(t) = -\frac{2eN}{4\pi\epsilon_0 c \mid \boldsymbol{r}_0 \mid} \int\limits_{-\infty}^{\infty} \left[ \frac{\varepsilon(t-\tau)\boldsymbol{e}_x}{[6\omega_0 \mid t-\tau \mid]^{1/3}} + \frac{\theta\boldsymbol{e}_y}{[6\omega_0 \mid t-\tau \mid]^{2/3}} \right] \frac{\mathrm{d}\,F(\tau)}{\mathrm{d}\,\tau}\,\mathrm{d}\,\tau \, , \quad (6.20)$$

where

$$\varepsilon(t-\tau) = 1 \qquad \text{for} \quad 0 < (t-\tau) < \infty \, , \qquad (6.21)$$

$$\varepsilon(t-\tau) = -1 \qquad \text{for} \quad -\infty < (t-\tau) < 0 \, . \qquad (6.22)$$

It might be worth to remark that the ultimate reason for using the auxiliary times $\delta_{(1,2)}$ in the derivation of Eq. (6.20) is that they help recognizing the validity of the asymptotic substitution, since otherwise a direct integration by parts of Eq. (6.4) would immediately give

$$\boldsymbol{E}_{\text{CSR}}(t) = \frac{-e}{4\pi\epsilon_0 c \mid \boldsymbol{r}_0 \mid} \int\limits_{-\infty}^{\infty} \left[ \frac{\boldsymbol{n} \times [(\boldsymbol{n} \times \boldsymbol{\beta})]}{(1-\boldsymbol{n}\cdot\boldsymbol{\beta})} \right]_{(t-\tau)} N \frac{\mathrm{d}\,F(\tau)}{\mathrm{d}\,\tau}\,\mathrm{d}\,\tau \, . \qquad (6.23)$$

Under the accepted limitation on the axial gradient of the beam current expressed by conditions (6.6), this equation transforms to Eq. (6.20).

As an example we show how to use Eq. (6.20) in order to calculate the CSR pulse. Let us concentrate on the CSR radiation produced in the orbital plane. In this case $\theta = 0$ and it is obvious that the radiation for an observer in that plane is horizontally polarized. To be specific, we consider an electron beam with a Gaussian axial profile of the current density

$$F(t) = \frac{1}{\sqrt{2\pi}\sigma_{\text{T}}} \mathrm{e}^{\left(-\frac{t^2}{2\sigma_{\text{T}}^2}\right)} \, , \qquad (6.24)$$

where $\sigma_{\text{T}}$ is the rms electron pulse duration. The rms is assumed to be large, $\sigma_{\text{T}} \gg R/(c\gamma^3)$. When $\theta = 0$ and the bunch profile is Gaussian, we can write Eq. (6.20) in the form

$$E_x(t) = \frac{2eN}{4\pi\epsilon_0(2\pi)^{1/2}6^{1/3}\sigma_{\text{T}}^3\omega_0^{1/3}c \mid \boldsymbol{r}_0 \mid} \int\limits_{-\infty}^{\infty} \frac{\varepsilon(t-\tau)\tau}{\mid t-\tau \mid^{1/3}} \mathrm{e}^{\left(-\frac{\tau^2}{2\sigma_{\text{T}}^2}\right)}\,\mathrm{d}\,\tau \, . \qquad (6.25)$$
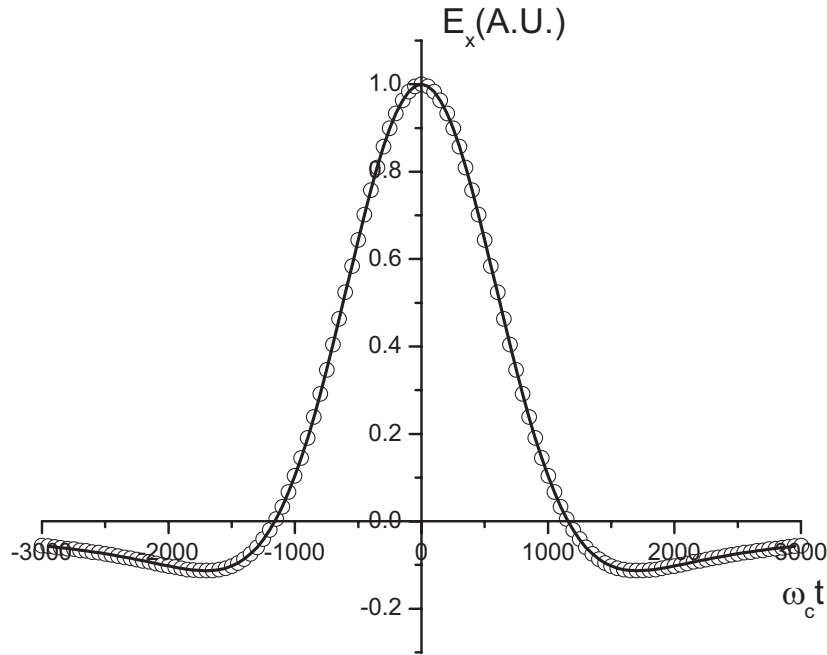
**Figure 6.9:** *Time structure of a CSR pulse from a Gaussian electron bunch moving in a circle. Here $\theta = 0$. The circles represent the results obtained from direct superposition of single particle pulses, while the solid line corresponds to the shape calculated by means of Eq. (6.25). The rms bunch duration is $\sigma_{\mathrm{T}} = 100\lambda_{\mathrm{c}}/c$, where $\lambda_{\mathrm{c}} = 4\pi R/(3c\gamma^3)$.*

Fig. 6.9 presents comparative results obtained by means of analytical calculations (solid curve, calculated with Eq. (6.25)) and numerical results (circles, calculated by direct superposition of single pulses from Eq. (6.4)). These plots constitute a simple cross-check between numerical (full Liénard-Wiechert espressions) and analytical results.

It is relevant to make some remarks about the region of applicability of Eq. (6.20). Eq. (6.20) is valid only when the electrons are moving in a circle and the observer is located in such a way that both the velocity term in Liénard-Wiechert formula can be neglected and the unit vector $\boldsymbol{n}$ can be considered constant. Another basic assumption is that the current density changes slowly on the scale of $R/\gamma^3$. This condition is well satisfied in the majority of practical cases, although not for very short bunches at low energies, like the ones produced by the RF photogun in Eindhoven [13], characterized by $\sigma_{\mathrm{T}} \sim 100$ fs and $\gamma \sim 10$. It should also be mentioned that the above expressions are good approximations for small enough vertical angles (even though they may be immediately generalized). In fact we used the replacement $\cos\theta \simeq 1$ in the retardation equation and, in practice, such an assumption is valid for the range $\theta^2 \ll (\sigma/R)^{2/3}$, where $\sigma$ is the characteristic length of electron bunch.

### 6.3.3   Arc of a circle case

Let us now extend the previous results to the case of an arc of a circle, relaxing the assumption $\phi_m \ll 1/\gamma$ made in Section 6.3.1. We will focus only on the radiation seen by an observer located at large distance from the sources, on the tangent to the electrons orbit at the middle point of the magnet. In this case we can continue to use the fixed coordinate system $(x, y, z)$ shown in Fig. 6.8. The observation point and the vector $\boldsymbol{n}$ are within the $(y, z)$-plane and the radiation is emitted at an angle $\theta$ with respect to the $z$-axis. Let us start expressing the total CSR pulse as a superposition of single particle fields at a given position in the far-zone. In the case of an arc of a circle Eq. (6.4) modifies as follows:

$$\boldsymbol{E}_{\mathrm{CSR}}(t) = \int_{t-T}^{t+T} \boldsymbol{E}_{\mathrm{r}}(t - \tau)NF(\tau)\,\mathrm{d}\tau \; . \tag{6.26}$$

Here the time $T$ in the integration limits is *in loco* of a window function in the integrand, in order to cut the contributions of the single particle radiation pulse when the electron is not in the arc. This expression contains the observation time interval $T$, which should be replaced by the retarded time interval $t'_{\mathrm{e}}$. The two times are related by

$$2T = 2t'_{\mathrm{e}} + \frac{1}{c} \mid \boldsymbol{r}(t'_{\mathrm{e}}) \mid -\frac{1}{c} \mid \boldsymbol{r}(-t'_{\mathrm{e}}) \mid \; , \tag{6.27}$$

where $t'_{\mathrm{e}} = \phi_m/(2\omega_0)$, $\phi_m$ being the bending magnet angular extension. Our analysis focuses on the case of a long bending magnet, $\gamma\phi_m \gg 1$. Using Eq. (6.2) and condition (6.3), the field of the CSR pulse is readily shown to be

$$\boldsymbol{E}_{\mathrm{CSR}}(t) = \int_{t-T}^{t-\delta} \boldsymbol{E}_{\mathrm{r}}(t - \tau)NF(\tau)\,\mathrm{d}\tau - NF(t)\int_{-\infty}^{t-\delta} \boldsymbol{E}_{\mathrm{r}}(t - \tau)\,\mathrm{d}\tau$$

$$+ \int_{t+\delta}^{t+T} \boldsymbol{E}_{\mathrm{r}}(t - \tau)NF(\tau)\,\mathrm{d}\tau - NF(t)\int_{t+\delta}^{\infty} \boldsymbol{E}_{\mathrm{r}}(t - \tau)\,\mathrm{d}\tau \; . \tag{6.28}$$

As we have already done previously, we assume that $\delta$ satisfies conditions (6.6). Adding and subtracting suitable edge terms one can still perform integration by parts, thus obtaining:

$$\boldsymbol{E}_{\mathrm{CSR}}(t) = NF(t + T)\int_{-\infty}^{t+T} \boldsymbol{E}_{\mathrm{r}}(t - \tau)\,\mathrm{d}\tau - NF(t - T)\int_{-\infty}^{t-T} \boldsymbol{E}_{\mathrm{r}}(t - \tau)\,\mathrm{d}\tau$$

$$- \int_{t-T}^{t-\delta} \Phi\left[\boldsymbol{E}_{\mathrm{r}}\right](t - \tau)N\frac{\mathrm{d}\,F(\tau)}{\mathrm{d}\,\tau}\,\mathrm{d}\,\tau - \int_{t+\delta}^{t+T} \Phi\left[\boldsymbol{E}_{\mathrm{r}}\right](t - \tau)N\frac{\mathrm{d}\,F(\tau)}{\mathrm{d}\,\tau}\,\mathrm{d}\,\tau \; . \tag{6.29}$$

Since conditions (6.6) hold for $\delta$ we may substitute the 3rd and the 4th integral in Eq. (6.29) with a single integral in which the primitive, $\Phi\left[\boldsymbol{E}_{\mathrm{r}}\right]$, is replaced by its

asymptote for large values of the argument, $\Phi\left[\boldsymbol{E}_r^A\right]$. Under the assumption of a long bunch ($\omega_c T \gg 1$) the 1st and the 2nd integral can be expressed by means of the asymptote of the primitive too. Moreover, we can perform a change of variables in all the integrals $t - \tau \to \tau$. As a result Eq. (6.29) can be written in the form:

$$\boldsymbol{E}_{\mathrm{CSR}}(t) = NF(t+T)\int\limits_{-T}^{\infty} \boldsymbol{E}_r^A(\tau)\,\mathrm{d}\tau + NF(t-T)\int\limits_{\infty}^{T} \boldsymbol{E}_r^A(\tau)\,\mathrm{d}\tau$$

$$- \int\limits_{-T}^{T} \Phi\left[\boldsymbol{E}_r^A\right](\tau)N\frac{\mathrm{d}\,F(t-\tau)}{\mathrm{d}\,\tau}\,\mathrm{d}\,\tau \ . \tag{6.30}$$

Using the ultrarelativistic approximation we can calculate a primitive $\Phi\left[\boldsymbol{E}_r\right]$ using Eq. (6.14) and Eq. (6.15). Again we assume that the vertical angle is very small so that we may use the replacement $\cos\theta \simeq 1$. In this situation we have again:

$$\frac{\boldsymbol{n} \times [(\boldsymbol{n} \times \boldsymbol{\beta})]}{(1 - \boldsymbol{n} \cdot \boldsymbol{\beta})} \simeq \frac{\omega_0 t' \boldsymbol{e}_x + \theta \boldsymbol{e}_y}{(\omega_0 t')^2/2} \ . \tag{6.31}$$

This quantity must be evaluated at the retarded time $t' \simeq [6\tau/\omega_0^2]^{1/3}$. Substitution of these expressions in Eq. (6.30) gives

$$\boldsymbol{E}_{\mathrm{CSR}}(t) = \frac{-2eN}{4\pi\epsilon_0 c \mid \boldsymbol{r}_0 \mid} \left\{ \int\limits_{-T}^{T} \left[ \frac{\varepsilon(\tau)\boldsymbol{e}_x}{[6\omega_0 \mid \tau \mid]^{1/3}} + \frac{\theta\boldsymbol{e}_y}{[6\omega_0 \mid \tau \mid]^{2/3}} \right] \frac{\mathrm{d}\,F(t-\tau)}{\mathrm{d}\,\tau}\,\mathrm{d}\,\tau \right.$$

$$+ \left[F(t+T) + F(t-T)\right] \frac{\boldsymbol{e}_x}{(6\omega_0 T)^{1/3}}$$

$$\left. - \left[F(t+T) - F(t-T)\right] \frac{\theta\boldsymbol{e}_y}{(6\omega_0 T)^{2/3}} \right\} \ , \tag{6.32}$$

where $T = \phi_m^3/(48\omega_0)$. Eq. (6.32) is a new result, which generalizes Eq. (6.20) to the case of a bunch moving in an arc of a circle.

As an example of the application of this expression, consider the situation when $\theta = 0$ and the bunch profile is a Gaussian. According to Eq. (6.32) the CSR field in this case is given by

$$E_x(t) = G_1(t) + G_2(t) \tag{6.33}$$

where

$$G_1 = \frac{2eN}{4\pi\epsilon_0(2\pi)^{1/2}6^{1/3}\sigma_T^3\omega_0^{1/3}c \mid \boldsymbol{r}_0 \mid} \int\limits_{-T}^{T} \frac{\varepsilon(\tau)(t-\tau)}{\mid \tau \mid^{1/3}} \mathrm{e}^{\left(-\frac{(t-\tau)^2}{2\sigma_T^2}\right)}\,\mathrm{d}\,\tau \ , \tag{6.34}$$

$$G_2 = \frac{-2eN}{4\pi\epsilon_0(2\pi)^{1/2}6^{1/3}\sigma_T(\omega_0 T)^{1/3}c \mid \boldsymbol{r}_0 \mid} \left[ \mathrm{e}^{\left(-\frac{(t+T)^2}{2\sigma_T^2}\right)} + \mathrm{e}^{\left(-\frac{(t-T)^2}{2\sigma_T^2}\right)} \right] \ . \tag{6.35}$$
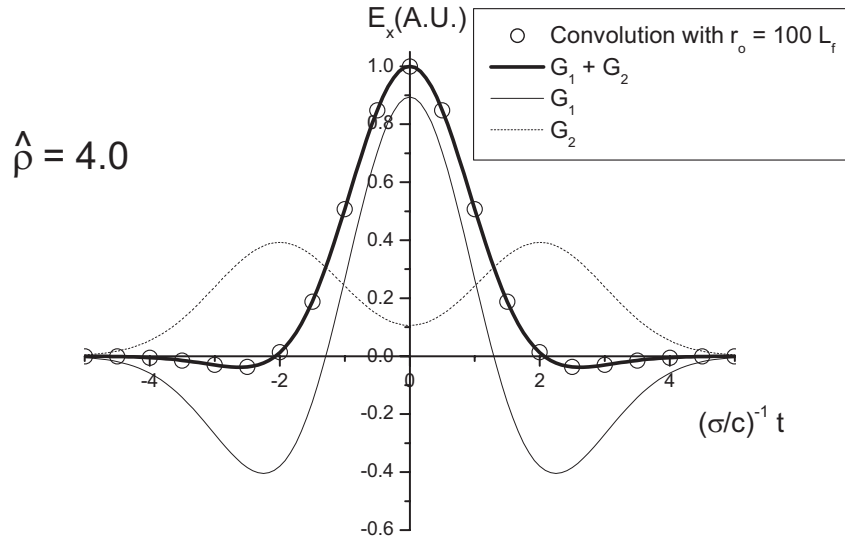
**Figure 6.10:** *Time structure of the CSR pulse from a Gaussian electron bunch moving along an arc of a circle. Here $\theta = 0$, $\hat{\rho} = \phi_m^3/(24\omega_0\sigma_T) = 4$. The physical meaning of the magnet length parameter $\hat{\rho}$ will be clear after reading Section 6.4. Circles present the results obtained from direct superposition of single particle pulses. The solid line corresponds to the shape calculated by means of Eq. (6.33).*

Fig. 6.10 presents the results of calculations obtained using Eq. (6.33). As expected, a simple cross-check with numerical results shows a very good agreement. Note how the finite magnet length chosen in Fig. 6.10, $\hat{\rho} = \phi_m^3/(24\omega_0\sigma_T) = 4$, modifies the shape of the CSR pulse with respect to Fig. 6.9: the tails shrink and the integral of the total field deviates from zero (which is the expected result for the circular case). This can be directly ascribed to the fact that Schwinger formulas can not be used to describe the long wavelength asymptote of the single particle radiation.

## 6.4    LIMITATIONS OF STANDARD RESULTS

As already anticipated in Section 6.1, besides failing in the long wavelength limit for the dipole magnet case, Schwinger's approach relies on several other assumptions: first, the observer is located in such a way that the velocity term in the Liénard-Wiechert formula can be completely neglected and that the unit vector $\boldsymbol{n}$ can be considered constant throughout the electron evolution. Second, a circular trajectory is postulated. Finally, no aperture limitation is considered at all. These assumptions must be analyzed in order to understand how the CSR pulse is altered in realistic situations. In this Section we will deal separately with all of them.

Let us imagine that our electron bunch moves along an arc of a circle and that there is no aperture limitation. We can take into account, then, effects as a finite distance between source and observer, a finite magnet length and the presence of velocity

fields by means of Eq. (6.4), where the expression for the electric field is given by the strict Liénard-Wiechert formula. Analytical methods are of limited use in the study of CSR in the near-zone, and numerical calculations must be selected. The application of similarity techniques will allow us to present numerical results in such a way that they are both general and directly applicable to the calculation of specific device situations. This technique not only allows one to reduce the number of parameters of the problem but also helps to reformulate it in terms of variables possessing a clear physical interpretation. Each physical factor influencing the CSR production is matched by its own reduced parameter. For the effect under study this reduced parameter is a measure of the corresponding physical effect. When some effect becomes less important for coherent radiation, it simply falls out of the number of the parameters of the problem.

For our present purposes we will concentrate on the temporal structure of a CSR pulse and we will consider the case of an electron beam with a Gaussian axial profile of the current density. The behavior of the CSR pulse profile as a function of dimensionless parameters provides information on the spectrum distortion. When comparing the temporal structure of CSR pulses in different conditions, it is convenient to use a normalized field amplitude. The rms electron pulse duration is assumed to be $\sigma_T \gg R/(c\gamma^3)$ and we focus on the radiation pulse seen along the tangent to the orbit at the middle point of the magnet. When the vertical angle $\theta = 0$, the normalized coherent field amplitude $E_x(t)/E_{\max}$ is a function of six dimensional parameters:

$$t \,, \quad v \,, \quad R \,, \quad \phi_{\mathrm{m}} \,, \quad \sigma_T \,, \quad \mid \boldsymbol{r}_0 \mid \,. \tag{6.36}$$

It is relevant to note that only two dimensions (length and time) are sufficient for a full description of the field profile. After appropriate normalization it is a function of four dimensionless parameters only:

$$E_x(t)/E_{\max} = \hat{E}_x = D(\hat{t}, \hat{\sigma}, \hat{\rho}, \hat{r}_0) \,, \tag{6.37}$$

where $\hat{t} = t/\sigma_T$ is the dimensionless time, $\hat{\sigma} = \omega_0 \sigma_T \gamma^3$ is the dimensionless electron pulse duration, $\hat{r}_0 = \mid \boldsymbol{r}_0 \mid (c\sigma_T)^{-1/3} R^{-2/3}$ is the dimensionless distance between source and observer and $\hat{\rho} = \phi_{\mathrm{m}}^3/(24\omega_0\sigma_T)$ is the magnet length parameter. In the general case the universal function $D$ should be calculated numerically by means of strict Liénard-Wiechert formulas.

The changes of scale performed during the normalization process imply that we are measuring time, bunch length, distance from the source and magnet length as multiples of "natural" CSR units. There is a physical reason for being able to write the field profile as in Eq. (6.37): let us explain this fact beginning with a qualitative analysis of the radiation from an electron moving in a circle, in the long wavelength asymptote. Synchrotron radiation is emitted from a rather small area and we need to determine this area for observers whose detection systems collect information over a long time period $\sigma_T$. The radiation pulse length is equal to the time taken for the electron to travel along any arc $AB$, reduced by the time taken for the radiation to travel directly from $A$ to $B$. Between point $A$ and point $B$ we have a deflection angle $\phi$, so that $\sigma_T \simeq R\phi/(\beta c) - 2R\sin(\phi/2)/c$, and $\sin(\phi/2)$ can be approximated by $\sin(\phi/2) \simeq \phi/2 - \phi^3/48$ for small angles. Then the pulse duration reduces to $\sigma_T \simeq R\phi^3/(24c)$. The radiation source extends over some finite length $R\phi \sim L_{\mathrm{f}} = (c\sigma_T)^{1/3}R^{2/3}$ along the particle path. We see that the reduced distance can be expressed as $\hat{r}_0 = \mid \boldsymbol{r}_0 \mid /L_{\mathrm{f}}$. One

can find that the ratio $(R\phi_{\mathrm{m}})^3/(24L_{\mathrm{f}}^3)$ is equal to $\hat{\rho}$, which we use now as a measure of finite magnet length effects.

### 6.4.1   Diffraction effects

In realistic situations, the long wavelength synchrotron radiation from bending magnets passes through many different vacuum chamber pieces with widely varying apertures. For example, in the presence of a vacuum pipe, the SR will be collected out of an aperture a couple of centimeters away from the source at most, and this will perturb the CSR spectrum.

Consider an electron moving in a circle, as in Fig. 6.11. Between the observer and the source there is an aperture with a characteristic dimension $d$. Qualitatively, an observer looking at a single electron is presented with a cone of radiation characterized by an aperture angle of order $\theta \simeq \sqrt{2d/R}$. Fig. 6.11 shows part of the trajectory of an electron travelling along an arc of a circle of radius $R$. The presence of a finite aperture introduces diffraction effects specific to the geometry and clearly dependent on the wavelength. For structures such as pinholes it is found that these diffraction patterns propagate away at angles of order $\theta_{\mathrm{d}} \simeq \lambda/d$, where $d$ is the characteristic aperture dimension. The region of applicability for the far diffraction zone is given by the relation $L_{\mathrm{p}} \gg L_{\mathrm{d}} \simeq d^2/\lambda$, where $L_{\mathrm{p}}$ is the distance between observer and aperture and $L_{\mathrm{d}}$ the typical diffraction distance. When the wavelength is about $R\theta^3/24 \simeq \sqrt{2}(d^3/R)^{1/2}/12$, the latter condition transforms to $L_{\mathrm{p}} \gg L_{\mathrm{d}} \simeq 6R\theta$. The significance of the discussed limitation cannot be fully appreciated until we determine typical values of the parameters that can be expected in practice. For example, if $R = 3$ m and $\lambda = 100$ $\mu$m, $\theta \simeq 0.08$, a 1 cm diameter hole will significantly perturb the SR spectrum at wavelengths in this region for distances greater than about 1 m. In order to solve the diffraction problem we must characterize the field at the aperture position: since the aperture is expected to be only a couple of centimeters away from the sources finite distance effects play an important role in the overall determination of the CSR pulse at the detector position.

### 6.4.2   Finite distance effects

Let us now imagine that our electron bunch moves in a real circle and there is no aperture limitation. We can first consider the contribution given by the acceleration field alone and then focus on the contributions by the velocity field.

**Acceleration field effects.**   When the electron bunch radiates from a circle the spectrum is obviously independent of the $\hat{\rho}$ parameter. In the long wavelength asymptote ($\hat{\sigma} \gg 1$) the acceleration field is described by one dimensionless parameter only: $\hat{r}_0$.

The region of applicability of Schwinger formulas requires the dimensionless distance to have a value $\hat{r}_0 \gg 1$. In fact, as previously explained, the radiation source extends over some finite length $R\phi \sim L_{\mathrm{f}}$, and this length corresponds to a transverse size of the radiation source $d \sim R\phi^2$. The vector $\boldsymbol{n}$ changes its orientation between point $A$ and point $B$ by an angle of order $d/r_0$, where $r_0$ is the distance between source and observer. Our estimates show that in the case $d/r_0 \ll \phi$, the vector $\boldsymbol{n}$ in the Liénard-Wiechert
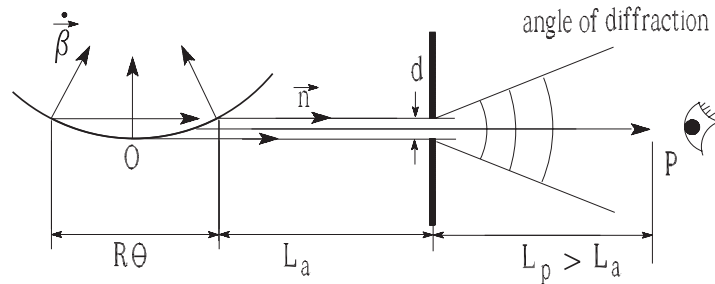
**Figure 6.11:** *Depiction of the effects of an aperture limitation.*

formula is almost constant when the electron moves along the formation length $R\phi$. Thus, we can conclude that the unit vector $\boldsymbol{n}$ can be considered constant throughout the electron evolution only if $r_0 \gg L_{\mathrm{f}}$.

The results of numerical calculations for several values of $\hat{r}_0$ are presented in Fig. 6.12. Calculations have been performed using the strict Liénard-Wiechert formula. The plots in Fig. 6.12 give an idea of the region of validity of the far-zone approximation considered above. At large distance the CSR pulse profile is simply the far-zone profile Eq. (6.25). One can see that Eq. (6.25) works well at $\hat{r}_0 = 100$. Then, at $\hat{r}_0 = 3$, the CSR pulse envelope is visibly modified. As the distance is decreased, the difference between the approximate and the strict pulse profile becomes significant. From a practical point of view this set of plots covers all the region of interest for the distance between observer and sources. Note that, for example, for a rms bunch length of about 100 $\mu$m and a radius $R = 3$ m, the value $\hat{r}_0 = 3$ corresponds to $r_0 \simeq 30$ cm. If we detect CSR in vacuum at a distance smaller than 30 cm this effect must be taken into account. Also, if we have an aperture at a distance smaller than 30 cm (which is practically always the case), and we want to solve the diffraction problem, this effect must be taken into account: in fact, as already said, in this case one needs to calculate the fields at the aperture position and these will differ from the behavior predicted by Schwinger formulas.

To check that no mistakes have been made in our similarity techniques we evaluated the normalized CSR pulse profile for several sets of parameters. The reduced distance was held constant $\hat{r}_0 = 0.15$ or $\hat{r}_0 = 15$. The plots were calculated numerically, using the strict Liénard-Wiechert formula. Fig. 6.13 and Fig. 6.14 show our results. It is seen that there is a good agreement with the prediction that the acceleration field from a circle in the long wavelength asymptote is a function of the reduced distance only.

**Velocity field effects.** Usual theory of synchrotron radiation is based on the assumption that the acceleration field dominates: all the results presented above refer, in fact, to the case when there is no influence of the velocity field on the detector. Yet,
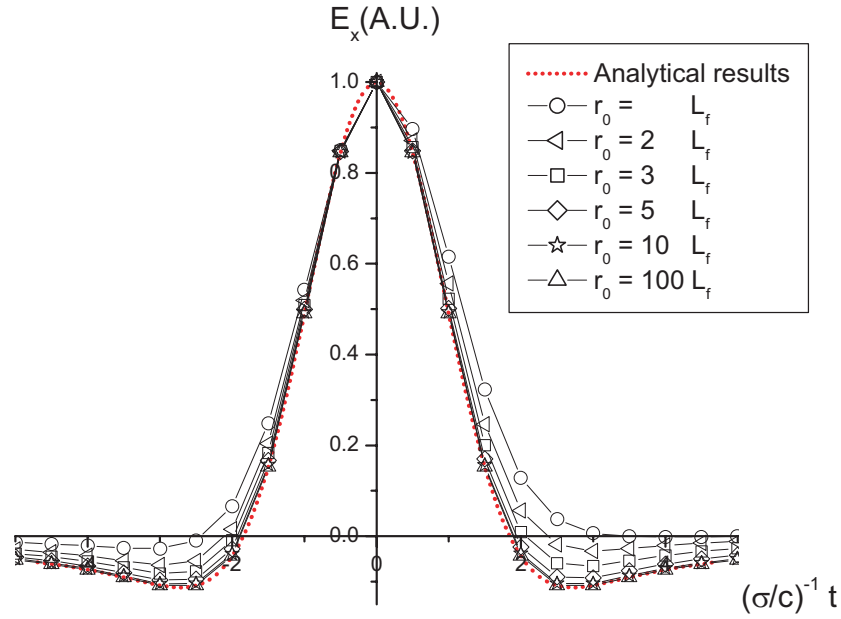
**Figure 6.12:** *Time structure of a CSR pulse from a Gaussian electron bunch moving in a circle at different reduced distance between source and observer. Here $\theta = 0$. The dashed curve is calculated within the far-zone approximation Eq. (6.25). Numerical calculations have been performed with the strict Liénard-Wiechert formula.*

the acceleration field dominates in the far-zone only, and we want to study near-zone effects too. The physics of coherent effects studied by means of general expressions for the Liénard-Wiechert fields is much richer than that of the simplified radiation field model considered above. In the long wavelength asymptote the velocity part of the coherent electric field from a particle in a circle is a function of two dimensionless parameters: the reduced distance parameter $\hat{r}_0$ and the reduced electron pulse duration parameter $\hat{\sigma}$:

$$E_{\mathrm{v}}(t)/E_{\max} = \hat{E}_{\mathrm{v}} = D(\hat{t}, \hat{\sigma}, \hat{r}_0) \; , \tag{6.38}$$

where the normalization of the velocity field is performed with respect to the maximal *acceleration* field amplitude.

To show that this is correct we can perform a simple check. In Fig. 6.15 we present numerical calculation results for the velocity field for different sets of parameters. The reduced distance and the reduced electron pulse duration are held constant. It is seen that all numerical results agree rather well.

Fig. 6.16 and Fig. 6.17 show the dependence of the normalized velocity field amplitude on the value of the reduced electron pulse duration for different values of the reduced distance. Using these plots we can give a quantitative description of the region of applicability of the radiation field model. It is seen from the plots in Fig. 6.17 that in the near-zone we can not neglect the influence of the velocity field on the detector.
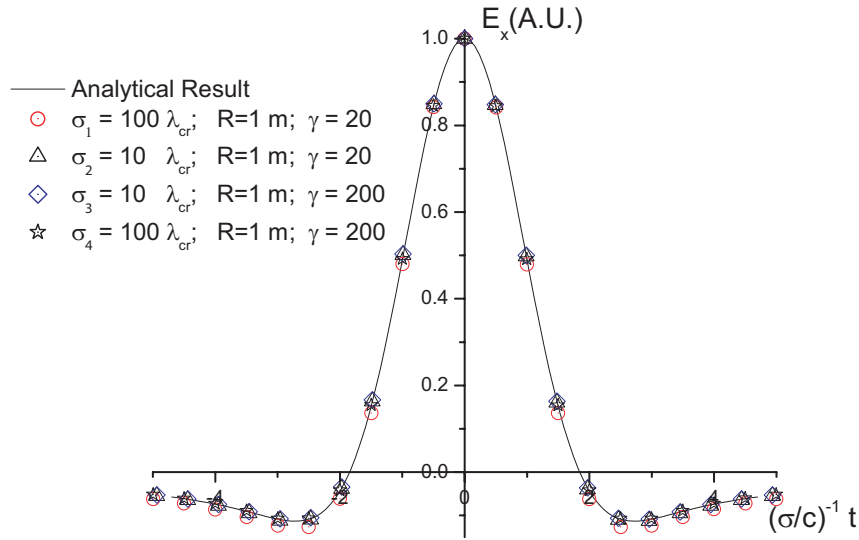
**Figure 6.13:** *Illustration of similarity techniques. Time structure of a CSR pulse from a Gaussian electron bunch moving in a circle for various sets of parameters. The reduced distance is held constant, $\hat{r}_0 = 15$. The solid curve is calculated within the far-zone approximation Eq. (6.25). Numerical calculations have been performed with strict Liénard-Wiechert formula.*

Let us now estimate the importance of the velocity field effect. Let us start considering the total velocity field pulse as a superposition of single particle fields at a given position in the far-zone. To calculate the integral one should take into account the property of its kernel. In the far-zone the velocity field from one electron is close to an antisymmetric function and the average of the electric field over time is close to zero. The approach used in Section 6.3 can be also used to compute the coherent velocity field. Under the "smooth" electron bunch condition the kernel (velocity field from one electron) can be substituted by its asymptotic behavior. If we wish to estimate the normalized amplitude of the coherent velocity field we can get it simply by dividing the asymptotic behavior of the velocity field kernel by the asymptotic behavior of the acceleration field kernel, so that, in the far-zone, the normalized velocity field is of order $E_v/E_{\mathrm{acc}} \sim R/(\gamma^2 \theta r_0)$, where $\theta \simeq (c\sigma_{\mathrm{T}}/R)^{1/3}$ is the natural synchrotron radiation opening angle for a frequency $\omega \simeq \sigma_{\mathrm{T}}^{-1} \ll c\gamma^3/R$. Using normalized variables we get

$$\hat{E}_{\mathrm{v}} \sim \hat{r}_0^{-1}\hat{\sigma}^{-2/3} \quad \text{for} \quad \hat{\sigma},\ \hat{r}_0 \gg 1 \ . \tag{6.39}$$

As we can see from Fig. 6.16, numerical calculations in the far-zone confirm this simple physical consideration. The value of $\hat{E}_{\mathrm{v}}$ is found remembering that, in the example given in Fig. 6.16, $\hat{r}_0 = 100$, $\hat{\sigma} = 100$; therefore the normalized velocity field would be about 0.0004, which is the same order of magnitude as results of numerical calculations (0.0002). Also, $\hat{E}_{\mathrm{v}}$ varies roughly as $\hat{\sigma}^{-2/3}$.

The normalized velocity field amplitude decreases, as we see from our estimations, linearly with distance, which means that if we are in the near-zone at $\hat{r}_0 = 1$ there will
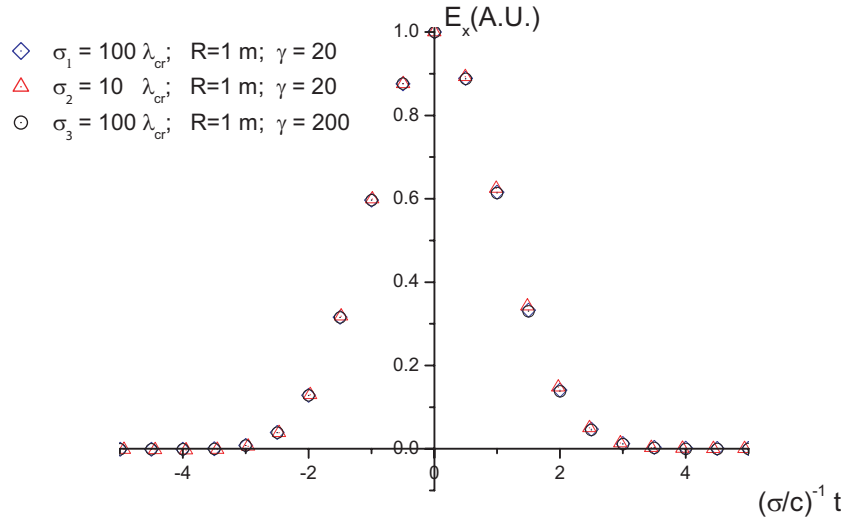
**Figure 6.14:** *Illustration of similarity techniques. Time structure of a CSR pulse from a Gaussian electron bunch moving in a circle for various sets of parameters. The reduced distance is held constant, $\hat{r}_0 = 0.15$. Numerical calculations have been performed with strict Liénard-Wiechert formula.*

be $\hat{E}_\mathrm{v} \simeq 0.04$. A numerical calculation of the precise fields, presented in Fig. 6.17, shows that, at the value $\hat{r}_0 = 1$, we have $\hat{E}_\mathrm{v} = 0.2$: in the case for $R = 3$ m and bunch length of 100 $\mu$m, this means that the velocity field contributes 20% of the total field at $r_0 \simeq 10$ cm. Our approximate treatment of the coherent velocity field breaks down once source and observer get as close as they are at $\hat{r}_0 \simeq 1$: this is not surprising, since we derived Eq. (6.39) in the limit for $\hat{r}_0 \gg 1$. There is an intuitive explanation for this discrepancy: in fact, in addition to the antisymmetric part of the kernel we have just described, there is also a symmetric part. When source and observer are far apart the observer sees only the antisymmetric part and the average of the electric field from one electron is close to zero. At very close distances there begins to be some extra symmetric contribution to the kernel. This symmetric field, which also varies with the separation, should, of course, be included in more precise estimates.

## 6.4.3   Finite magnet length effects

Until now we have considered the case in which electrons move in a circle. Here we will study the case where the electrons move along an arc of a circle by means of Eq. (6.33). Normalizing Eq. (6.33), we obtain that, under the far-field approximation, the CSR pulse profile is a function of only one dimensionless parameter $\hat{\rho} = \phi_\mathrm{m}^3/(24\omega_0\sigma_\mathrm{T})$, where $\phi_\mathrm{m}$ is the magnet angular extension. The applicability of Schwinger formulas require $\hat{\rho} \gg 1$. Using the plots presented in Fig. 6.18, one can characterize quantitatively the region of applicability of the circular motion model. Note that the tail in Fig. 6.18 is completely modified for $\hat{\rho} = 6$ which, for our example
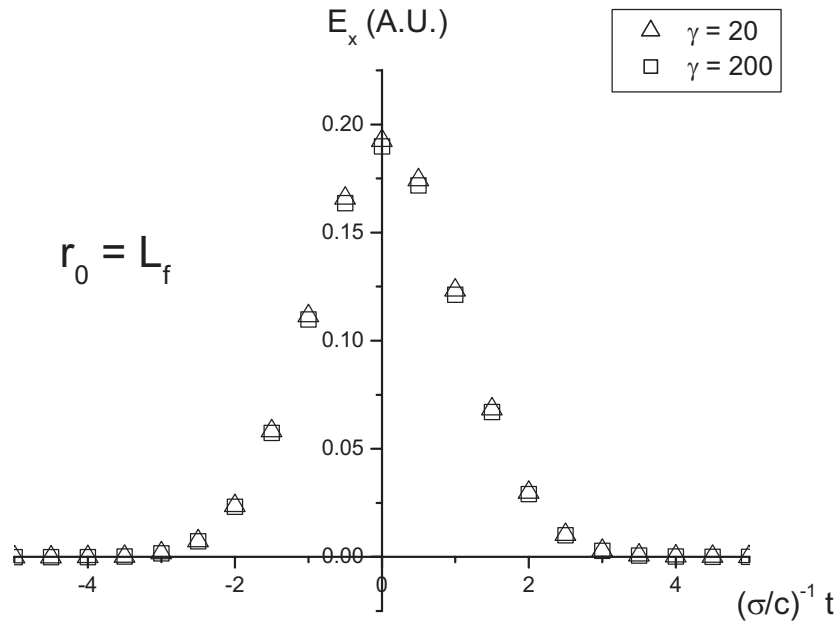
**Figure 6.15:** *Illustration of similarity techniques. Electric field pulse due to the velocity term from a Gaussian electron bunch moving in a circle for various sets of parameters. The reduced distance and reduced bunch length are held constant, $\hat{r}_0 = 1$ and $\hat{\sigma}_{\mathrm{T}} = 100$ respectively. Numerical calculations have been performed with strict Liénard-Wiechert formula.*

of $R = 3$ m and rms bunch length of 100 $\mu$m translates to $\phi_{\mathrm{m}} \simeq 0.17$. This means that a 50 cm magnet is short enough to give spectral distortions.

## 6.5 Conclusions

In this Chapter we treated subjects related to both longitudinal bunch diagnostics and CSR sources characterization. We found a new, simple analytical expression to describe the CSR pulse from a bunch moving in an arc of a circle. Our expression depends on the long wavelength asymptotic of Schwinger formula for the electric field from a particle in a circle, and the magnet length plays a crucial role here, since it substantially modifies, with respect to the case of circular motion, the behavior of the field at long wavelengths. Our formula applies for a generic bunch density distribution and can be used for a quick estimation of the CSR field pulse from a bunch moving in a dipole magnet. Yet, in almost any practical application, where the radiation pulse is collected through a finite aperture, one has to take into account diffraction effects too. Since the solution of the diffraction problem involves the knowledge of the field at the aperture position, which is usually at short distance from the sources, we have to take into account finite distance effects. We treated these effects from a quantitative viewpoint in the framework of a similarity technique which provided very
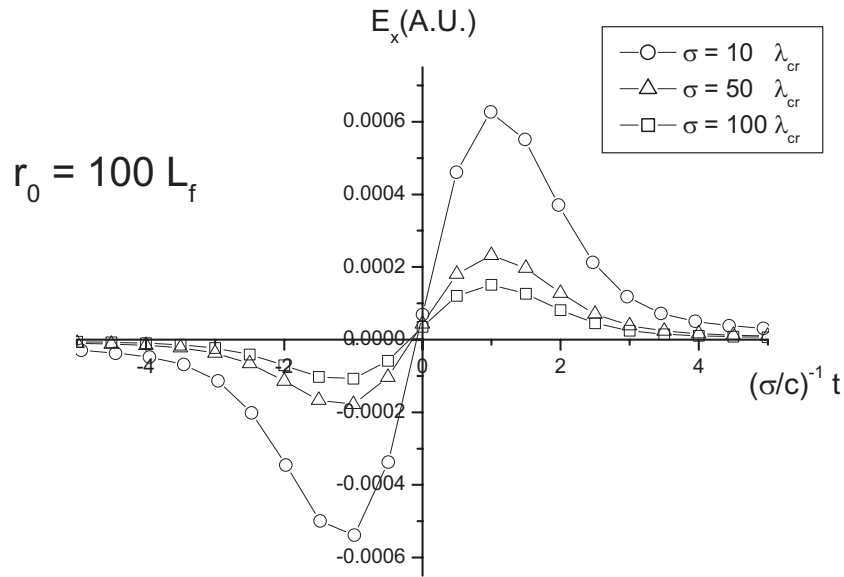
**Figure 6.16:** *Electric field pulse due to the velocity term from a Gaussian electron bunch moving in a circle at different reduced bunch lengths. The reduced distance is held constant, $\hat{r}_0 = 100$. Here $\theta = 0$ and the normalization is performed with respect to the maximal acceleration field amplitude.*

general results, immediately applicable at any practical parameter range. By doing this, we produced the basis elements for numerical simulations of the full behavior of the CSR fields in realistic situations.

For a more complete investigation of bunch diagnostics techniques and CSR, including the use of undulators as an alternative to bending magnets and constrained deconvolution techniques to recover information on the bunch density function, we refer to [5].
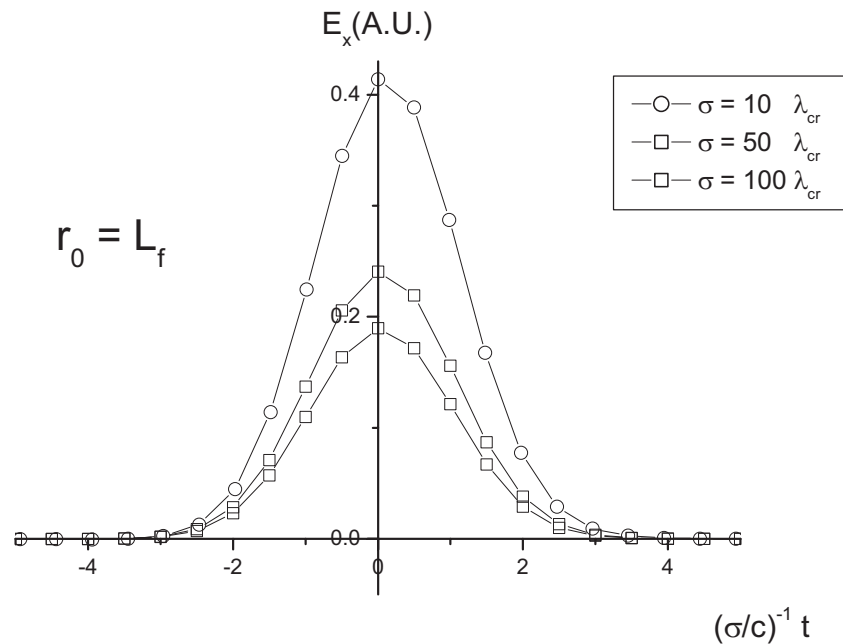
**Figure 6.17:** *Electric field pulse due to the velocity term from a Gaussian electron bunch moving in a circle at different reduced bunch lengths. The reduced distance is held constant, $\hat{r}_0 = 1$. Here $\theta = 0$ and the normalization is performed with respect to the maximal acceleration field amplitude.*

# Bibliography

[1] G.L. Carr et al. Nature, November 2002, 153

[2] M. Abo-Bakr, J. Feikes, K. Holldack et al. Phys. Rev. Lett. 88, 254801 (2002)

[3] B. Faatz et al. Nucl. Instr. and Meth. A 475 (2001), 363

[4] G. Krafft et al., Appl. Phys. Lett. 70 (4), 1997

[5] G. Geloni, E. Saldin, E. Schneidmiller and M. Yurkov, DESY 03-31, ISSN 0418-9833, 2003

[6] V. G Bagrov, N. I. Fedosov, and I. M. Ternov, Phys. Rev. D 28, 2464 (1982)

[7] J. D. Jackson, *Classical electrodynamics*, John Wiley and Sons, New York, 1975

[8] P. J. Duke, *Synchrotron radiation*, Oxford University Press, Oxford, 2000

[9] H. Wiedemann, *Particle Accelerator Physics*, Springer, Berlin, 1995

[10] J. Schwinger, Phys. Rev. 75, 1912 (1949)
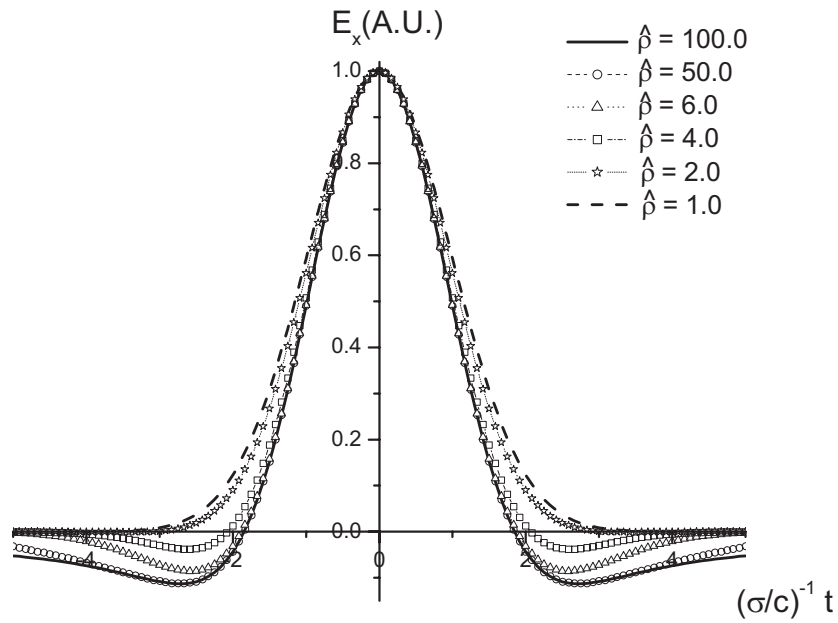
[11] V. Ayvazyan et al., Phys. Rev. Lett. 88(2002)104802

**Figure 6.18:** *Time structure of a CSR pulse in the far-zone from a Gaussian electron bunch moving along an arc of a circle at different reduced magnet lengths. Here $\theta = 0$. Calculations have been performed with Eq. (6.32). Results at $\hat{\rho} = 100$ (solid curve) agree with our analytical expression Eq. (6.25) for circular motion within 1%.*

[12] V. A. Bordovitsyn (Editor), *Synchrotron Radiation Theory And Its Development*, World Scientific, Singapore-London, 1999

[13] F. B. Kiewiet, O. J. Luiten, G. J. H. Brussaard, J.I.M. Botman and M.J. van der Wiel in *Proceedings of Eurpean Particole Accelerator Conference, Wien, 2000*, edited by J.L. Laclare, W. Mitaroff et al.

# Summary

The production of high brightness, ultrarelativistic electron beams to be used, for example, in X-ray Free-Electron-Lasers is a challenge for accelerator physicists. One of the effects which may spoil the characteristics of such beams is constituted by the interactions between particles and electromagnetic fields produced by the particles themselves during their motion.

This work is devoted to the study of theoretical aspects of self-interactions within ultrarelativistic electron bunches induced by transverse acceleration. The problem of a full quantitative determination of the electron bunch behavior belongs to a class of self-consistent issues which can be solved only with the help of numerical methods. In this thesis, though, we limited ourselves to the characterization of the self-interactions from an electrodynamical viewpoint (i.e. without considering the dynamical problem). This appears to be possible analytically: we performed such a task with in mind the double purpose of providing knowledge and understanding of the self-field interaction and of creating cross-checks and benchmarks for numerical computations.

Self-interactions can be naturally divided in a longitudinal component (parallel to the particle velocities) and a transverse component. We studied the longitudinal component first. We provided a new, flexible expression for the fields which can be both used as a basis for the development of a numerical code and for new theoretical investigations: with the help of our expression we were, in fact, able to study from a quantitative viewpoint the energy-dependence of the longitudinal self-fields, which is particularly relevant in the low-energy region of any injector for a large accelerator.

Next we dealt with the transverse component of the self-interaction. We profited, in this study, of a fruitful collaboration with DESY (Hamburg), where these problems are particularly important in relation to the XFEL project. A preliminary analysis of the self-forces by means of the code $\texttt{TraFiC}^4$ shows unexplained and counterintuitive features which we were able to understand, both qualitatively and quantitatively, only by means of thorough analytical investigations. We found that the electron bunch can be divided, in relation to the self-interaction issue, in different zones. In each zone, the electrons are sources of self-interactions with peculiar characteristics. In particular we were able to explain the sudden jump of the self-force at the entrance of a magnetic system in terms of the interaction between the head and the tail of the bunch. We also discovered that this has a local character and that, although completely neglected in the analysis of simulation results of the last two decades, it is of the same order of magnitude of the total self-interaction field. Our study has, moreover, the practical feature of providing the first quantitative benchmark for numerical studies of transient transverse effects.

From a very fundamental viewpoint, we found that the results of our study are

related to the nature of the energy-momentum pair: we showed that, in the case under study, this pair does not constitute a four-vector. This result can be explained in very simple terms by the fact that, within an electron bunch, the electromagnetic forces are not compensated by any other kind of interaction (as, for example, happens in an atomic nucleus). In other words, the system is intrinsically unstable.

In the last Chapter we considered the Coherent Synchrotron Radiation (CSR) from a bend. The longitudinal self-fields are responsible, in the wave-zone, for CSR phenomena, and CSR may be used both as a radiation source and as a tool for monitoring the longitudinal distribution of an electron bunch. Both these applications call for a thorough characterization of the CSR pulse. We derived analytically, for the first time, the CSR field pulse from an arc of a circle and we pointed out the presence of spectral distortions caused by finite distance effects between sources and observer and by diffraction effects. We provided a first quantitative study of these by means of numerical calculations, using a similarity technique to present our results which are, thus, in form of universal plots valid at any parameter range. Our study provides the first description of the physical phenomena responsible for spectral distortions which must be accounted for in the characterization of a CSR source or in the development of a diagnostic system based on CSR.

# Samenvatting

De productie van zeer heldere, ultrarelativistische elektronenbundels, die bijvoorbeeld in vrije-elektronenlasers in het röntgengebied toegepast kunnen worden, vormt een uitdaging voor versnellerfysici. En van de effecten die de eigenschappen van zo'n bundel kunnen verslechteren vindt zijn oorzaak in de wisselwerking tussen deeltjes en het electromagnetische veld dat door de elektronen zelf tijdens hun beweging wordt opgewekt.

Dit proefschrift is gewijd aan de studie van theoretische aspecten van zelfinteractie binnen korte ultrarelativistische elektronenpakketjes ('bunches') ten gevolge van transversale versnelling. Het probleem van een volledige kwantitatieve bepaling van het elektronenbunch gedrag behoort tot een klasse van zelfconsistente problemen die slechts met behulp van numerieke methoden kan worden opgelost. In dit proefschrift, beperken we ons echter tot de beschrijving van de zelfinteractie vanuit een electrodynamisch gezichtspunt, dus zonder het dynamische probleem te beschouwen. Dit blijkt analytisch mogelijk: deze taak werd uitgevoerd met voortdurend het dubbele doel voor ogen kennis en begrip te verschaffen van de zelf-veld wisselwerking en tevens kruiscontroles en referentiestandaarden voor numerieke berekening te creren.

Zelf-interactie kan op natuurlijke wijze worden verdeeld in een longitudinale component, parallel aan de deeltjessnelheid, en een transversale component. Als eerste bestudeerden we de longitudinale component. We vonden een nieuwe flexibele uitdrukking voor het veld, die zowel als basis kan dienen voor een numeriek programma als voor nieuw theoretisch onderzoek: met behulp van onze uitdrukking waren we in feite in staat de energieafhankelijkheid van longitudinale zelf-velden vanuit kwantitatief oogpunt te bestuderen, hetgeen in het bijzonder van belang is in het lage-energie gebied van injectoren zoned die bij van grote deeltjesversnellers gebruikt worden.

Vervolgens behandelden we de transversale component van de zelf-interactie.Hierbij profiteerden we van de vruchtbare samenwerking met DESY (Hamburg), waar deze problemen bijzonder belangrijk zijn bij het XFEL project. Een voorlopige analyse van de zelf-krachten met het programma TRAFIC[4] laat onverklaarde en zelfs tegen de intutie indruisende verschijnselen zien, die wij evenwel toch zowel kwalitatief als kwantitatief konden verklaren met behulp van gedegen analytische studie. We vonden dat, met betrekking tot het zelf-interactie vraagstuk, de elektronen bunch in verschillende zones kan worden ingedeeld. In iedere zone zijn de elektronen bronnen van zelf-interactie met speciale karakteristieken. In het bijzonder konden we de plotselinge sprong van de zelf-kracht aan de ingang van een magnetisch systeem verklaren in termen van wisselwerking tussen voor- en achterkant van de bunch. Ook ontdekten we dat dit een lokaal karakter heeft en dat dit, hoewel volledig genegeerd in de analyse van simulatieresultaten van de afgelopen twintig jaar, van de zelfde orde van grootte is als het totale zelf-interactie

veld. Onze studie verschaft bovendien het praktische nut voor het eerst kwantitatief vergelijkingsmateriaal te leveren voor numerieke studies van transversale effecten.

Vanuit een zeer fundamenteel gezichtspunt vonden we dat de resultaten van onze studie verbonden zijn met het wezen van het energie-impuls paar: we toonden aan dat in ons geval dit paar niet een viervector is. Dit resultaat kan worden verklaard in heel simpele termen door het feit dat binnen een elektronen bunch de elektromagnetische krachten niet worden gecompenseerd door enige andere wisselwerking (zoals dit bijvoorbeeld gebeurt in een atoomkern). Met andere woorden, het systeem is intrinsiek instabiel.

In het laatste hoofdstuk beschouwden we Coherente Synchrotron Straling (CSR) in een buigmagneet. De longitudinale zelf-krachten zijn in het 'verre veld' verantwoordelijk voor CSR verschijnselen, en CSR kan worden gebruikt zowel als bron van straling alswel als middel om de longitudinale dichtheidsverdeling van een elektronen bunch te meten. We karakteriseerden analytisch, en voor de eerste keer, de CSR veldpuls vanuit een cirkelboog en we merkten de aanwezigheid op van spectrale vervormingen ten gevolge van eindige-afstands effecten tussen bron en waarnemer en tengevolge van diffractie-effecten. We gaven een eerste kwantitatieve studie van deze effecten met behulp van numerieke berekeningen, waarbij we een vergelijkingstechniek gebruikten in de vorm van universele grafieken met een geldigheid voor ieder bereik van de parameters. Onze studie geeft de eerste beschrijving van fysische verschijnselen die verantwoordelijk zijn voor spectrale vervormingen waarmee rekening gehouden moet worden bij de karakterisatie van een CSR-bron of bij de ontwikkeling van een diagnostisch systeem gebaseerd op CSR.

# Acknowledgements

It is time to thank many people. Those who worked with me during the last three years and a half, those who supported me during the difficult moments, those I had fun with.

Parents, relatives, friends, colleagues, people from many nations which I met, sometimes even for a short time, and people I should have mentioned in these Acknowledgements but I did not (because I forgot to do so)... Thanks, grazie, bedankt, merci, spassiba, igracias, danke, takk, tack, obrigado, shiéshié...

I will never thank Evgeni Saldin enough for the wonderful collaboration we had in the last year and a half. Evgeni, you have been really a guide for me, you are an outstanding scientist and a very good person: I will always be grateful to you... Amazingly our cooperation took place almost completely (and with this I must thank your wife Galina for her terrific hospitality in Hamburg!) by email and fax! It will be great to continue it in the future!

Also, I want to express my sincere gratitude to Vladimir Goloviznin for his scientific support during the first phase of my Ph.D. studies: I only regret we couldn't go on with it, and I hope that, some day, we will work together again...

Marnix van der Wiel is another person I am much indebted with. Marnix, you were always there with your support and advice both as a leader and as a physicist when I needed it, especially in the difficult moments.

Jan Botman is the first person I met here in The Netherlands. Jan, I always admired the calm and the style you have in facing every situation. Together with Marnix, you were giving me a lot of support and advice during these years and you were there whenever I needed your help. For this I am grateful to you both, Marnix and Jan!

Next to them I want to thank my second promotor, Theo Schep, for the nice scientific discussions we had during the last year.

Jom, after tasting the real *Pesto ä Zeneize*[1] (instead of the AH fake!), you almost became a fellow genovese citizen, whether you like it or not... I will always look forward to our discussions! When is the next one scheduled, by the way?

Annette, Bas, Charlotte, Christian, Cyrille, Dimitri, Fred, Inge, Jaap, Jimmy, Marieke, Nicoline, Seth, Walter, Wim: I had a lot of fun working (and not only working!) with you guys! Thanks to you all!

---

[1] Pe'primma cosa méttite o scosa, poi piggia baxaicó ben fresco e noéllo, un spigo d'aggio, di pigneu, da sa, do sbrinso o parmixan prórpio de quello e caccia tutto quanto in to morta. Cantando na canson o un ritornello, pesta e remescia sensa fa schitta travaggiando de gómio e de pestello. Quando l'é tutto unio comme 'na pasta, piggia dell'euio nostro do ciú bon e remesciando, allunga quanto basta. Ed ecco o pesto profumóu da mette in ta pugnatta isemme a-o minestron o sorvia un bello piatto de trenette!

I wish to thank several people at DESY, in particular Joerg Rossbach for the hospitality granted, Evgeni Schneidmiller and Mikhail Yurkov for the scientific collaboration we had during the last year and a half. Also, thanks to Bart Faatz, Christopher Gerth and Philippe Piot for their pleasant welcome to Hamburg.

I am grateful to all the CASA staff at Jefferson Lab: in particular to Lia Merminga and Geoffrey Krafft for giving me the opportunity of spending three months at JLAB, to Kevin Beard who spent a lot of his time helping me with computer matters and of course, to Rui Li, Yuhong Zhang and Yaroslav Derbenev for the nice period spent working together: even if sometimes we had different views I had a great time with all you guys, and I hope this can be repeated in the future!

Thanks go also to the Italian and French groups at the FEL2002 conference in Chicago, with whom I had a terrific time, and in particular David, Hervé, Giovanni, Luca, Mauro...

How many other people I should thank for the nice time together! Thanks to Carlo, Roberto, Silvia, Sylvie, Sergio, Evgeni, Natasja, "De as van het Kwaad" fencing board (*Hoc Habet, haec melior magnis data victima divis*) and all the Hoc Habet fencers... did I forget anybody?

In Italia, non posso non ringraziare Mario Conte, mio maestro e amico.

Un grazie particolare va poi a Vittorio Sicolo, senza il cui consiglio questo lavoro sarebbe finito ancora prima di cominciare!

Signora Nene, mi piacerebbe che potesse leggere queste righe: posso solo aggiungere che il Suo ricordo sará sempre con me. Nene, Piero, Chiara, Maria, Raffaella, Tatiana (e a loro unisco tutta la Fondazione Zavattaro): grazie per l'affetto e l'amicizia che mi avete dimostrato in tutti questi anni.

Bobo, Emilio, Eugenio, i due Franceschi, Gianluca, Pablo, Roberto, Valerio, insomma la banda di Recco (e va be', anche Camogli): grazie per le rimpatriate piú o meno alcoliche e per la vostra amicizia. Un ringraziamento va anche a Teresa per la bella corrispondenza degli ultimi tempi.

Infine, sono riconoscente a tutta la mia famiglia: i miei zii Luisa e Arrigo, mio cugino Alessandro, mio padre Gianfranco e mia madre Lina in particolare, per essermi sempre stati vicini.

# Curriculum Vitae

June $7^{th}$, 1975    Born in Genova, Italia

1989-1994      Liceo Scientifico *Nicoloso da Recco*, Recco, Italia

1994-1999      Laurea in Physics, *Universitá degli Studi di Genova*, Genova, Italia

2000-2003      Ph.D. research project, FTV group,
*Technische Universiteit Eindhoven*, Eindhoven, Nederland

2002: Three months working visit at the
Center for Advanced Studies of Accelerators (CASA)
*Thomas Jefferson National Accelerator Facility*,
Newport News, Virginia, USA

2003-      ...Hey, who knows the future anyway?